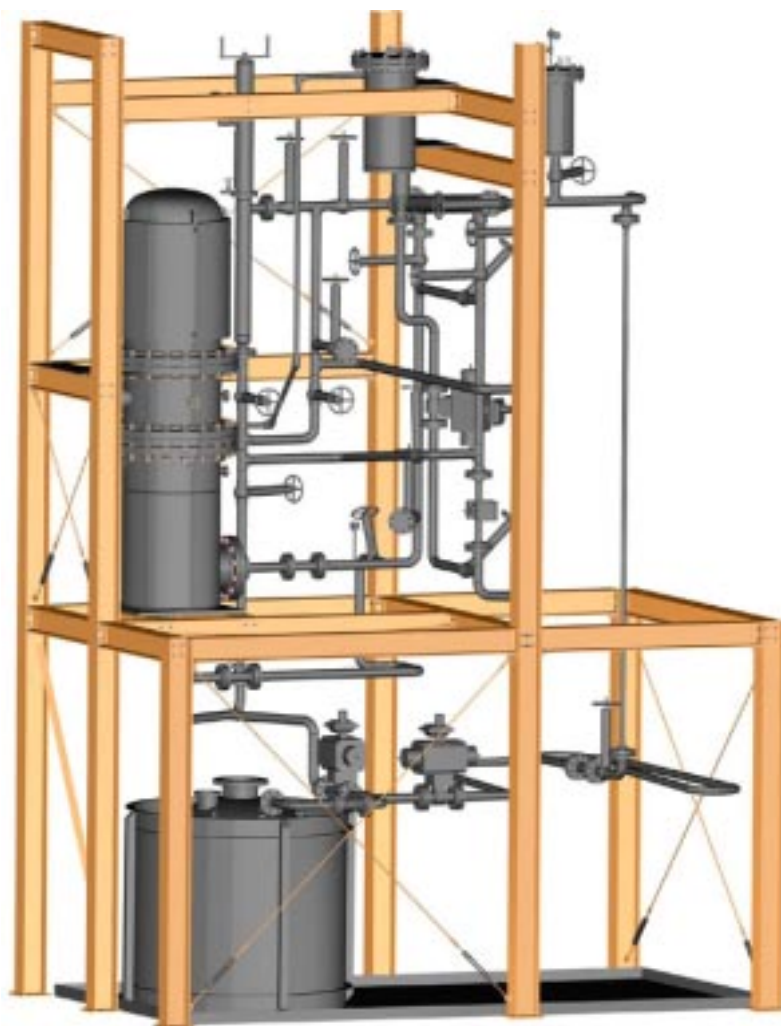

**DELTA Loop for Testing and Development of
Lead-Bismuth Eutectic Spallation Target Technology for
Accelerator-Driven Transmutation Systems**



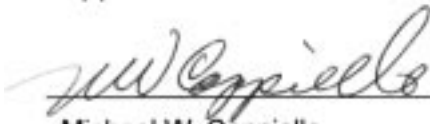
Los Alamos National Laboratory, Argonne National Laboratory
Oak Ridge National Laboratory, Pacific Northwest National Laboratory
Brookhaven National Laboratory, Lawrence Livermore National Laboratory
Idaho National Engineering and Environmental Laboratory, Idaho Accelerator Center
University of Nevada, University of Michigan, University of California, University of Texas
Burns & Roe, Enterprises, Inc., General Atomics, Westinghouse Savannah River Company

Blank Page

**AAA Technical Quarterly Report
January–March 2002**

LA-UR-02-2630

Approval



Michael W. Cappiello
LANL AAA Program Manager
Advanced Accelerator Applications

5/6/02
Date

Blank Page

Table of Contents

Major Contributors	ix
Acronyms and Symbols	xi
I. INTRODUCTION.....	1
II. HIGHLIGHTS	3
III. TECHNOLOGY DEVELOPMENT	7
1. FUELS DEVELOPMENT	7
Scope	7
Highlights	7
Fabrication Development	8
Metal Fuel.....	8
Nitride Fuel.....	12
Dispersion Fuel Fabrication.....	17
TRISO Fuel Fabrication.....	19
Fuels Irradiation Testing.....	21
ATW-1 Irradiation Test	21
ATW-3 Irradiation Test	25
Fuel Performance	26
Assessment of Radiation Tolerance	26
Radiation Damage	26
Helium Release Effects	26
Modeling and Fuel Properties	26
Continuum Scale Modeling of Nuclear Fuels	26
Atomic Scale Modeling of Nuclear Fuels	28
TRISO.....	29
Metal Fuels.....	29
Thermal Conductivity of Actinide Elements	29
Thermal Conductivity of Multi-Phase Alloys	31
2. SEPARATIONS TECHNOLOGY	36
Scope	36
Highlights	36
Oxide Fuel Processing—Electrolytic Oxide Reduction (PYROX) Process.....	37
Anode Development for the PYROX Process.....	41
UREX Process Development.....	45
Optimized UREX Process Demonstration	45
Plutonium Distribution Measurements with AHA.....	53
Plutonium Acetohydroxamic Acid Interaction	55
Dissolution of Dresden Reactor Fuel.....	57
Modified Direct Denitration (MDD) Demonstration.....	58
Sodium Iodide Production from Molten Salts	59
SANEX Process Studies	61
Alternative Fuel Treatment Process Development	62
TRISO Spent Fuel Reprocessing.....	62
Waste Form Development – Ceramic Waste Form from LiCl Salt System	69

3. TRANSMUTATION SCIENCE	70
3.1 Integration and Analytical Support	70
Scope	70
Highlights	71
Transmutation Science R&D Plan	71
LBE-Sodium Compatibility Experiments	73
MEGAPIE Technical Review Meeting	74
Analytical Support for LBE-Target Experiments	74
3.2 Materials	75
Scope	75
Highlights	76
PNNL Activities	76
Materials Handbook	77
3.3 Lead-Bismuth Eutectic Technology	77
Scope	77
LBE Technology Development	77
DELTA Loop Operations	78
Highlights	78
LBE Technology Development	78
DELTA Loop Operations	79
3.4 LANSCE Irradiation Experiments	81
Scope	81
Sodium Activation Tests	81
Neutron Yield and Spectrum Tests	81
Helium and Hydrogen Production Tests	82
Corrosion Studies	82
Highlights	82
Sodium-Activation Tests	83
Neutron Yield and Spectrum Tests	83
Foil Counting	83
Helium and Hydrogen Production Tests	87
Corrosion Studies	90
3.5 High-Energy Physics	94
Scope	94
MCNPX Code Development	94
Nuclear Data Evaluations	94
Highlights	95
MCNPX Code Development	95
Nuclear Data	96
3.6 Reactor Physics	100
Scope	100
Experiment and Safety Analysis	100
Physics Needs and Methods Development	100
Physics Experiment Planning	100
Highlights	101
MUSE Benchmark	101
MUSE Experimental Activity	101

PROFIL Experiment	101
Safety Analysis	102
Uncertainty Assessment.....	102
Method Development	102
TREAT-Coupling Experiments.....	103
3.7 International Support.....	103
Scope	103
Highlights	104
Summary	104
MEGAPIE General Description.....	105
Current Status of MEGAPIE.....	105
US MEGAPIE Activities	107
3.8 LANL-Sponsored University Programs	109
Scope	109
University of California – Berkeley	109
University of Michigan	109
University of Texas – Austin.....	109
North Carolina State University.....	110
University of California – Berkeley	110
Optimization of an Accelerator-Driven Molten-Salt Transmuting Reactor	110
Transmutation Capability of Accelerator-Driven Pebble-Bed Reactor	113
A Simplified Model for Fuel Isotope Evolution in ATW Systems	113
Comparison Between Na and Pb-Bi as Coolants for Liquid-Metal ATW	113
Cost/Risk Analysis of Candidate Approaches for P&T	113
Neutronics Computational Laboratory	113
University of Michigan	114
Transmutation of Transuranics in Pressurized Water Reactors.....	114
Analysis in Support of the LANSCE Experiments.....	114
Space-Time Analysis of Coupled Accelerator-Core Dynamics	114
Cross-Section Processing with the NJOY Code	115
Radiation Effects in Candidate Materials for Spallation Neutron Environments.....	115
University of Texas (UT) Austin	116
Proliferation Resistance Assessments	116
Spallation Product Studies	116
4. SYSTEMS TECHNOLOGIES	117
Scope	117
Accelerator-Driven Test Facility (ADTF).....	117
ADS Preconceptual Reference Design.....	118
Micro Accelerator-Driven System Proof-of-Principle.....	118
Highlights	118
Accelerator-Driven Test Facility (ADTF).....	119
Preconceptual Cost Estimate	119
Preconceptual Design	120
Transmutation Technology Development Plan	120
ADS Reference Design	121
Sodium-Cooled ADS Engineering Design	121
Micro Accelerator-Driven System (ADS) Proof-of-Principle (POP).....	124
Coupling Experiments	124
Fuels and Materials Experiments.....	127
Advanced Cavity Development.....	129

5. PROJECT INTEGRATION	131
5.1 Systems Studies.....	131
Scope	131
Highlights	131
Transmutation System Selection Studies	131
Report To Congress	134
5.2 University Programs.....	135
Scope	135
Highlights	136
LANL University Programs.....	136
University Participation Program	136
Idaho Accelerator Center	136
University Research Alliance	136
Directed University Research	136
Technical Progress.....	137
References	138

Major Contributors

Fuels Development:	D. Crawford (ANL) K. Chidester (LANL) M. Meyer (ANL) S. Hayes (ANL) R. Margevicius (LANL) K. McClellan (LANL)
Separations Technology:	J. Laidler (ANL)
Transmutation Science:	K. Pasamehmetoglu (LANL) E. Pitcher (LANL) L. Waters (LANL) M. James (LANL) M. Chadwick (LANL) N. Li (LANL) V. Tcharnotskaia (LANL) S. Wender (LANL) S. Maloy (LANL) B. Haight (LANL) G. Morgan (LANL) S. Lillard (LANL) R. Klann (ANL) G. Palmiotti (ANL)
Systems Technologies:	M. Cappiello (LANL) S. McConnell (LANL) K. Pasamehmetoglu (LANL) J. Roglans (ANL) R. Guffee (LANL) H. Cohen (BREI/GA) J. Herceg (ANL) W. Chaves (LANL) G. Willcutt (LANL) J. Elson (LANL) H. Ludewig (BNL) M. Todosow (BNL)
Project Integration:	L. Guillebaud (LANL) W. Davidson (LANL) D. Beller (LANL) A. Hechanova (UNLV) J. Lee (Univ Michigan) E. Greenspan (UC Berkeley) W. Charlton (UT Austin)

Blank Page

Acronyms and Symbols

AAA	Advanced Accelerator Applications
AC	Accelerating cavities
ADS	Accelerator-Driven System
ADTF	Accelerator-Driven Test Facility
ADMAB	Accelerator-Driven Minor Actinide Burner
AES	Advanced Energy Systems (formerly Northrup-Grumman Corp.)
AET	Ability Engineering Technology
AFM	Atomic Force Microscopy
Ah	Ampere-Hour
AHA	Acetohydroxamic acid
Am	Americium
AMUSE	Argonne Model for Universal Solvent Extraction, the generic TRUEX model expanded to include UREX and PUREX processing
ANL	Argonne National Laboratory (Chicago)
ANL-W	Argonne National Laboratory-West (Idaho Falls)
ANRC	Amarillo National Research Center
ANS	American Nuclear Society
ANSYS	structural analysis modeling code
appm	atomic parts per million
APT	Accelerator Production of Tritium
ASME	American Society of Mechanical Engineers
ATR	Advanced Test Reactor (INEEL)
ATW	Accelerator Transmutation of Waste
Ba	Barium
BCM	Beam-Current Monitor
BCP	Baseline Change Proposal
BCP	Buffered Chemical Polishing
Be	Beryllium
Beta (β)	Ratio to the speed of light
Bi	Bismuth
BISTRO	Two-Dimensional Discrete Ordinates Code
BNFL	British Nuclear Fuels, Ltd
BNL	Brookhaven National Laboratory
BOF	Balance of Facility
BOL	Beginning of Life
BOP	Balance of Plant
BOR-60	Sodium-Cooled Fast Reactor (Dmitrovgrad, Russia)
BPM	Beam-Position Monitor
CCDTL	Coupled-Cavity Drift-Tube Linac
CCL	Coupled-Cavity Linac
Ce	Cerium
CEA	Commissariat à l'Energie Atomique (France)
CEM	Cascade Exciton Model code (Model-based Monte-Carlo particle transport code)
CERCA	Compagnie Pour L'Etude Et La Realisation De Combustibles Atomiques
cercer	Ceramic-Ceramic
cermet	Ceramic-Metal
CFD	Computational Fluid Dynamics
CINDER90	Computer Code
CLWR	Commercial Light-Water Reactor
Cm	Curium
CMPO	Neutral Extractant

CMR	Chemistry and Metallurgy Research (facility at LANL)
CONCERT	COmbined Neutron Center for European Research and Technology
Cs	Cesium
Cu	Copper
CVD	Chemical Vapor Deposition
cw	Continuous Wave (100% duty factor)
DACS	Data Acquisition and Control System
DAS	Data Acquisition System
DCR	Design Change Request
DDN	Design Data Need
DIAMEX	Aqueous Solvent Extraction Process for TRU Recovery
DOE	Department of Energy
dpa	Displacements per Atom
EBR	Experimental Breeder Reactor
ED&D	Engineering Development and Demonstration
EDS	Energy Dispersive Spectrometry
EFPD	Effective Full-Power Day
EFTTRA-T4	Radiation Test Sponsored by the European Union
EIS	Electrochemical Impedance Spectroscopy
EIS	Environmental Impact Statement
ENDF	Evaluated Nuclear Data File – Evaluations that can be used in MCNPX for more accurate predictions of fission, criticality, transport, and radiation damage
EOI	End of Irradiation
EOL	End of Life
EPICS	Experimental Physics and Industrial Control System
ERANOS	Computer modeling code
ERC	External Review Committee
ES&H	Environmental, Safety, and Health
ESS	European Spallation Source
ESSAB	Energy System Acquisition Advisory Board (DOE)
Eu	Europium
FDD	Facility Design Description
Fe	Iron
FFTF	Fast Flux Test Facility
FMF	Fuel Manufacturing Facility
FODO	Focus-Drift-Defocus-Drift
FPY	Full-Power Year
FWHM	Full Width Half Maximum
FZJ	Forschungs Zentrum Jülich (German Laboratory)
FZK	Forschungs Zentrum Karlsruhe (German Laboratory)
g/L	Grams per Liter
GA	General Atomics Inc.
GNASH	Nuclear Reaction Code
GSI	Gesellschaft für Schwerionenforschung (Darmstadt, Germany)
GT-MHR	Gas Turbine Modular Helium Reactor
H	Hydrogen
HAN	Hydroxylamine
HCP	Hazard Control Plan
He	Helium
HEBT	High-Energy Beam Transport
HEU	Highly enriched uranium
Hf	Hafnium
HFIR	High Flux Isotope Reactor (ORNL)
HFR	High Flux Reactor (Petten, Netherlands)
Hg	Mercury
HIP	Hot Isostatic Process (for bonding materials)

HM	Heavy metal
HPRF	High-Power Radio Frequency
HS/WS	Halo-Scraper/Wire-Scanner (diagnostic device)
HX	Heat exchanger
I&C	Instrumentation and Control
IAC	Idaho Accelerator Center
IAEA	International Atomic Energy Association (Vienna, Austria)
ICP-MS	Inductively Coupled Plasma-Mass Spectrometry
ICS	Integrated Control System
IFMIF	International Fusion Materials Irradiation Facility
IFR	Integral Fast Reactor
IHX	Intermediate Heat Exchanger
IMS	Information Management System
INEEL	Idaho National Engineering and Environmental Laboratory
IPBT	In-Pile Beam Tube
IPPE	Institute of Physics and Power Engineering, Obninsk, Russia.
ISABEL	Physics Modeling Code
ISTC	International Science and Technology Centre (Moscow)
ITER	International Thermonuclear Experimental Reactor
ITU	Institute for Transuranium Elements (Karlsruhe, Germany)
JAERI	Japan Atomic Energy Research Institute
JCNNM	Johnson Controls Northern New Mexico
JLAB	Jefferson Laboratory (VA)
K	Potassium
KAERI	Korean Atomic Energy Research Institute
KEK	National Laboratory for High-Energy Physics (Tsukuba, Japan)
keV	Kiloelectron Volt
LA150n	Los Alamos generated nuclear data library, extending up to 150 MeV
LAHET	Los Alamos High-Energy Transport
LANL	Los Alamos National Laboratory
LANSCE	Los Alamos Neutron Science Center
LBE	Lead-bismuth eutectic
LBHM	Low- β Hot Model
L/d	Length-to-diameter ratio
L/hr	Liter per hour
LEBT	Low-Energy Beam Transport
LEDA	Low-Energy Demonstration Accelerator
LINAC	A computer code based on PARMILA that has been modified to include CCDTL and SCRF elliptical cavities as options
LLFP	Long-lived fission product
LLNL	Lawrence Livermore National Laboratory
LLRF	Low-level radio frequency
LME	Liquid-metal embrittlement
LMR	Liquid-metal reactor
LWR	Light-water reactor
M	Molar
MA	Minor actinide
mb	Millibarn
MCA	Multi-criteria analysis
mCi	Millicurie
MCNP	Monte Carlo N-Particle Transport Code
MCNPX	Merged code—Los Alamos High-Energy Transport (LAHET) and Monte Carlo N-Particle Codes (MCNP)
MDD	Modified Direct Denitration
MEGAPIE	Megawatt Pilot Experiment
MFM	Magnetic Flow Meter

MIT	Massachusetts Institute of Technology
mL	Milliliter
Mo	Molybdenum
MOX	Mixed oxide fuel
mR	Millirad (a measure of radiation)
MT	Metric Ton
MTL	Materials Test Loop
MW	Megawatt
MWD/T	Megawatt Days per Ton (standard unit for burnup)
MWth	Megawatt thermal
N	Nickel or nitride
Np	Neptunium
n/p	Neutrons per proton
NDA	Nondestructive analyses
NEA	Nuclear Energy Agency (Paris)
NEPA	National Environmental Protection Agency
NERAC	Nuclear Energy Research Advisory Committee
NERI	Nuclear Energy Research Initiative
NFC	Nuclear Fuel Cycle
NFF	Nonfertile Fuel
O	Oxygen or Oxide
O&M	Operations and Maintenance
OECD	Organization for Economic Cooperation and Development (Paris)
ORIGEN	A computer code system for calculating the buildup, decay, and processing of radioactive materials
ORNL	Oak Ridge National Laboratory
P&ID	Piping and Instrumentation Diagram
P&T	Partitioning and transmutation
PACS	Personnel Access Control System
PARMTEQM	RFQ simulation code
Pb	Lead
PCM	Pulse Control Modulation
Pd	Paladium
PFD	Process Flow Diagram
PHA	Preliminary Hazards Assessment
PHENIX	Fast Reactor in France
PIE	Post-irradiation examination
PNNL	Pacific Northwest National Laboratory
POP	Proof of Performance, Proof of Principle
PRAD	Proton Radiography
PRISM	Power Reactor Innovative Small Module
PSAR	Preliminary Safety Analysis Report
PSS	Personnel Safety System
PSI	Paul Scherrer Institute (Switzerland)
Pu	Plutonium
PUREX	Plutonium-Uranium Extraction
PWR	Pressurized Water Reactor
PYRO	Pyrochemical process
Q	Quality factor
QA	Quality Assurance
QAC	Quick ATW Costing
R	Rad (a measure of radiation)
RAMI	Reliability, Availability, Maintainability, and Inspectability
RBS	Rutherford Backscattering Spectrometry
RERTR	Reduced Enrichment for Research and Test Reactors program
RF	Radio Frequency

RFQ	Radio-Frequency Quadrupole
RCCS	Resonance-Control Cooling System
RIA	Rare Isotope Accelerator
RIAR	Russian Institute of Atomic Reactors
rms	root mean square
RRR	Residual Resistance Ratio
RSICC	Radiation Safety Information Computational Center
RTD	Surface Temperature Detector
RTH	Royal Institute of Technology (Stockholm, Sweden)
Ru	Ruthenium
SAA	Systems Approaches Analysis
SANEX	Aqueous Solvent Extraction Process for Am and Cm Recovery
SAR	Safety Analysis Report
SC	Superconducting
SCM	Subcritical Multiplier
SCRF	Superconducting RF
SDD	System Design Description
SEM	Scanning Electron Microscopy
SFT	Stacking-Fault Tetrahedral
SHR	shutdown heat-removal
SINQ	Spallation Neutron Source at Paul Scherrer Institute (Switzerland)
SNF	Spent Nuclear Fuel
SNL	Sandia National Laboratory
SRS	Savannah River Site
SRTC	Savannah River Technology Center
Star-CD	Computational fluid dynamics code
STAYSL	A computer code to analyze results of activation foil measurements
STAYSL2	A computer code to analyze results of activation foil measurements in both a proton and neutron flux
STP	Standard Temperature and Pressure
STIP	Spallation Target Irradiation Program (at PSI)
T/p	Tritons (nucleii of tritium atoms) per Proton
T/B	Target / Blanket
Ta	Tantalum
TBP	Tri- <i>n</i> -butyl Phosphate or Tributylphosphate
Tc	Technitium
TEM	Transmission Electron Microscopy
TESLA	International Collaboration on a TeV Superconducting Linear Accelerator
TGA	Thermal Gravimetric Analysis
TJNAF	Thomas Jefferson National Accelerator Facility
TMT	Target and Materials Test Station
TRAC	Transient Reactor Analysis Code
TRACE 3-D	Interactive computer code that calculates the envelopes of a bunched beam through a user-defined transport system
TREACS	TReat Experiment for ACcelerator-driven System
TREAT	Transient Reactor Test Facility
TRISO	Tri-isotropic, referring to a multi-layered fuel-particle coating consisting of pyrolytic carbon and silicon carbide
TRISPAL	Refers to the French APT Program
TRL	Technical Readiness Level
TRU	Transuranics (americium, curium, neptunium, and plutonium)
TRUEX	Aqueous solvent extraction process for TRU recovery
U	Uranium
UFP	University Fellowship Program
UNLV	University of Nevada Las Vegas
UPP	University Participation Program

UREX	Uranium Extraction (an aqueous partitioning process)
URP	University Research Program
USQD	Unreviewed Safety Question Determination
V	Vanadium
VPS	Vapor Plasma Spray
VARIANT	Three-Dimensional Nodal Transport Code
W	Tungsten
WBS	Work Breakdown Structure
WNR	Weapons Neutron Research (facility at LANL)
WPPT	Working Party on Partitioning and Transmutation
WSRC	Westinghouse Savannah River Company
Xe	Xenon
XRD	X-ray Diffraction
Y	Yttrium
ZPPR	Zero Power Physics Reactor
Zr	Zirconium

Advanced Accelerator Applications

Quarterly Report

January – March 2002

I. INTRODUCTION

The Advanced Accelerator Applications (AAA) Program, a Department of Energy (DOE) program commissioned by Congress in FY2000, is a national effort consisting of DOE laboratories (Los Alamos, Argonne, Savannah River, Livermore, Oak Ridge), industry (Burns and Roe Engineering Inc, General Atomics) and universities (UC-Berkeley, Texas, Michigan, Nevada). The primary mission of the AAA Program is to develop the technology base for the transmutation of nuclear waste and to demonstrate its practicality and value for long-term waste management.

The AAA Program was constituted by combining two programs: the Accelerator Production of Tritium (APT) Program and the Accelerator Transmutation of Waste (ATW) Program. The APT Program was established in 1995 with a commercial light-water reactor (CLWR) program as part of a dual-path strategy for development of a new tritium-production technology for the nation. From 1995 through 2001, DOE-Defense Programs invested in the design and development of an accelerator to produce tritium, including a full-scale prototype of the front end of the accelerator. In December 1998, the DOE chose the CLWR as the primary technology for tritium production, leading to the closeout of APT at the end of FY01. The ATW Program, which was investigating the feasibility of accelerator-driven systems to transmute long-lived toxic components of spent nuclear fuel, benefitted from the technology development of APT.

The goal of the AAA Program is to evaluate the effectiveness of transmutation of spent nuclear fuel against the following criteria:

- (1) Reduce the long-term radiological impact of waste;
- (2) Enable development of a simpler, cheaper repository;
- (3) Reduce proliferation risk; and
- (4) Improve long-term prospects for nuclear power.

Improving the long-term prospects for nuclear power means not only demonstrating through proof-of-performance the practicality of the transmutation of nuclear waste and its meaningful impact on nuclear materials, waste management, and economics, but also defining and executing activities designed to support the country's nuclear science and engineering infrastructure.

For the short term, the AAA Program is focusing its efforts on the following:

- (1) Evaluating the most effective systems for transmutation of spent nuclear fuel;
- (2) Developing separations technologies to partition long-lived radioactive waste from reusable nuclear material;
- (3) Developing and testing potential transmutation fuels;
- (4) Developing a spallation target to provide an effective environment for transmutation;

- (5) Establishing and supporting a national university program to re-energize development and training in nuclear-related fields; and
- (6) Collaborating in international research efforts with nations involved in evaluating nuclear waste management.

Through these efforts, the AAA Program is defining the key experiments, analyses, and facilities needed to demonstrate the technical viability of partitioning and transmutation of long-lived nuclear wastes.

Additionally, a key future objective of AAA is the construction of an accelerator-driven test facility (ADTF). The goal of the facility would be to demonstrate the transmutation of nuclear waste and to function as a national nuclear science and engineering user facility.

II. HIGHLIGHTS

Fuels Development

- The first AAA PuN and (Pu, Zr)N pellets were sintered. High density in ZrN pellets using Pd as a sintering aid was achieved.
- The first AAA PuN powder was successfully synthesized from PuO₂ feed.
- Fabrication of Pu-60Zr and Pu-10Np-40Zr alloy fuel slugs for irradiation in the ATW-1 experiment was completed and substantial characterization performed.
- The AAA Fuel Development Five-Year Plan was drafted and submitted to DOE.

Separations Technology

- We have demonstrated better than 99% conversion of UO₂ to U metal in the direct electrolytic reduction process being developed for the treatment of LWR spent fuel.
- An optimized flowsheet prepared for the UREX hot demonstration at SRTC is predicting performance at the program target levels (>99.9% recovery of U and TRU, >95% recovery of Tc).
- Two conceptual processes have been developed for the treatment of TRISO fuel that would convert the fuel materials to chlorides for subsequent recovery of the actinides by pyrochemical means.

Transmutation Science

- The initial draft of the Transmutation Science 10-year R&D plan was issued.
- The remaining tests in the test matrix for the LBE-Na compatibility experiments were completed.
- At the MEGAPIE technical review meeting, we identified a number of areas for US support tasks to MEGAPIE.
- LANL hot-cell activities at the CMR Building resumed after completion of the facility upgrades.
- During this quarter, the DELTA Loop was operated for a total of 35 hours for operational testing.
- A final report was issued for the Na-activation experiments. A preliminary report was written for the neutron yield of LBE target experiments.
- MCNPX version 2.4.j, fully updated, rewritten in Fortran90 and available on seven platforms, was released to the Beta Test Team.

- We completed our new data evaluation for the LA150 nuclear data library of inelastic scattering to the first excited state in Pb at 2.61 MeV, which will be made available for use in MCNPX and other codes.
- A preliminary analysis of the MUSE benchmark, corresponding to the critical configuration of the MUSE-4 experiment, was performed.
- An uncertainty assessment relevant to the neutronic design of an ADS has been carried out for systems containing fuels with high content of minor actinides.
- In partial fulfillment of the MEGAPIE collaboration agreement, a resident engineer from LANL is stationed at PSI for a 5-month duration, working on the MEGAPIE target engineering design and development tasks.

Systems Technologies

- We issued the ADTF Preconceptual Cost Study, providing parametric estimates for the Total Project Cost of four alternate design concepts for the ADTF.
- We revised the ADTF Missions, Functions, and Requirements document to reflect the removal of the tritium production mission from the AAA Program.
- We initiated the preparation of the Transmutation Technology Development Plan.
- The Na-cooled ADS reference design for the reactor core shroud was completed.
- Discussion of the engineering feasibility of coupling the IAC accelerator to the TREAT reactor at ANL-W identified no show-stoppers.

Systems Studies

- The AAA report on the CORAIL-Pu deep burn analyses was completed, and three papers on the CORAIL fuel cycle analyses were submitted to upcoming nuclear conferences.

University Programs

- An annual report describing all FY01 AAA University Programs was completed and distributed.
- UNLV hosted a University Workshop to bring together researchers from a number of the AAA university programs.
- UNLV hosted a week-long training course for the MCNPX radiation transport code.
- UNLV coordinated and hosted the second AAA Quarterly Technical Review.

- UNLV received a third round of research proposals, four for continuation of ongoing research, and seven for new funding. Two proposals were selected for funding beginning this summer.
- The University Research Alliance (URA), formerly the Amarillo National Research Center, conducted the selection of ten AAA Fellows.

Blank Page

III. TECHNOLOGY DEVELOPMENT

1. FUELS DEVELOPMENT

Scope

AAA fuels development activities are directed toward the development and qualification of fuels for safe transmutation of actinides at maximal rates. The objective of the effort is to provide one or more transmutation fuel forms at Technical Readiness Level (TRL) 6 at the time that transmutation technology overall is to begin integral demonstration. Thus far, requirements for such fuels include nonfertile compositions in forms suitable for fast-spectrum transmuters and a homogenous fuel cycle (i.e., all minor actinides would be maintained in the same fuel and processing stream). However, the AAA transmutation program is considering additional transmuter architectures, the use of which would imply different requirements for fuels; therefore, the fuel development program is evolving as the nature of and approach for the overall transmutation mission evolves.

The specific R&D activities include development of techniques to fabricate transmutation fuels from LWR fuel-derived actinide feed and from actinide feed recycled from transmuters. As-fabricated samples are chemically and microstructurally characterized to evaluate the success of fabrication processes and to better understand the nature of the fuel materials. Evaluation of proposed fuel forms (nitride, oxide, metal, carbide, dispersion, etc.) requires irradiation testing, so near-term irradiation tests are being planned and will be performed through the course of this program. Finally, the understanding of in-service fuel behavior is best demonstrated through the development and validation of fuel behavior models that are eventually incorporated into fuel performance codes. Such models are being developed, concurrent with an effort to develop thermal models that allow calculation of fuel and cladding temperatures in service and during testing.

Highlights

- The ATW-1 fuel rodlet endplug weld procedures were qualified.
- Fabrication of Pu-60Zr and Pu-10Np-40Zr alloy fuel slugs for irradiation in the ATW-1 experiment was completed and substantial characterization of these alloys performed.
- High density in ZrN pellets at moderate temperatures (~1500°C) using Pd as a sintering aid was achieved.
- Technical collaboration with the Institute for Transuranium Elements (ITU) on He release effects in ZrN was initiated.
- In modeling and analyses, we assessed the high-temperature domain of the Ce-O phase diagram, modeled the partial pressure of oxygen in sub-stoichiometric plutonia, and determined the equilibrium volume, bulk modulus, and elastic constants of ZrN.

- Using electronic structure calculations, the thermal analysis of the ATW-1 test specimens showed that rodlet endplug and cladding temperatures are acceptable at a pin power of 300 W/cm.
- The final design of the borated aluminum ATW-1 test outer basket was completed. Neutronics indicate that ATW-1A and ATW-1B will reach discharge burnup after approximately 110 days of irradiation.
- We synthesized DyN by nitriding Dy metal powder at 1200°C under nitrogen for 24 hours.
- The first AAA PuN powder was successfully synthesized from PuO₂ feed.
- The first AAA PuN and (Pu, Zr)N pellets were sintered. The pellets were strong but the density varied between 65% to 75% TD (lower than the 80%–90% TD desired). Powder milling tests with ZrN increased final sintered densities to 92% TD.
- Spherical DUO₂ particles were transported from ORNL to ANL for use in dispersion fuel particle coating experiments.
- Processes for fabrication of TRUO_x particles for fabrication of ATW-1 dispersion fuel test specimens were defined.
- Modifications were made to the ATW-1 test capsule to allow cask transport of the entire capsule assembly.
- A sol-gel method for making hafnia (HfO₂) microparticles was developed (the microparticles are used as nonradioactive surrogate kernels in development of TRISO-coated particle fuel).
- The AAA Fuel Development 5-Year Plan was drafted and submitted to DOE.

Fabrication Development

Metal Fuel

Weld qualification for ATW-1 irradiation specimen closure welds was finalized. The final end plug design is shown in Fig. 1. Documents specifying specific weld and weld inspection requirements for ATW-1 were completed and approved. Welding procedures are given in the ANL documents *Fuel Element First Plug Welding Procedure Specification (W7520-0475-ES-00)* and *Fuel Element Second Plug Welding Procedure Specification (W7520-0476-ES-00)*.

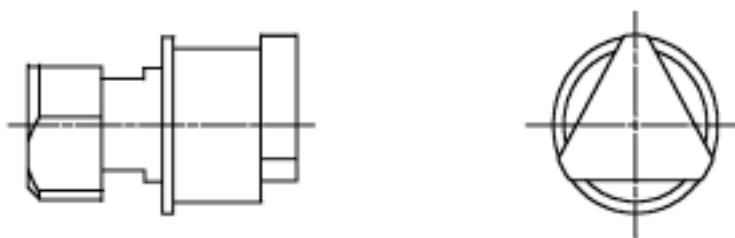


Fig. 1. Endplug design for ATW-1 fuel rodlets.

Fabrication of the first two batches of metal fuel slugs for irradiation in the ATW-1 test was completed. Short rods of Pu-60Zr and Pu-10Np-40Zr alloys were fabricated by

arc casting into a zirconium-oxide-coated silica mold. Transverse sections taken from the two Pu-60Zr specimens were characterized using XRD (x-ray diffraction) and SEM/EDS/WDS (scanning electron microscopy/energy dispersive spectroscopy/wavelength dispersive spectroscopy) to determine the effects of some processing variables on fuel-slug microstructure. Section MA002 was taken from a rod that was remelted and recast four times; section MA005 was from a rod that was cast only once. Analysis of both Pu-60Zr and the Np-bearing specimens are continuing.

Figure 2 is an SEM micrograph that shows the overall microstructure of sample MA002; the microstructure is uniform from the center of the sample to the edge. Figure 3 shows a higher-magnification image of this sample, showing the grain boundaries and a relatively large globular precipitate phase favoring grain boundaries. Some random precipitates were observed to form within individual grains. These microstructural features are similar to those observed in U-20Pu-10Zr fuel fabricated and irradiated in EBR-II. The matrix appears to be a two-phase mixture of an acicular precipitate phase and a more brightly contrasted matrix phase.

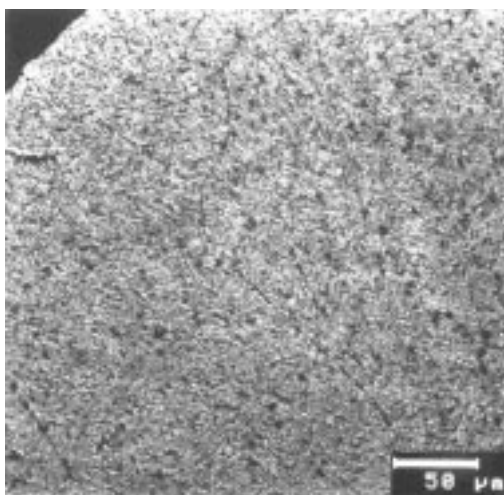


Fig. 2. SEM micrograph of the microstructure observed in sample MA002.

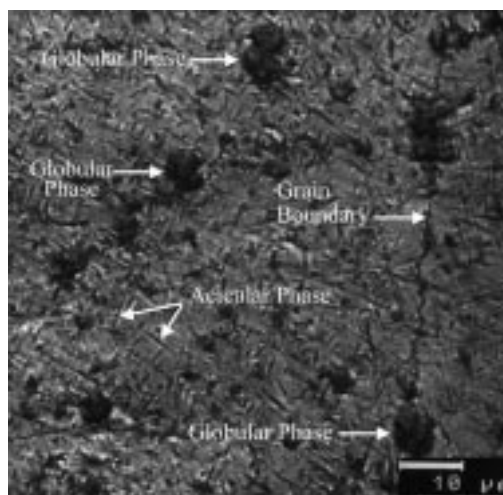


Fig. 3. SEM micrograph of sample MA002. Three possible phases were observed: a dark-contrasted, globular, precipitate phase; a dark-contrasted, acicular precipitate phase; and a light-contrasted matrix phase.

X-ray maps in Fig. 4 show the variations of Zr, Pu, and O in a selected region of MA002. In these maps, areas that are light in contrast relative to the background indicate increased concentration of an element. Figure 4(a) shows a BSE (back-scattered electron) image of a grain boundary containing a precipitate phase (seen in dark contrast). It was observed that the globular phase was depleted in Pu and enriched in oxygen relative to the two-phase mixed matrix. Both the two-phase mixture and the globular phase contained similar Zr concentrations. The acicular phase was also slightly enriched in oxygen. Point-to-point standardless analysis gives a relative picture of the variation in composition between the globular precipitate phase and the two-phase matrix. Based on this analysis, the globular precipitate contained roughly 52 wt% Zr, 35 wt% Pu, and 13 wt% O ($\pm 2-3$ wt%). The two-phase mixture contained approximately 48 wt% Zr, 51 wt% Pu, and negligible oxygen. The compositions of the individual phases in this mixture could not be determined because of the small size of these features relative to the probe spot size.

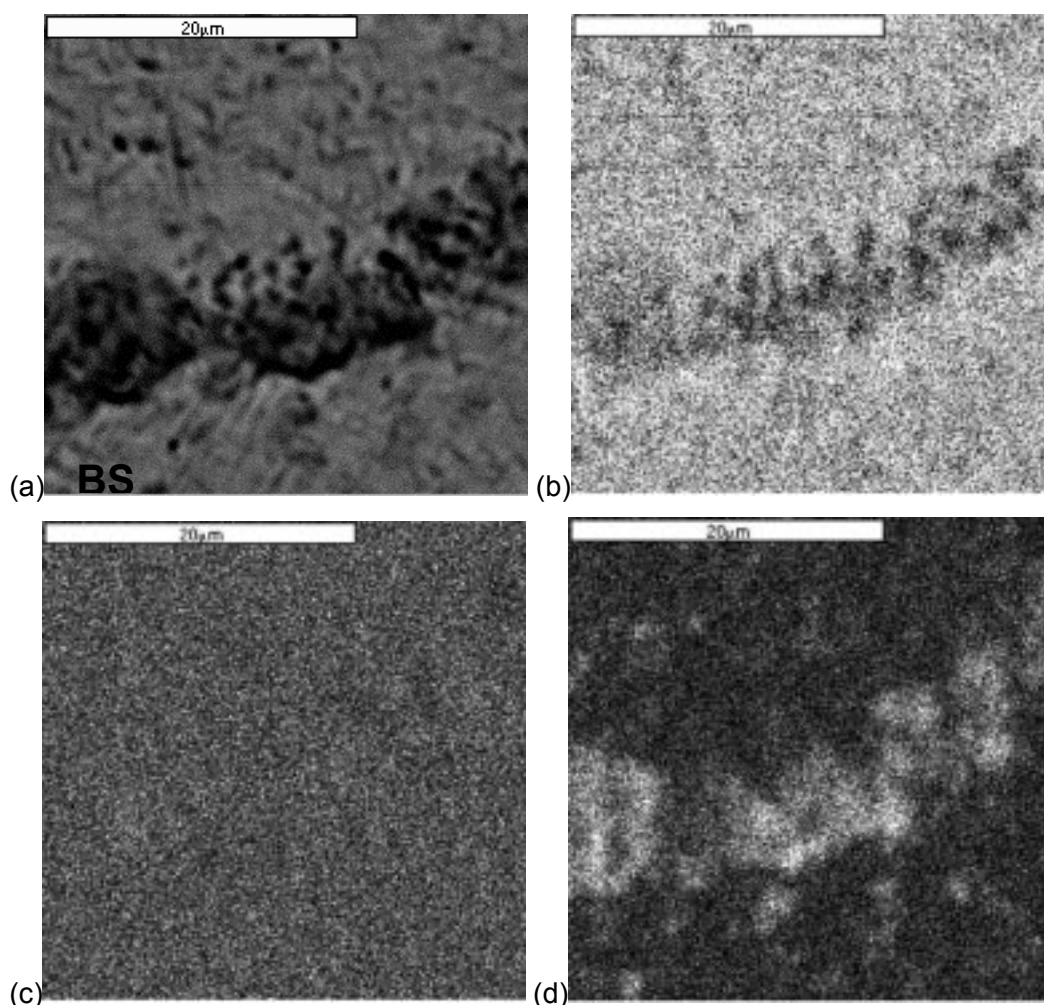


Fig. 4. (a) A backscattered electron image of sample MA002 along with x-ray maps of (b) plutonium, (c) zirconium, and (d) oxygen content. Light areas indicate higher concentrations of the element being mapped.

Sample MA005, cast only once, had a slightly different overall microstructure than sample MA002 (see Fig. 5). MA005 contained some of the same types of phases as MA002, viz., a dark-contrasted, globular, precipitate phase, a dark-contrasted, acicular precipitate phase, and a light-contrasted matrix phase. Less of the dark-contrasted, globular, precipitate phase was observed moving from the center of the sample to the edge of the sample. Regions of the sample were enriched in Pu (light areas in Fig. 5), suggesting the presence of some incompletely alloyed metal. Dendritic structures were present at the edge of the sample that were not seen in sample MA002. SEM/EDS/WDS analyses performed on sample MA005 showed that the compositions of the globular precipitate phase and two-phase mixture areas agreed with what was measured for the same phases in sample MA002.

Thus, based on SEM/EDS/WDS analysis, three primary phases seem to comprise the as-cast Pu-60 wt% Zr alloy microstructure: a globular precipitate, an acicular phase, and a matrix phase. Additional phases are introduced as a result of insufficient melt times for complete alloying. Based on the approximate composition of 50 wt% Zr and

the presence of oxygen, the globular phase may be the k-phase. The k-phase has been reported to exist only in the presence of oxygen¹.

Figure 6 shows an x-ray diffraction (XRD) pattern taken from samples MA002 and MA005. Diffraction patterns were taken from a setup that produces relatively high background; solid specimens were placed in an environmental chamber in a polyethylene sample holder. Diffraction peaks were very broad, with typical widths on the order of $\sim 0.4^\circ$ two-theta.

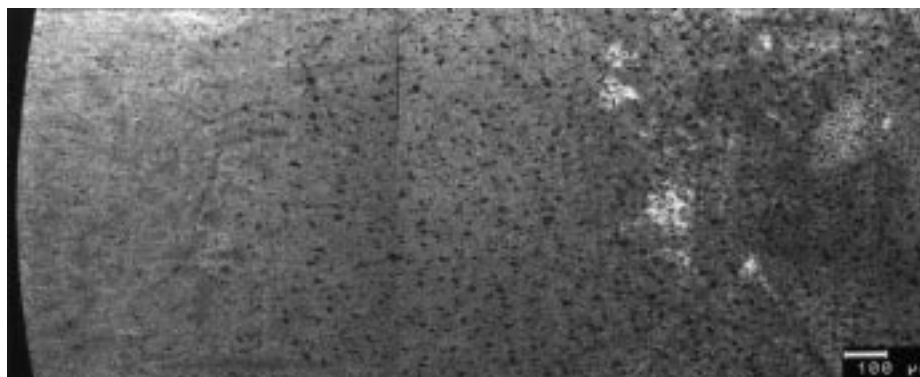


Fig. 5. Montage of SEM micrographs for sample MA005. The amount of the dark-contrasted, globular, precipitate phase decreases moving from the center of the sample (right) to the edge of the sample (left). Bright-contrasted regions are enriched in Pu. A dendritic structure can be observed at the edge of the sample.

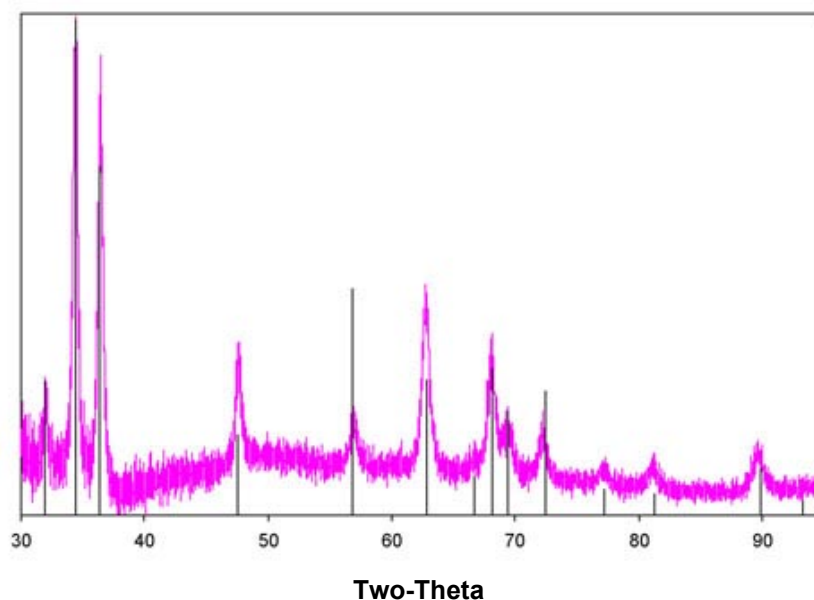


Fig. 6. X-ray diffraction pattern of Pu-60Zr specimen. Markers represent peak positions and calculated intensity for a random solid solution of α -(Pu,Zr) with lattice parameters of $a=0.324$ nm and $c=0.532$ nm.

¹ See for example, J.A.C. Marples, *Journal of Less-Common Metals* 2 (1960) 331-351, Y. Suzuki *et al.*, *Journal of Alloys and Compounds* 182 (1992) L9-L14, and J.C. Lauthier *et al.*, *Journal of Nuclear Materials* 23 (1967) 313-319.

As it is, all peaks in the pattern are accounted for by a calculated pattern for a hexagonal α -Zr phase (Mg structure) with approximate lattice parameters of $a=0.324$ nm and $c=0.532$ nm. No second-phase peaks could be identified; however, the high background and peak broadening present in this pattern may be masking the presence of the minor second phases observed by SEM. Peak intensities are also likely to be skewed. The broad peaks may indicate the presence of a range of Pu-Zr solid solutions, each with slightly different lattice parameters. Further SEM and XRD analyses of annealed specimens, along with differential thermal analysis, will be required to definitively establish the microstructural state of the specimens.

Nitride Fuel

Surrogate and Nonactinide Nitride Studies

ZrN pellets with an L/d ~ 0.5 can typically be cold pressed to a green density of 75% theoretical density (TD) and additional densification can be achieved with sintering above $\sim 1650^\circ\text{C}$ for -325 mesh powders. However, with the anticipated length/diameter (L/d) ~ 1.5 for fuel pellets for the ATW-1 irradiation, the desired final density of 85% TD will not be able to be reached without use of a sintering aid to allow significant densification at $\leq 1400^\circ\text{C}$.

A study is being conducted with three classes of sintering aids which have been identified as having promise for providing densification at $\sim 1400^\circ\text{C}$ while still providing a stable microstructure during irradiation. The three classes can be categorized as “noble” metals, mononitride-forming rare-earth type metals, and oxides. The noble type and rare-earth type metals have been the focus of the processing during this quarter.

ZrN-based matrices were successfully pressed and sintered with the addition of Pd, Ni, Cu, V, and Zr metals as candidate sintering aids, with contents ranging from 0.3 vol% to 5.0 vol%. Of the experimental runs performed to date, Pd shows the most promise (Table 1), with a relative increase in density on the order of 20% from the green state demonstrated. However, there is substantial scatter in the data, which is most likely due to the need for equipment modification and process refinement. Densification is dependent upon residual oxygen content during firing, and furnace optimization is an ongoing process.

Table 1. Density Data for Initial Pd Sintering Aid Survey
(density expressed as percent of theoretical density accounting for density of sintering aid)

Composition	As-Pressed Density		Sintered Immersion Density	
	mean	error	mean	error
ZrN	63.093	N/A	85.011	N/A
ZrN-Pd 0.5%	66.903	+1.88/-3.00	88.029	+2.69/-1.91
ZrN-Pd 1%	67.082	+1.70/-2.60	82.691	+5.85/-6.55
ZrN-Pd 5%	70.036	N/A	81.482	N/A

Density evaluations of the Ni, Cu, Zr, and V samples identified physical expansion, which was confirmed by the observation of significant porosity under optical and

scanning electron microscopy. The physical expansion of these pellets is attributed to a high oxygen partial pressure in the sintering furnace for these early experiments. Recent process optimization has significantly reduced this effect for the Pd-bearing samples, and these sintering aids will undergo reevaluation.

Studies carried out by JAERI indicate that the physical properties of Dyn, specifically its volatility, closely match that of AmN. The initial objective of this study is to determine phase formation in the Dy/Zr/N system. Following these initial studies, the next objective will be to study the volatility and thermodynamics of DyN in ZrN matrices prepared by different synthetic routes such as from Dy and Zr powders and from pre-made Dy-Zr alloys.

Dysprosium nitride was prepared by reacting the metal (-40 mesh) with nitrogen gas at 1200°C for 24 hours. This reaction was carried out in an alumina boat lined with Zr metal foil to protect against unwanted oxidation. Based on powder x-ray diffraction, the starting material nitrated completely (Fig. 7). TGA and DSC measurements indicate that DyN is stable under inert atmosphere and does not undergo any structural-phase transitions up to 1100°C as shown in Fig. 8.

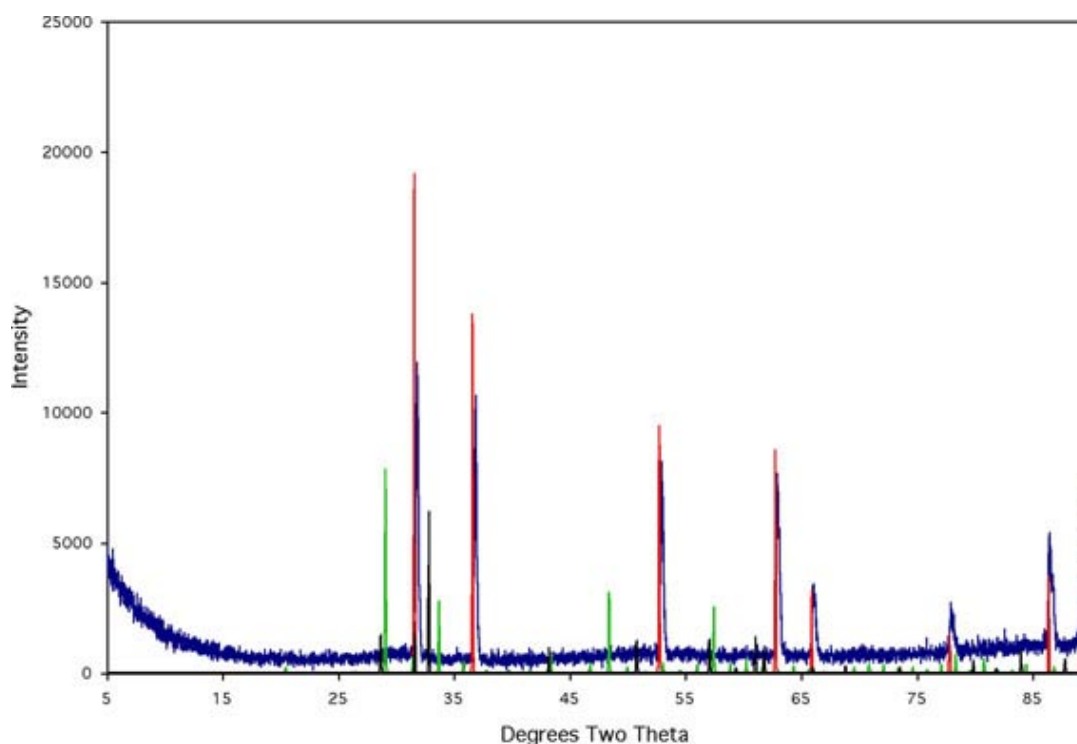


Fig. 7 Powder diffraction pattern of DyN prepared by heating Dy metal to 1200°C for 24 hours under a nitrogen atmosphere. Blue peaks are experimental DyN, red peaks are calculated DyN, green peaks are calculated Dy₂O₃, and black peaks are calculated Dy metal.

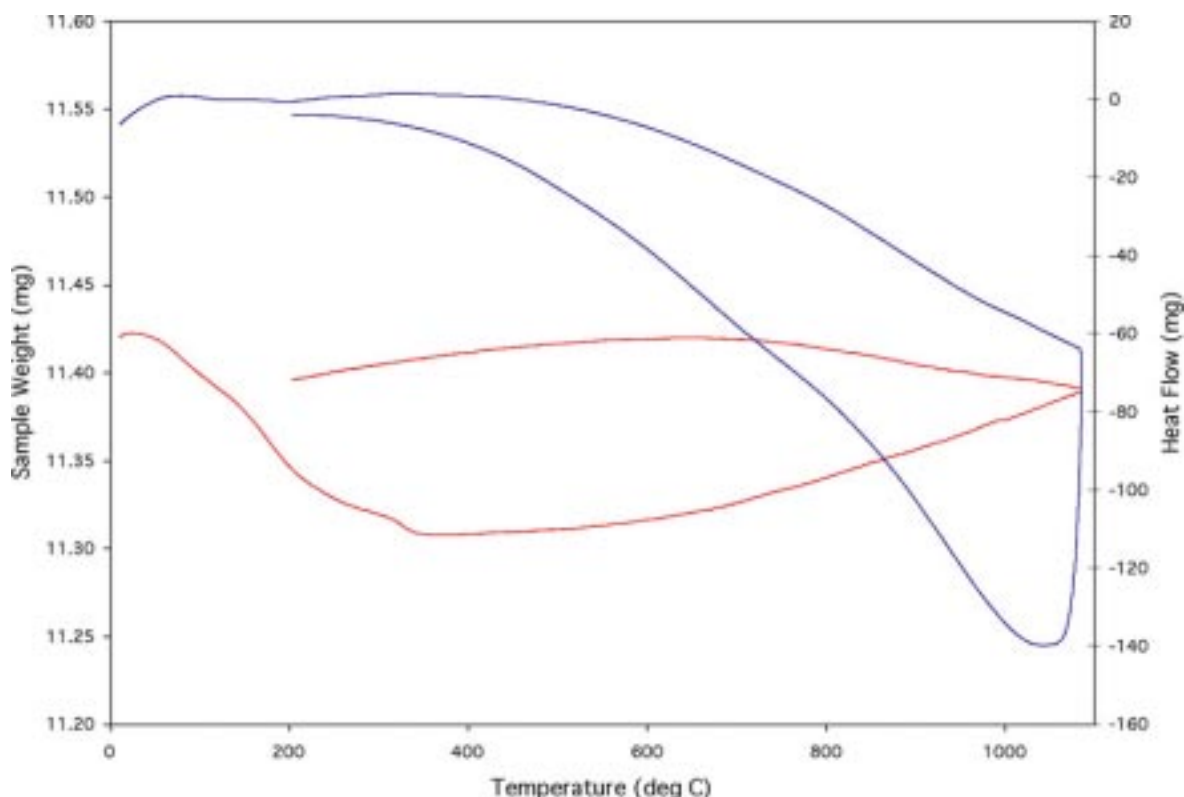


Fig. 8. Thermogravimetric analysis (red) and differential calorimetry (blue) of DyN. Both experiments were carried out under flowing argon. The TGA curve shows no significant changes in sample weight that would occur with decomposition. The DSC curve does not contain any peak that would indicate some type of structural-phase transition.

Dy/Zr/N Reactions

Dysprosium/zirconium nitride pellets were prepared via two different routes. One set of pellets were prepared using Dy metal and pre-made ZrN powder. Another set of pellets were prepared using Dy metal and Zr metal powder where the ZrN matrix was formed during the sintering process. The green compacts were sintered in a tube furnace in alumina boats lined with Zr metal foil. The sintering conditions were 1400°C for 24 hours.

In both sets of Dy/ZrN pellets the Dy metal forms DyN during the sintering process (Fig. 9). It appears that three phases are present in the pellet after sintering. Two of the phases are DyN and ZrN while the third phase is unidentified but initial examination suggests a DyN-ZrN solid solution. Further experiments including thermal analysis are required to further characterize this system.

A final significant result of these experiments concerns the atmospheric stability of DyN/ZrN pellets. These pellets are sensitive to both air and moisture. Pellets brought in contact with water completely convert to powder (mixed oxide-nitride) within two hours.

Pellets left exposed to air begin to show signs of decomposition within 12 hours and completely convert to powder within 24 hours. This behavior is significantly different than what is seen with pellets containing only ZrN.

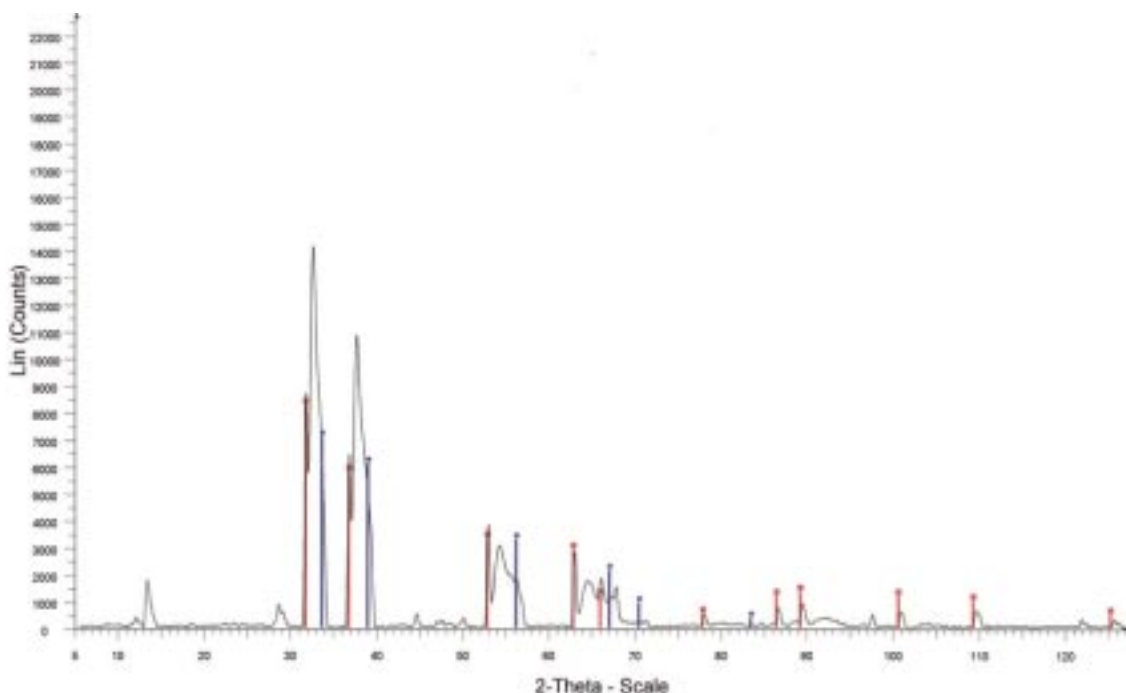


Fig. 9. Powder diffraction pattern of a pellet with the starting composition of 43 wt% Dy in Zr. The ZrN matrix was formed during the sintering process. The blue peaks are ZrN and the red peaks are DyN,

Actinide Nitride Studies

Success was achieved in synthesizing the first PuN powder. Figure 10 shows the results of carbothermic reduction, the conversion of oxide to nitride using graphite, nitrogen, and 6% hydrogen gas. The weight loss of 16.2% was very close to the predicted weight loss of 16.0%, and the color of the powder turned to gold, a classic nitride color. The x-ray diffraction data showed complete conversion to nitride, with no remaining oxide or carbon peaks. Parts per million levels of residual oxygen and carbon are expected in the final nitride.

The PuN powder was either kept unblended or it was blended with ZrN to produce the composition for the ATR tests. Figure 11 shows the 100% PuN pellets and the 64% PuN 36% ZrN pellets. The final sintered densities of these pellets were 65%–75%TD; this is, however, lower than the 80%–90%TD required for the ATW-1 test fuel.

Other studies were performed in the plutonium glovebox line to examine how powder-processing parameters could influence the densities. Three initial powder sizes of pure ZrN were examined: -325 mesh, -200+325 mesh, and a mixed powder of 75% -200+325 and 25% -325. Three pressing pressures were tried, 200 MPa, 300 MPa, and 400 MPa. The powders were milled in a Spex Mill for 0.5, 15, 30, 45, or 60 minutes. The results are given in Fig. 12. The relative densities against milling time for pellets sintered at 1750°C for 10 hours in Ar are plotted. The overall trend is that longer milling times produced higher sintered densities, with the highest density being 92%. Milling at 60 minutes, however, produced two samples that end-capped

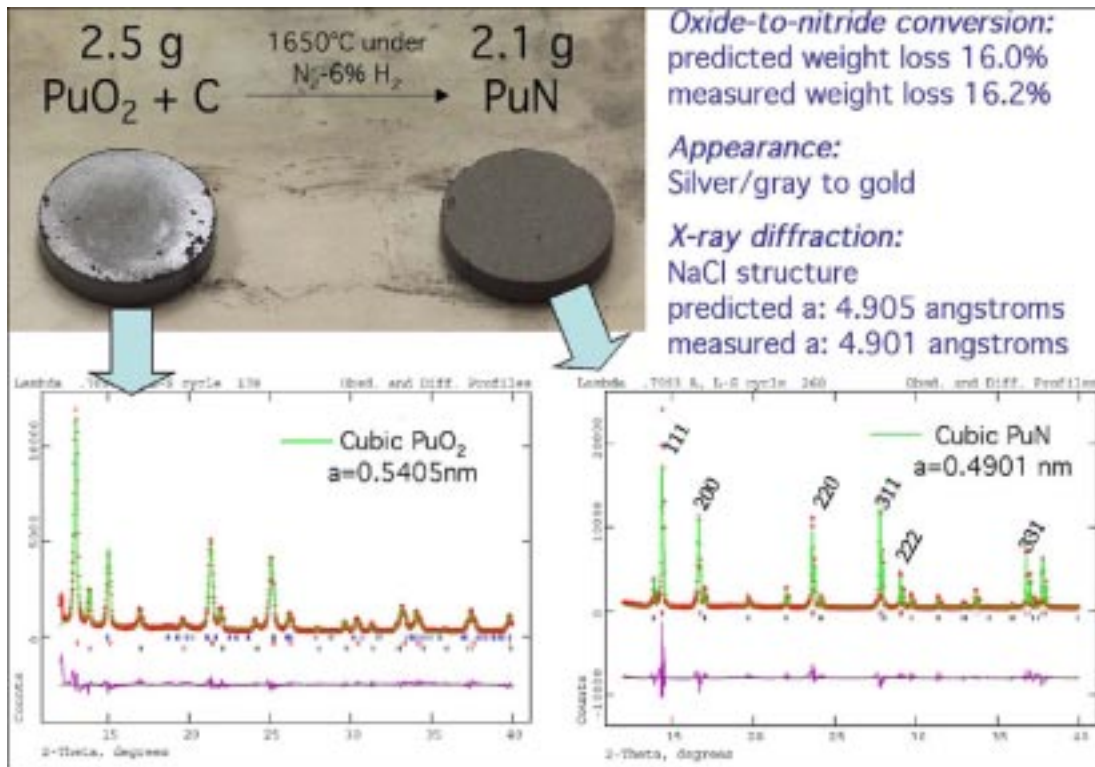


Fig. 10. Conversion of plutonium oxide to nitride.



Fig. 11. Sintered PuN and PuN/ZrN pellets.

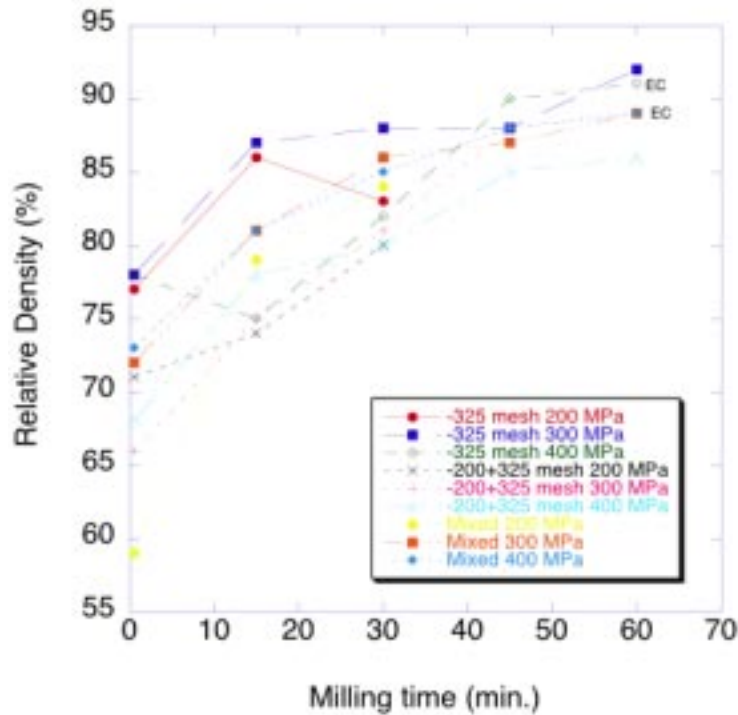


Fig. 12. Effect of processing parameters on sintered density of ZrN.

(“EC” in Fig. 12). The end-cap flaw is created during pressing as the pellets are extruded from the die, and are normally the result of pellet spring-back. It seems likely that milling for 45 minutes will be sufficient. Caution must be exercised in consideration of this data: (1) these samples had no actinide content, which will likely change the sinterability of ZrN, and (2) these were sintered at 1750°C, about 350°C–400°C higher than the estimated required sintering temperature of AmN-bearing pellets.

Dispersion Fuel Fabrication

Cermet fuels are a candidate fuel form for transmutation, and will be irradiated as part of the ATW-1 fuel irradiation test series. Fabrication of these specimens involves preparation of TRU particles, particle coating, and fuel specimen consolidation and cladding.

TRU fuel particles are being prepared at ORNL in a nominal 100-g batch scale by the resin-loading process. This process is used for the preparation of Am and Cm microspheres for fabrication isotope targets. This process uses a sulfonic acid ion-exchange resin as the matrix for adsorbing the cations of choice from acid solutions. The resins are loaded to breakthrough, washed with water, and dried. The resin is then transferred to a crucible for final sintering at 1050°C for 12–16 hr. The sintered microspheres are then characterized by sieving and tap-density measurement. Microspheres for Am/Cm isotope targets are ~20 µm diameter for mixing with aluminum powder for pellet fabrication. In the AAA Program, the desire is for kernels of 80 µm diameter and 150 µm diameter for kernel coating work.

A plan for preparing the resin-loaded kernels was developed and submitted for review and comment. The original direction was to prepare a minor actinide fraction of ~60% Pu and 40% Am. The quantity of Am needed for this kernel preparation was not available in the ORNL inventory and the recommendation was made to purchase the needed Am material from the Isotope Program (NE-70). The equipment for preparing the kernels is being assembled and prepared. The initial effort focused on dissolver equipment for preparing a feed solution for resin loading. Most of the candidate materials are available as oxide products that are sometimes difficult to dissolve in acid solution, especially if the material has been high-fired when originally prepared. To accomplish this dissolution in a timely manner, an electrolytic dissolver has been fabricated to utilize the cerium (Ce(IV)) promoted dissolution of the Pu oxides. The equipment components can be seen in Fig. 13, which shows the platinum anode, the cathode compartment with a fritted glass bridge, and the dissolution vessel that will contain the components and oxide/acid mixture. A glove box has been prepared for use with the electrolytic dissolution equipment when initial testing with surrogate materials is completed.

The resins for use in the preparation of the kernels were ordered and received from the vendor, and the equipment for hydraulic classification of the resin fractions has been prepared. The resin fractions will be classified according to initial particle diameter, and a size will be selected to yield the desired particle size of the final product fraction.



Fig. 13. Photograph of electrolytic dissolution equipment.

After the review of the proposed experimental plan, a desire to change the isotope distribution of the Pu fraction in the kernels was expressed so that the kernel would have a significant fissionable material fraction during the irradiation testing. To accomplish this increase in the fissionable material fraction, the distribution of the Pu fraction will be changed to give a ^{239}Pu fraction around 90% with the ratio of Pu/Am remaining the same. A review of available candidate materials for this change is in progress.

Zr metal is the baseline matrix metal selected for the ATW-1 test fuel, although alternative matrices will be considered as the project progresses. The use of a Zr matrix with nitride or oxide fuel particles requires measures to prevent reaction of the particles with the matrix during irradiation. The initial focus of this work is to develop coating methods to place a Nb barrier layer onto oxide microspheres that simulate the mixed TRU oxide microspheres described above. The fuel particles will be approximately 50% to 70% dense. Natural uranium oxide microspheres (UO_2), ~500 μm in diameter were received at ANL from ORNL to serve as surrogates for coating method development. These particles were manufactured via internal gelation processing in the late 1970s or early 1980s and may not be representative of the final microsphere morphology as the smaller TRU particles.

Imaging of the natural urania (UO_2) particles using SEM determined that they exhibit variations in surface morphology. All are polycrystalline but exhibit varying levels of consolidation, apparent binder (precursor) content and cracking. Most of the microspheres exhibited a continuous surface with some outgassing porosity. Other microspheres exhibited cracking with evidence of transgranular spalling. The cracks seem to have occurred prior to sintering as examination of the crack surface revealed they were healed over, apparently by heat treatment. These results indicate that the submitted spheres had been sintered which precludes our repeating the heat treatment operation. Figure 14 shows a micrograph representative of the various surface finishes observed on the natural urania particles.

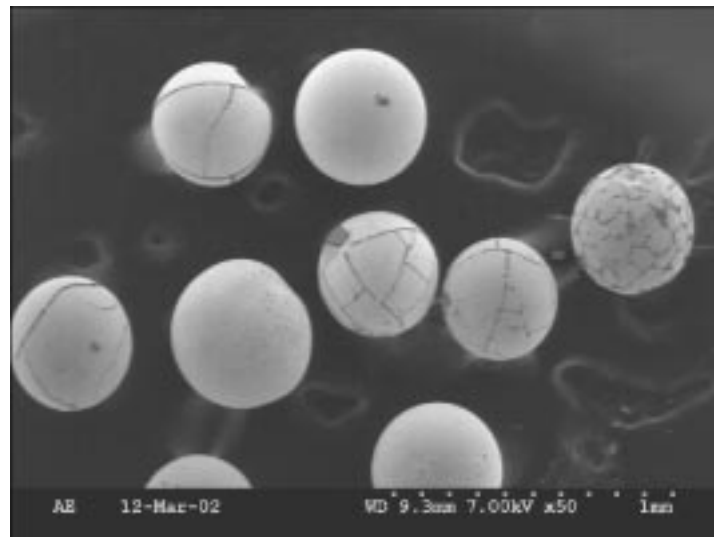


Fig. 14. Representative sample of natural urania microspheres.

TRISO Fuel Fabrication

Efforts in the TRISO fuels area were divided between laboratory work on synthesis of surrogate HfO_2 microparticles and preparation of laboratories for U- and TRU-coated-particle fuel fabrication. The uranium labs are necessary to re-establish the basic coated-particle fabrication capability, and to make preliminary test specimens to prove fabrication methods produce the necessary fuel quality. The labs for handling TRU are necessary for the fabrication of the irradiation test samples of the “deep-burn” fuel materials—the contact-handled driver fuel (containing Pu/Np), and the remote-handled transmutation fuel (containing Pu/Am/Cm).

Rapid progress was made in establishing an internal gelation method for making HfO_2 microparticles for use as coated-particle kernel surrogates. A sample of this material after room-temperature drying is shown in Fig. 15. Optimum gel-sphere processing conditions were identified, and 250 g of hafnia spheres (~200-micron sintered diameter) were made in five separate experiments. TGA/DTA analyses were conducted to define the proper treatments to remove volatile constituents and densify these hydrous gel-spheres. Using an optimized heat treatment schedule, this material has been calcined to 1050°C with little cracking. These spheres will be used in the initial coating work because of their close match to the density of actinide oxides, and will be very useful for testing of thermal stress models for coating integrity and other analysis that can be done more easily in a nonradioactive environment. Existing coating-furnaces have been modified for making TRISO-coated hafnia. The instruments have been calibrated and tested and laboratory safety documentation completed.

Preparation of labs for fabrication of U- and TRU-containing materials proceeded on many fronts. Documentation for NEPA review of the entire scope of AAA TRISO-fuel activities was submitted to the local DOE site office and guidance has been issued. Laboratory safety documentation was completed for work with existing equipment to make U dioxide kernels by the internal gelation chemistry. Enclosures were ordered to contain the coating equipment that will process the U kernels, and the basic coating laboratory design and layout was completed.

Activities to support work with TRU-containing materials benefited from the synergism of the dispersion fuels activity and the Pu/Np kernels (driver fuel) fabrication activity. Both activities use the same head-end treatments for contact-handled actinides (dissolution, ion-exchange, solution adjustment) and require roughly the same scale of operation. Flowsheets for both of these activities were developed and nominal batch sizes were established based upon existing facility limits and practical considerations. Glovebox resources have been identified to support these head-end treatment activities. A simple lab-scale electrolytic dissolver has been fabricated for glovebox dissolution of high-fired actinide oxides. Resins for use in preparation of the dispersion fuel kernels were ordered and received, and equipment for the hydraulic classification of the resin fractions has been prepared for operation.

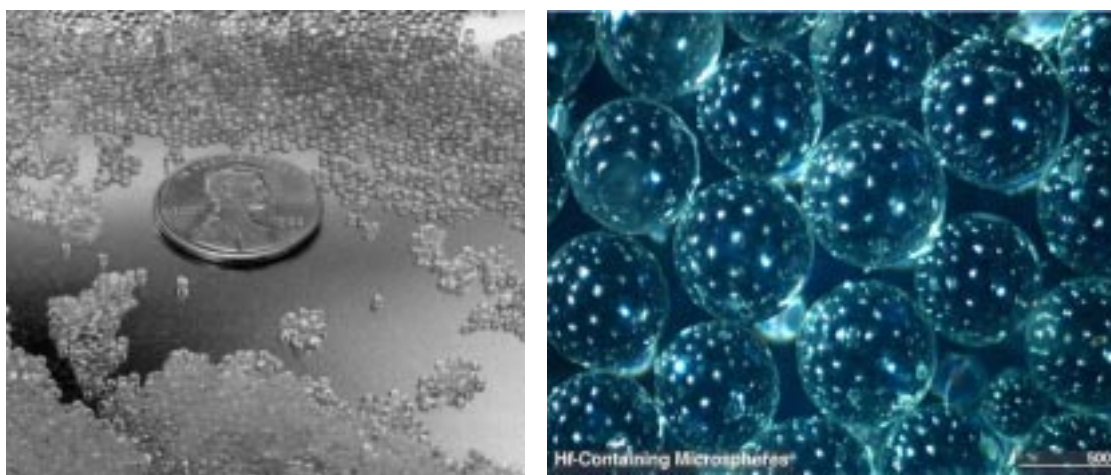


Fig. 15. Air-dried hydrous hafnium oxide microspheres made by internal gelation at ORNL.

TRISO Fuel Design

To guide the designs of the fuel and the reactor core and the development of fabrication processes, initial designs of the driver fuel (DF) and transmutation fuel (TF) were recommended. The DF design uses a 300- μm -diameter substoichiometric oxide kernel with a thick-buffer conventional TRISO coating, and the TF design uses a 200- μm -diameter kernel with a conventional TRISO coating.

Preliminary limits on the in-core environment of the fuel were also defined. The limits on the in-core environment proposed for the DF and TF were taken from the temperature, burnup, and fast neutron fluence limits achieved with highly enriched U and Pu fuels.

Fuels Irradiation Testing

ATW-1 Irradiation Test

During this quarter, the final design of the ATW-1A, -1B, -1C, and -1D irradiation tests neared completion. These four irradiation tests include two nitride-fueled and two-metallic fueled-irradiation test vehicles, each loaded with six miniature fuel rods. Simplified design drawings for the capsule and rodlet are shown in Figs. 16–17.

The overall capsule length was shortened to 52 inches. This was done at INEEL's request to allow for the possibility of shipping the entire capsule (as is) directly from the ATR canal to an off-site hot cell facility using the GE-2000 cask. Plans currently call for the experimental capsules to be disassembled at the TRA (Test Reactor Area) hot cell, with only the individual rodlets being shipped using the GE-100 cask. While this is still the preferred option, there is some uncertainty regarding the operation and availability of the TRA hot cell during the time projected for experiment disassembly and shipping. Calculations conservatively predicting the maximum pressure inside the capsule were revised for the shortened design, resulting in a maximum pressure of 230 psi in ATW-1C, assuming all 6 rodlets failed at 25% burnup.

The last iteration on the neutronics calculations was completed, and the design specifications for the borated-aluminum basket that will hold each experiment in the Advanced Test Reactor (ATR), as well as serve as a thermal neutron filter, were established. The baskets will limit the maximum linear heat generation rate (LHGR) produced in the peak rodlet of each experiment to ≤ 300 W/cm; this maximum occurs at the end of the basket's operational lifetime due to depletion of B-10 by neutron absorption. The basket operational lifetime was set at 110 days of full power irradiation; the basket wall thickness is 0.070 inches and will be fabricated from Al-6092 aluminum alloy with 29 wt% natural boron carbide added. The 110-day lifetime of the basket will suffice to complete the irradiations of the two low-burnup experiments, ATW-1A and -1B. The baskets will be replaced every 110 days for the high-burnup ATW-1C and -1D experiments.

Table 2 gives the fuel test matrix for the ATW-1A, -1B, -1C, and -1D experiments, showing the irradiation test predictions based on the final basket design. Depletion of initial ^{239}Pu is being used as the experiment discharge criterion. ^{239}Pu burnup will be $\geq 5\%$ for ATW-1A and -1B and $\geq 20\%$ for ATW-1C and -1D. As seen in the Table 3, discharge of ATW-1A and -1B should occur after 110 days of irradiation. Final projections for discharge of ATW-1C and -1D are not yet complete, although preliminary estimates indicate that approximately 280 full-power days of irradiation will

be required to reach their target discharge burnups of $\geq 20\%$ ^{239}Pu . Also shown in Table 3 is the predicted burnup for all heavy metals, which is low due to the predominantly thermal neutron flux provided by the ATR test environment. Finally, ^{241}Am transmutation in excess of 10% is predicted at the low-burnup discharge level.

Table 2. ATW-1A, -1B, -1C, and -1D Test Matrix

Rod	EXPERIMENT	
	ATW-1A and -1C	ATW-1B and -1D
1	(Pu _{0.2} ,Am _{0.8})N-36ZrN	Pu-12Am-40Zr
2	(Pu _{0.8} ,Am _{0.2})N-36ZrN	Pu-10Am-10Np-40Zr
3	(Pu _{0.5} ,Np _{0.5})N-36ZrN	Pu-40Zr
4	PuN-36ZrN	Pu-12Am-40Zr
5	(Pu _{0.50} ,Am _{0.25} ,Np _{0.25})N-36ZrN	Pu-10Np-40Zr
6	(Pu _{0.5} ,Am _{0.5})N-36ZrN	Pu-60Zr

Table 3. Irradiation Test Predictions for ATR Tests ATW-1A, -1B, -1C, and -1D

Test	Rod	LHGR (W/cm)			^{239}Pu Depletion		Heavy Metal Burnup		^{241}Am Depletion	
		0 Days	60 Days	110 Days	60 Days	110 Days	60 Days	110 Days	60 Days	110 Days
ATW (1A) Nitride	1	42.9	45.9	48.2	0.029	0.055	0.008	0.015	0.031	0.059
	2	162.9	179.3	211.8	0.034	0.065	0.018	0.034	0.051	0.097
	3	126.7	147.9	168.1	0.042	0.081	0.014	0.026	—	—
	4	202.6	232.8	275.6	0.034	0.066	0.021	0.040	—	—
	5	119.5	133.8	156.4	0.037	0.072	0.014	0.026	0.046	0.088
	6	114.1	129.3	148.7	0.037	0.071	0.013	0.025	0.041	0.078
ATW (1B) Metal	1	127.7	140.1	154.6	0.027	0.052	0.014	0.026	0.040	0.075
	2	141.9	163.3	185.3	0.035	0.069	0.015	0.028	0.053	0.100
	3	202.7	234.7	264.4	0.036	0.069	0.020	0.039	—	—
	4	197.6	226.4	264.0	0.043	0.084	0.021	0.041	0.059	0.112
	5	191.0	215.7	249.2	0.035	0.069	0.017	0.033	—	—
	6	129.3	151.6	175.5	0.042	0.081	0.022	0.044	—	—
ATW (1C) Nitride	1	46.1	49.4	53.3	0.032	0.060	0.009	0.016	0.034	0.063
	2	166.8	185.7	218.6	0.034	0.067	0.018	0.035	0.049	0.092
	3	145.6	166.8	198.6	0.047	0.091	0.015	0.030	—	—
	4	221.2	260.5	297.3	0.038	0.074	0.023	0.045	—	—
	5	123.1	145.6	166.1	0.039	0.078	0.014	0.028	0.049	0.096
	6	105.5	121.2	137.3	0.033	0.065	0.014	0.026	0.040	0.075
ATW (1D) Metal	1	133.7	149.0	163.3	0.029	0.056	0.014	0.027	0.044	0.082
	2	154.9	173.5	194.0	0.039	0.076	0.016	0.031	0.049	0.093
	3	210.6	253.9	294.1	0.038	0.074	0.021	0.041	—	—
	4	175.7	201.5	234.3	0.039	0.075	0.019	0.037	0.064	0.121
	5	193.3	216.0	259.4	0.037	0.070	0.017	0.033	—	—
	6	144.2	161.1	179.3	0.046	0.088	0.024	0.047	—	—

Thermal analyses for the experiments are being performed using the commercial software package ABAQUS. Figure 18 shows the results of the analysis for the bottom endplug of a rodlet operating at the peak linear power of 300 W/cm. A peak temperature of 483°C is predicted, which is acceptable. Similar analysis shows that the peak cladding temperature will be approximately 450°C. Stress analyses of these experiments were also initiated, but are not yet complete. Nevertheless, initial results indicate that component stresses, especially weld joints, are all at acceptable levels.

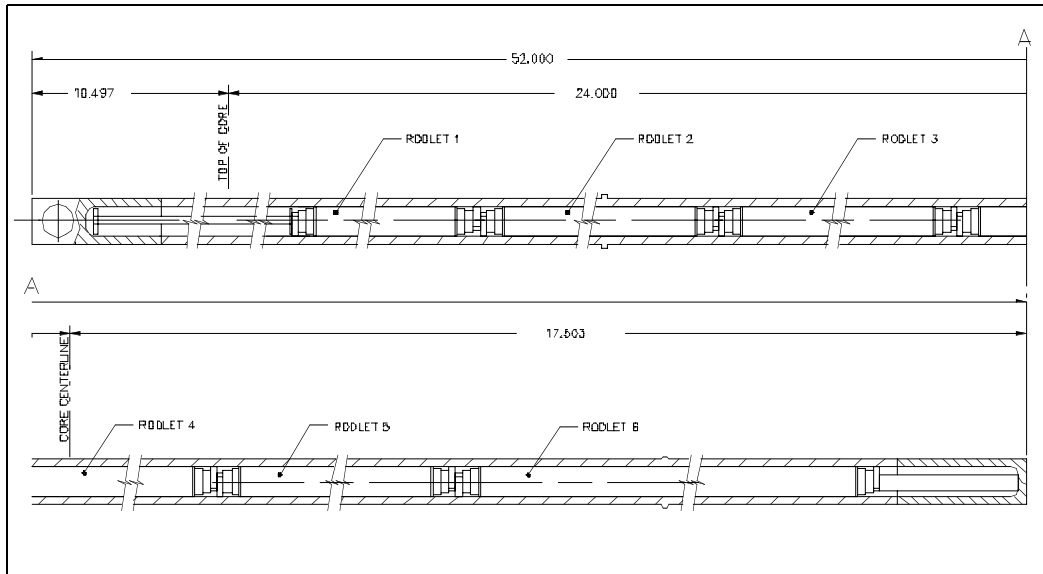


Fig. 16. ATW-1 stainless steel containment capsule design.

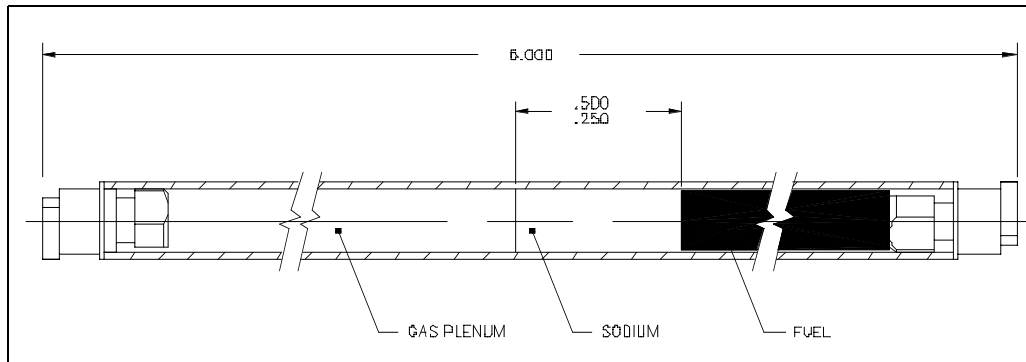


Fig. 17. ATW-1 rodlet design.

Calculations of the heat generation rate as a function of fast fluence for a hypothetical $\text{MgAl}_2\text{O}_4+\text{AmO}_x$ specimen in the ATR were made for comparison to calculations performed for the EFTTRA-T4 test. The T4 test was irradiated in the HFR (High-Flux Reactor) at Petten, and heat generation rates are published. ^{241}Am neutron captures to ^{242}Cm , which α -decays to ^{238}Pu . ^{238}Pu in turn captures a neutron and transmutes to ^{239}Pu ; the buildup of ^{239}Pu causes an increase in fission power with in-core residence time. The MCWO methodology, a validated depletion tool that applies the Monte Carlo code MCNP coupled with the isotope depletion code ORIGEN-2, was used to calculate heat generation rates for T4 specimens in the ATR. The MCWO-calculated

total heat rate vs. fast neutron fluence calculated for the ATR is compared to the $\text{MgAl}_2\text{O}_4 + \text{AmO}_x$ heat rate in HFR in Fig. 19. The MCWO-calculated results show the same trend of total heat rate increase vs. irradiation time as the T4 experiment, showing that calculations performed using the MCWO method provide a credible calculation of total power during actinide irradiation in an ATR experiment.

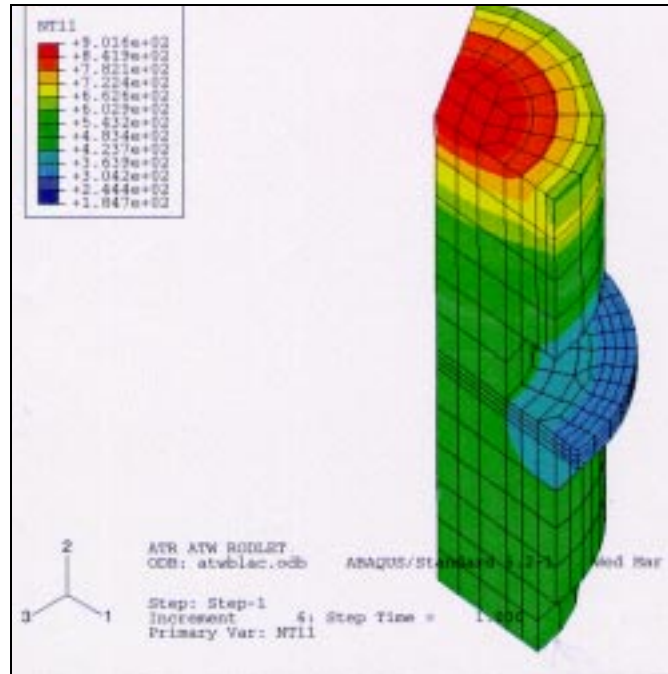


Fig. 18. Thermal analysis of ATW-1 rodlet bottom end plug.

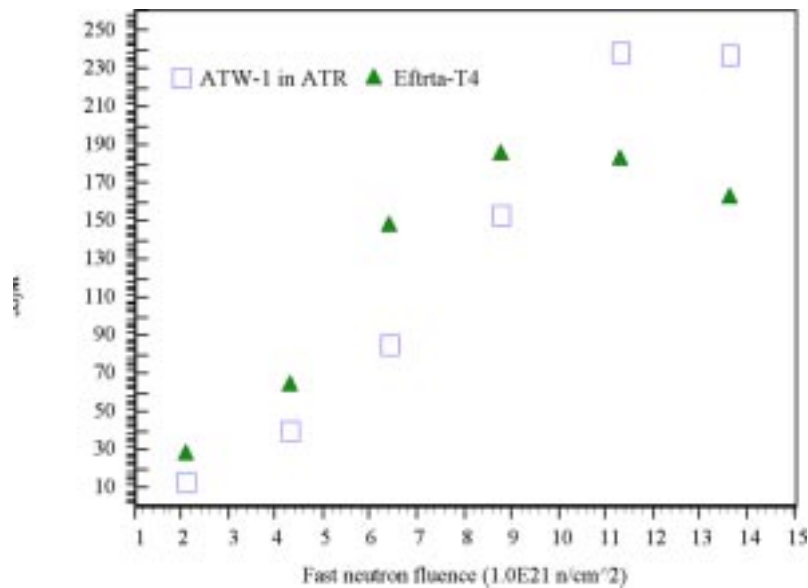


Fig. 19. Comparison of $\text{MgAl}_2\text{O}_4 + \text{AmO}_x$'s heat rate in ATR and HFR at Petten vs. fast neutron fluence ($E > 0.1 \text{ MeV} \times 10^{21} \text{ n/cm}^2$).

ATW-3 Irradiation Test

Geometry, fabrication arrangements, and schedule for the ATW-3 fuels test in the Phénix reactor were addressed by CEA, ITU (Institute for Transuranium Research, Karlsruhe), DOE, and ANL/LANL personnel during a visit to the CEA installations at Cadarache and Marcoule in January. Meetings at the CEA Cadarache Research Center focused on planning for a joint DOE/CEA/ITU fast-spectrum transmuter-fuel irradiation test in the Phénix reactor. Major points of the collaborative effort are as follows:

- The experiment will be limited to 8 pins of experimental transmuter fuel due to the licensing burden of irradiating more fuel. Two pins will be supplied by CEA, two by ITU, and four by the US program.
- The pin geometry is essentially that of a standard full length Phénix pin (1.8 m length). The experimental subassembly design consists of a central tube containing up to 19 experimental pins, surrounded by standard driver fuel. The cladding tubes will be of standard Phénix diameter and alloy. Flow through the central experiment tube can be controlled through orifices.
- Fuel column length will be 10 cm, governed primarily by difficulties in procuring and handling larger quantities of Am. This amount has been deemed sufficient for all post-irradiation examination and separation studies.
- The two CEA fuel pins will be microdispersions of (Pu,Am)O₂ in MgO. One pin will be fabricated using a powder metallurgy route at Cadarache, the other using an aqueous process (sol gel) at the ATALANTE facility at Marcoule.
- ITU will fabricate one fuel pin containing (U,Pu,Am)O_{2-x} pellets (similar to the previously irradiated SUPERFACT experiment), and the other a dispersion of (Zr,Pu,Am)O_{2-x} in a metal matrix (CERMET). CEA and the US program will have input on the CERMET matrix composition and microstructure.
- The US program will provide two (Pu, Am, Np, Zr)N and two Pu-Am-Np-Zr metallic fuel slugs. These will be Na-bonded.
- Due to the Na bonding requirement for US fuels coupled with the desire to have all pins welded at one location to avoid duplication of weld QA requirements, all fuel pins for this experiment will be encapsulated and welded at ITU.
- Gas reactor fuel specimens may also be irradiated in the same test subassembly.
- Common costs for the experiment should be shared on the basis of the number of pins being tested. All post-irradiation examination data should be shared among all participants in this test, and all participants should be equal partners.
- Based on scheduling requirements for fuel fabrication and licensing and the Phénix operating schedule, the most likely scenario for irradiation will be December 2005, allowing irradiation for two 120-day cycles (240 EFPDs) in 2006–2007 prior to Phénix shutdown in mid-2007.
- It was learned that a statutory shutdown related to maintenance will occur in 2008, and it is unknown if Phénix will be restarted after this shutdown, regardless of the actual number of full-power days accumulated.

Fuel Performance

Assessment of Radiation Tolerance

Various techniques are being used to evaluate radiation damage under heavy ions and fission product implantation in ZrN. Using both cross-section and plan view transmission electron microscopy (TEM) samples, irradiation damage from Xe and He ion implantation (300 KeV and 50 KeV respectively, both at 5×10^{16} fluence) are being characterized.

Radiation Damage

Plan-view samples reveal extensive microtwinning in the Xe-irradiated ZrN, along with very small (~ 5 nm) voids or bubbles at grain boundaries. Cross-sectional TEM samples should elucidate how these microstructural features depend on deposited nuclear-energy density as well as their relation to the implanted Xe ion profile. Unfortunately, the current quality of cross-sectional TEM samples is not yet sufficient to make clear interpretations of these issues. Work continues to improve the quality of the cross-sectional TEM specimens.

Helium Release Effects

A study on He release effects in MgAl_2O_4 , in collaboration with scientists at the Institute for Transuranium Elements (ITU) in Karlsruhe, Germany, has been completed [25]. Discussions have begun between LANL and ITU about the initiation of similar experiments on ZrN samples. Los Alamos will implant He into ZrN and deliver these to ITU for similar He release investigations.

Modeling and Fuel Properties

Continuum Scale Modeling of Nuclear Fuels

Thermodynamic data for nitrides were collected from the literature, available commercial databases, and other sources. The modeling process consists of analyzing the data using an uncertainty evaluation procedure based on Bayesian statistics. Calculations of phase diagrams are being conducted for specific oxide and nitride systems to provide information about the stability of phases in the various thermodynamic systems of relevance for the fuels development effort.

The Ce-O system is being used to tune up the phase-stability modeling process. Important progress on the assessment of the Ce-O phase diagram was made, specifically, the high-temperature area (1600 K–3200 K) of the phase diagram was modeled (Fig. 20). The immiscibility of the liquid is a result of the models for the Gibbs Free Energy and must be confirmed experimentally. However, experimental confirmation of the calculated liquidus line is difficult since the temperatures involved are up to 3100 K.

Assessment of the Pu-O phase diagram continued by modeling the partial pressure of oxygen in substoichiometric plutonia (Fig. 21). PuO_{2-x} was modeled as a solution of PuO_2 and Pu_2O_3 and compared with previous models [26,27]. A more sophisticated atomistic model that accounts for the mobility of oxygen atoms is under development.

Work on the Pu-N phase diagram concentrated on modeling the thermodynamic properties of the liquid. The partial pressure of nitrogen was examined and nonequilibrium calculations revealed the nonstoichiometry of the compound.

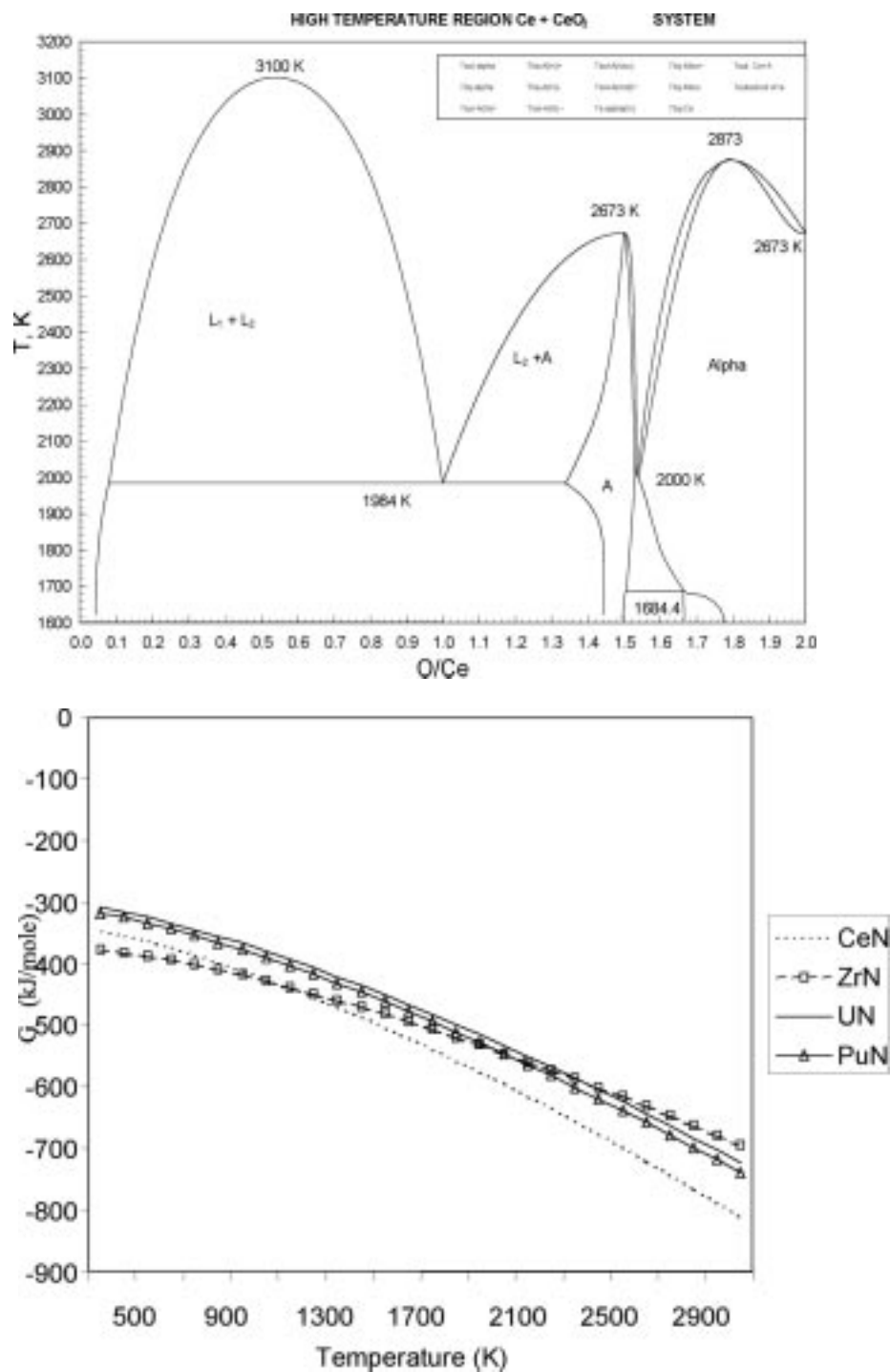


Fig. 20. Calculated high-temperature-phase equilibrium in the Ce-O system.

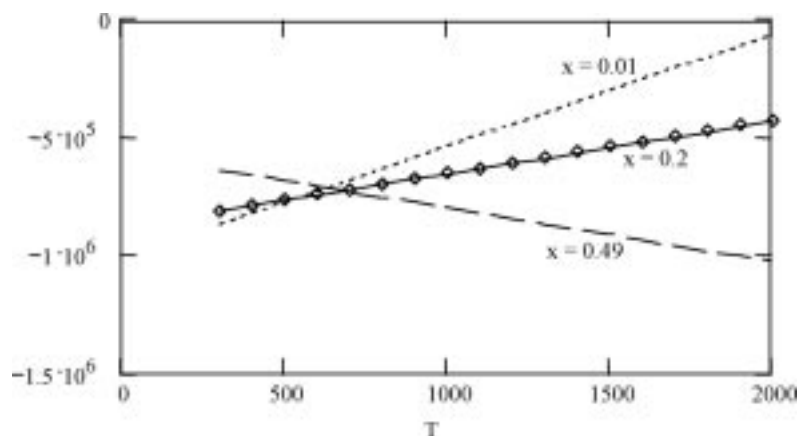


Fig. 21. Model for the partial pressure of oxygen in PuO_{2-x} . For comparison, the diamonds represent values calculated using Besmann's model for $\text{PuO}_{1.8}$ [26,27].

Atomic Scale Modeling of Nuclear Fuels

Electronic structure calculations for ZrN are being conducted in collaboration with LANL's T Division. The plan is to eventually calculate the free-energy of formation for compounds such as NpN, AmN, CmN, etc., for which it is difficult, if not impossible, to get accurate, equilibrium experimental data. Calculated free energies will be used in modeling the phase stability of TRU-nitrides. Initial work is focused on ZrN matrix material.

The elastic properties of ZrN have been investigated by means of electronic structure calculations at 0 K. The approach is based on density functional theory. The total energy density functional minimization was used, within a Kohn-Sham scheme, implemented in a full potential liberalized muffin-tin orbital basis. The equilibrium volume ($V=164.4$ a.u., Fig. 22), bulk modulus ($B=254$ GPa), and the C_{11} - C_{12} elastic constant (C_{11} - $C_{12}=388$ GPa), were calculated. The volume is correct within 1.1% of the experimental volume. No experimental data was found for the elastic constants. Upon calculating the C_{44} elastic constant, a possible anomaly was found, indicating a small ground state distortion of the crystal structure. Further investigations will be performed.

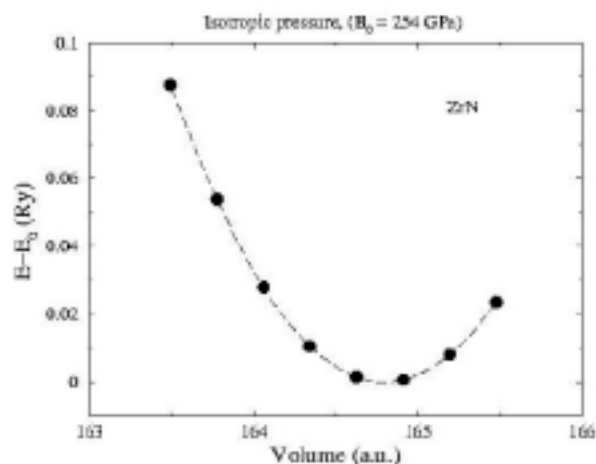


Fig. 22. Electronic structure calculation of the energy as a function of volume for ZrN.

TRISO

Design calculations for the DF and TF coatings have begun using the GA PISA coated-particle structural-analysis code. Material property information is being prepared for input to the code.

A proposal for coated particle design work has been received from MIT. The proposal covers use of their coated particle performance model for DF and TF coating design, and upgrade of the model to model the unique chemistry of the DF and TF kernels.

Metal Fuels

Data on the heat capacity, enthalpy content, phase transition enthalpies, and heat capacity for elemental Zr, Pu, Am, Np, and Cm (and alloys of these elements) were critically reviewed and data was selected for inclusion in the first edition of AAA fuels handbook. Thermal conductivity of elements and alloys relevant to ATW-1 metal fuels were also reviewed. Where data were not available, correlations were developed. Data and correlation for heat capacity of elements and alloys are given below.

Thermal Conductivity of Actinide Elements

Data for the thermal conductivity of actinide elements is scarce. For example, known thermal conductivity data for Np consists of only two data points, both at room temperature; there is no known data for Am and Cm. To estimate values for these elements, indirect derivations and comparisons with other actinides were made, thus this data is also presented here.

Uranium

Touloukian *et al.* [1] summarized the thermal conductivity data for U metal available before 1970. The only data added after this is by Takahashi *et al.* [2] A simple correlation for thermal conductivity of U metal is generated as a polynomial using the least squares fitting of the data.

$$k_U(T) = 21.73 + 1.591 \times 10^{-2} T + 5.907 \times 10^{-6} T^2, \quad (1)$$

where k is in W/m-K and T temperature in K. Equation 1 is valid in the temperature range of $255.4 \leq T \leq 1173.2$ K.

Zirconium

The thermal conductivity data of Zr up to 1970 were reviewed by Touloukian [1] and the recommended values tabulated. Fink [3] produced a correlation, including available data after 1970, as

$$k_{Zr}(T) = 8.853 + 7.082 \times 10^{-3} T + 2.533 \times 10^{-6} T^2 + 2.992 \times 10^{-3} T^{-1}. \quad (2)$$

Equation 2 is valid in the ranges of $298 \leq T \leq 2000$ K.

Plutonium

Data for the thermal conductivity of the unalloyed metal are found only for α -Pu. Thermal conductivity for higher-temperature phases such as δ - and ϵ -Pu can be estimated using the Wiedemann-Franz-Lorentz law, $k = LT / \rho$, where ρ is the

electrical resistivity and L is the Lorentz number. The electrical resistivity of Pu is obtained from Ref. 4. The estimated thermal conductivity of Pu is as follows:

$$k_{\delta-Pu}(T) = 3.225 + 0.0296T \quad (593 \leq T \leq 736 \text{ K}), \quad (3a)$$

$$k_{\epsilon-Pu}(T) = 9.507 + 0.0184T \quad (756 \leq T \leq 913 \text{ K}). \quad (3b)$$

Thermal conductivity data for δ -stabilized Pu with 1 wt% Al were obtained from Ref. 1. A polynomial correlation of the thermal conductivity data is obtained as

$$k_{Pu-1Al} = 1.213 + 2.018 \times 10^{-2} T + 2.857 \times 10^{-6} T^2 \quad (4)$$

for temperatures between 373 K and 873 K. As shown in Fig. 23, pure Pu has generally higher thermal conductivity than Pu-1Al. This is attributed to the aluminum alloying effect, although Al has an extremely high thermal conductivity relative to Pu.

Because of its low density, however, 1 wt% Al in Pu+Al occupies about 7% of the alloy volume. This large volume fraction limits the applicability of Pu-1Al data for pure Pu element. The temperature dependence, however, is useful to approximate data for other actinides whose measured data are scarce in the literature.

The thermal conductivity data for the remaining TRU elements are scarce, so further estimations must be made at this time to allow calculation of in-reactor operating conditions.

Neptunium

Thermal conductivity data for Np at room temperature are found in several references [1,5,6]. They are consistent among themselves, and the value 6.3 W/m-K at 300 K is taken.

The electrical resistivity given by Lee [7] was compared at 300 K to the consistent data in the literature [1,5,6]. As a result, a Lorenz number of $1.63 \times 10^{-8} \text{ Volts}^2 / \text{K}^2$ is found, which is also the recommended value by Touloukian [1]. Based on the electrical resistivity data by Lee [7], the thermal conductivity correlation of Np is obtained by the Wiedemann-Franz-Lorentz law:

$$k_{Np} = 4.562 + 3.674 \times 10^{-3} T + 6.845 \times 10^{-6} T^2 \quad (5)$$

Np has a melting temperature at 912 K, which limits the validity of Eq. 5 to below this temperature.

Americium

Touloukian's recommendation for the thermal conductivity of Am is 10 W/m-K at room temperature [1]. Tamura [8] predicted the thermal conductivity of Am to be 22.8 W/m-K at room temperature by using an empirical correlation between electrical conductivity and thermal conductivity. Another estimate can be made through direct application of the Wiedemann-Franz-Lorentz law. The typical Lorentz number for metal is given at room temperature as $2.44 \times 10^{-8} \text{ Volts}^2 / \text{K}^2$. Adopting this value and $\sigma = 0.0015 \text{ GS/m}$ [8] puts k at about 11 W/m-K, which is very close to the value suggested by Touloukian [1] and Muller [6]. In this work, therefore, the conservative value of 10 W/m-K is selected.

The change in the conductivity as a function of temperature is assumed to be similar to that of Pu-1Al, i.e., the expression takes the form, $k_{Am} = k_{Pu-1Al} - (k_{Pu-1Al}^0 - k_{Am}^0)$ where k_{Pu-1Al}^0 and k_{Am}^0 are the thermal conductivity values of Pu-1Al and Am at room temperature. Therefore, the thermal conductivity of Am is estimated to be

$$k_{Am} = 4.118 + 0.018T + 5.35 \times 10^{-6} T^2. \quad (6)$$

Curium

The thermal conductivity of Cm is also supposed to be 10 W/m-K at room temperature [1]. Therefore, applying the method used for Am, the thermal conductivity of Cm is estimated to be

$$k_{Cm} = 4.118 + 0.018T + 5.35 \times 10^{-6} T^2. \quad (7)$$

Figure 23 shows the thermal estimated thermal conductivities of the minor actinides, Pu, Pu-1Al alloy, U, and Zr as a function of temperature provided in Eqs. 1–7. Notice the similarity of the shape of the thermal conductivity curves for U and Pu-1Al.

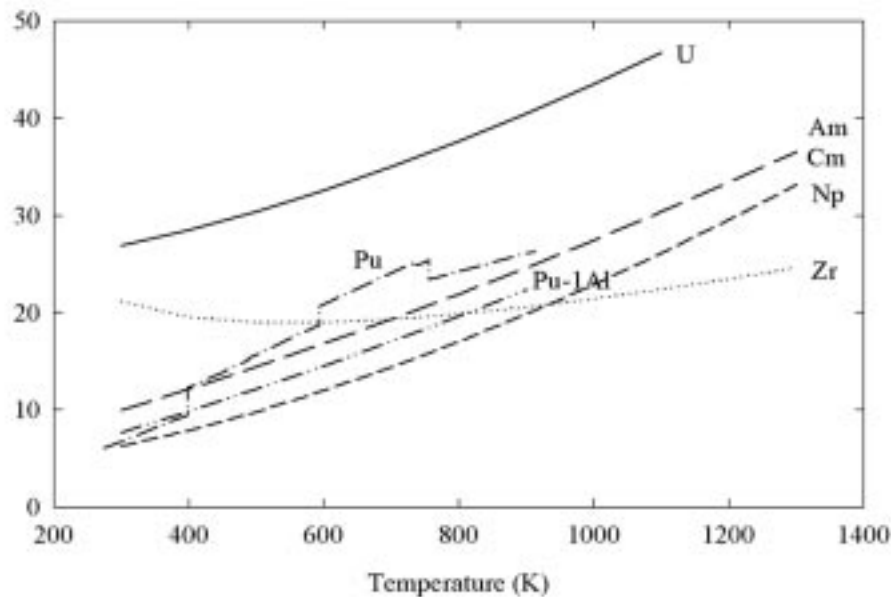


Fig 23. Thermal conductivity of TRU elements. U and Zr are included for comparison.

Thermal Conductivity of Multi-Phase Alloys

Bruggeman [11] developed a method of averaging to obtain the thermal conductivity of a heterogeneous phase mixture. Landauer [12] obtained the same result for a binary metallic mixture that had a random distribution of different phases. The Bruggeman model has been proven to be the reliable method to the purpose by many authors [13–16]. The formula for the thermal conductivity of a two-phase mixture was given as follows:

$$k = \frac{1}{4} \left[A + \left(A^2 + 8k_1k_2 \right)^{\frac{1}{2}} \right], \quad (8)$$

where $A = (3v_1 - 1)k_1 + (3v_2 - 1)k_2$. Here, k is thermal conductivity, and v is the volume fraction. For a two-phase mixture, k_1 and k_2 must be the conductivities of each phase at the phase boundaries contacting the two phases, which means they also have some impurity effects in them.

The Bruggeman scheme has been proven to be the most accurate when applied to composites of heterogeneous phases. For the solid solution cases, however, it significantly overpredicts because it does not fully appreciate the impurity effects. Therefore, the Bruggeman equation applying to a solid-solution phase is considered to provide the upper limit values of the thermal conductivity.

Ternary Solid Solution Model

Consider a ternary solid solution that is composed of A, B and C with $a_C < a_B \ll a_A$, where a is atom fraction. For instance, consider an ATW fuel, which is composed of 85 atm% Zr + 10 atm% Pu + 5 a% Am. Since A is the major component playing the dominant role, addition of C in A-B alloy, maintaining the same total impurity content, is replacing B impurity atoms with C impurity atoms in the crystalline lattice of A. If the perturbation in A crystalline lattice caused by C atoms is slightly greater than that of B atoms, the thermal conductivity of A-B-C will decrease from that of A-B. If C atoms completely replace B atoms, then the thermal conductivity becomes that of A-C. From this, it is expected that the thermal conductivity of the ternary alloy will decrease monotonically, $k_{A-C} \leq k_{A-B-C} \leq k_{A-B}$; there is no minimum between two bounding values, which does not hold for the binary solid solution cases. In this context, if the third element has similar size and valence to the major component, it does not further penalize the alloy thermal conductivity.

The thermal conductivity of ternary A-B-C alloy modeled in this manner [17–19] has the following relationship,

$$k_{A-B-C} = k_{A-B} v_{A-B}^2 + k_{A-C} v_{A-C}^2 + 4v_{A-B}v_{A-C} \frac{k_{A-B}k_{A-C}}{k_{A-B} + k_{A-C}}, \quad (9)$$

where v is the volume fraction. The subscript denotes the corresponding alloy. It is notable that, if $k_{A-B} \approx k_{A-C}$, Eq. 9 simply reduces to k_{A-B} .

U-Zr Alloys

Thermal conductivity data for U-Zr alloys is used as the basis for estimation of the thermal conductivity of some TRU-Zr alloys. After Touloukian reviewed and summarized the thermal conductivity data of U-Zr alloys [1], Takahashi *et al.* [2] were the only authors to report further measured data. Both data sets revealed the alloy thermal conductivity is lower than the simple interpolation of values between U and Zr. This is due to the impurity effects discussed above.

A correlation to predict the thermal conductivity of U-Zr alloys for U-rich (50 wt% < U) cases has been developed at ANL [20]. This correlation, however, is not directly applicable to ATW fuel cases where Zr content is beyond the limit of the correlation.

Including all U-Zr data from Touloukian and Takahashi [1,2], and Zr data from Fink [3], a new correlation, applicable to any Zr content, is produced as follows:

$$k_{Zr-U} = \left(1 - \sqrt{1 - x_{Zr}}\right) k_{Zr} + \sqrt{1 - x_{Zr}} \left\{x_{Zr} k_{c,U} + (1 - x_{Zr}) k_U\right\} \quad (10)$$

where x_{Zr} is the Zr weight fraction, k_U is the thermal conductivity of U given by Eq. 1, k_{Zr} the thermal conductivity of Zr given by Eq. 2 and $k_{c,U}$ is a thermal conductivity correction due to the alloying effect. $k_{c,U}$ is obtained by fitting the data to Eq. 10 to yield

$$k_{c,U} = -102.0 + 200.1 x_{Zr} - 109.2 x_{Zr}^2 + 9.435 \times 10^{-3} T + 3.459 \times 10^{-5} T^2 - 0.02093 x_{Zr} T$$

The standard error of estimate for data fitting was 1.29 W/m-K. Equation 10 is applicable to any Zr content.

Pu-Zr Alloys

No measured data for the thermal conductivity of Zr-Pu alloy is available in the literature; therefore, estimates have to be made. Thermal conductivity of the alloy is modeled for four separate phase fields, namely, δ -Pu, α -Zr, δ -Pu+ α -Zr, and (ϵ -Pu, β -Zr) solid-solution phases.

δ -Pu Phase – δ -Pu has a high solubility for Zr; up to about 40 wt% Zr can be dissolved in solid solution. In order to estimate the effect of Zr dissolving into δ -Pu, an alloy that has similar alloying behavior must be used as an analog. The γ -U phase in U-Mo alloy was used for this purpose; it has also a cubic structure and a wide range of Mo solid solubility—up to ~20 wt% Mo. Thermal conductivity data for U-Mo were available from Refs. 1 and 21–23. Among these, only data from Refs. 21 and 23 deal with the γ -U phase. The decrease in the thermal conductivity of γ -U as a function of Mo content was correlated. Assuming that Zr dissolution in δ -Pu also has the same effect as Mo does in the γ -U, the decrease correlation was scaled by the ratio of $k_{\delta-Pu}/k_U$. As a result, the thermal conductivity correlation for Zr dissolved in δ -Pu is estimated as

$$k_{\delta-Pu(Zr)} = \left(1 - \sqrt{1 - x_{Pu}}\right) k_{\delta-Pu} + \sqrt{1 - x_{Pu}} k_{c,Zr} \quad (11)$$

where x_{Pu} is the Pu weight fraction and $k_{\delta-Pu}$ is given by Eq. 2. In this case, $k_{c,Zr}$ is obtained as

$$k_{c,Zr} = 29.469 - 118.811 x_{Pu} + 88.893 x_{Pu}^2 + 0.0117 T + 1.922 \times 10^{-5} T^2 - 0.00716 x_{Pu} T.$$

The valid temperature range is 540K–870 K.

α -Zr Phase – α -Zr has high solubility for Pu; α -Zr can accommodate up to ~20 wt% Pu. The same argument made for the Pu-rich side is applied here, and the thermal conductivity for this phase is correlated as

$$k_{\alpha-Zr(Pu)} = \left(1 - \sqrt{1 - x_{Zr}}\right) k_{Zr} + \sqrt{1 - x_{Zr}} k_{c,Pu} \quad (12)$$

where $k_{c,Pu}$ is given by

$$k_{c,Pu} = 30.57 - 82.301 x_{Zr} + 71.456 x_{Zr}^2 + 0.01895 T + 8.111 \times 10^{-6} T^2 - 0.02453 x_{Zr} T$$

α -Zr+ δ Pu – In this two-phase region, alloy thermal conductivity can be modeled by the Bruggeman equation (Eq. 8). The weight fractions of each phase, δ -Pu or α -Zr, are calculated by the lever rule, and the volume fractions of each phase are determined by the following formula:

$$v_{\delta-Pu} = \frac{\rho_{\alpha-Zr} x_{\delta-Pu}}{\rho_{\delta-Pu} - (\rho_{\delta-Pu} - \rho_{\alpha-Zr}) x_{\delta-Pu}}, \quad (13)$$

and $v_{\alpha-Zr} = 1 - v_{\delta-Pu}$, where x is the weight fraction and ρ is the density of each phase. Temperature-dependent densities of δ -Pu and α -Zr were used.

Figure 24 shows the thermal conductivity of Zr-Pu alloy as a function of Zr concentration for δ -Pu, α -(Pu,Zr), and the two-phase δ -Pu+ α -Zr mixture above 540 K. Each isothermal line was generated by three composite equations given by Eqs. 8, 11, and 12.

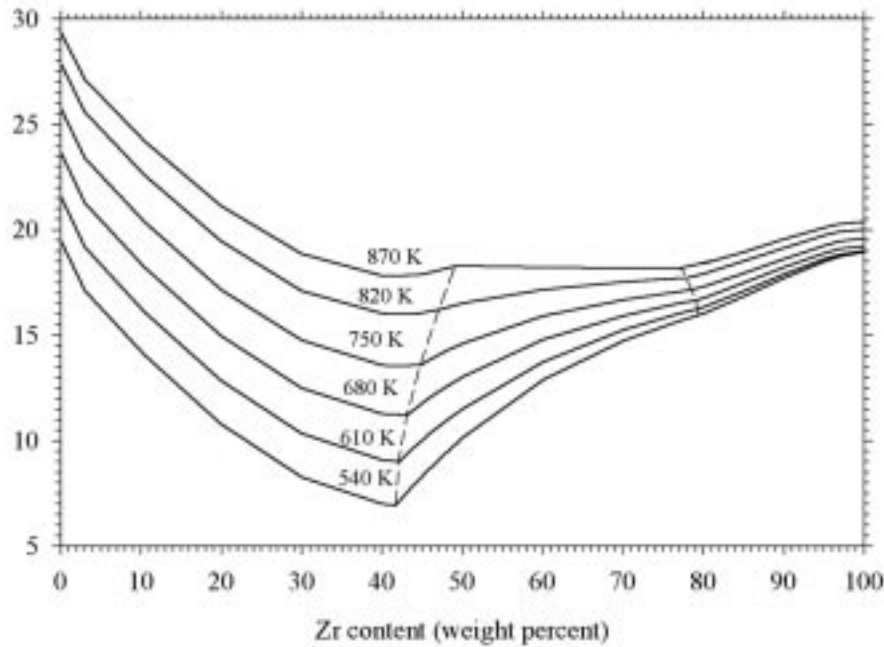


Fig. 24. Thermal conductivity of Pu-Zr alloys vs. Zr content 540–870 K. The dashed lines indicate the phase transitions.

ϵ -Pu, β -Zr – For this higher-temperature phase, the thermal-conductivity correlation of U-Zr (Eq. 10) was considered applicable. Prediction results by Eq. 10 for temperatures above 873 K were scaled to fit the correlation, and the correlation is analogous to Eq. 10, namely,

$$k_{\epsilon-Pu, \beta-Zr} = (1 - \sqrt{1 - x_{Zr}}) k_{Zr} + \sqrt{1 - x_{Zr}} \{ x_{Zr} k_{c,Pu,Zr} + (1 - x_{Zr}) k_{\epsilon-Pu} \} \quad (14)$$

where k_{Zr} is given by Eq. 2, k_{e-Pu} by Eq. 3b, and

$$k_{c,Pu,Zr} = -98.806 + 147.895 x_{Zr} - 26.883 x_{Zr}^2 + 0.0512 T + 8.699 \times 10^{-6} T^2 - 0.0601 x_{Zr} T.$$

In Fig. 25, the thermal conductivity of Pu-Zr at temperatures above 873 K is plotted. The alloying effect is salient at low temperatures, but diminishing at high temperatures.

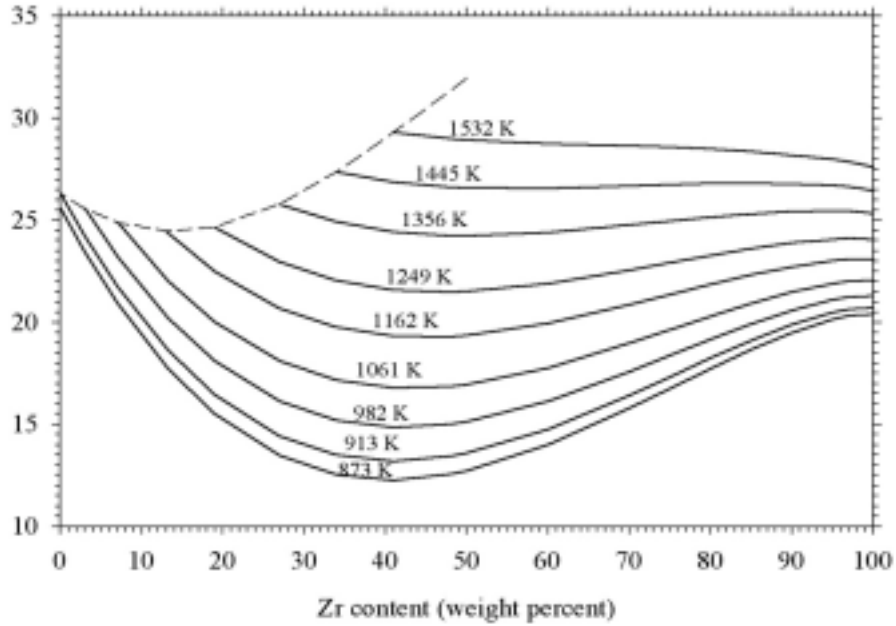


Fig. 25. Thermal conductivity of Pu-Zr alloy vs. Zr content 873 K–1532 K. The dashed line indicate the phase transition (solidus line).

Pu-Am-Zr and TRU-Zr Alloys

As discussed above, the thermal conductivity of Zr-Pu-Am alloy is provided by Eq. 9, namely

$$k_{Zr-Pu-Am} = k_{Zr-Pu} v_{Zr-Pu}^2 + k_{Zr-Am} v_{Zr-Am}^2 + 4 v_{Zr-Pu} v_{Zr-Am} \frac{k_{Zr-Pu} k_{Zr-Am}}{k_{Zr-Pu} + k_{Zr-Am}}.$$

Due to the lack of data for the Am-Zr binary system and any higher-order systems, the thermal conductivity of Zr-Pu alloys must be used for Zr-Pu-Am alloy at this time. Pu content should be increased according to the amount of Am.

The addition of up to 8 w% Np in Pu had almost negligible effect on the thermal conductivity of Pu, even at room temperature [24]. This suggests that the impurity effect produced by the existence of a small amount of Np and other actinides typical in TRU-Zr fuel will be negligible at the fuel operating temperatures. As a result, the Zr-Pu-Am alloy correlation given in Eq. 9 or the Zr-Pu correlations again should be applied to the higher alloy cases for the present.

2. SEPARATIONS TECHNOLOGY

Scope

The separations technology activity consists of three tasks addressing the various stages in the process of partitioning irradiated fuels for subsequent fissioning of transuranic elements and transmutation of long-lived fission products. The tasks are as follows:

Light-Water Reactor Spent Fuel Treatment – This task involves the development and demonstration of efficient and economic means for the separation of uranium, transuranic elements, specific long-lived fission products, and other fission products from LWR spent fuel. An aqueous partitioning process (UREX) is envisioned for the initial treatment of LWR fuel, involving the extraction of U for disposal as a low-level waste. A pyrochemical process (PYRO-A) will follow to separate the transuranic elements from fission products. Pyrochemical processes for the direct treatment of LWR spent fuels are also being developed for possible future use.

Transmutation Fuel Treatment – Fertile or nonfertile fuel that has been irradiated in the transmuter to fission transuranic elements must be processed to recover and recycle the unburned transuranics and to extract newly generated, long-lived fission products for transmutation. This task accomplishes the development and demonstration of the means for processing that blanket fuel. A pyrochemical process (PYRO-B) is planned for the separation of unburned transuranics and long-lived fission products. Such processes are favored because the reagents are stable under high-radiation fields, and because the processes are normally operated at elevated temperatures with the use of molten salts and can thus accommodate high levels of decay heating. In certain cases, aqueous separations processes may prove appropriate, and methods are being developed that will enable the optimum combination of aqueous and non-aqueous processes.

Waste Form Production – One of the overarching criteria for AAA separations technology development is the minimization of high-level waste generation. Design of the hybrid LWR fuel-treatment process has been oriented toward the elimination of liquid high-level waste streams, and the pyrochemical processes are similarly being designed to minimize high-level waste volumes. This task involves the development and qualification of durable high-level waste forms to accommodate the two principal waste streams (salt and metal) that emanate from the separations process as well as the waste form for the disposal of the pure U extracted from the spent LWR fuel.

Highlights

- In the development of the direct electrolytic reduction process for the treatment of LWR spent fuel, it has been shown that better than 99% conversion of UO_2 to U metal can be achieved. Work in progress will establish the conversion rate and its dependence upon particle size.
- The AMUSE code was used to prepare an optimized flowsheet for the UREX hot demonstration at SRTC. This process flowsheet is expected to provide performance at the program target levels (>99.9% recovery of uranium and transuranics, >95% recovery of Tc).

- A laboratory-scale rotary furnace was designed for testing the modified direct denitration process, for use in converting the UREX TRU-bearing liquid raffinate to oxide powder for feed to the PYRO-A process.
- Analyses using available thermodynamic data suggest that it will be possible to obtain pure NaI for iodine transmutation target preparation by passing the dissolver outgas through molten NaOH.
- A couple of conceptual processes for the treatment of TRISO fuel have been developed, one involving acid leaching to dissolve the fuel kernel and the other a carbochlorination-based process that would convert the fuel materials to chlorides for subsequent recovery of the actinides by pyrochemical means. These steps would be preceded by head-end processing that could be the conventional crush and burn method or the halide volatility process originally proposed by ANL.

Oxide Fuel Processing—Electrolytic Oxide Reduction (PYROX) Process

Uranium oxide reduction experiments carried out during the quarter used crushed UO_2 particles as the feed material and platinum as an oxygen electrode. Four particle size ranges were selected for the kinetic study: 0.045–0.6 mm, 0.6–1.18 mm, 1.18–2.8 mm, and 2.8–4.0 mm. The mass of UO_2 in these experiments varied between 18 and 20 g. UO_2 was contained in a cylindrical fuel basket, 1.5 cm in diameter and 2.2 cm in height, constructed from permeable stainless steel screen material. Experiments have been performed with the 0.045–0.6 mm and 0.6–1.18 mm particle-size ranges thus far.

The results of the three recent electrolytic reduction experiments with UO_2 are shown in Table 4. In this table, the second column shows the mass and the particle size range of UO_2 used in the experiments. The third column shows the termination point of the experiment in charge per mole (4 F/mol is the theoretically required charge for 100% conversion). The fourth column shows the average current concentration in the cathode during the experiment. These values were computed using the current concentration (cell current/volume of the oxide bed) for every incremental time step and averaging it over the whole time period. The increasing average current concentration from experiment to experiment is an indication of improved cell operation. The last two columns show the measured conversion of oxide to metal using the two quantitative analytical methods.

Table 4. UO_2 Conversion in Reduction Experiments

Experiment No.	Mass of UO_2 (g), Particle Size Range (mm)	Termination Point (F/mol.)	Average Current Concentration (A/cm^3)	Conversion wt% (methanol-washed product)	Conversion wt% (water-washed product)
EWR-32	18.9 g, 0.045–0.6 mm	5.3	0.22	71	(Not analyzed by this method)
EWR-33	17.8 g, 0.045–0.6 mm	6.8	0.27	58	95
EWR-34	20.0 g, 0.6–1.18 mm	7.3	0.32	95	>99

At the end of each experiment, the fuel basket with the electrolytic reduction product was sectioned longitudinally into two halves. One half was further sectioned longitudinally into two segments. Each segment was then analyzed by one of the two quantitative techniques. The major difference between the two techniques was that methanol was used as the solvent to remove the salt phase in one method while water was used as the solvent in the other. In both cases (water or methanol), the dissolved salt was separated from insoluble U phases by filtering the solution through a 5- μm Teflon-membrane filter. The isolated U phases were washed with the pertinent solvent and then rinsed with methanol and dried by pulling a stream of argon through the material on the filter. With the listed cell-product samples, the U phases consisted of sizeable pieces of metallic material and varying amounts of powder that ranged in color from brown to black. Shiny faces were visible on the metal pieces where they had been cut during segmenting. These faces remained shiny after the washing process, and indicated that no oxidation of the metal took place during the washing, regardless of solvent. Distribution between metal and oxide in the U phases was determined by igniting the collected product to U_3O_8 and calculating the fractions of metal and oxide from the gain in mass on ignition, assuming the initial material consisted of a mixture containing only U metal and UO_2 . The validity of this approach has been demonstrated with samples of pure U metal (apparent conversion of $98.9 \pm 1.2 \text{ wt}\%$) and pure UO_2 (apparent conversion of $<1 \text{ wt}\%$).

The results in Table 4 show that the products analyzed after an initial methanol wash step showed conversions of 71, 58, and 95 wt%, respectively, for the three experiments. Samples from the EWR-33 and EWR-34 experiments, analyzed after a water-wash step, showed conversions of 95 and $>99 \text{ wt}\%$. There is a large difference between the results for the methanol-washed and water-washed product in EWR-33 (58% vs. 95%). The difference is much smaller for EWR-34. Since no evidence was found for tarnishing of the metal surfaces during salt removal with either solvent, the difference between the two methods could be attributed to nonuniformity of the U/ UO_2 -phase distributions in the two segments from a given specimen. The large difference in segments from experiment EWR-33 is puzzling since the sectioned faces of these samples showed no visual indication of unreduced UO_2 . It is possible that the postulated nonuniformity arises from oxide trapped inside or between aggregated metal particles and can only be observed through a microstructural examination of such samples. The results of EWR-34 show that its reduction product was at least 95% reduced and was more than 99% reduced in some areas.

The starting particle size range for EWR-34 was 0.6–1.2 mm while the starting particle size range for EWR-33 was 0.045–0.6 mm. Both the cells were operated for about 13 hours, but as a result of higher current concentrations in EWR-34, more charge was passed in EWR-34 than in EWR-33. From the cell characteristics of the two experiments, there does not seem to be a significant effect of particle size on the conversion extent or rate over these particle size ranges. The products from EWR-32 and EWR-33 experiments are shown in Figs. 26–27, respectively.



Fig. 26. Transverse cross-section of fuel basket showing a partially reduced product in experiment EWR-32.

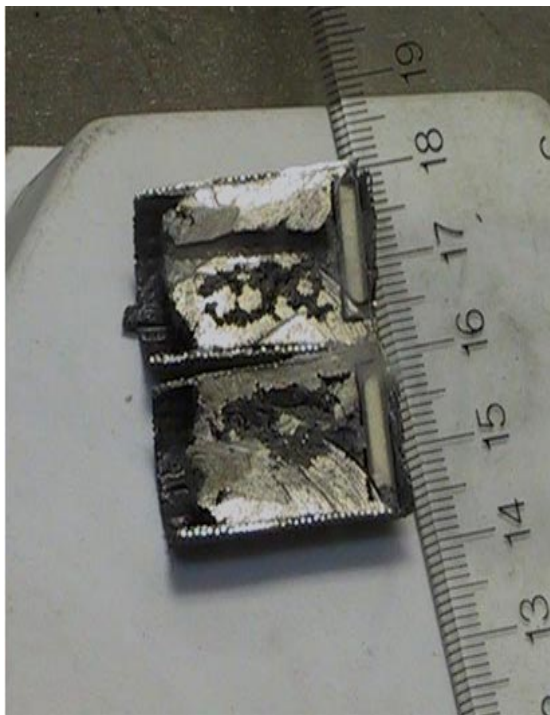


Fig. 27. Longitudinal cross-section of fuel basket showing a highly reduced product in experiment EWR-33.

Using the same electrolytic cell, three experiments were performed with Nd_2O_3 to evaluate the feasibility of direct electrochemical reduction of rare-earth oxide fission products in a LiCl electrolyte at 650°C . The experimental conditions for these are summarized in Table 5. All three experiments were performed in an MgO cell container with no dissolved Li_2O in the electrolyte at the start of the experiment. Cell voltage, electrode potentials, current, oxygen- and chlorine-evolution rates were measured and recorded with an automated data acquisition system. The total charge passed and F/mol for Nd_2O_3 were calculated from the recorded data (6 F/mol is the theoretical charge required for complete reduction of any given mass of Nd_2O_3 at 100% efficiency).

The first two experiments, LRNd-8 and LRNd-9, were performed with a gold-wire anode. Although gold proved to be an excellent oxygen electrode at low oxide ion concentrations, it was unstable near the standard chlorine evolution potential, 3.6 V vs. lithium. Gold appears to dissolve anodically as gold chloride. It was also observed that some gold was redeposited near the gold wire anode, suggesting the dissolved gold chloride might have thermally decomposed at 650°C . While only a small portion of the gold wire anode was lost by dissolution in LRNd-8, the entire wire in LRNd-9 was lost by dissolution. This may be explained by the longer duration of the second experiment (100 hours) as compared to that of the first (26 hours). The longer duration of the cell operation in the second experiment was primarily designed to provide enough time for the chlorine gas to purge any residual oxygen in the electrolyte. The reaction between the evolved chlorine at the anode and the dissolved oxide in the electrolyte will drive the oxide activity lower, thus providing more favorable conditions for the cathode reaction.

Post-cell examination of the cathode compartments in both experiments revealed a gray layer of particles under a distinguishable blue layer of unreduced Nd_2O_3 . X-ray diffraction (XRD) analysis of the gray particles revealed the presence of NdOCl in addition to Nd_2O_3 . NdOCl formation is not expected under these conditions according to available thermodynamic data. The gray particles were also equilibrated with tin metal to separate any Nd metal, if present. ICP-AES analysis of the tin alloy showed that a small amount (0.06 g) of Nd metal was present in the gray material.

The appearance of the cathode product in the third experiment, LRNd-10, was distinctly different from that of the earlier two. The whole cathode product in LRNd-10 was dark gray with a metal-like deposit on the Ta wire pan. However, the analysis of these two samples, the gray material and the metal-like deposit, has been deferred until a reliable analytical method for detection and measurement of Nd metal is established. One problem in evaluating the degree of reduction of rare-earth oxides is the lack of a reliable quantitative analytical technique for determining and measuring the mass of rare-earth metal in the reduction product. Currently, efforts are underway to develop a reliable technique for quantitative analysis of these reduction products.

The graphite anode behavior during the cell run in LRNd-10 was also interesting. Graphite appears to be a highly reversible chlorine electrode. However, during this process some oxygen evolution also occurs. Graphite appears to disintegrate to some extent during this process, forming CO_2 gas and some colloidal graphite in the melt. The genesis of colloidal graphite in the melt is not clear. One possible explanation is as follows: graphite also reacts with lithium forming a Li_xC_6 compound. This reaction appears to take place during the open-circuit phase of the experiment when the graphite anode is not protected by high anode potentials and gas evolution. When the current is turned back on, the Li_xC_6 compound is oxidized to graphite, as evidenced by a current flow even at low anode potentials well below chlorine evolution. This reoxidation reaction may be the source of colloidal graphite in the melt.

Table 5. Summary of Nd_2O_3 Reduction Experiments

Cell No.	LRNd-8	LRNd-9	LRNd-10
Anode	Au wire	Au wire	Graphite rod
Reference Electrode	Ni/NiO	Ni/NiO	None
Cathode Lead	Ta wire pan	Ta wire pan	Ta wire pan
Mass of Nd_2O_3 in Cathode Compartment, g	1.08	2.03	1.00
Electrolyte	LiCl	LiCl	LiCl
Temperature, °C	650	650	650
Number of hours of cell operation	26	100	28
Termination Point, F/mol	5.9	4.4	14.2

Anode Development for the PYROX Process

The pyrochemical processes to treat spent LWR fuel and Pyro-A UREX product involve the direct electrochemical reduction of oxides in a molten LiCl electrolyte at 650°C. In this process, the oxide fuel is reduced to metal at the cathode while oxygen, and possibly chlorine, are evolved at the anode. The anode environment is very oxidizing and the challenges to the anode material are significant. Platinum has been used in the lab-scale development of the process, but it has practical limitations in large-scale cell designs because it will react with chlorine, and the cost is prohibitive as a consumable anode. Development of advanced anode materials for the direct electrochemical reduction process is being pursued. Of two possible solutions to consider, namely nonconsumable inert anodes and consumable graphite anodes, we have selected the first option as having the best chance of success without introducing detrimental impurities into the process.

We are screening candidate materials for this application through a series of performance tests. Both metals and ceramics are being evaluated with the understanding that high-surface area anodes are required for typical gas-generating electrodes. Candidate materials were screened for thermodynamic stability and electrical conductivity at 650°C. Materials considered include platinum, gold, and ceramics including Li_2SnO_3 , LiFeO_2 , CoFe_2O_4 , and BaCrO_4 , and a commercially available doped SnO_2 . We are also investigating various ruthenium-containing materials.

The lab-scale cell design for testing ceramic disk anodes is shown in Fig. 28 and a photograph of the assembled cell is shown in Fig. 29. As indicated in Fig. 28, the cell consists of (1) a stainless steel foam counter electrode that will contain lithium metal, (2) a Ni/NiO reference electrode, and (3) a disk-shaped metal or metal-oxide working electrode. The same electrolyte and temperature conditions used in the wire cell will be used here. The working electrode will be roughly 1 cm in diameter and 0.5 cm in height, depending on the material used. Contact with the working electrode is made via a 3-mm-diameter stainless steel rod enclosed in a magnesia tube. A 5-cm-O.D. magnesia crucible has been machined to allow the electrolyte to flow through the base of the crucible, but also allows the anode assembly to be lifted when necessary for inspection, testing, or replacement.

Several candidate anode materials have been tested during this reporting period. These were CoFe_2O_4 , LiFeO_2 , a commercial SnO_2 electrode material (Stannex), and gold. Results for the Co and Li materials were reasonable, and the samples survived the tests in fairly good condition. Test results on the latter two materials were not satisfactory. Repeat tests on the Stannex and gold and new experiments with ruthenium oxide are planned. A more complete summary of these tests is provided below.

Before these tests were carried out, a new anode current lead was constructed and installed to replace the stainless steel rod previously described. Corrosion of the stainless steel had been observed in earlier tests. The new lead was made from a 6-inch length of 0.1-inch-diameter gold rod welded to 1/8-inch-diameter copper rod. Not enough gold was available to construct this entirely out of gold. Heavier gauge wire was then installed to connect the potentiostats to the cell inside the glove box being used for this work. Several test experiments were then conducted on candidate materials of interest. As explained previously, the cell consists of a stainless steel

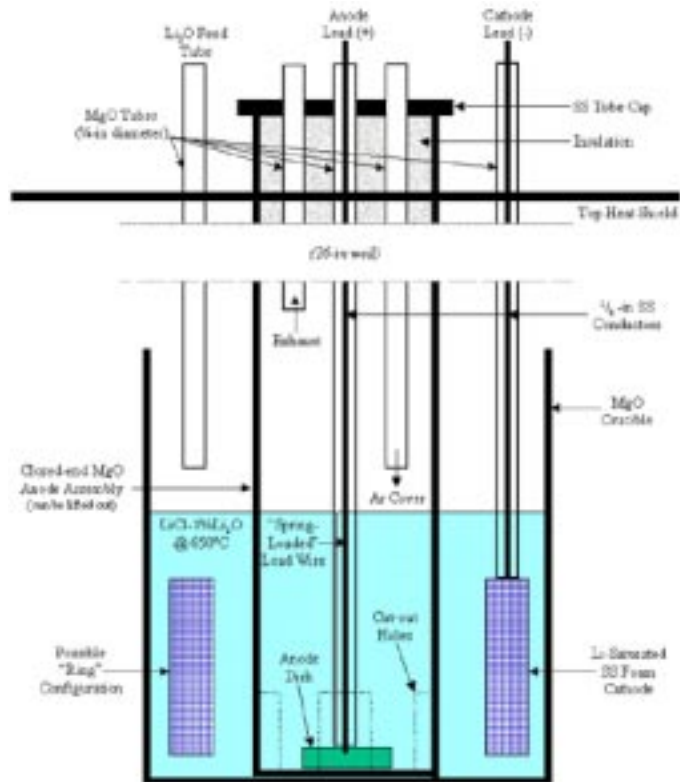


Fig. 28. Schematic of lab-scale anode development test cell.

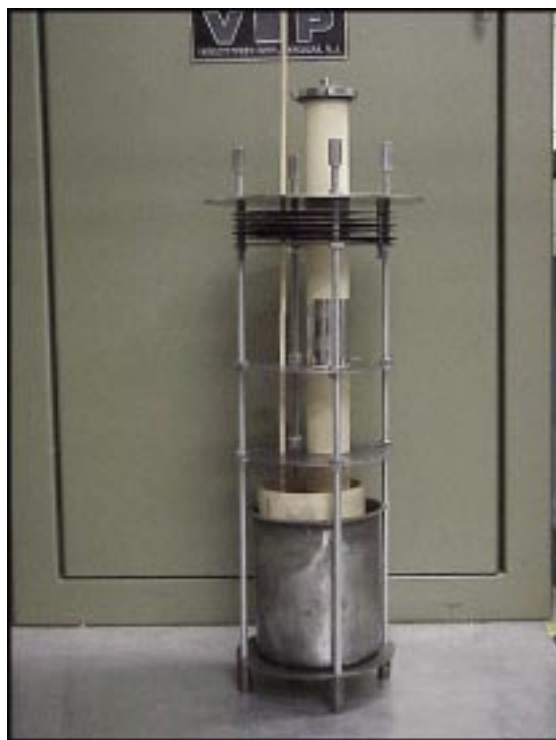


Fig. 29. Lab-scale anode development test cell assembly.

foam counter electrode, a Ni/NiO reference electrode, and a metal or metal-oxide working electrode. The materials examined during this reporting period were CoFe_2O_4 , LiFeO_2 , a commercial SnO_2 electrode material (Stannex), and gold. The exposed area of all materials was about 1 cm^2 and all tests were conducted at $\sim 650^\circ\text{C}$. The electrolyte was LiCl containing 1 wt% Li_2O . Results were mixed and indicate that some additional refinements of the cell design are desirable.

One of a number of cyclic voltammetry results for CoFe_2O_4 is shown in Fig. 30 with repeated scans. The potential of the Ni/NiO reference electrode is 1.6–1.7 V relative to Li. Note that an increase in current begins at about 0.75 volts about the potential oxygen generation would be expected (i.e., $\sim 1.6\text{V} + 0.75\text{V} = 2.35\text{V}$ and the O_2 generation potential is $\sim 2.3\text{V}$). A slight diminution follows in the rate of increase of current that could signal diffusion limits to the availability of oxide ions at the anode. A slight turn up in the curve is then seen, and we are tentatively assigning it to the onset of chlorine evolution. At the conclusion of these tests, the sample was retrieved from the cell. The surface appeared to be slightly pitted but otherwise not significantly attacked. Thermodynamic calculations indicate that this material should perform reasonably well in this system.

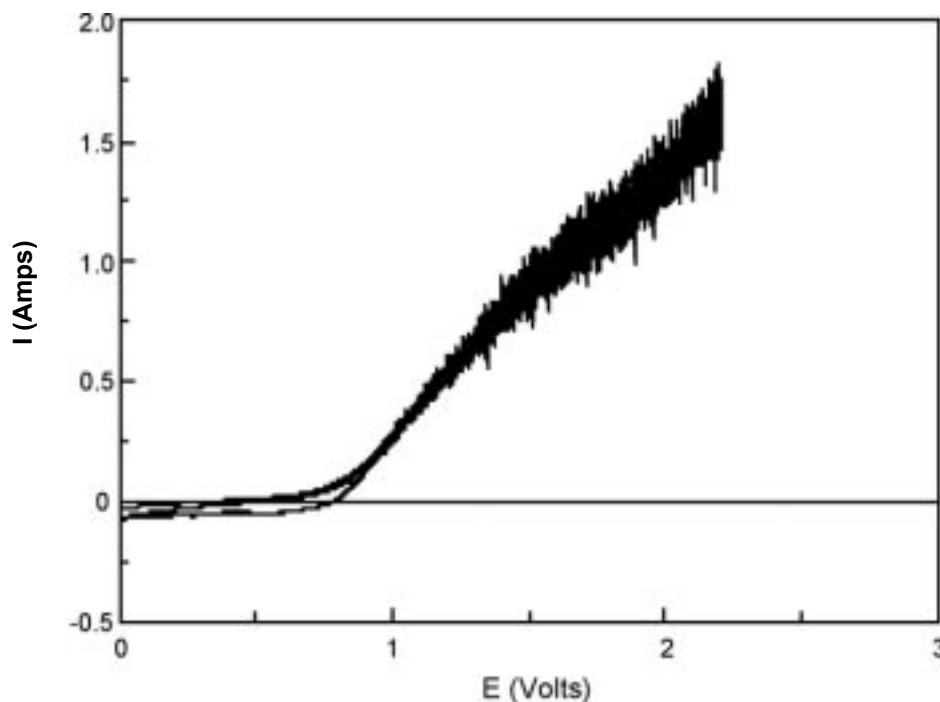


Fig. 30. CoFe_2O_4 anode: cyclic voltammetry at 40 mV/sec vs. Ni/NiO reference electrode.

A typical cyclic voltammetry result for LiFeO_2 is shown in Fig. 31. The general features of the curves are similar to those obtained with CoFe_2O_4 although with somewhat greater noise and slightly higher current. The electrical conductivity of LiFeO_2 is higher than that of CoFe_2O_4 , possibly accounting for the higher current. The surface of the sample at the conclusion of these tests was somewhat more pitted than the CoFe_2O_4 . Thermodynamic calculations indicate that LiFeO_2 would be less stable in this environment than the Co compound. The noise could be attributed to bubble formation, but may be a consequence of the electrical contact between the

anode lead and the sample. Improving this contact is one of the modifications being contemplated.

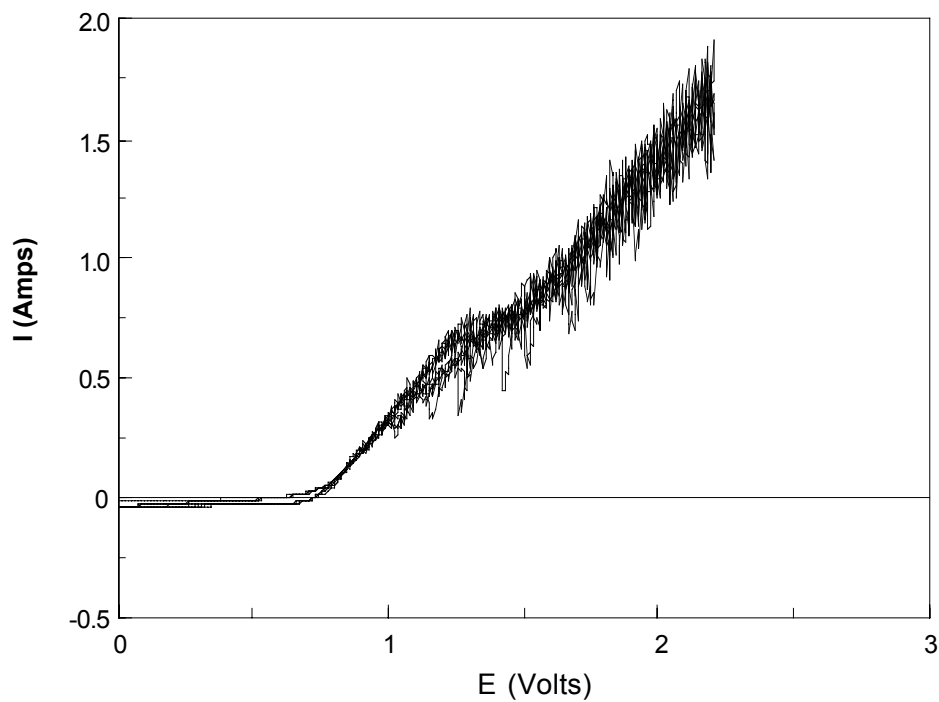


Fig. 31. LiFeO_2 anode: cyclic voltammetry at 40 mV/sec vs. Ni/NiO reference electrode.

Tests with SnO_2 were unsuccessful in that the sample appeared to be changing during the course of the tests. During electrical conductivity measurements, reported previously, it was observed that this material showed low conductivity until the sample had been held for about 12 hours at 650°C whereupon the conductivity increased by about a factor of 100. In our cell tests the sample was held overnight in the furnace, but not in the salt. It was hoped that this treatment would result in a stable sample but obviously did not. An annealed sample is currently being prepared and the electrical conductivity will be measured prior to insertion into the cell for testing. Thermodynamic calculations indicate that this material should perform quite poorly under these conditions; however, the sample retrieved from the tests run was intact and not badly corroded. (Past experience states that SnO_2 should perform reasonably well in this system, despite the thermodynamic calculations.)

Current plans are to run a gold sample in the current cell configuration followed by annealed SnO_2 . A sample of RuO_2 is also ready and will be tested as soon as possible. Thermodynamic calculations indicate that the latter material should be quite stable under these conditions. Also, a sample of SrRuO_3 is presently being prepared for testing.

UREX Process Development

Optimized UREX Process Demonstration

Using the solvent extraction modeling code AMUSE 1.08, an optimized flowsheet was derived for the UREX hot demonstration to be performed in the SRTC hot cells later this year. Using the existing 36-stage, 2-cm centrifugal contactor in the SRTC hot cell put important restrictions on the flowsheet design. The contactor is divided into two tiers, with 20 stages on top and 16 stages on bottom. Because of this break, only the extraction/scrub section can be performed on the top tier, and, more importantly, only sixteen stages are available for the Tc-strip section. Uranium-stripping must be performed outside the hot cell. Because the contactor is also being used for demonstrating the Caustic-Side Solvent Extraction process, it is good practice to not use the first stages of the top tier, thus keeping cross-contamination effects to a minimum. The flowsheet that was developed is shown in Figs. 32–33. The bases for the design of each section is discussed below.

Extraction/Scrub Section

In the extraction section, U and Tc are extracted from the feed, and Np, Pu, and the fission products remain in the aqueous solution and exit the process in the raffinate. Process goals are:

- >99.9% of the U is extracted for recovery;
- >95% of the Tc is extracted for recovery;
- <0.01% of the Pu is extracted; and
- <10% of the Np is extracted.

The U-loading in the solvent must be $\geq 70\%$ to achieve 10^4 decontamination factors from fission products².

The completeness of extraction of U and Tc is primarily influenced by (1) the number of extraction stages and (2) the organic/aqueous (O/A) flow rate ratio. The U-loading of the solvent is primarily influenced by the feed-to-solvent O/A ratio. It is also significantly affected by the flow rate and nitrate concentration of the scrub feed.³ Increasing nitrate concentrations makes U more and Tc less extractable. Pertechetate extraction has a strong inverse dependency on the process temperature.

The effectiveness of making Pu(IV) and Np(IV) inextractable is primarily affected by the concentration of acetohydroxamic acid (AHA); however, increasing the concentrations of both hydrogen and nitrate increase their extractability. The extraction of Np(V), which will be the major Np species in the feed, is increased by increasing nitrate and unaffected by AHA. Under the flowsheet conditions, Np(V) will be more extractable than Np(IV); therefore, only Np(V) was followed in the design analysis. Loading the solvent also decreases the extraction of Pu and Np. Because AHA is not stable for long periods of time in ≥ 1 M HNO₃, it is added only in the scrub.

² This is a new requirement suggested by Major Thompson based on SRS PUREX-process experience. Because it requires two moles of tributyl phosphate (TBP) to extract one mole of uranyl nitrate, loading to 70% means that the uranium concentration in 30 vol% (1.1 M) TBP should equal $(0.7 \times 1.1)/2 = 0.385$ M.

³ Under the low-acid scrub condition required for the UREX process, uranium is pinched in the scrub section, and its highest organic-phase concentration is in the later stages of the scrub section.

The results of the 49-stage countercurrent UREX demonstration run last September at ANL showed (1) the temperature in the extraction scrub section must be kept at ~25°C to provide good extraction of Tc, and (2) four scrub stages were not sufficient to provide required decontamination from Pu. Optimization studies have led to the conclusion that 10 extraction and 6 scrub stages, maintained at 25°C, will meet all process goals at the influent flow rates shown in Fig. 32. Figures 34–37 show the concentration profiles for U(VI), Pu(IV), Np(V), and Tc(VII) for this flowsheet.

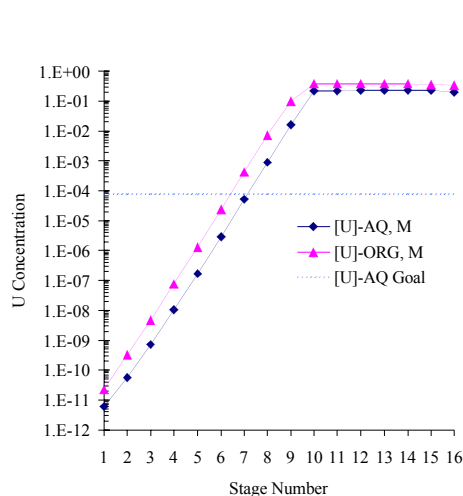


Fig. 34. U profile for the extraction/scrub section of the optimized UREX flowsheet for the SRTC hot demonstration. Fig. 32 shows conditions.

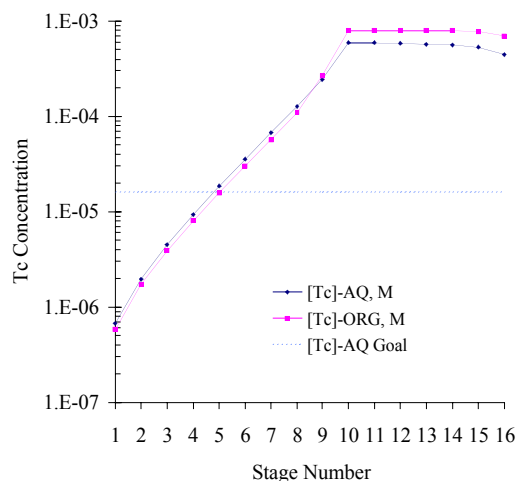


Fig. 35. Tc profile for the extraction/scrub section of the optimized UREX flowsheet for the SRTC hot demonstration. Fig. 32 shows conditions.

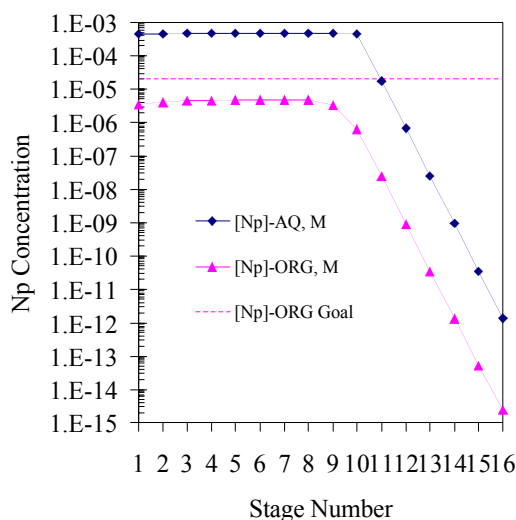


Fig. 36. Np(V) profile for the extraction/scrub section of the optimized UREX flowsheet for the SRTC hot demo. Fig. 32 shows conditions.

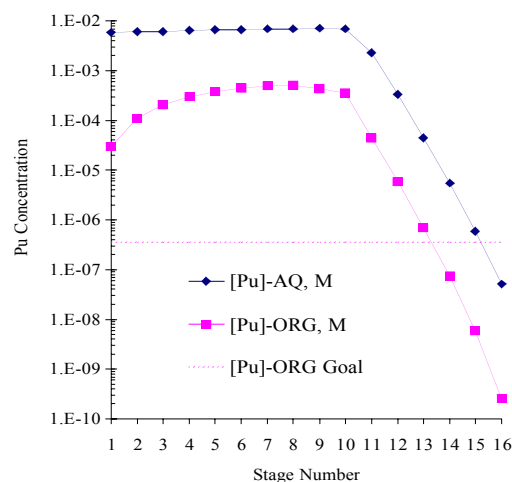


Fig. 37. Pu(IV) profile for the extraction/scrub section of the optimized UREX flowsheet for the SRTC hot demonstration. Fig. 32 shows conditions.

A new consideration to be met by this flowsheet is loading the solvent to 70% to increase U decontamination from fission products. Because of the low concentration of nitric acid in the scrub section, loading of the solvent is maximized in the scrub section, not at the feed stage. Figure 38 shows the effect of feed rate on solvent loading. A flow rate of 5.6 mL/min was chosen for the process because (1) loading was almost 70% at this flow rate, and (2) flow rates higher than 5.8 mL/min made convergence of the flowsheet calculation by AMUSE difficult; in many cases, it would not converge. Experience has taught us that problems in converging the mathematics are consistent with physical and chemical problems with running the flowsheet. Another concern with this low-acid scrub is that the density of the solvent will approach that of the aqueous phase, making phase separation difficult to impossible. Hydraulic testing should be done to verify performance of the flowsheet at high loading. Figure 38 shows how changes in feed flow rate effects solvent loading.

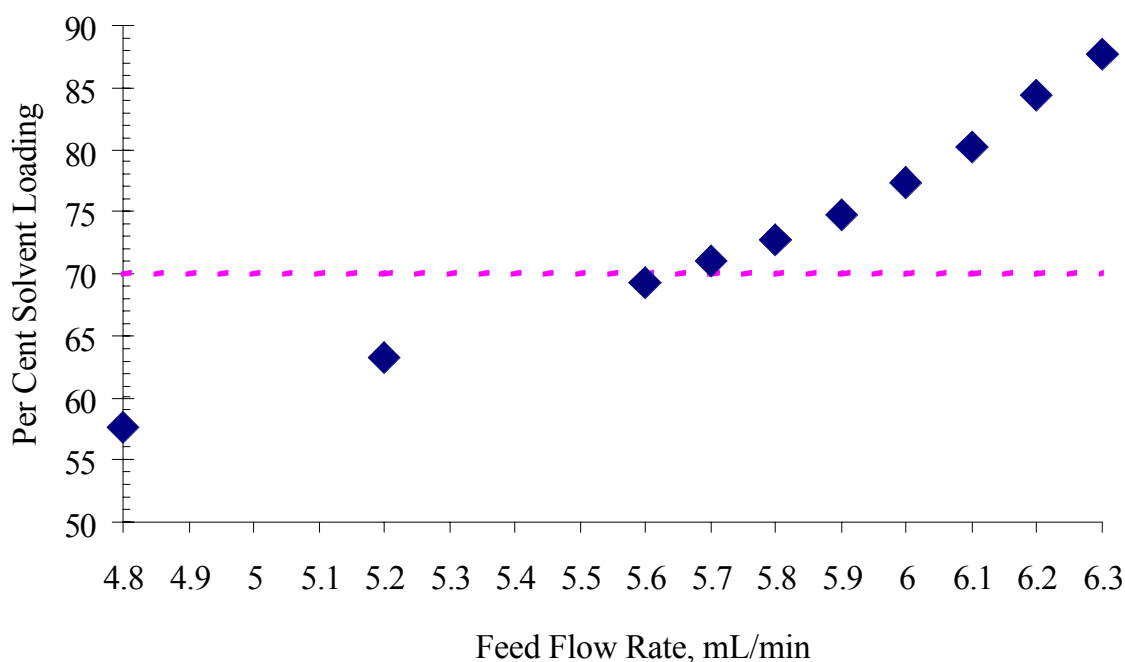


Fig. 38. Solvent loading vs. the feed rate of the dissolved-fuel solution entering the feed stage of the extraction section. Scrub and solvent feed rates were as shown in Fig. 32. A loading of 70% is considered ideal for PUREX processing at the Savannah River Site.

The effects of temperature on the distribution ratio of HTcO_4 are an important consideration. Figure 39 shows how allowing the extraction/scrub section to reach a temperature above 31°C will not lead to meeting the Tc-recovery process goal.

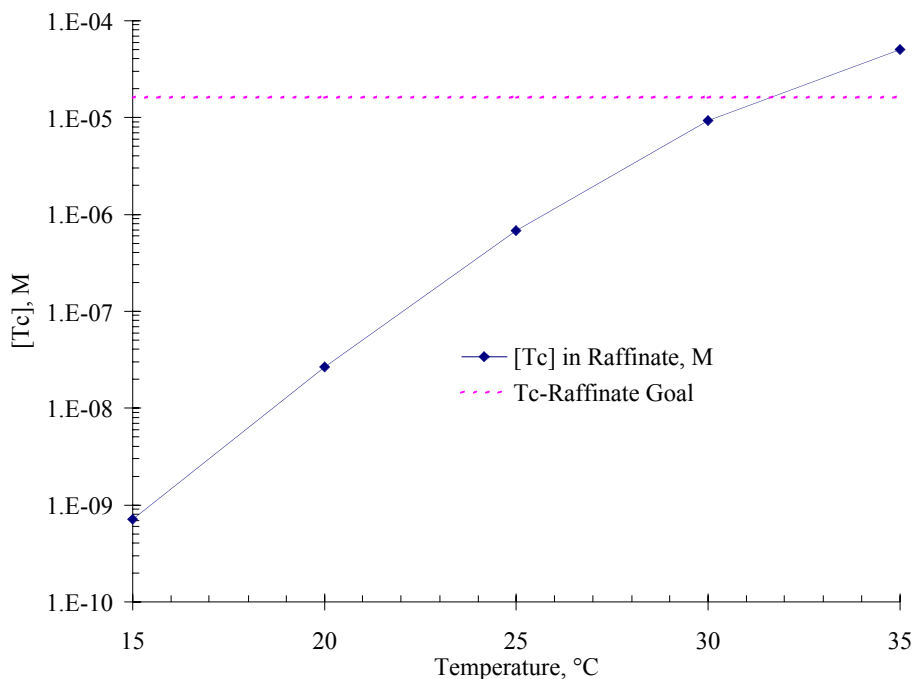


Fig. 39. Effects of process temperature on the extractability of the Tc in the UREX flowsheet shown in Fig. 32.

Technetium-Strip Section

The Tc-strip section is actually three sections (see Fig. 32). The loaded solvent from the scrub section (stage 16) enters the contactor at stage 24, where it is stripped of Tc in stages 24–30. By contacting clean solvent, the stripped Tc product is then scrubbed from the fraction of uranium nitrate that was also stripped from the loaded solvent in the U re-extraction section (stages 17–23). At the other end of the Tc-strip section, acid is scrubbed from the U-loaded solvent in the acid-scrub section (stages 31–32). This part of the flowsheet is not optimized for the UREX process; rather, it is optimized for the hot demonstration in the SRTC hot cell. More than the 16 available stages are required to optimize this section. Because of the limitation of available stages, the flow rates of (1) the solvent in the U re-extraction section, (2) the Tc-strip solution, and (3) the acid-scrub solution are all higher than would be required for an optimized flow sheet. Further, acid-stripping from the U-loaded solvent was less than ideal. The stage temperatures used in calculating this section were those calculated for the ANL demonstration. Because ambient conditions, flow rates, and stages are not identical, they do not correspond directly to what will be seen in the SRTC contactor. Once conditions are set for the SRTC demonstration, the temperature profile can be calculated, followed by re-calculation of this flowsheet. Figures 40–42 show the stage concentration profiles for Tc, U, and H ion in the flowsheet shown in Fig. 32. The Tc-strip section of the flow sheet had several variables to examine:

- Stage distribution between the three subsections;
- Flow rates of clean solvent, Tc-strip, and acid-scrub feeds; and
- Nitric-acid concentration in the Tc-strip feed.

A limited parametric study was performed to find the best values for these parameters.

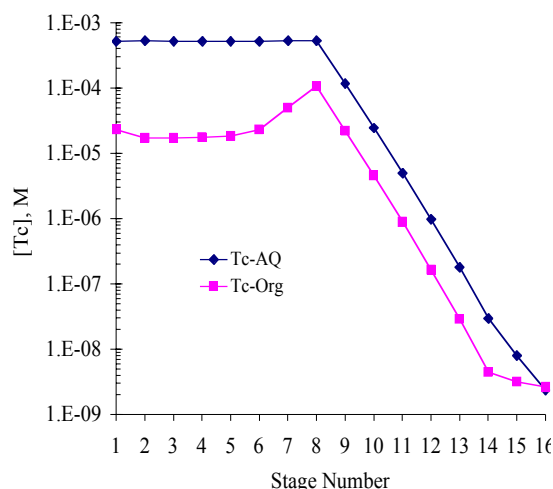


Fig. 40. Technetium profile for the Tc-strip section of the optimized UREX flowsheet for the SRTC hot demonstration. Fig. 32 shows conditions.

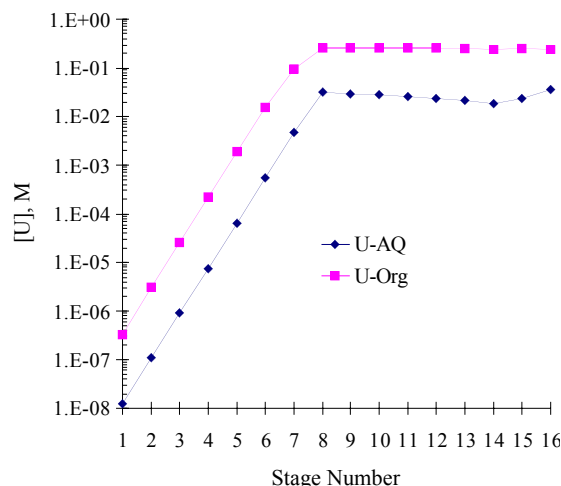


Fig. 41. U profile for the Tc-strip section of the optimized UREX flowsheet for the SRTC hot demonstration. Fig. 32 shows conditions.

The distribution of stages for the three subsections was not studied thoroughly during this analysis. Earlier development studies for the ANL demonstration showed that the best split between the Tc-strip and the U re-extraction sections was to make the number of stages equivalent. We made that decision here also. The addition of the acid scrub section cut into the already limited stages available for the other operations; therefore, we chose two stages as the maximum for that operation. This led to the 7-7-2 stage configuration shown in Fig. 32.

The flow rates for the three feeds in the Tc-strip section were varied to get a feeling for their effects. Minimizing all three flow rates was a process goal. Increasing the two aqueous feeds acts to dilute the Tc product; increasing the clean-solvent feed dilutes the U going to the U-strip section. Keeping the U concentration low in the Tc product is a yet undefined goal, but we chose to make the mass of U in the product less than 1% of the Tc mass. Because the U mass entering the section in the Tc-strip section is ~1200 times that of Tc, this calls for a DF from U of >120,000. The flow rate in the U re-extraction operation was set to meet this goal.

The nitric acid concentration in the acid-scrub feed was set to a value equal to that used in the U-strip feed, 0.01 M. The nitric-acid concentration in the Tc-strip feed was varied from 5 to 7 M. Over this range, it did not greatly effect the U and Tc concentrations of the effluent streams. Figures 43–45 show how the Tc, U, and H-ion profiles varied in a 7-7-2 stage configuration with the flow rates of both the clean-solvent and Tc-strip feeds set at 7 mL/min. Only the H-ion profiles show significant differences.

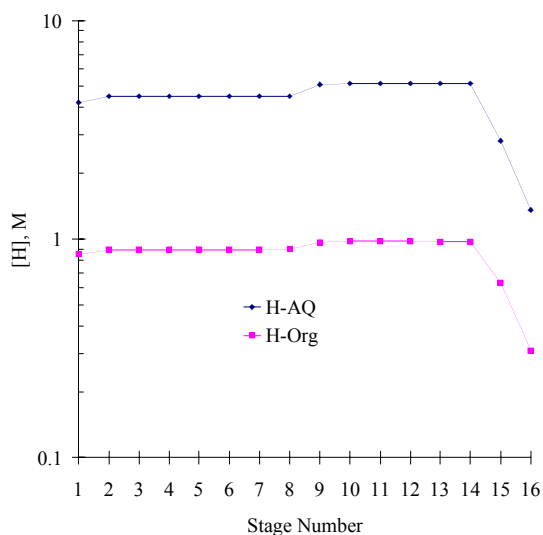


Fig. 42. H-ion profile for the Tc-strip section of the optimized UREX flowsheet for the SRTC hot demonstration. Fig. 32 shows conditions.

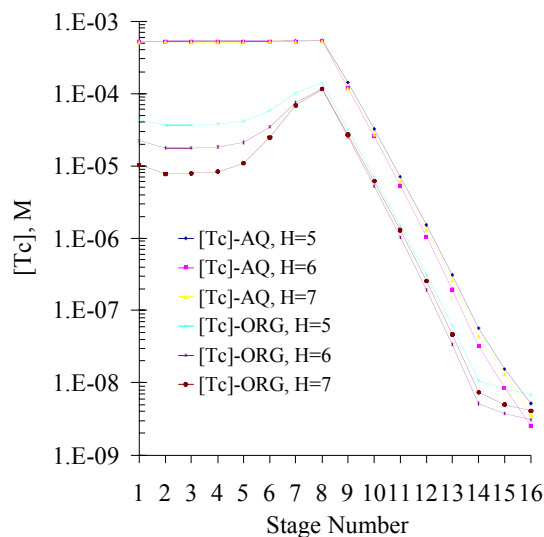


Fig. 43. Tc profile for the Tc-strip section of a UREX flowsheet for the SRTC hot demonstration with all condition as in Fig. 32, except (1) the clean-solvent flow rate is 7 mL/min and (2) the nitric acid in the Tc-strip feed was varied from 5 to 7 M.

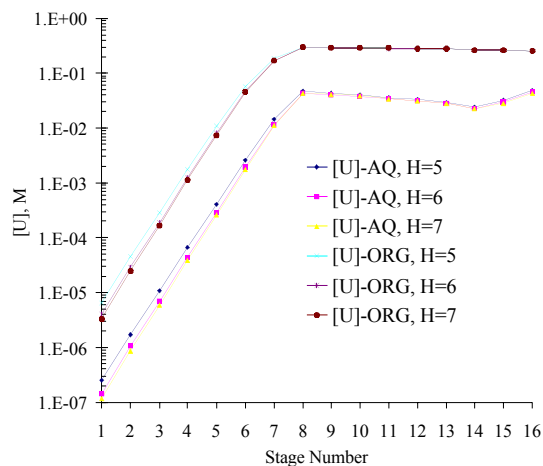


Fig. 44. U profile for the Tc-strip section of a UREX flowsheet for the SRTC hot demonstration with all condition as in Fig. 32, except (1) the clean-solvent flow rate is 7 mL/min and (2) the nitric acid in the Tc-strip feed was varied from 5 to 7 M.

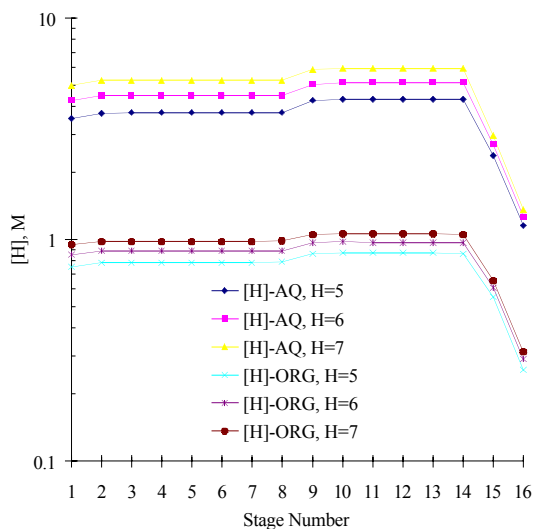


Fig. 45. H-ion profile for the Tc-strip section of a UREX flowsheet for the SRTC hot demonstration with all condition as in Fig. 32, except (1) the clean-solvent flow rate is 7 mL/min and (2) the nitric acid in the Tc-strip feed was varied from 5 to 7 M.

The relative flow rates for the influent streams were varied to find where the most robustness could be given to this undersized section. Table 6 gives examples of how the flow rates of the clean solvent and the acid-scrub flow rates were varied to find one that met process goals and allowed some variability in the actual flow rates during the demonstration.

Table 6. Effects of Varying Flow Rates of the Clean-Solvent (U-Scrub) and Acid-Scrub Feeds to the Tc-Strip Section*

Acid-Scrub flow rate mL/min	ORG-Scrub flow rate mL/min	[U] in Tc product, <u>M</u>	[Tc] in Loaded solvent, <u>M</u>	[H] in loaded solvent, <u>M</u>
7	7	1.436E-07	3.110E-09	2.881E-01
7	8	3.617E-08	2.838E-09	2.990E-01
7	9	1.211E-08	2.646E-09	3.098E-01
7	10	4.767E-09	2.502E-09	3.203E-01
8	8	5.228E-08	2.419E-09	2.540E-01
9	9	2.404E-08	2.007E-09	2.256E-01

*The Tc-strip feed flow rate was set at 20 mL/min. Feed compositions are as shown in Fig. 32. The row with bold typeface is for the optimized flowsheet

Uranium-Strip Section

The major goals for this section are to (1) concentrate the U product as much as possible, (2) remove enough U from the solvent to guarantee it could be recycled to stages 1 and 17 with no adverse effects to process goals, and (3) be robust enough to allow 5% variation in feed flow rates. Goals 2 and 3 are necessary; goal 1 is nice to do. Acid scrubbing the solvent at the end of the Tc-strip section did not have as much benefit as had been hoped. As was seen in Fig. 33, the optimized flowsheet has an O/A flow ratio of 1/1.8 (compared to 1/2 in the ANL demonstration), meaning U concentration in the U-product solution is only 11% of that of the dissolved-fuel feed to the process. Adding more stages to the Tc-strip section can help this situation.

Figure 46 shows how the U concentration in the recycled solvent exiting stage 33 is influenced by the O/A flow-rate ratio in the U-strip section. The organic-phase U-concentration profiles in Fig. 47 show this effect dramatically. A flow ratio of 1.6 would meet processing goals; using 1.8 assures robustness.

Conclusions

A UREX demonstration run in the SRTC hot cell using the flowsheet described in Figs. 32–33 should meet all process goals. The sheet has been optimized for that purpose. The flowsheet run in an actual UREX plant would be different. Specifically, more stages would be allotted to Tc-strip and U-strip sections. Adding stages to both these sections would make the flowsheet more robust and allow higher concentrations of product in both sections.

High loading of U in the extraction/scrub section is a time-tested means to lower fission-product contamination of U and was employed in this flowsheet. However, because this is a low-acid flowsheet, small density differences between the solvent

and the aqueous solution will be present in the scrub section. Hydraulic testing will be required to assure smooth operation during the hot demonstration.

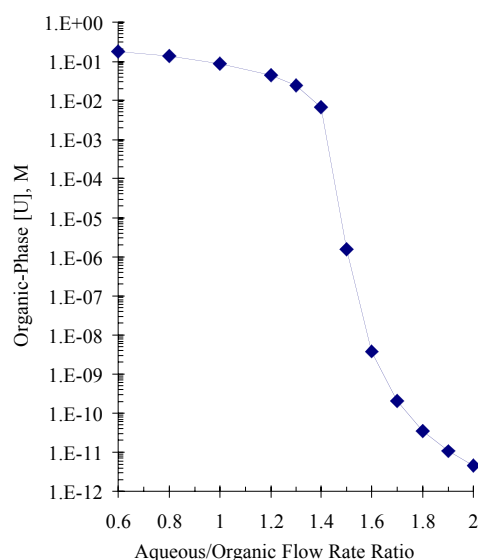


Fig. 46. Effect of aqueous-to-organic (A/O) flow rate ratio on the stripping of U for the UREX solvent. Shown is the organic-phase U concentration in the stripped solvent.

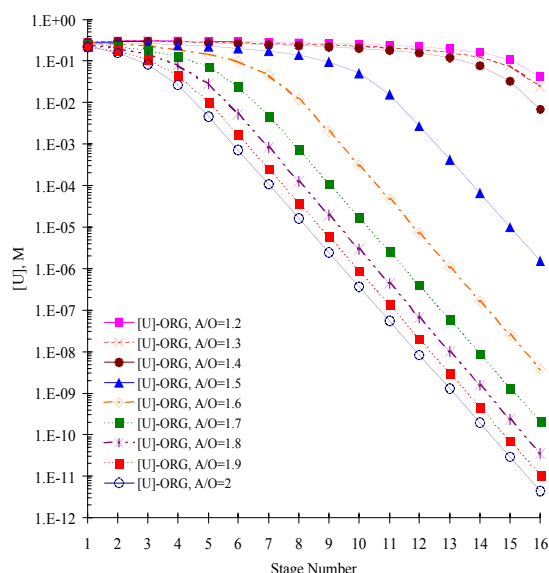


Fig. 47. Effect of aqueous to organic (A/O) flow rate ratio on U-stripping for the UREX solvent. Shown is the organic-phase U-concentration profile in the U-strip section.

Plutonium Distribution Measurements with AHA

Additional Pu distribution measurements were requested for AMUSE model development. The AMUSE solvent extraction model is being used to calculate conditions for the UREX hot demonstration. Accurate data are required to ensure that results of calculations match experimental data from contactor experiments. All distribution measurements were performed with tracer concentrations of Pu from a solution purified by anion exchange. The data were generated by contacting 3 mL of 30 vol% TBP three times with an equal volume of aqueous phase. The aqueous phase for the third contact was spiked with Pu. The emulsions were centrifuged after contact, the phases sampled and counted by liquid scintillation. A test was made with 1 M HNO₃ acid in the aqueous phase to demonstrate that three contacts brought the solution to acid equilibrium. The results showed that little acid is extracted in the third contact (Table 7).

Table 7. Extraction of 1 M HNO₃ in 30 Vol% TBP

Contact Number	Aqueous HNO ₃ after Extraction
1	0.75
2	0.94
3	0.99

Distribution was measured at different acid concentrations and AHA concentrations with the results shown in Table 8. Note that points taken at acid concentrations below

0.5 M usually gave poor material balance so the data points are not considered reliable. It is believed that the Pu may have polymerized and adhered to the glassware. The data are plotted in Fig. 48. As expected, the distribution increases with increasing acid concentration at constant AHA concentration. Distribution decreases with increasing AHA concentration at constant acid concentration. The point at 2 M HNO₃ with 0.3 M AHA appears to be slightly lower than expected based on the curves with 0 or 0.1 M AHA.

**Table 8. Distribution of Tracer Plutonium
as a Function of HNO₃ and AHA Concentration**

	AHA Concentration, M				
HNO ₃ , M	0 ^a	0.1	0.3	0.5	1.0
0.1	NM	NM	NM	NM	0.018 ^b
0.2	NM	0.04	NM	NM	0.023 ^c
0.5	0.837	0.10	0.05	0.049	NM
1.0	2.7	0.34	0.15	0.12	0.070
2.0	8.06	0.95	0.27	0.21	NM
3.0	16	1.57	0.65	0.34	0.210

NM=Not Measured

^a Data measured previously

^b Bad material balance 2.5% data unreliable

^c Bad material balance 70%

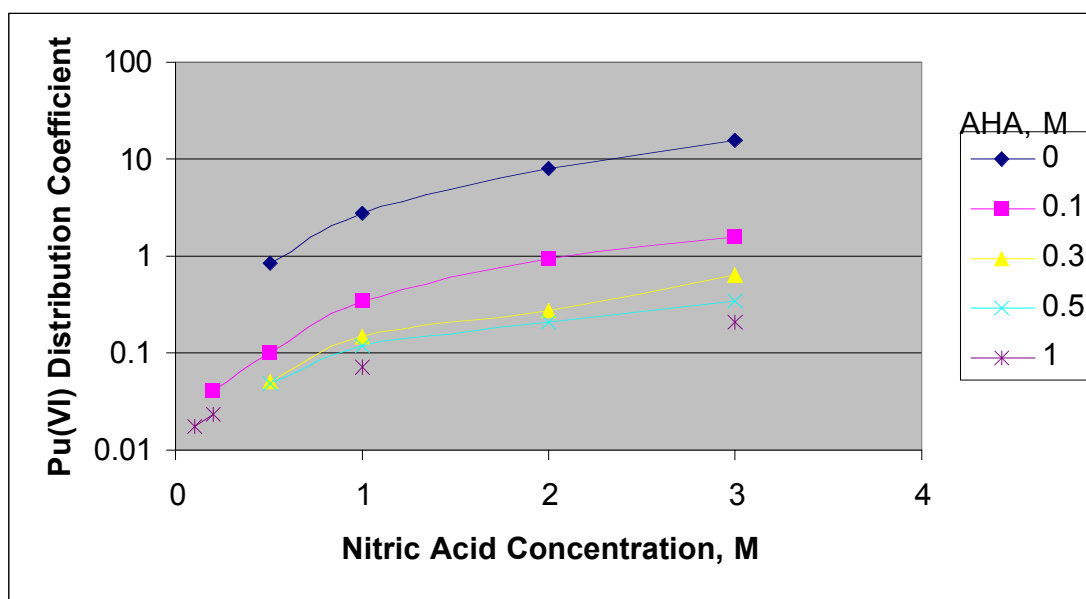


Fig. 48. Pu(IV) distribution at different HNO₃ and AHA concentrations.

Similar data were collected at 0.5 and 1 M HNO₃ with addition of 2 M NaNO₃. Table 9 shows the distribution of Pu(IV) in the various solutions.

Table 9. Pu(IV) Distribution from 2 M NaNO₃ at Different HNO₃ and AHA Concentrations

HNO ₃ , M	AHA Concentration, M			
	0.1	0.3	0.5	1.0
0.5	0.84	0.34	0.30	0.17
1.0	0.64	0.41	0.33	0.22

The value of 0.84 at 0.5 M HNO₃ and 0.1 M AHA is believed to be in error. Figure 49 shows a plot of the data, which emphasizes that the point is probably in error. The plot also shows that the point at 0.5 M AHA and 0.5 M HNO₃ is probably slightly high.

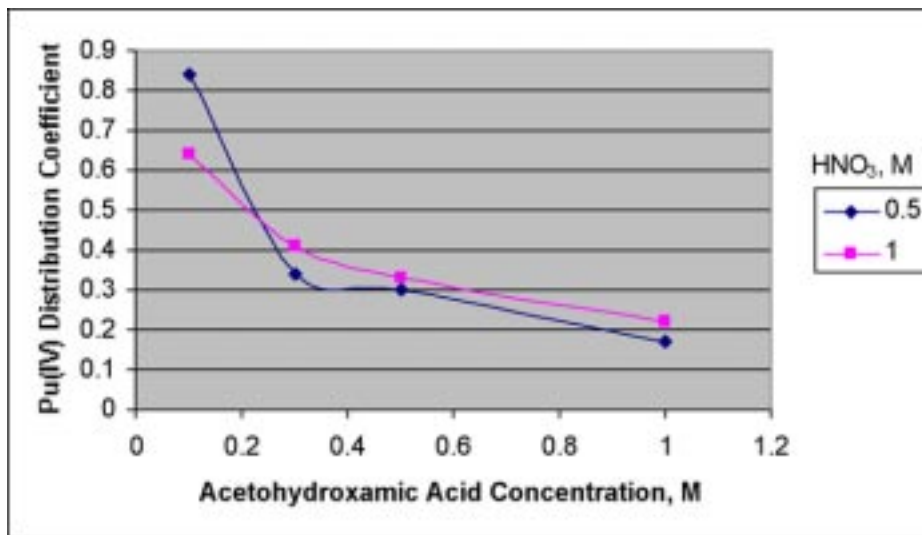


Fig. 49. Pu(IV) distribution from 2 M NaNO₃.

Plutonium Acetohydroxamic Acid Interaction

An experiment was done to look at the number of molecules of AHA complexed to Pu. The experiment was done by titrating AHA into a solution which was 1 M HNO₃ and 0.0035 M Pu(IV). The Pu solution (2.7 mL) was placed in a cuvette for spectrophotometry, eight 0.025 mL increments of 0.1 M AHA solution added, and the absorbance was measured at three different wavelengths after each addition. The AHA-to-Pu mole ratio was calculated for each addition and the data plotted in Fig. 50. The data show increasing values up to about 5 moles of AHA per mole of Pu. The absorbance at 455 nm is the most consistent, since the other wavelengths had some contribution from the ingrowth of Pu(III). The AHA is expected to be a bidentate ligand, so Pu(IV) is expected to complex only 4 AHA molecules.

The experiment was repeated at 0.5 and 2 M HNO₃ with the results shown in Fig. 51. The data for 0.5 and 2 M HNO₃ show the absorbance increasing up to mole ratios greater than 5. The data for 0.5 M is erratic at mole ratios of 1 and 2 compared to the remaining data. It is obvious from this data that the system is complex. The total time to collect data for all 8 points is about 45 minutes. Significant hydrolysis of the AHA can occur in that time, especially at 2 M acid.

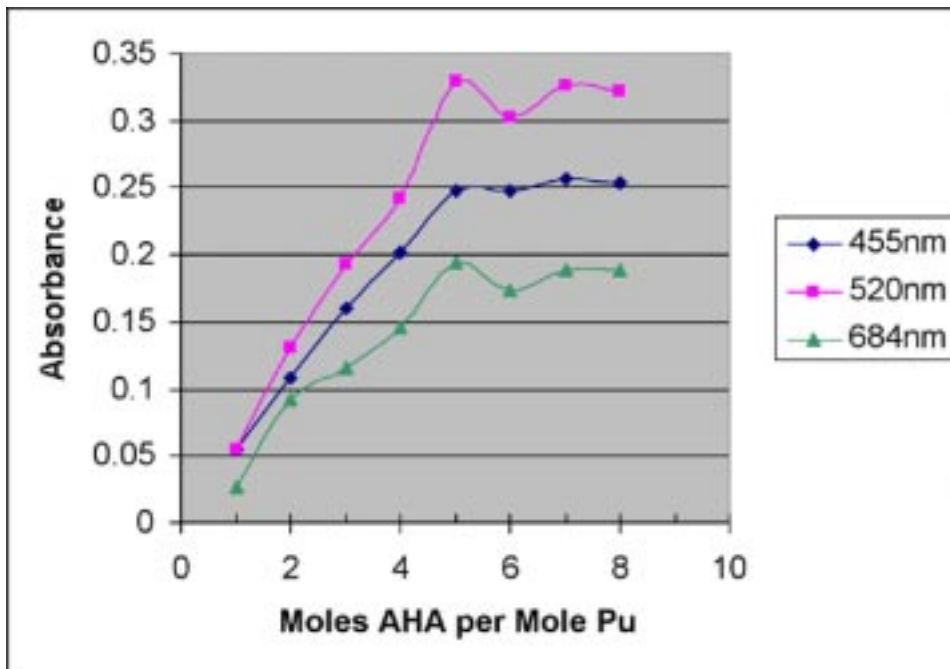


Fig. 50. Absorbance of the Pu-AHA complex at three wavelengths.

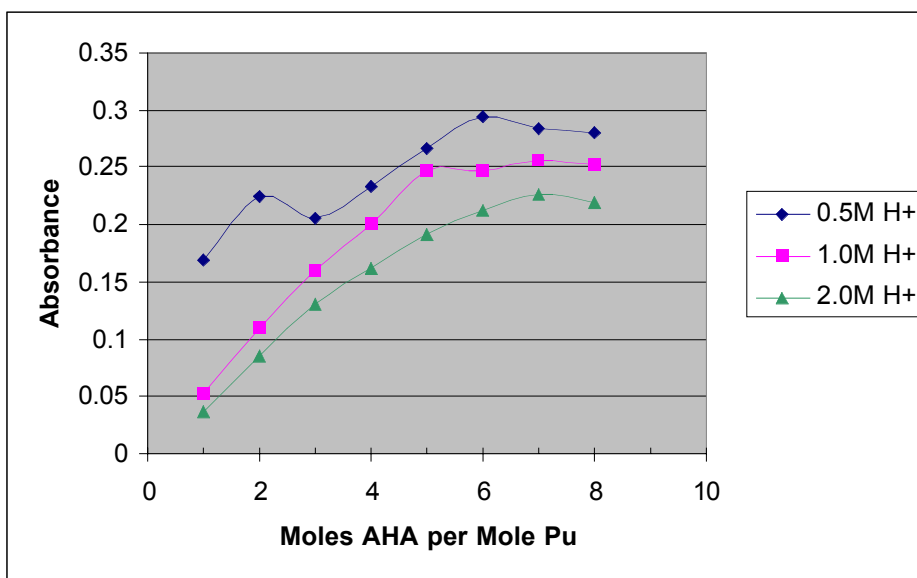
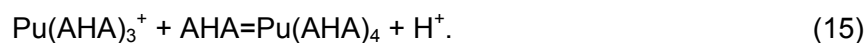


Fig. 51. Absorbance of the Pu-AHA complex at 455 nm.

The average increase in absorbance at 1 and 2 M HNO₃ is essentially linear with each AHA addition, but the fourth addition is 73% and 62%, respectively, of the first three for 1 and 2 M acid. On the assumption that there is an equilibrium as shown,



Equilibrium constants of $K=3.4 \times 10^3$ and $K=3.7 \times 10^3$, respectively, were calculated for the reaction in 1 and 2 M acid. There is also the possibility that some of the AHA is monodentate rather than bidentate. The data in 0.5 M HNO_3 does not fit in the proposed equilibrium, possibly due to complications from hydrolysis of Pu(IV) .

Dissolution of Dresden Reactor Fuel

The hot demonstration of the UREX process will be done with solution prepared by dissolution of 3.9 kg of irradiated fuel from the Dresden power reactor. The Dresden fuel has been in storage at SRTC since the late 1970s. The fuel was examined to determine the condition and the need for further cutting of the cladding. The fuel is in three cans inside one of the shielded cells at SRTC. Two of the cans contain cladding and powder while the third can contains only powder. Figure 52 shows a picture looking into one of the cans. The fuel cladding pieces can be distinguished and some pieces appear to not have fuel in them. However, the entire length of the cladding piece was not visible.

A 6-liter glass dissolver vessel was designed which will allow 1.3 kg to be dissolved per batch. The dissolver contains a removable steel basket to hold the cladding. The dissolver will have a condenser and a means to purge the solution with air or air containing NO_x gas to remove ^{129}I from the dissolver solution. A caustic scrubber can be attached to the offgas stream to remove ^{129}I and nitrogen oxides.



Fig. 52. Dresden fuel can.

Modified Direct Denitration (MDD) Demonstration

In the reference flowsheet, following the UREX step, the stream containing the minor actinides (Pu, Np, Am, and Cm) and fission products must be converted from a liquid nitrate form to a solid oxide form prior to delivery to the PYRO-A process. Direct conversion by means of the modified direct denitration (MDD) process is planned. This process was developed for the conversion of uranyl nitrate solutions to UO_3 to provide an oxide powder with acceptable ceramic properties for fabrication of nuclear fuel pellets. The ceramic characteristics of the oxide produced by the MDD process have been found to be similar to that produced by the ammonium diuranate (ADU) precipitation/filtration/calcination process and to be significantly improved when compared to the low-density, hard glass shards produced by early thermal denitration processes. While not yet proven, it is believed that the actinide and fission product oxides produced from the modified direct denitration process would also have better ceramic properties than similar oxides produced from other precipitation processes. The effects of the ceramic properties in the pyrochemical processing may be of no consequence; however, the properties could be important in the handling and transfer of the materials, i.e., uniform free-flowing powders, as feeds to the PYRO-A process.

Testing of this process in a lab-scale rotary furnace is planned. The initial testing will be with nonradioactive simulants, followed by installation of the unit in a glove box and testing with the actinide elements Pu and Np and simulated fission products. If these tests prove successful, the equipment could be moved into a hot cell for further testing with additional actinides (Am, Cm, Np, and Pu) and actual fission products.

A conceptual design of the test unit has been prepared based on a unit used for the development of the MDD process for U and a larger (1 kg/h) U demonstration unit operated at ORNL. The design parameters were established to keep the equipment sizes and operating parameters appropriate for glove box operation. A simplified schematic of the unit and the operating parameters is shown in Fig. 53.

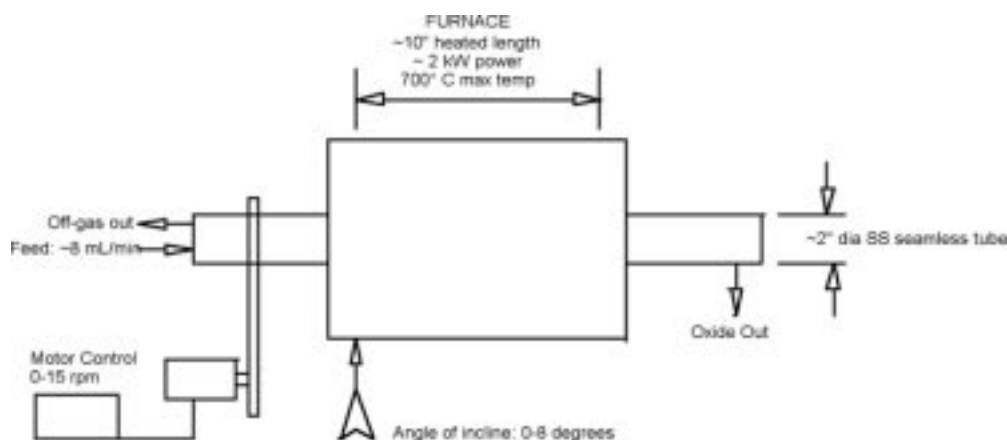


Fig. 53. Schematic of conceptual MDD unit.

The ends of the tube will be equipped with rotating seals to prevent the release of the offgas or powder into the glove box. The offgas will be routed through a scrubber for the capture and analysis of potentially volatile actinides or fission products. A vendor is currently reviewing the design for possible fabrication. During the fabrication

process, batch testing will be conducted with simulants to determine appropriate metal/ NH_4 ratios for testing in the rotary furnace.

Sodium Iodide Production from Molten Salts

The purpose of this work is to demonstrate and develop a method for scrubbing iodine-containing gases (e.g., I_2 , HI, or CH_3I) from fuel processing offgas streams via reaction and dissolution in molten salts. Specifically, the iodine-containing gas stream is bubbled through molten NaOH where it reacts and enters the molten salt as iodide. The phase diagram of the NaOH/NaI system indicates that at sufficiently high iodine concentration, NaI will precipitate as a relatively pure solid phase as the melt is cooled. A pure NaI precipitate has advantages from the point of view of later processing (i.e., transmutation).

The task to be performed is to experimentally demonstrate the efficacy of iodine trapping by molten NaOH and to demonstrate the NaI precipitation suggested by analyses of the phase diagram. Thermodynamic analysis of baseline gas processing scenarios will also be carried out. Since other gases that could react with NaOH may also be present in offgases from fuel processing (e.g., CO_2 , NO_x , H_2O), their interaction with the molten-salt system will also be evaluated.

Experimental Work

Preliminary experimental work was aimed at examining the freezing behavior of mixed hydroxide/iodide molten salts. The general procedure was to prepare a mix from the pure ingredients, melt it in a glassy carbon or graphite crucible under an inert atmosphere (He), and then cool the melt according to a predefined, controlled temperature program. Post-experiment examination was conducted by visual and photographic examination of the crystalline material and by titration of the hydroxide content of various subsamples of these materials.

A few scoping experiments were conducted using the KI/KOH system. In all cases, the salt, after melting and refreezing, visually showed two phases distinct in their crystal morphology. Acid-base titration of subsamples of the two phases were done for two of these experiments and indicated enrichment of hydroxide in one phase and depletion in the other, though not complete separation. In one run, which had been carried out at higher temperature for longer duration, an apparent solid sublimate appeared well above the molten-salt level. Titration results indicated that hydroxide was not present (i.e., that the solid was pure KI).

The NaOH/NaI system is the one of primary interest. The most recent experiments being made are on this system. Following blank runs using pure NaOH or NaI, two experiments were run on mixtures. The first showed crystal morphology differences in the salt similar to those observed for the potassium system. Titration indicated enrichment of hydroxide in one of the phases, though not complete separation. No effort was made, however, to separate NaI from the melt as cooling progressed (e.g., by “drawing” a crystal from the melt). A second NaOH/NaI experiment also visually showed two distinct phases after freezing; titration has not been performed on subsamples of those phases as yet.

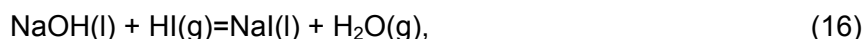
Glassy carbon crucibles appeared to be reasonably resistant to the molten hydroxide/iodide salts studied in these experiments. Since these were in short supply, some of our experiments were carried out in crystalline graphite crucibles. These were resistant to pure iodide salts, but leaked slightly when exposed to hydroxides.

We have ordered and received a supply of glassy carbon crucibles for further experiments.

The iodine content calculated from simple acid/base titration of salt samples dissolved in water assumes that no material is present other than the hydroxide and the iodide salts. The presence of water, CO₂, or metals (e.g., from the gas sparge tube) would be interpreted as iodide. To obtain a more direct measure of iodine content, we are in the process of assembling the capability to do iodine analyses via selective ion electrode methods. Upcoming experimental efforts will be directed at the trapping of iodine from the incoming vapor stream.

Thermodynamic Analyses

Preliminary thermodynamic analyses were carried out using the commercial thermodynamics software package HSC (ver. 4.1). These calculations were done to analyze the equilibria in simple reactions relevant to scavenging of iodine-containing compounds with molten sodium hydroxide. For example, in the reaction



the equilibrium lies very strongly on the product (right-hand) side of the equation, indicating that little HI(g) should escape the melt (at equilibrium). Similar calculations for other potential gaseous components of fuel processing offgases (I₂, CH₃I, H₂O, CO₂, NO₂, and NO₃) suggested all but water would be scrubbed by the molten hydroxide at reasonable operating temperatures (500°C–750°C). In particular, iodine in any form should, per these analyses, be captured with high efficiency by the melt. Calculations using this single-reaction technique are simple to perform but may overlook critical reactions which might have less favorable outcomes. Further, the single-reaction technique does not capture solution effects or the interaction of other components. HSC is capable of generalized equilibrium calculations (calculations in which the equilibrium of all components of the system is calculated regardless of the route to equilibrium). Unfortunately, HSC is not able handle the effects of solution non-ideality.

Phase diagrams are available in the literature for binary mixtures of the sodium salts of primary interest (e.g., OH⁻, CO₃⁼, NO₃⁻) and for some of the binary mixtures of these anions with anions of secondary interest (O⁼ and NO₂⁻). All the binary phase diagrams suggested that non-ideal solution effects would be important in assessing stability of solid phases and partial pressures (gaseous) of components in the system. No information was found for ternary, quaternary, or higher mixtures of these sodium salt mixtures. Since plausible compositions of gases to be treated may include more than simply H₂O and iodine-containing gases, multi-component thermodynamic analyses incorporating non-ideal solution effects are needed.

A second commercial thermodynamic software package, ChemSage (ver. 3.1) is capable of performing generalized chemical equilibrium calculations incorporating non-ideal solution effects in multi-component solutions. This program contains an extensive database of thermodynamic properties of inorganic compounds, including most of those needed for this molten-salt work. The ChemSage database does not have non-ideal solution parameters, however. Binary non-ideal solution parameters were therefore determined by (a) assuming regular solution behavior, then (b) adjusting the non-ideal solution parameter values until (c) critical phase diagram characteristics such as eutectic temperatures and melting points matched published phase diagrams. Thermodynamic data were not available in the ChemSage database

or standard references for a few intermediate compounds shown on phase diagrams (for example, $3\text{NaI} \cdot 2\text{NaOH(s)}$ from the NaI/NaOH phase diagram). In such cases, the necessary thermodynamic data were estimated and adjusted so that the melting point in ChemSage calculations matched the melting point plotted on the corresponding published phase diagram.

The result of this effort is a data set that is capable of approximately duplicating the phase diagram behavior in all the available published binary phase diagrams. A common first order approximation to treating ternary and higher multi-component non-ideal solutions is to simply use the binary interaction parameters, ignoring higher terms. Within the constraints of this approximation, we now have a data set for ChemSage capable of analyzing any gas-scrubbing scenario involving the components previously mentioned. We would envision such an analysis computing the iodine fraction escaping the molten salt, the partitioning of iodine between NaI (or other solid compounds) during cooldown, and the precipitation of other solids from the melt. At present, no such analyses have been carried out other than for the binary hydroxide/iodide system.

SANEX Process Studies

In the TRISO spent fuel-processing flowsheet, an actinide/lanthanide separation step must be used to prepare the Am and Cm for transmutation. The European community studies have focused on a number of new reagents for accomplishing trivalent actinide (An(III))/trivalent lanthanide (Ln(III)) separation. The desire of this study is to develop a system that selectively extracts An(III) over Ln(III) from an aqueous nitric acid feed solution and avoids some of the drawbacks of these types of processes such as precipitation, third-phase formation, difficult pH control, and reagent loss due to radiation damage or solubility. The process for accomplishing this separation, SANEX, has utilized several classes of reagents as the development progressed. A review of the European work in this area was made and promising results were noted for two of the SANEX processes in particular. Further study of these systems was proposed. The SANEX-III process utilizes a bis-triazinylpyridine compound and SANEX-IV utilizes a dithiophosphinic acid compound. Both processes have shown promising results for $\text{An(III)}/\text{Ln(III)}$ separation in an acid range of 0.5 to 1.0 M HNO_3 , however, both exhibited problems with interfering elements that would be present unless a separate pretreatment process is included.

Some of the early work in this area utilized a commercial reagent, CYANEX 301, which showed promising results with purified reagents and in synergistic systems with tributyl phosphate, trioctylphosphine oxide, and other similar compounds. The SANEX-IV reagent is a variation of this commercial compound but designed to increase the acidity of the ligand so that it would extract in a lower pH range. The reagent, bis(chlorophenyl)-dithiophosphinic acid, is not available commercially and must be synthesized. A diphenyldithiophosphinic acid reagent is available commercially and a sample was acquired for initial testing to determine satisfactory techniques and analysis schemes for testing the other SANEX extractants. Researchers in the Chemical Sciences Division (CSD) at ORNL were requested to review the synthesis of the bis(chlorophenyl)-dithiophosphinic acid compound and prepare a nominal 100-g batch of the reagent for performing solvent extraction tests. The purity of the initial batch of material was in the 98% range so a sample was recrystallized and a 45-g batch of >99% purity has prepared for initial testing. Recovery and further purification of the remaining reagent will follow. An

actinide/fission product feed sample from the processing of irradiated target material containing Am, Cm, and their associated fission products has been identified for use in the initial testing, and an experimental plan for testing the An(III)/Ln(III) separation at various acid conditions and in combination with other synergistic compounds is being developed.

After the recovery and purification of the remaining dithiophosphinic acid reagent the CSD group will focus on the preparation of the SANEX III reagent, 2,6-bis(5,6-*n*-propyl-1,2,4-triazin-3-yl)-pyridine. The synthesis of this reagent will be more difficult in that some of the starting compounds must also be synthesized. The testing of this compound, if successfully synthesized, will follow the SANEX IV extractant testing.

Alternative Fuel Treatment Process Development

TRISO Spent Fuel Reprocessing

Head-End Spent Fuel Disassembly/Oxide Dissolution

An effort is underway to evaluate the various options for the processing of TRISO-coated spent-fuel particles imbedded in graphite-block fuel elements to recover and recycle the actinide elements. The main goal is to study early work in the field and to propose some innovative options. The different process options will be ranked based on their technical merit and maturity, relative costs, and waste generation. As a result of these studies, a technical plan will be developed to further analyze two or three of the highest rated options and to prepare proposals to address technical needs and to reduce the technical risks. Additionally, the TRISO fuel-reprocessing plan will be incorporated into the ORNL/GA GT-MHR Fuel Development Plan.

Figure 54 shows a cross-section of an entire fuel element. The hexagonal fuel block contains about 3000 TRISO fuel compacts. Each compact is a cylinder, 2 inches long and 0.5 inches in diameter (Fig. 55), and is comprised of TRISO-coated fuel particles embedded in a graphite matrix. The actinide loading of TRISO fuel particles in the compact ranges from 15% to 30%. At present, the plans call for a 15% loading for the driver fuel and 30% loading for the transmutation fuel. The Pu/Np driver fuel and Am/Cm transmutation fuel are simultaneously present in the fuel block in different channels according to an elaborate fuel design.

A common feature of all practical processing schemes will be the removal of the compacts from the fuel element block. This will require precision boring of the top and bottom of each channel in the spent fuel blocks and the use of push rods to release the compacts from each channel. Each fuel type, driver, and transmutation might be processed separately or a decision can be made to reprocess only the driver fuel component. Either way, the first step is to remove the fuel compacts to be processed from the fuel block. The fuel blocks, along with any portions of the compacts that will not be processed, will be disposed as a waste.

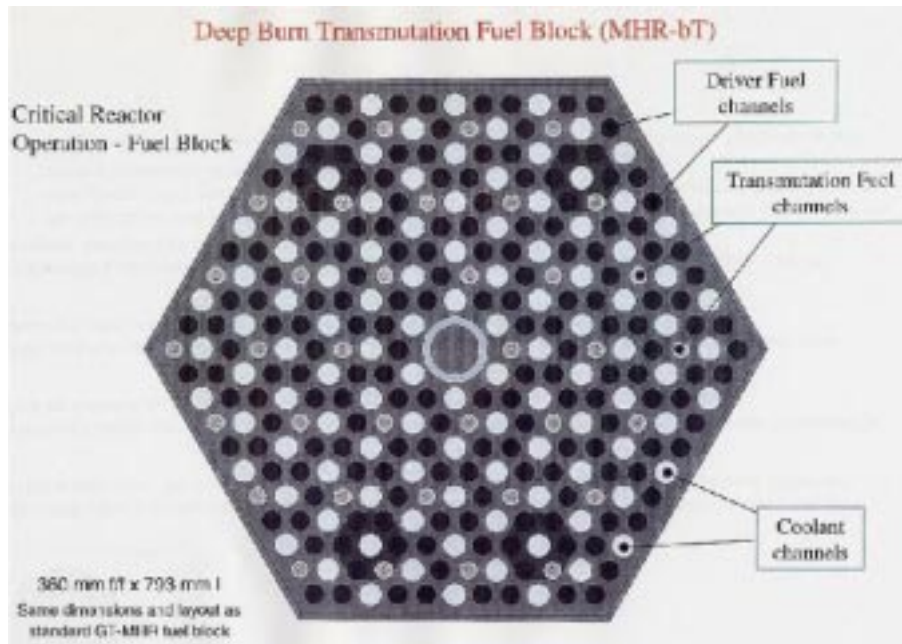


Fig. 54. Cross-section of a GA fuel block.



Fig 55. TRISO fuel compacts.

Figure 56 depicts a cutaway view of a TRISO fuel particle showing the fuel kernel surrounded by a layer of porous graphite followed by successive layers of pyrolytic carbon, silicon carbide and finally an external pyrolytic carbon layer. Table 10 shows the estimated percentages of metal oxide, carbon, and silicon carbide in the individual fuel particles and compacts. As shown, about 90% of the weight of each fuel compact is carbon and only 2% to 4% is the heavy metal-oxide that will be recovered.

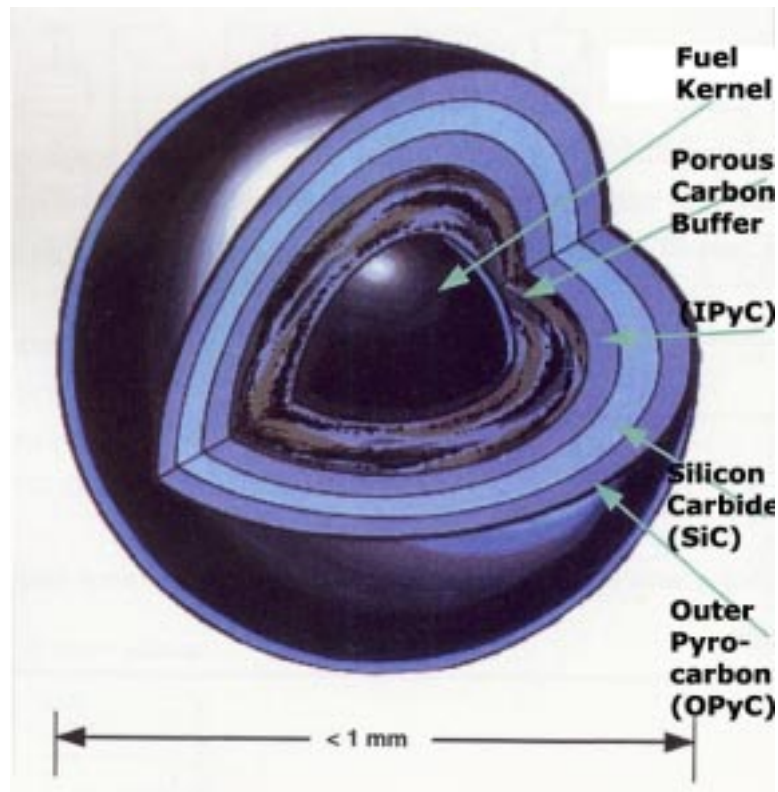


Fig 56. Cutaway view of a TRISO fuel particle.

Most methods reported in the literature involve burn-crush-burn-leach operations to remove the carbon, open the SiC shells, and burn the inner carbon layers prior to nitric acid leaching. Variations of this general method range from whole-block burning to dry mechanical separation of the coated particles before crushing and burning. Chemical methods to remove the coating were also identified, including dissolution of the SiC in acids or alkali, dissolution in fused salts, and a burn-fluorinate-burn method that uses limited fluorination to target the SiC shell. Figures 57–58 show the wide range of treatment possibilities identified.

During the irradiation, the carbon that constitutes the great majority of the spent fuel will grow significant amounts of ^{14}C . Regulations will prohibit release of the carbon to the environment, e.g. as CO_2 . Accordingly, the management of the carbon will constitute one of the most important considerations in the processing of the fuel. Because of the great importance of adequately dealing with the carbon, several companies specializing in carbon and graphite were contacted to probe the possibility of utilizing their expertise. In particular, the UCAR Carbon Company Inc. appears to be a very promising collaborator. The UCAR Company appears to possess many elements of the technology needed to better process the TRISO fuels. During an initial conference call with the UCAR R&D staff, it was determined that UCAR might be very helpful in providing support related to the crushing, grinding and milling of the compacts, physical separation of the carbon fraction, and acid leaching and filtering. A nondisclosure agreement is being formalized to get detailed information from UCAR to fully evaluate the technologies already available that may be applied to carbon management related to TRISO-coated fuel processing.

Table 10. Estimated Fractions of Materials in Compact

Layer	Material	Dimensions (μm)		Density g/cm ³	Volume cm ³	Mass (g)	Wt%	Wt% in Compact
Kernel	Metal oxide	300	(dia)	11	1.41E-05	1.56E-04	23.8	7.1
Buffer layer	Porous carbon	150	(thick)	1	9.90E-05	9.90E-05	15.2	4.6
	I-PyC	Pyrolytic carbon	35 (thick)	1.85	4.44E-05	8.21E-05	12.6	3.8
	SiC	Silicon carbide	35 (thick)	3.2	5.47E-05	1.75E-04	26.8	8.0
	O-PyC	Pyrolytic carbon	40 (thick)	1.85	7.65E-05	1.42E-04	21.7	6.5
Subtotal						6.53E-04	100.0	30.0
Compact	Carbon Filler	Packing Factor		0.3		1.52E-03		70.0
TOTAL						2.18E-03		100.0
	Metal oxide					1.56E-04	7.1	
	Carbon					1.85E-03	84.8	
	SiC					1.75E-04	8.0	
TOTAL						2.18E-03	100.0	

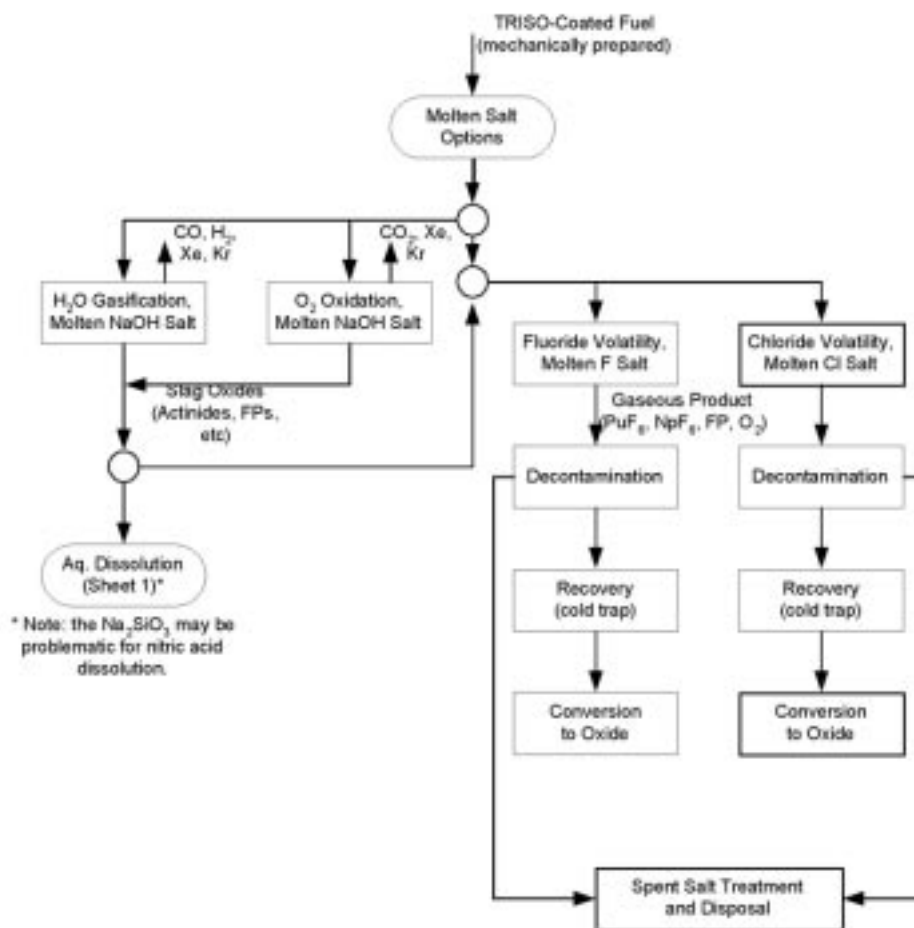


Fig. 57. TRISO-coated fuel-processing options, 1 of 2.

As a result of the initial interaction with UCAR, a preliminary head-end flow sheet was developed. This head-end process should precede and apply to any process scheme. As shown in Fig. 59, the TRISO fuel compacts would be separated from the fuel blocks, the compacts would be initially crushed but the fuel particles would remain largely intact. A physical separation based on particle size and density (e.g., cyclonic separation) would separate a significant fraction of the carbon used to agglomerate the individual particles into a compact (70% to 85% of the total). The fraction that contains the TRISO particles would be further milled to smaller particles so that the SiC layer would be broken. Again, the material would be physically separated according to particle size and density. The concentrated heavy metal-oxide fraction would then be ready for processing. The amount of carbon to be removed by this head-end operation is yet to be determined; however, it is clear that the initial separation step will be very crucial to the entire operation.

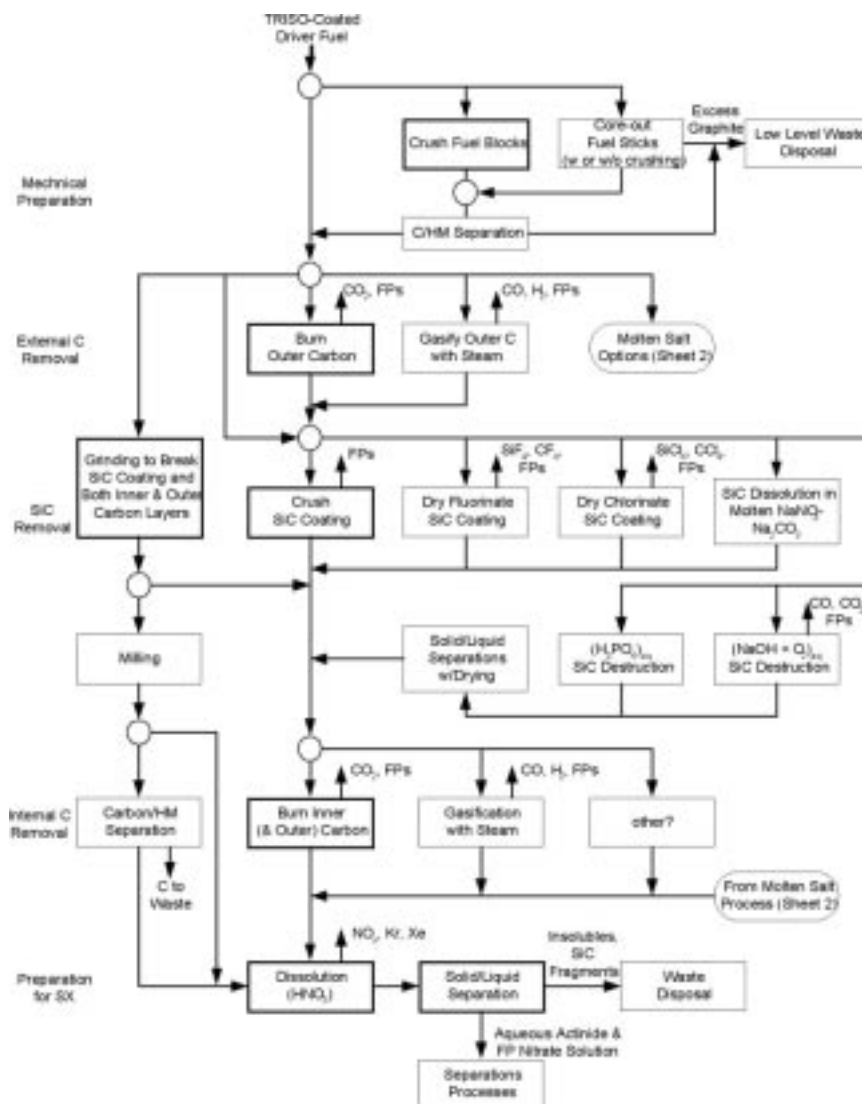


Fig. 58. TRISO-coated fuel-processing options, 2 of 2.

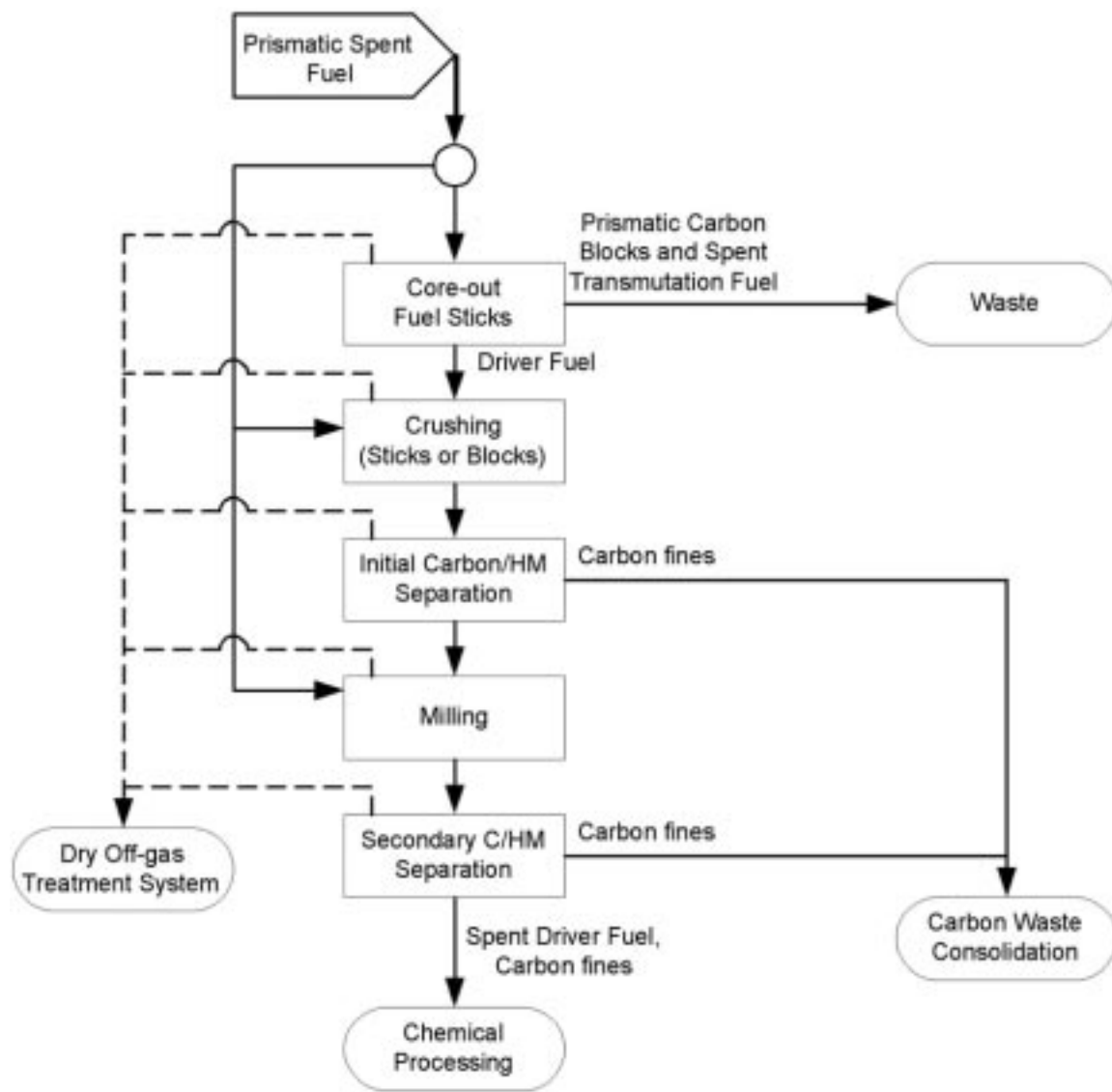


Fig. 59. Head-end processing options.

After the head end, several processing options can be envisioned. In particular, we are analyzing two promising options. The first is based on acid leaching and the second is based on carbon chlorination. The acid leaching scheme is shown in Fig. 60 and includes two leaching steps, followed by washing and drying. The washing solution is mixed with concentrated nitric acid to make-up the second acid leaching step that is then further used for the primary leaching step, resulting in essentially a two-stage countercurrent leaching process. The leachate would be used as the starting material in conventional solvent extraction processing.

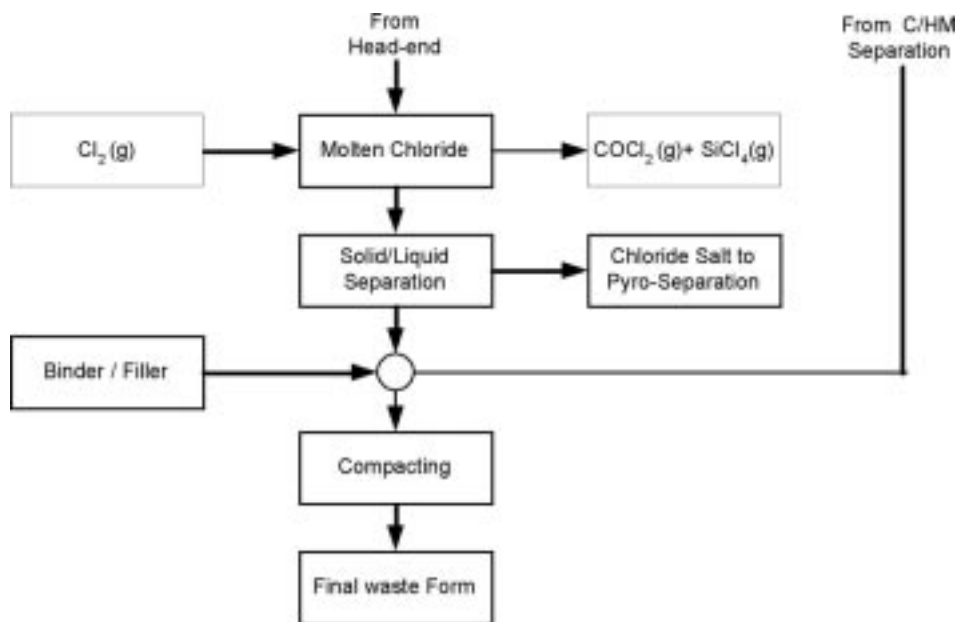


Fig. 60. Direct acid leaching flowsheet.

In the carbon chlorination option (see Fig. 61), the concentrated heavy metal fraction is fed into a molten chloride bath along with chlorine gas. The chlorine would react with the metal oxides and a small fraction of the carbon to transform the oxides into chloride salts, e.g., $\text{MO}_2 + 2\text{C} + 4\text{Cl}_2 = \text{MCl}_4 + 2\text{COCl}_2$. The COCl_2 , along with the SiCl_4 that would be produced by reaction between the chlorine and SiC , would need to be trapped (e.g., using NaOH). One crucial step in this process is the separation of the excess carbon from the molten salt. Once separated, the chloride molten salt can be processed using some of the already developed pyroprocessing schemes.

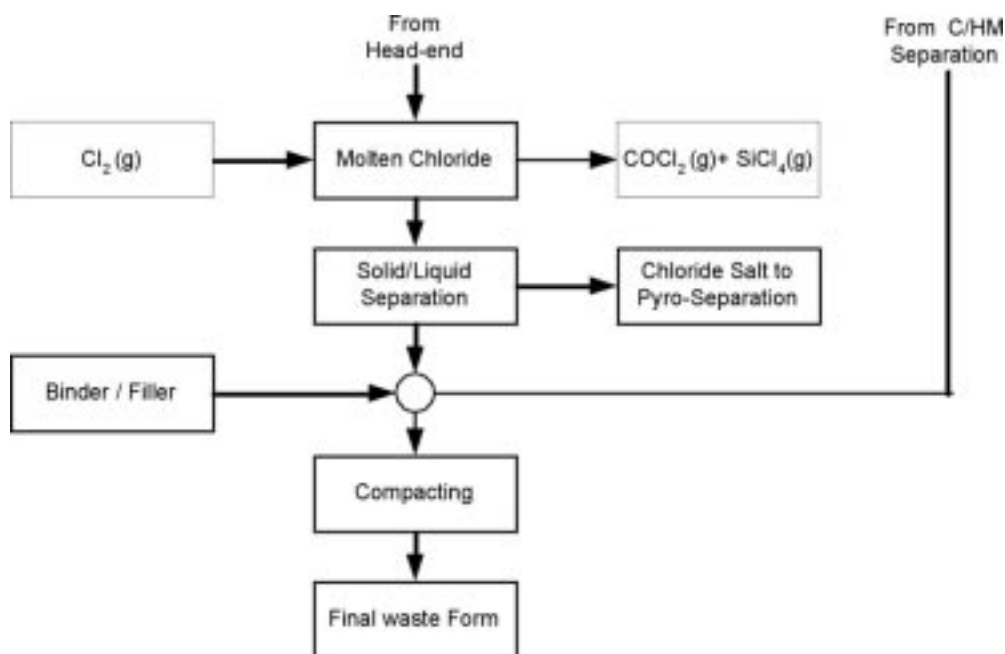


Fig 61. Carbon chlorination flowsheet.

Waste Form Development – Ceramic Waste Form from LiCl Salt System

The ceramic waste form production process, as previously developed for the disposal of a LiCl-KCl-based ($T_m=355^\circ\text{C}$) waste salt, calls for blending dehydrated zeolite 4A with ~10 wt% waste salt at 500°C for 20 hours. The waste salt from the oxide reduction process is LiCl-based ($T_m=613^\circ\text{C}$). The higher melting point involved necessitates a higher blending temperature, and the stability of zeolite 4A under these conditions is in question.

An experiment addressing this problem has been performed where 270 g of dehydrated zeolite 4A granules and 30 g of LiCl powder were placed in an alumina crucible. Under constant mechanical stirring, the mixture was heated up to 650°C , held at temperature for 20 h, and allowed to cool down. Two samples of the resulting material were examined by XRD (see Fig. 62). The bulk of the material appears to have the structure of zeolite 4A with no LiCl present. However, a number of diffraction peaks consistent with the presence of faujasite can be clearly seen. The consequences of this novel phase formation to waste form performance will be evaluated by producing a ceramic waste form using the blended material.

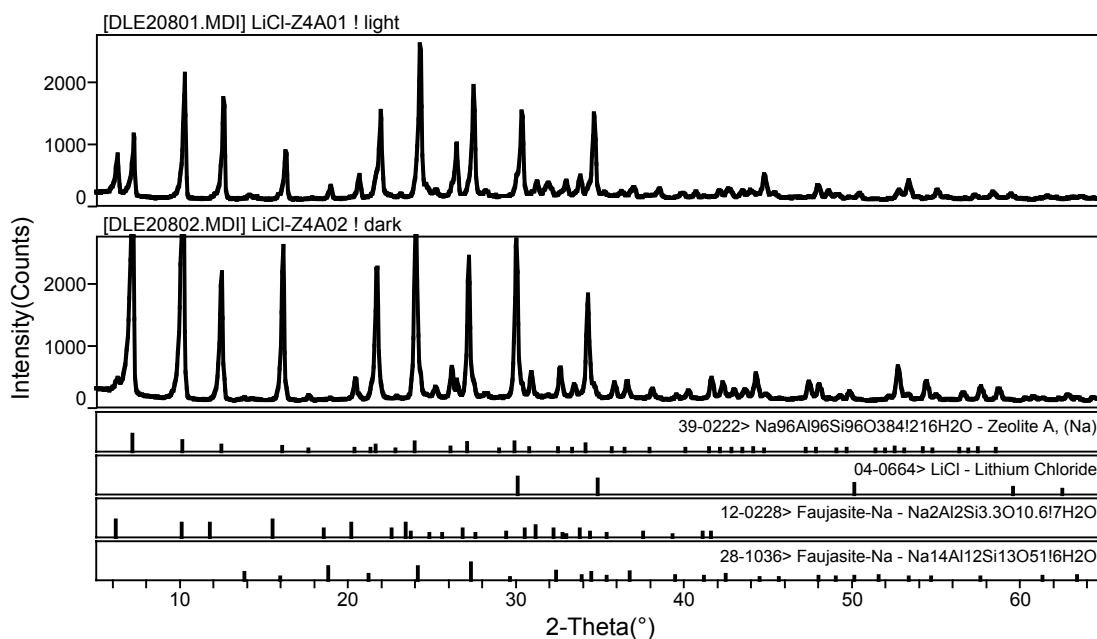


Fig. 62. Powder x-ray diffraction patterns of zeolite blended with LiCl.

Additional insight into the processes occurring in mixtures of LiCl and zeolite 4A upon heating will be investigated by simultaneous DSC/XRD at the APS on March 7, 2002. Mixtures to be studied will contain 30 wt% LiCl corresponding to complete occlusion. This method will yield data pertaining to the correlation of thermal and structural changes in the zeolite upon occlusion.

3. TRANSMUTATION SCIENCE

Transmutation science research is divided among seven major categories:

- Integration and Analytical Support
- Materials
- Lead-Bismuth Eutectic (LBE) Technology
- Irradiation Experiments
- High-Energy Physics
- Reactor Physics
- International Support
- LANL-Sponsored University Projects

The quarterly progress in each area is presented in the subsections that follow.

3.1 Integration and Analytical Support

The major objective of the integration and analytical support activities is to define and implement a consistent research plan for transmutation science.

Scope

Integration and analytical support activities include project management and integration of activities under transmutation science. The specific technical scope includes the following:

- Implement/maintain the 10-year research plan for transmutation science (experiments and supporting analyses);
- Maintain and coordinate international work packages (DOE international coordination agreements) relevant to transmutation science topics;
- Assist AAA Program management in generating other international collaboration work packages in transmutation science; and
- Participate in safety and hazard control plan (HCP) reviews for project experiments.

In general, analytical support tasks involve defining and designing the experiments, defining the test requirements and the data quality objectives, and converting the test data into technology readiness input. Defining and designing experiments involve scaling analyses, assessment of the facility limits and parametric ranges, and comparing those to the technology development needs. During this process, the specific requirements for tests as a function of a Technology Readiness Level (TRL) also are defined in terms of data quality objectives (with emphasis on accuracy requirements). Generated data must be analyzed and assessed in terms of TRL achievements and used to define design parameters or the need for supplementary and complementary tests. Specifically, tasks include:

- Integration of the Weapons Neutron Research (WNR) facility gas production test results with Blue Room neutron-yield results to map out buffering effects;
- Assessment of the data provided through international collaboration in terms of its impact on the TRL and definition of US experiments;

- Input to international test plans; and
- Completion of LBE-Na compatibility experiments begun in FY01.

Highlights

- The initial draft of the Transmutation Science 10-year R&D plan was issued and reviewed by DOE and the task leaders. The plan is currently being revised based on the comments.
- The remaining tests in the test matrix for the LBE-Na compatibility experiments were completed.
- We participated in the MEGAPIE technical review meeting held in Bologna, Italy. In subsequent conversations with task leaders, we identified a number of areas for US support tasks to MEGAPIE.
- We organized the Third International Workshop on Utilization and Reliability of High-Power Proton Accelerators to be held in Santa Fe, NM, on May 12–17, 2002. The workshop is commissioned by the OECD Nuclear Energy Agency (NEA).

Transmutation Science R&D Plan

This draft document presents the research and development (R&D) plan for the high-energy physics, spallation targets and materials portion of the accelerator driven transmutation program. The plan covers the proof-of-principle phase of the research program spanning from FY01 through FY10. The planned research is divided into four general categories. The general categories and the major issues covered under each category are as follows:

- High-Energy Physics:
 - Improvements, benchmarks, verification and validation of the high-energy physics codes
 - Cross-section measurements and evaluations up to 100–150 MeV neutron energies
- Materials:
 - Structural properties of materials exposed up to 100 dpa and helium-to-dpa ratios ranging from 1 to 100 appm
 - Thermal fatigue limits
 - Maintenance of an International Materials Handbook
 - Development of a structural design criteria
- Lead-Bismuth Eutectic Technology:
 - Liquid metal corrosion and corrosion control strategies
 - Thermal-hydraulics performance
 - Instrumentation development
 - Chemical thermodynamics (impact of spallation and impurities)
 - Liquid-metal embrittlement (with and without radiation)
- Target Technologies:
 - Compatibility of target and multiplier coolants
 - Dose-conversion factors for the spallation and activation products

The main research objectives of the proof-of-principle phase are as follows:

- Verified and validated high-energy physics codes via the use of separate effect and integral effect experiments;
- The definition of the performance envelop for the materials and the coolants including achievable flux and fluence limits and limits on thermodynamic and thermal-hydraulic parameters; and
- Demonstration of the spallation target operations with the essential support systems at ~1-MW beam power.

To achieve these objectives, even though the resolution strategy includes both experimental and analytical studies, the strategy relies heavily on separate-effect and integral-effect experiments. In general, the required experimental facilities exist to complete the proof-of-principle phase of the research. However, one essential facility, which is a test station at the end of the LANSCE beam, requires major upgrades and improvements. This facility must be available by 2006 to achieve the stated research objectives. The research roadmap, in terms of the experimental facilities needed to complete the proof-of-principle leading up to proof-of-performance in an Accelerator-Driven Test Facility (ADTF) by FY10, is summarized in Fig. 63.

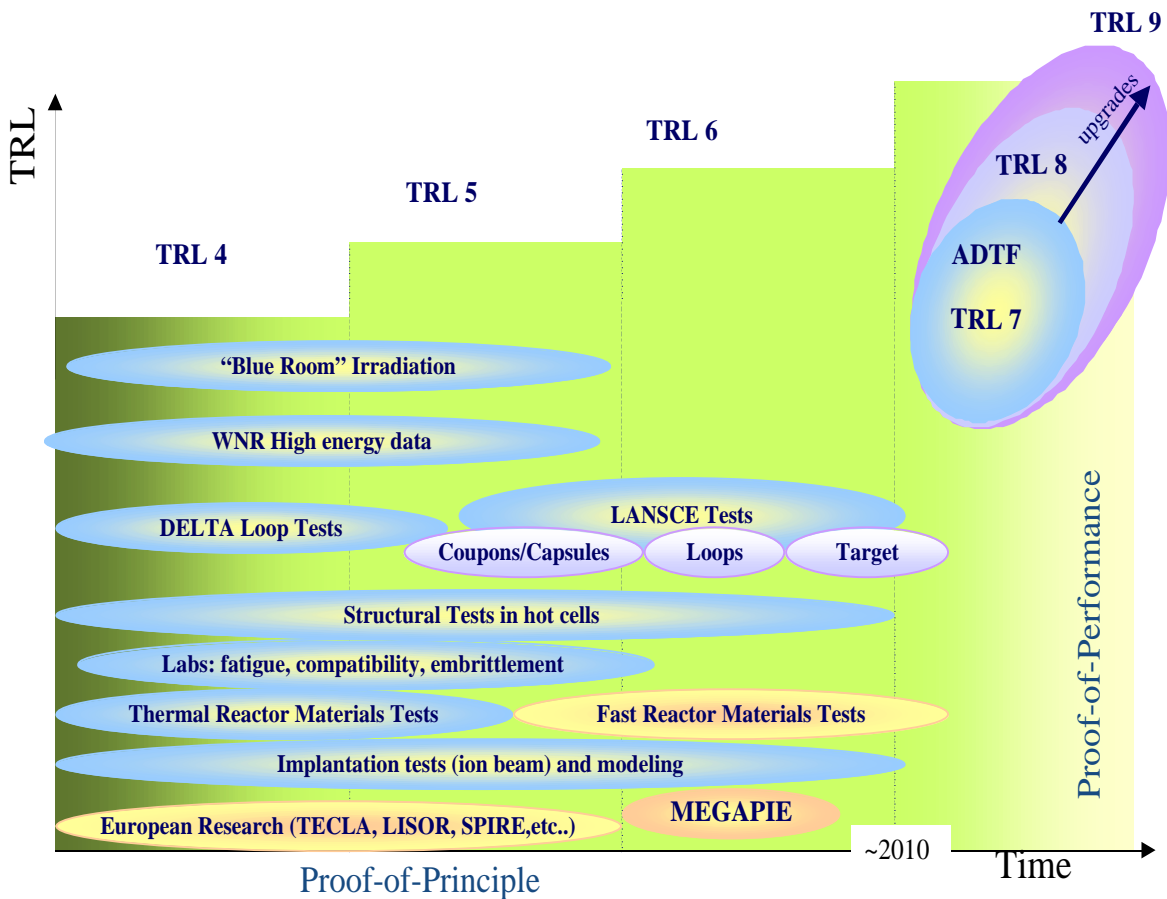


Fig. 63. Summary of the R&D plan.

An initial estimate for the budget required to achieve the stated research objectives is provided in the report. In developing the budget estimate, considerable credit is taken for the ongoing international collaborations with the French CEA and the MEGAPIE initiative in Europe. Additional collaboration opportunities also exist, which may result in further savings in the upcoming years. The budget estimate also includes considerable funding for university participation in programmatic research.

LBE-Sodium Compatibility Experiments

For transmutation scenarios where an LBE target is used inside a Na-cooled subcritical blanket, the compatibility of the two coolants are of interest in the event of accidental mixing of the coolants. A less likely scenario where the two fluids can be used together is when a Na-bounded metallic fuel is deployed inside a LBE-cooled blanket. A more detailed description for the experiments was provided in the previous quarterly report. In this second quarter, we completed the remaining few tests. The complete test matrix and the results are summarized in Table 11.

Table 11. Test Matrix for LBE-Na Compatibility Experiments

Test Date (YMD)	Initial Temp (°C)	Injection Speed (Area)	Sodium Volume (cm ³)	Heavy Metal		Max. Temp Increase (°C)
				Injection Material	Volume (cm ³)	
011023	600	Fast (2 cm ²)	50	Pb	2.5	110
011026	600	Fast (2 cm ²)	50	Bi	2.5	285
011102	600	Fast (2 cm ²)	50	LBE	2.5	165
020208	600	Slow (2 mm ²)	50	LBE	2.5	150
011018	400	Fast (2 cm ²)	50	Pb	2.5	115
020215	400	Fast (2 cm ²)	50	Bi	2.5	225
020212	400	Fast (2 cm ²)	50	LBE	2.5	235
011120	400	Slow (2 mm ²)	50	LBE	2.5	310
011115	200	Fast (2 cm ²)	50	LBE	2.5	60
020206	200	Slow (2 mm ²)	50	LBE	2.5	20

The temperature spikes typically occurred at the bottom of the mixing chamber and within one second of the injection. The magnitude of the temperature increases were generally consistent with pretest calculations, and showed that a stronger exothermic reaction resulted from the bismuth than the lead, with the LBE predictably in between. Exothermic reactions were observed at all temperatures and both injection rates. The temperature increase during the 200°C tests was immediate but without a noticeable spike as in the higher-temperature tests. This may have been because the reaction occurred higher in the crucible. However, in analyzing the peak temperature data, one must remember that those are obtained by discrete thermocouples and it is difficult to assume that the initial reaction always occurs where the thermocouple is located. The most meaningful data would be the equilibrium temperatures, which are being calculated as detailed analyses of the discrete thermocouple data continue.

An unexpected result was the temperature rise measured in the three slow-injection tests, which lacked consistency. This may have been caused by not all of the heavy

metal being injected into the Na and possibly the overall inhomogeneity that occurs when mixing small volumes of materials.

Preliminary examination of the post-test mixtures indicated the gritty texture of the reacted Na. The product did not form large particles at any of the temperatures or at either injection rate, but rather formed a very fine submicron-sized particulate that explains the grittiness of the reacted Na. Additional examination of these materials will continue.

MEGAPIE Technical Review Meeting

We attended the MEGAPIE technical review meeting, which was held in Bologna, Italy. In addition to participating in this meeting, we visited the ENEA/Brasimone facilities where considerable LBE research is being conducted, as well as the Paul Scherrer Institute (PSI) in Switzerland where we met with task leaders to identify efforts that can be performed in the US as part of the MEGAPIE support. The major highlights of these meetings are as follows:

- MEGAPIE is making good progress; however, the irradiation schedule is moved up to 2005, with a beam current of only 2 mA.
- Additional US support to MEGAPIE is requested in the areas of neutronics, thermal-hydraulics, and materials irradiation.
- An international working group is proposed to address the LBE technology development. Specifically, the group will address the issues of oxygen control standards, probe calibration standards, corrosion testing and data analyses procedures. A 3–4 year deliverable of a parametric performance envelope, including material selections, is envisioned. The US side will draft the charter for the working group for review among the parties (presently thought to include AAA, ENEA-Brasimone, CEA, and FZK).

Analytical Support for LBE-Target Experiments

Much progress was made in analysis of the neutron yield from the thick Pb-Bi target (Section 3.4). The counting of the 14 stacks of activation foils was completed, with many of the significant foils counted more than once to verify isotopes with decay information. Most of the counting in this period was performed to sample the longer-lived isotopes.

The beam history data for the Blue Room irradiation and the Target-4 irradiation were assembled to create the production histories of the isotopes from their measured activities using the BCF program. The group of foils placed in Target-4 were analyzed with STAYSL and compared to the known spectrum in that location (Fig. 64). Based on those initial results, a “best fit” spectrum was determined based on the isotopic results that fit the known spectrum extremely well.

As part of this process, numerous evaluations and additions of cross-section data have also been made to the STAYSL package, including additions of Bi and Tb (n,xn) reactions.

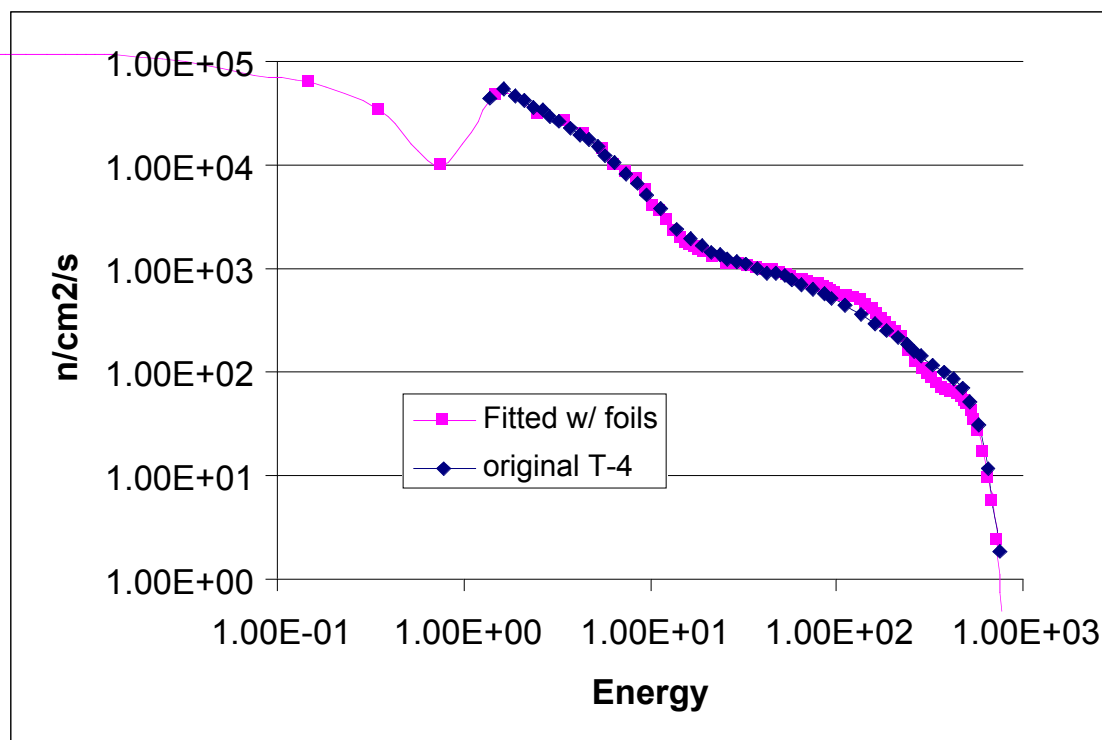


Fig. 64. Preliminary results of Target-4 foil analysis.

3.2 Materials

The major objective of the materials activities is to test and quantify materials properties under proton and neutron irradiation.

Scope

The major activities in this area are continuation of the high-temperature testing of irradiated materials, irradiation test plans, collaborations with the Paul Scherrer Institute (PSI) materials program, and updating and maintaining the *Materials Handbook*. Specifically, testing in hot cells will support the AAA Program by determining the mechanical properties of structural materials at prototypic temperatures after irradiation in a proton beam. This will involve testing some materials irradiated at LANSCE at low temperatures and testing materials irradiated at PSI at high temperatures. The following are the activities in support of this mission:

- Receive and test irradiated rods from PSI;
- Order and install a high-temperature furnace for performing mechanical tests on specimens in vacuum or argon at temperatures up to 700°C;
- Perform bend tests at 300°C, 400°C, and 500°C on F82H, 9Cr-1Mo, and SS-316L;
- Perform compression tests on W at 600°C;

- Perform mechanical tests on Ta at high temperature;
- Continue high-temperature testing of 9Cr-1Mo at PNNL;
- Complete and publish new chapters of the *Materials Handbook*, including 9Cr-1Mo, W, Ta, Hg, LBE, and corrosion on various steels;
- Prepare an irradiation test plan (mostly in reactors) for cladding duct materials; and
- Review the reactor irradiation database as applicable to transmutation.

Work in the materials area has been curtailed due to budget uncertainties.

Highlights

- LANL hot-cell activities at the CMR Building resumed after the facility upgrade activities were completed.
- Members of the materials team attended a workshop in La Jolla, CA, sponsored by DOE/NE on high-temperature materials for Generation IV nuclear reactors.
- Two drums containing 150 APT TEM specimens have been returned to LANL from PNNL as part of the agreement that LANL would handle any future examination and disposal of APT specimens. One drum containing APT tensile specimens has also been returned to LANL as part of the same agreement.
- A Pb shielding container was placed inside of a certified type-A 55-gallon drum and shipped to PSI for transporting the SINQ-irradiated material to LANL.
- An order for a high-temperature furnace for performing mechanical tests on irradiated materials at temperatures up to 700°C in argon in a hot cell was placed with Materials Research Furnaces.

PNNL Activities

Transmission Electron Microscopy – One-hour aging treatments at 300°C, 400°C, and 500°C have been performed on unirradiated and irradiated Mod 9Cr-1Mo and SS-316L in preparation for TEM examination of these materials.

Shear Punch Testing – Shear punch tests have been performed at 300°C on SS-316L irradiated to 9.7 dpa and 1.7 dpa. These results will be compared to results from tensile tests performed on SS-316L irradiated to similar doses.

Technology Transfer – Further development has been performed on a tensile test system, which can be used for tensile testing of delicate S1 tensile specimens. This work represents a revision to a system that was previously designed and tested at PNNL and transferred to LANL.

Russian Efforts – The second of three data installments on irradiation creep, void swelling, and embrittlement of Russian ferritic/martensitic steels EP-450 and EP-823 was received from the IPPE laboratory in Obninsk, Russia. This report concentrates on data from the range 305°C–335°C, temperatures unobtainable in Western reactors, to doses as high as 89 dpa. These data are being analyzed at PNNL and

will be combined with earlier data at higher temperatures. When all three data sets are available, a combined report will be submitted to AAA.

Materials Handbook

A new contract relative to efforts on the *Materials Handbook* was put into place and work immediately resumed. Meetings held at LANL determined the following:

- All activities scheduled in support of the handbook for the remainder of CY02 were considered acceptable;
- Data and information necessary for sections to be modified or added to the handbook were collected; and
- The review process and reviewers for the various necessary draft sections were identified.

Major additions scheduled for the handbook in the near-term involve chapters on T91 ferritic/martensitic steel, Pb-Bi eutectic, the Russian ferritic/martensitic steel EP823, and Ta. Additions are also planned to existing chapters on W (strength data for irradiated material), SS-304L and SS-316L (corrosion data), Al-6061-T6 (corrosion data), and Alloy 718 (corrosion data). The status of these activities is as follows:

- The T91 chapter from the Coordinator is more than 80% complete;
- The chapter on Pb-Bi is being prepared at PSI;
- The chapter on EP823 is being prepared by PNNL;
- The chapter on Ta is the responsibility of FZJ;
- Drafting of sections of Chapter 19 on 9Cr-1Mo-V ferritic/martensitic continued at ANL.

3.3 Lead-Bismuth Eutectic Technology

The major objective of LBE research activities is to develop a fundamental understanding of LBE performance parameters and measurement techniques when used as a nuclear coolant, with primary emphasis on spallation-target applications.

Scope

LBE Technology Development

The safe and reliable implementation of the LBE technology requires additional developments for the oxygen sensors. Development of other nonintrusive flow measurement and online corrosion measurements would significantly improve the reliable operations of an LBE target. The development will be carried out in collaboration with international partners (e.g., CEA and FZK) under DOE agreements. By collaborative testing, the objective is to achieve in 3–4 years a TRL-4 level where a parametric (velocity, temperature, materials, thermal gradients, etc.) is developed to Pb into the spallation-target conceptual design.

The scope of this work package involves developing new sensor technologies and corrosion data analyses with the long-term objectives listed above. Some of the actual tests will be performed in the DELTA Loop (Materials Test Loop) at LANL, and

testing must be closely coordinated with loop-operation work-package activities. The FY02 activities are as follows:

- Fabricate oxygen probes to be tested in the DELTA Loop;
- Develop a calibration standard in conjunction with international partners;
- Cross-calibrate oxygen sensors;
- Develop gas and solid-phase oxygen control methodology;
- Develop concepts for low-temperature oxygen probes;
- Develop ultrasonic laser velocimetry technique;
- Analyze corrosion data;
- Develop and design components for FY03 testing (with international collaboration); and
- Revise the DELTA Loop test plan according to international collaboration work packages.

DELTA Loop Operations

The DELTA Loop will be operated to validate key Russian LBE nuclear-coolant technology, to perform corrosion and thermal-hydraulic testing, and to develop diagnostics and probes for application in a high-powered spallation-target system. Again, the tests will be carried out in collaboration with international partners.

The scope of this work package involves operating, maintaining, and upgrading the DELTA Loop in accordance with the long-term objectives listed above. The actual test plans will be developed under the LBE technology work package, and operations must be closely coordinated with activities under that work package. The FY02 activities are as follows:

- Completing construction for operational and instrumentation testing;
- Addressing all post-start findings;
- Performing operational tests;
- Testing oxygen control techniques and procedures;
- Updating data acquisition and control (DAC) system and hazard control plans for unmanned operations;
- Installing new instruments (e.g., improved oxygen sensors and ultrasonic velocimetry) as delivered from the LBE technology team; and
- Performing 1000-hr corrosion tests (two different materials and/or two different velocities).

Highlights

- During the second quarter, the DELTA Loop was operated for a total of 35 hours for operational testing.

LBE Technology Development

We designed the hydrogen and steam gas-mixture system for gas-phase oxygen control and calibration of oxygen sensors to support the DELTA Loop operation and

the international collaborations. It consists of a gas flow-control manifold, a steam generator, a gas-mixing chamber, and RGAs for measuring compositions. Two RGAs were calibrated to measure hydrogen, helium, and oxygen to levels of a few parts per billion in mass concentration. Gas supply and system purity was tested. It was concluded that the residual oxygen levels in helium, although too high if directly used in LBE, should not affect the gas-mixture system's control of the oxygen level in LBE.

The mass flow valves and controller for the oxygen control system have been procured and received, and the reaction pressure vessel for mixing gases and steam is being constructed.

Two oxygen sensors were installed in the DELTA Loop. During one operation when the loop temperature reached 370°C, the sensors read approximately 0.12 V, the appropriate emf for oxygen saturated LBE (cover gas helium contains sufficient residual oxygen) at temperatures based on thermodynamic analysis. The signals were very steady. Some improvement is being made to the freeze-plug in the gas injection line. Once the gas control system is fully operational, additional oxygen sensors will be installed.

One team member visited PSI, FZK and CEA Saclay. Collaborative projects were discussed. Preliminary agreement on a joint test plan with CEA, detailing defined test conditions, was reached. A DELTA Loop test plan for FY02 was drafted based on discussions with the international partners and is being reviewed. The test matrix will contain materials for engineering tests (MEGAPIE candidate materials) and scientific investigations to understand LBE corrosion and protective oxide growth and repair mechanisms.

A water flow channel was set up to calibrate the ultrasonic Doppler system as part of the function.

Also, a Lattice Boltzmann Method was coded to simulate flow instabilities that may occur in MEGAPIE target coolant flow. Some results for two-dimensional test cases were obtained. It is now being adapted for corrosion modeling.

DELTA Loop Operations

During the second quarter DELTA Loop was continuously upgraded in preparation for unmanned operations and to improve ease of use, data quality and loop reliability.

Three additional pressure transducers were installed: one in the gas volume of the calibration tank, another in the Pb-Bi just before the main heating section, and a third in the cleaning gas inlet line. The pressure-transducers' signals were wired to the Data Acquisition and Control (DAC) program.

Two oxygen sensors were installed in the loop. Also, oxygen and hydrogen gas were connected to the loop cleaning gas system. Additionally, two heating zones were separated, allowing for better electrical load balance on the heaters' solid-state relays and better control.

A differential pressure-transducer was installed on the enclosure wall to measure pressure difference between the inside and outside. A heater was installed and connected to the DAC system, and all hand valves were marked.

The Data Acquisition and Control program was upgraded to improve user interface, control reliability, and functionality. The DAC program was upgraded for new

instruments and additional heaters and to incorporate suggestions collected during the first run cycle. A high-impedance electrometer was procured for the magnetic flow meter (its reading was connected to the DAC), and the DAC program was continuously upgraded to fulfill SCRAM conditions requirements.

In the second quarter of FY02, the DELTA Loop was operated for a total of 35 hours. The loop was run with a uniform temperature distribution and with the heat exchanger. Maximum temperature was 375°C. Maximum flow rate was 7.6 m³/hr or 33.5 gpm (3.8m/s in a 1-inch test section).

We conducted SCRAM conditions tests. Most of these conditions caused proper response from the control system. As the DAC program was modified for better SCRAM response, additional SCRAM tests were conducted.

Oxygen sensors provided readings expected for the loop conditions. The readings were stable. We calibrated the magnetic flow meter. The calibration results are shown in Fig. 65. The linear dependence of the flow rate on the measured voltage is as expected.

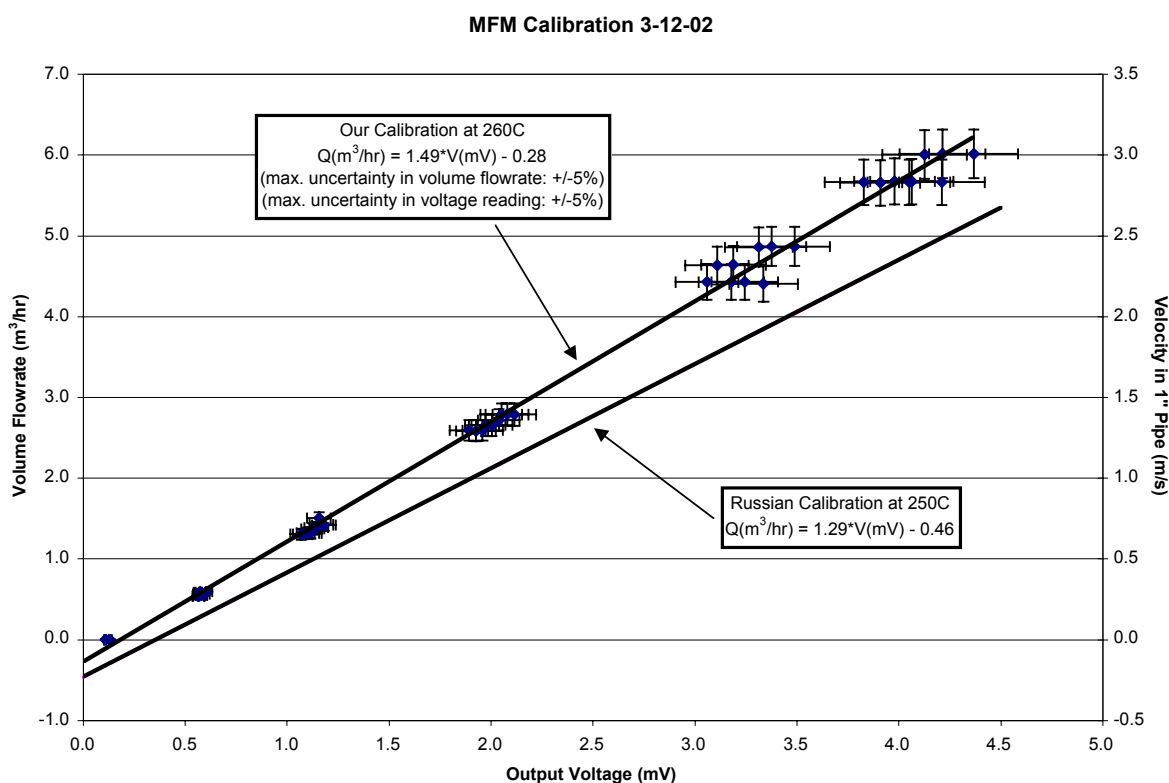


Fig. 65. Calibration results for the magnetic flowmeter.

We practiced using the cleaning gas injection system. A freeze plug that prevents Pb-Bi ingress into the gas line was melted out and gas was injected into the loop, maintaining the level of liquid metal in the injection line as needed.

We conducted a smoke test when the loop was at the highest temperature. So far, no air leaks from the enclosure were apparent.

The HCP was amended with additional considerations for Pb vapor hazards in case of a large spill. Controls already in place mitigate this hazard. The HCP and the operating procedures were upgraded for the unattended operations. We are working on these documents with the responsible safety line management.

3.4 LANSCE Irradiation Experiments

The major objective of the LANSCE irradiation experiments is to advance the TRL for transmutation in various areas up to TRL 6 by performing small-scale proton and neutron irradiation of materials to investigate various phenomena. Specific experiments to be performed in FY02 are as follows:

- Sodium activation tests;
- Neutron yield and spectrum tests;
- Helium and hydrogen production tests; and
- Corrosion studies.

Scope

Sodium Activation Tests

If a Na-cooled spallation target is used, accurate prediction of coolant activation is important for operational and safety reasons. In the summer of FY01, we performed a series of activation tests using an 800-MeV beam. Subsequent tests at other energies were postponed because of budget reduction. The FY02 activity is limited to completing the final data report.

Neutron Yield and Spectrum Tests

Spallation neutron sources create high-energy neutrons whose energies extend up to the incident proton-energy. In the design of accelerator-driven waste transmuters, the high-energy neutrons that leak from the spallation target have three practical implications:

- They dominate the shield design because they have long attenuation lengths (18 cm in steel);
- They lead to the production of source neutrons in the fuel region, which generates a spatially dependent neutron source that influences the power density distribution in the blanket; and
- They dominate the production of helium and hydrogen atoms in the steel structural elements that reside in the multiplier region near the target, while gas production limits the lifetime of structural materials near the target.

As a means of reducing gas production in structural materials in the multiplier region, a buffer region consisting of high-atomic-mass material may be placed between the target and the multiplier. This buffer attenuates high-energy neutrons that leak from the target into the multiplier. Additionally, the configuration of the buffer and the associated beam rastering parameters are variables available to the ADTF designer

for adjusting the multiplier power distribution. The objective of these experiments is to provide benchmark data for the analysis tools. The data from these tests will be combined with the gas-production test results and structural-properties test results to optimize the target and buffer design (which impacts the multiplier design). To evaluate the effectiveness of a buffer in reducing the leakage of high-energy neutrons, we propose making these measurements of high-energy neutron distributions a function of target radius.

Helium and Hydrogen Production Tests

Currently, considerable uncertainty exists in predicting the helium and hydrogen production at high energies. The objective of these experiments is to provide data to improve helium and hydrogen production cross-sections in materials near the spallation target. The data from these tests will be combined with data from spectrum tests and structural properties tests to optimize the target and buffer design (which impacts the multiplier design). Optimizing the design with large uncertainty in the design tool is not adequate and will result in a waste of time and money in the long run. Hydrogen and helium production on materials proposed for the AAA Program in the neutron energy range up to 100 MeV will be measured. Measurements of the double differential cross-sections for proton and alpha-particle emission will provide not only data for the total hydrogen and helium production by neutrons in these materials, but also data for transport of these elements by recoil into or out of zones of different composition in AAA designs. We will take the measurements for iron (Fe). As an integral test and to provide data quickly, an alloy of stainless steel such as SS-316 will also be studied.

Corrosion Studies

Liquid-metal corrosion is the major issue when LBE is used as a nuclear coolant or as a spallation target. If oxygen control is used to control the corrosion, it must be shown that stable oxide layers can be developed and maintained on the surfaces. This is affected by the initial conditioning of the surfaces, as well as changes in thermodynamic conditions during operations. For spallation target applications, we must also show that direct proton irradiation does not cause a drastic change in oxide layer properties adversely affecting corrosion rates. Finally, a more reliable operation is possible if a capability for online corrosion monitoring during actual operations can be developed for the loops. By collaborative testing, the objective is to achieve in 3 to 4 years a TRL 4, where a parametric is developed to lead into the spallation target conceptual design. The scope of this work package involves oxide film characterization, Blue Room irradiation of oxidized surfaces, and conceptual design of corrosion probes to be used in the test loop

Highlights

- A final report was issued for the Na-activation experiments.
- For the neutron yield of LBE target experiments, a preliminary report was written, the foil counting completed, and the initial neutron spectra generated from time-of-flight data.

Sodium-Activation Tests

The draft of the final report for the Na-activation tests was reviewed and comments incorporated. The document was issued as a LANL technical report, LA-13902-MS.

Neutron Yield and Spectrum Tests

Target irradiation was conducted December 1–4 (as discussed in the preceding AAA *Quarterly Report*).

A preliminary report was drafted and is being reviewed internally. Initial results from activation foil analysis and time-of-flight measurements indicate that both types of measurements produce useful results. It will take time to analyze the results and make comparisons between the two counting methods. Some preliminary findings and results are presented here.

Foil Counting

Foil counting continued throughout the quarter. The foils will be sent to the University of Michigan for additional low-background counting of the long-lived isotopes during the third quarter. A preliminary analysis has been performed using the Bi foils that were taken from the target and counted in December. The activities of the various Bi isotopes as a function of position along the target are shown in Fig. 66. It can be seen that there is a consistent trend in the results. The peak activity, and hence flux, occurs around 10 cm, which is consistent with the Monte Carlo calculations. Figure 67 shows the activities for several Bi isotopes normalized to one at 10 cm. These results indicate that the larger mass isotopes (205, 206, 207) drop off more quickly than the lower mass isotopes (199, 200, 201) as a function of axial position. This can be attributed to a hardening of the neutron-spectra further down the target. The higher-energy neutrons are more strongly forward-scattered. One possible anomaly in the results is the ^{199}Bi activity at 30 cm. The activity seem to be too high than can be attributed to a harder spectrum above 100 MeV—the threshold for the (n,11n) reaction. Figure 68 shows the measured activity of ^{207}Bi and ^{206}Bi in the bismuth (^{209}Bi) foils (normalized) in comparison to the total neutron flux above 20 MeV calculated using MCNPX (also normalized). ^{207}Bi is created from the (n,3n) reaction with a threshold of 14.42 MeV and ^{206}Bi is created from the (n,4n) reaction with a threshold of 22.55 MeV. So the thresholds are comparable to the MCNPX calculations with an energy tally boundary of 20 MeV. The measured activities are in reasonable agreement with the calculated flux, even though the activities have not been corrected for spectral variations along the length of the target. In addition, the measured activities demonstrate a consistent trend along the length of the target.

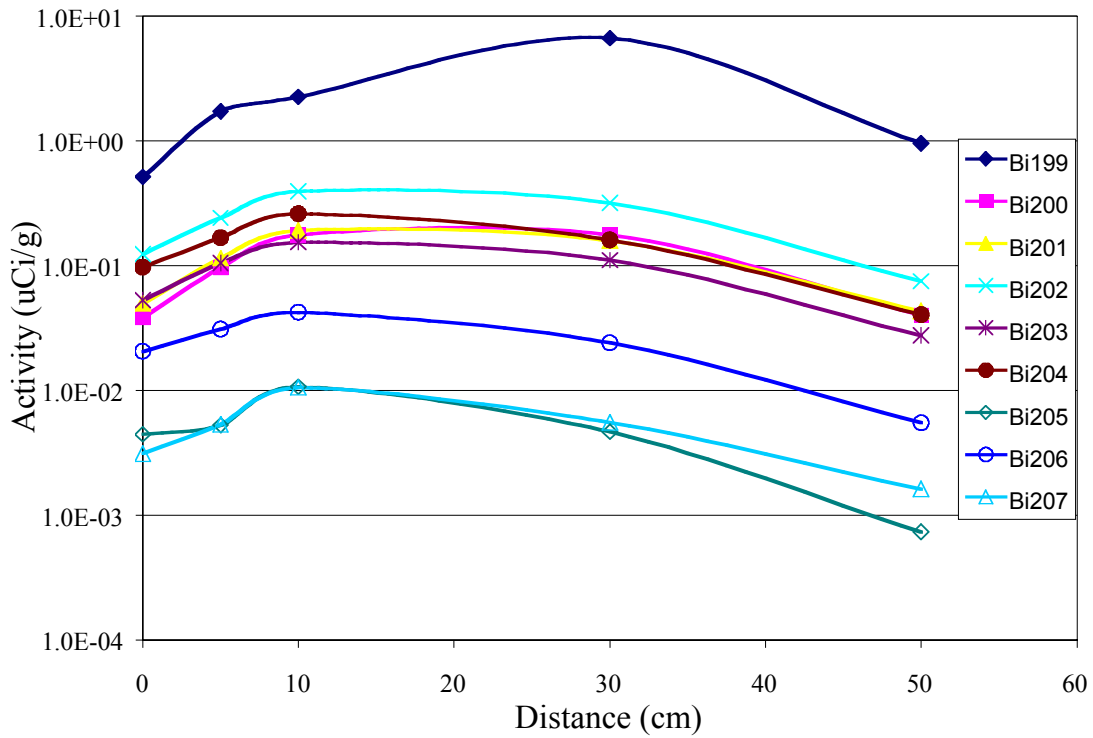


Fig. 66. The activity of bismuth isotopes as a function of distance along the target.

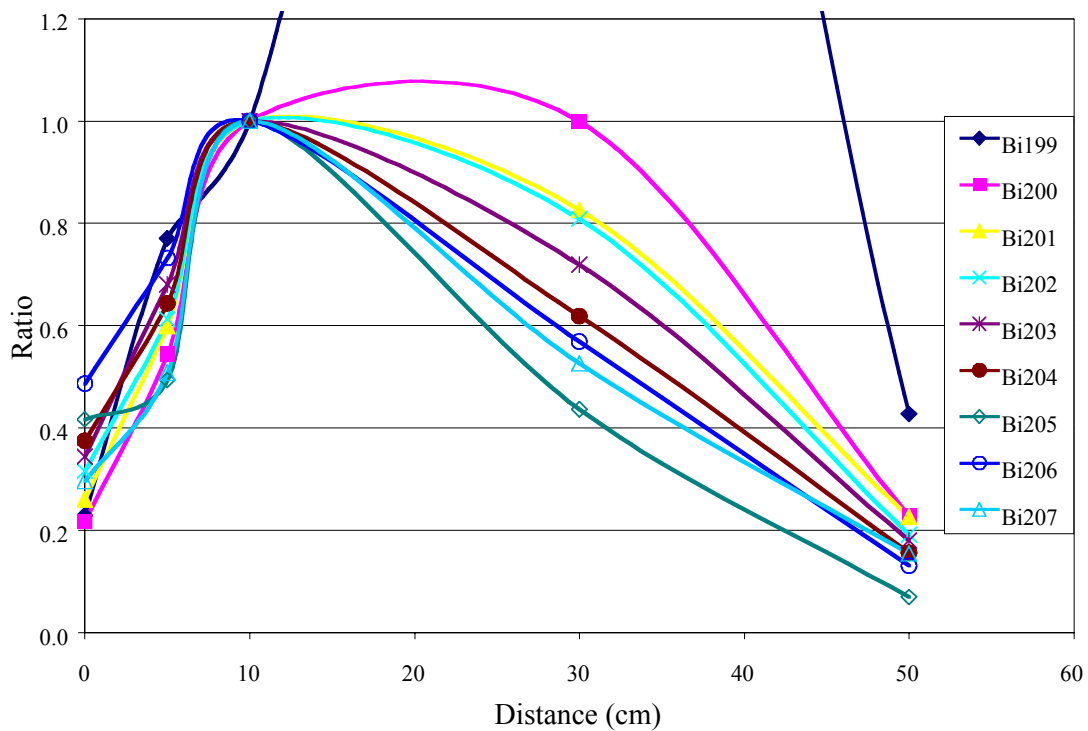


Fig. 67. The ratio of activities for bismuth isotopes normalized to 1 at 10 cm.

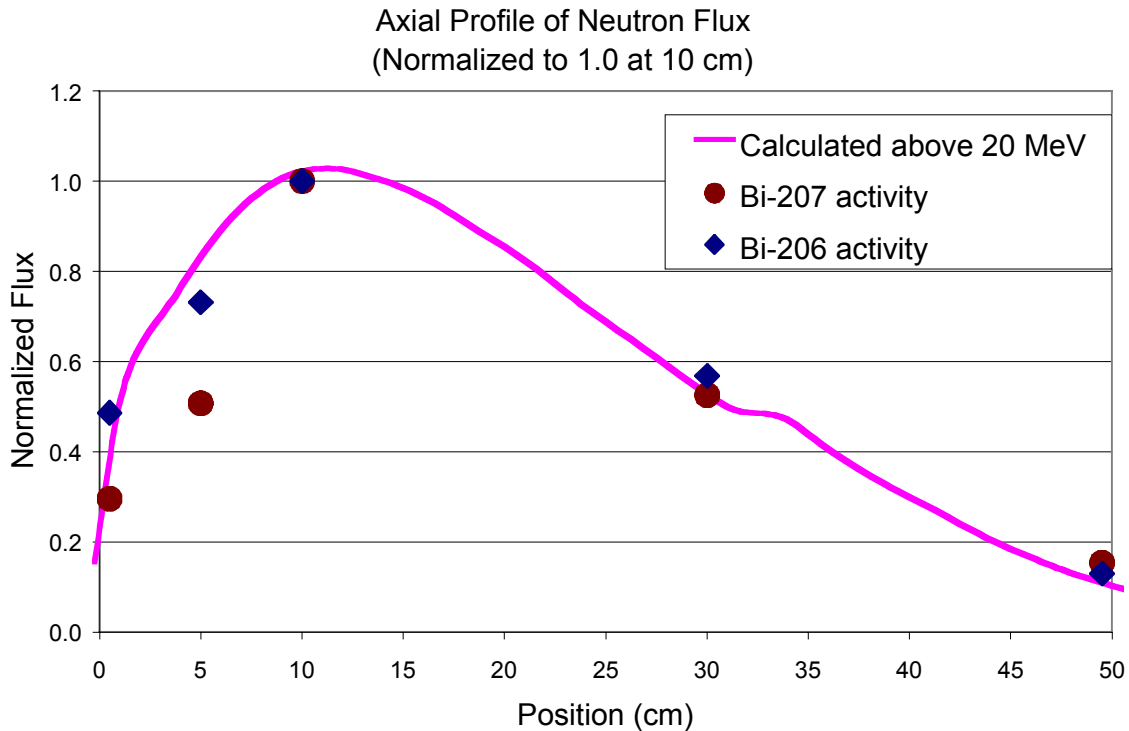


Fig. 68. This preliminary result compares measured ^{207}Bi and ^{206}Bi activities to the calculated total neutron flux at 20 MeV. Values are normalized to 1.0 at the 10-cm location.

For the time-of-flight measurements, two data acquisition sequences were performed at each of the three target positions. These target positions were with the face of the target at 0 cm, 20 cm (upstream), and 40 cm with respect to the intersection of the proton beam and flight path axes. The first data acquisition sequence used the plastic detectors to obtain data in the high-neutron-energy region (~ 0.5 to 800 MeV). This required about 1.5 hours of beam (~ 20 nA) on target at each target position and used 20 μs spacing for the beam pulses. The second sequence used the Li-loaded glass detectors to obtain data in the lower-energy region (~ 0.01 to 1 MeV). About 8 hours of beam time (~ 25 nA) were required for each target position, with a beam-pulse spacing of 40 μs .

Preliminary neutron spectra for each target position are shown in Figs. 69–71. The spectra have been generated by merging the data from each acquisition sequence (separate high- and low-energy measurements) and correcting for experimental characteristics (such as detector efficiencies, dead times, and normalization). Calculations are currently being performed and will be compared with the measurements during the next quarter.

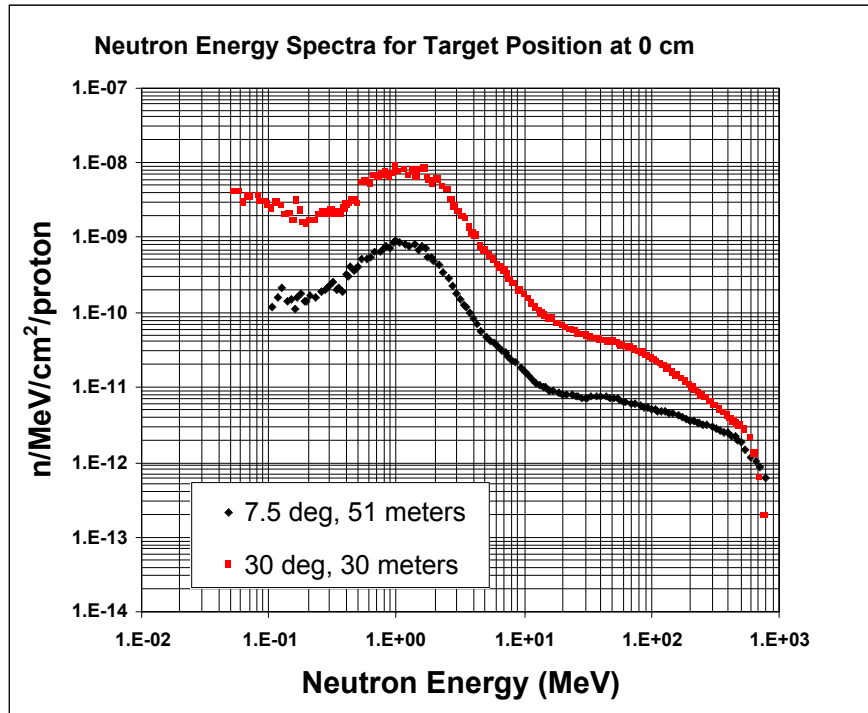


Fig. 69. Neutron-energy spectra for target position at 0 cm.

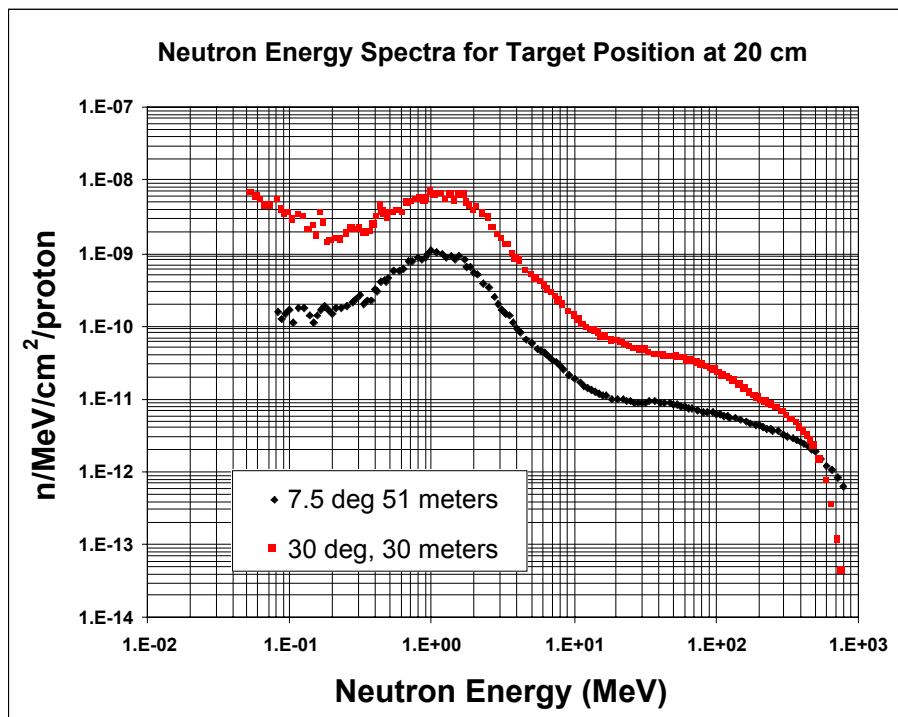


Fig. 70. Neutron-energy spectra for target position at 20 cm.

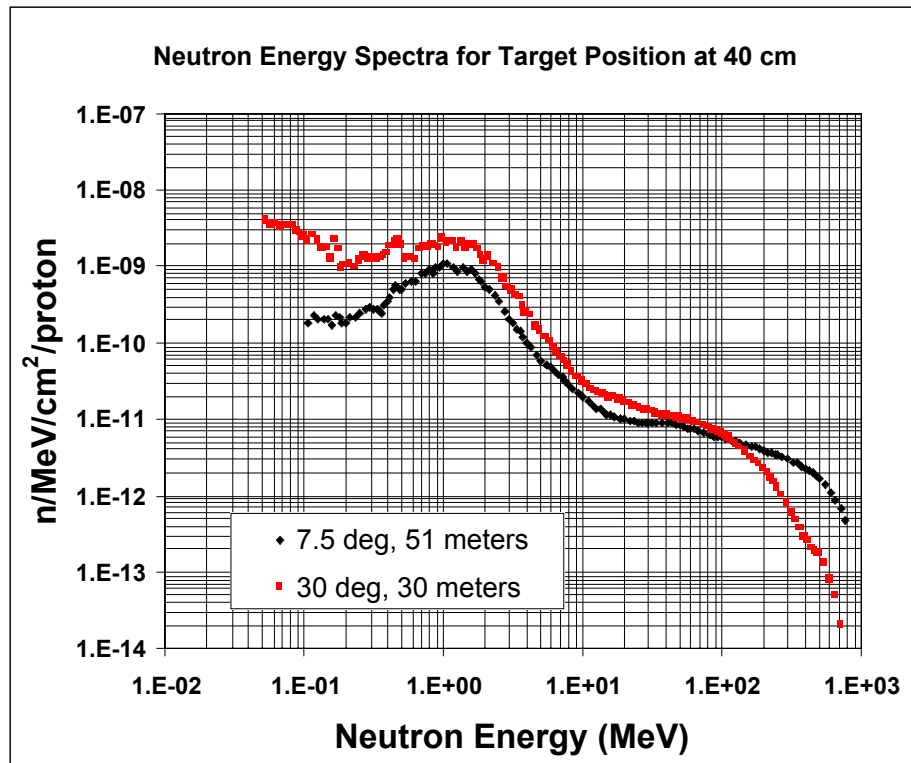


Fig. 71. Neutron-energy spectra for target position at 40 cm.

Helium and Hydrogen Production Tests

Hydrogen and helium are produced when energetic neutrons interact with materials, and these gases can lead to significant changes in material properties such as embrittlement and swelling. The goal of these tests is to measure hydrogen and helium production on materials proposed for the AAA Program in the neutron energy range up to 100 MeV, by detecting protons and alpha particles emitted in reactions induced by neutrons at the WNR/LANSCE spallation neutron source. Measurements of the double differential cross-sections for proton and alpha-particle emission provide not only data for the total hydrogen and helium production by neutrons in these materials, but also data for transport of these elements by recoil into or out of zones of different composition in AAA designs. Schematically, the measurement approach is shown in Fig. 72, where the correspondence of these microscopic measurements is made to the materials problem.

The test chamber is an evacuated chamber, 55.9 cm I.D., to accommodate the test materials and the detectors. The apparatus is located on the 30-degree right beam line at the LANSCE/WNR spallation neutron source. Detectors are coincidence counters consisting of low-pressure gas-proportional counters followed by silicon surface-barrier detectors and thick CsI(Tl) detectors to stop the most energetic hydrogen and helium nuclei. Signals from these detectors undergo preliminary processing near the chamber, and then the processed signals are transported to further electronics and a data acquisition system in a nearby building. The chamber and the detector layout are shown in Fig. 73.

During the second quarter, we analyzed the data taken in November and December 2001. These data were to commission the detector station, shielding, detectors and the data acquisition system. For this commissioning, we used an iron sample and concentrated on the proton emission (hydrogen production) at several angles. Detection of protons from the target is challenging because protons are easily produced by neutron interactions with shielding materials. A measure of the quality of data is the signal-to-background ratio. The signal-to-background ratios were found to be 6:1 in the forward angles and 3.5:1 at 90 degrees at a neutron energy of 100 MeV (Fig. 74). At lower neutron energies, the signal-to-background ratios are significantly better. These results show that the measurement program is possible as planned. Some improvements in the shielding will be implemented to make the measurement program even more solid.

To obtain beam time for the production measurements beginning in August 2002, we prepared a request for beam time. This proposal, together with many others, will be reviewed by the LANSCE Program Advisory Committee in late April 2002. We expect no problem with this review because, to our knowledge, there are no other requests to use this detector station.

Gas production by neutrons in materials

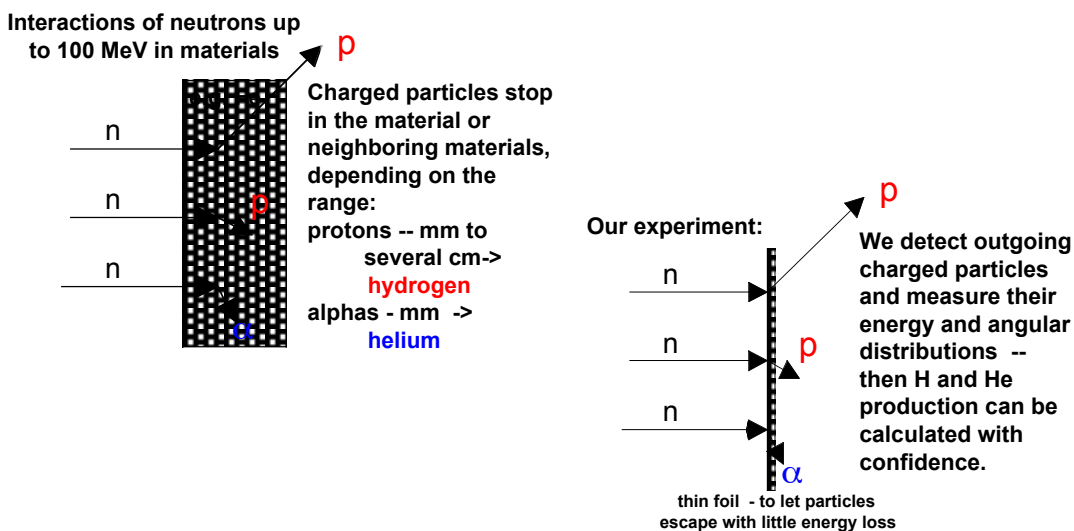


Fig. 72. The relationship of gas production in materials to our approach to measuring the production rate.

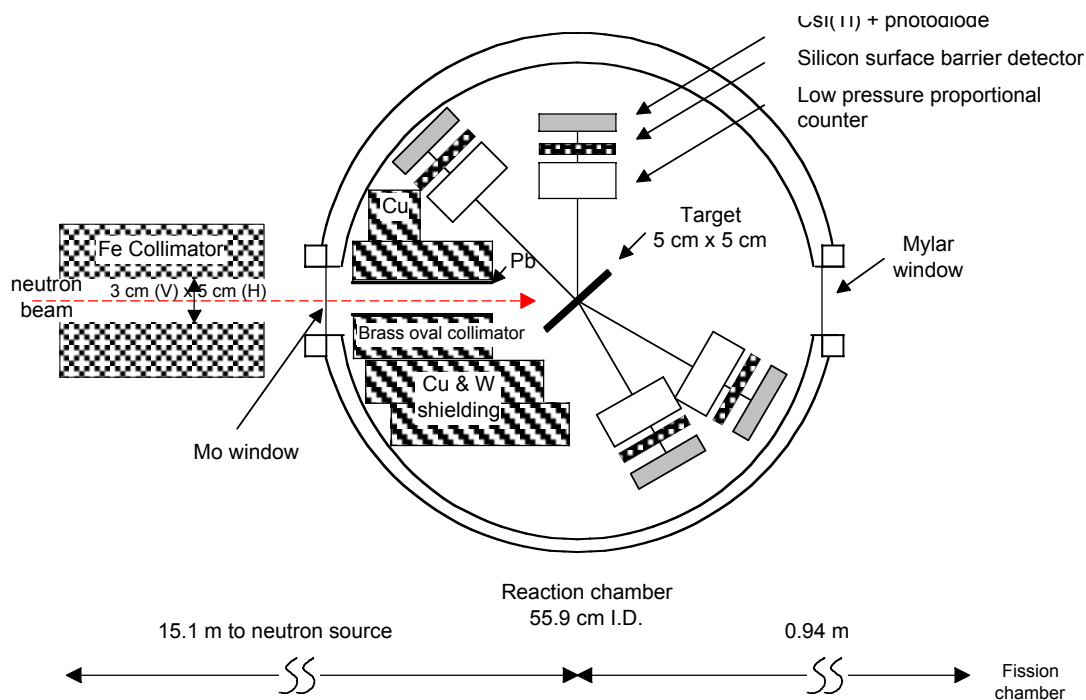


Fig. 73. Layout of apparatus for measuring hydrogen and helium production in materials showing collimation for the neutron beam, target position, and array of detectors.

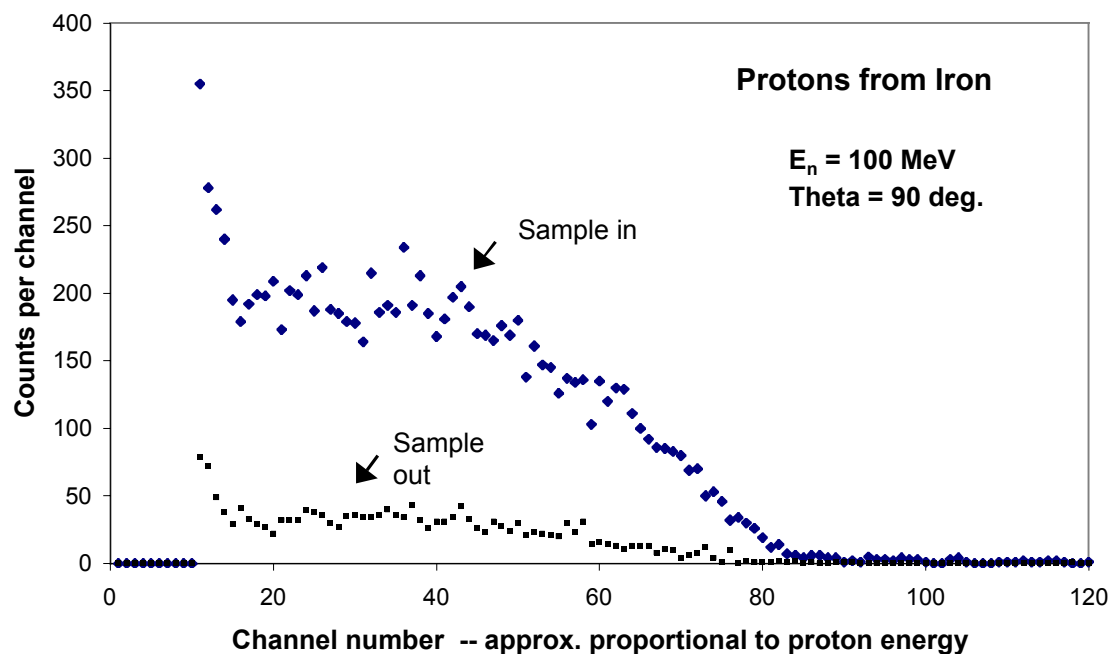


Fig. 74. Sample-in and sample-out measurements of proton production from an iron sample at a neutron energy of 100 MeV. The signal-to-background ratio is good at this neutron energy and significantly better at lower incident neutron energies.

Corrosion Studies

Samples of HT-9, 440A, and SS-316L were oxidized in LBE at 400°C for 330 hr and in air at 800°C for exposures of 48 hr and 64 hr. Initial microscopy on HT-9 and 440A exposed to LBE found a thick (2 mm), compact, and adherent oxide film (Fig. 75). EDS maps of the LBE/oxide/metal regions found that

- the oxide consisted predominantly of Fe and Cr,
- the oxide was bi-layer: inner Cr-rich, outer Fe/Pb/Bi-rich, and
- the LBE immediately adjacent to the oxide film contained considerable amounts of alloy constituents—Fe, Cr, and Mn (see Figs. 76a–76e).

Preliminary capacitance measurements on samples oxidized in air and then exposed to LBE as a function of time and temperature have found several trends in both oxide capacitance and resistivity. We are currently exploring the origin of these trends.

In comparison, microscopy of SS-316L exposed to LBE found no oxide film at the detectability limits of the SEM (Fig. 77). It is uncertain whether this is because (1) a thin oxide film (tens of nm) is protecting the surface, (2) the surface oxide has not been wetted by the LBE, or (3) no oxide is present and there is an indication that an appreciable amount of corrosion has occurred. We are currently analyzing the thin LBE layer on the surface of the sample for corrosion product and plan to examine cross-sections of this interface in TEM, which will allow us to establish whether or not an oxide film is present. Not surprisingly, given the lack of oxide scale, capacitance measurements on this sample were not successful. However, capacitance measurements on preoxidized SS-316 exposed to LBE as a function of time and temperature have found similar trends in both oxide capacitance and resistivity as observed in HT-9 and 440A steel.

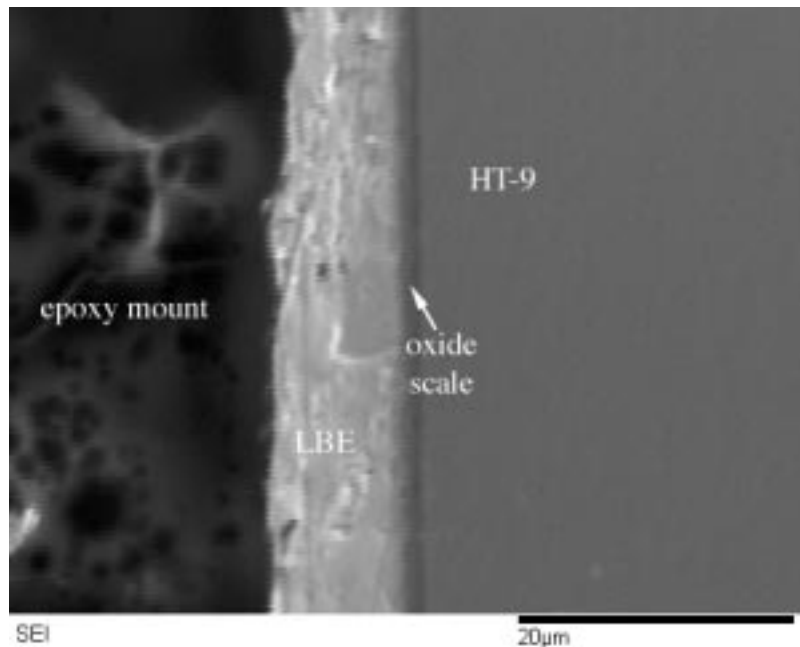


Fig. 75. Secondary electron image of HT-9 sample after exposure to LBE at 400°C for 330 hr (in cross-section). The image area, size, and orientation are identical to the x-ray maps presented in Figs. 76a–76e.

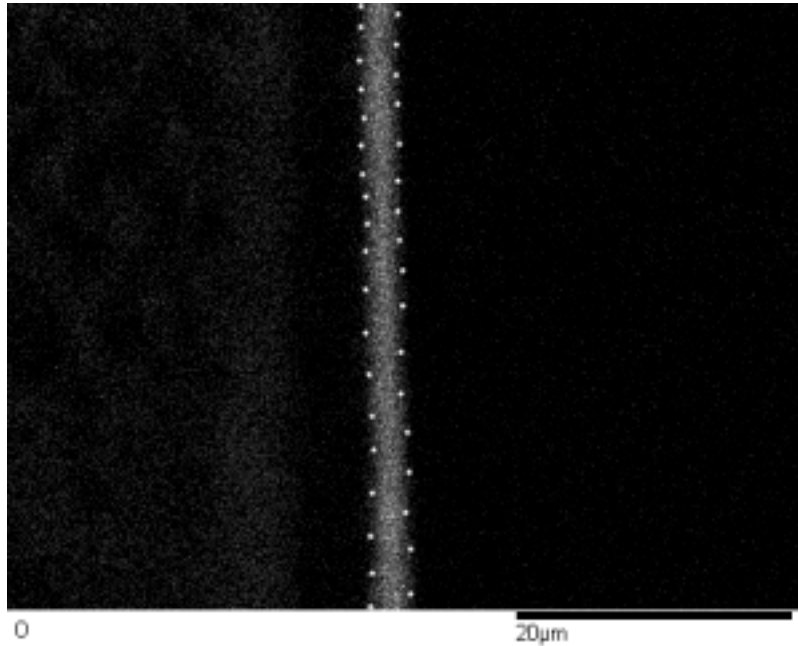


Fig. 76a. HT-9 energy dispersive x-ray spectroscopy map (EDS) for oxygen. Same area as in Fig. 75. Small white dots have been added to the map to show the oxide region. This region is reproduced in Figs. 76b and 76c.

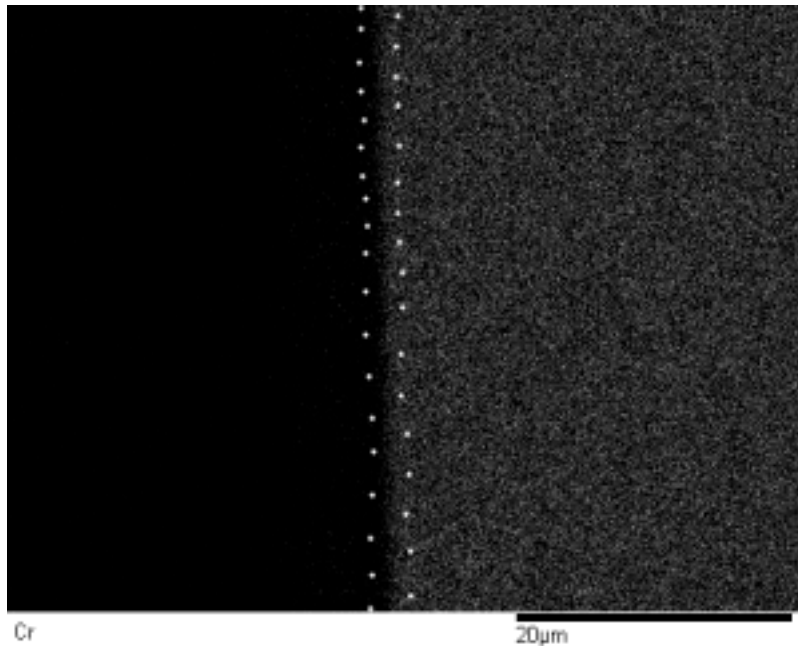


Fig. 76b. HT-9 energy dispersive x-ray spectroscopy map (EDS) for chromium. Same area as in Fig. 75. Small white dots show the oxide region. Note that the inner region of the oxide (right) has a Cr concentration similar to the bulk HT-9 while the outer region (left) is depleted in Cr.

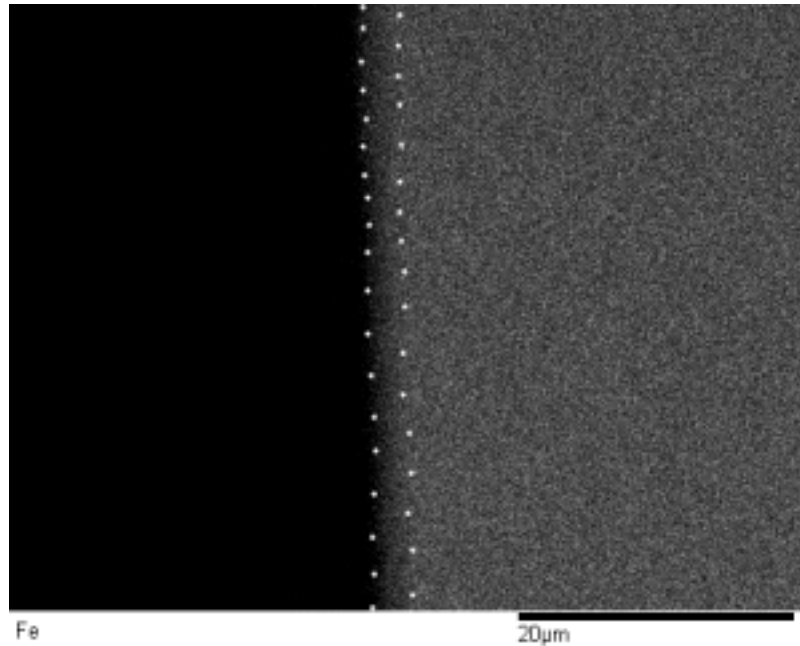


Fig. 76c. HT-9 energy dispersive x-ray spectroscopy map (EDS) for iron. Same area as in Fig. 75. Small white dots show the oxide region. Note that Fe is well distributed through the oxide at a similar concentration as the bulk HT-9.

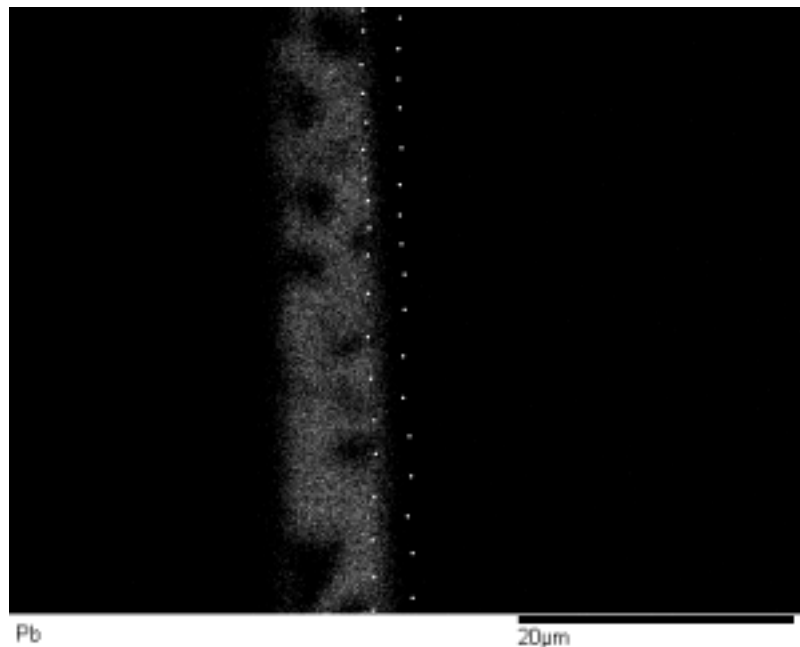


Fig. 76d. HT-9 energy dispersive x-ray spectroscopy map (EDS) for Pb. Same area as in Fig. 75. Small white dots show the oxide region. Note that Pb is present in the outer regions of the oxide (left). The black areas in the Pb map are due to the Bi-rich phase in Fig. 76e.

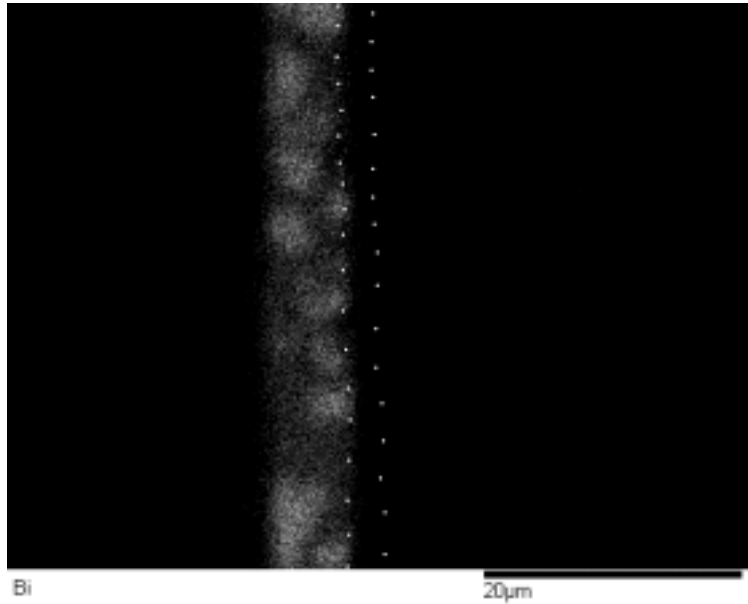


Fig. 76e. HT-9 energy dispersive x-ray spectroscopy map (EDS) for bismuth. Same area as in Fig. 75. Small white dots show the oxide region. Note that Bi is present in the outer regions of the oxide (left). The black areas in the Bi map are due to the Pb-rich phase in Fig. 76d.

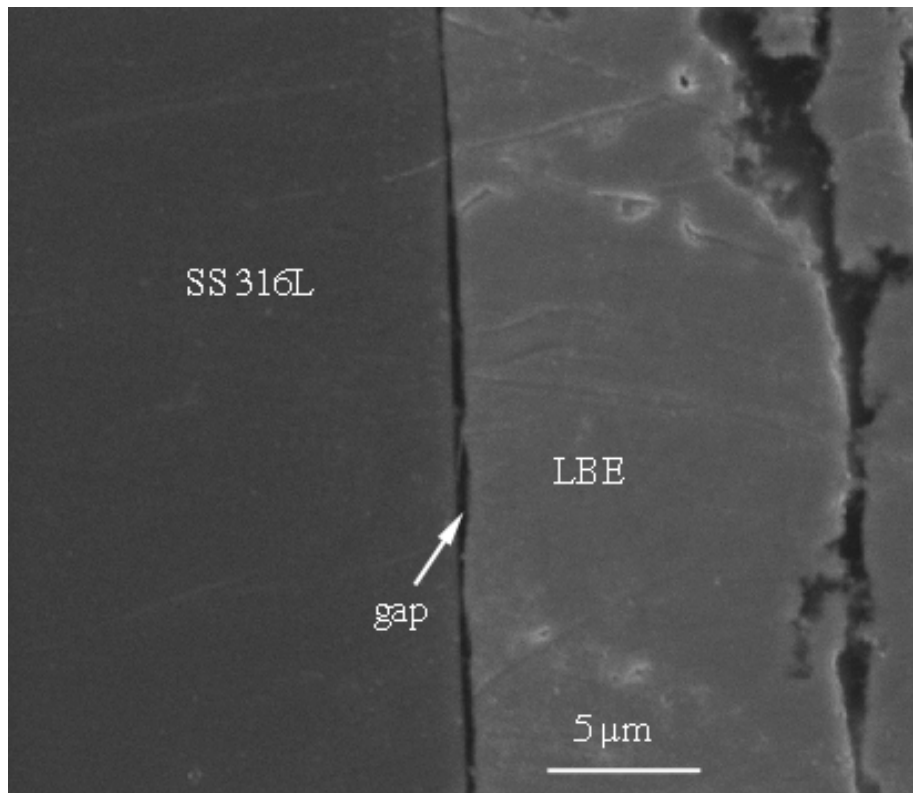


Fig. 77. Secondary electron image of SS-316L sample after exposure to LBE at 400°C for 330 hr (in cross-section). Note much higher magnification than Fig. 75.

3.5 High-Energy Physics

The major objective of high-energy physics activities is to improve and maintain the computer codes used in the analyses of accelerator-driven transmutation systems. As part of the improvement, the nuclear data accuracy will be reevaluated to match the desired objectives.

Scope

MCNPX Code Development

MCNPX code development consists of the following activities:

- Development of the mix and match capability within MCNPX, which requires production of a version of MCNPX in which evaluated data libraries with different upper-energy limits may be used within the same MCNPX run. This will allow the new LA150n data tables to be used simultaneously with the standard 20-MeV data tables for those isotopes that do not appear in LA150n. (LA150n refers to Los Alamos-generated nuclear data library, extending up to 150 MeV.)
- Incorporation of the Cugnon intranuclear cascade and Schmidt evaporation models into MCNPX, which will be carried out in collaboration with CEA-Saclay under the CEA-AAA collaboration framework. CEA will install the models in MCNPX, with LANL oversight. LANL will perform a quality check of this work and incorporate the code changes into the official release.
- MCNPX maintenance and beta testing, which involves maintaining an approved list of beta testers for the code and fixing bugs as beta testers report them. Regular releases of MCNPX will be transmitted to the Radiation Safety Information Computational Center (RSICC) as significant improvements to the code are made.

Nuclear Data Evaluations

The nuclear data activities include production of new neutron fission and capture ENDF (Evaluated Nuclear Data File) evaluations to 150 MeV for two actinide isotopes of highest priority. This involves the following:

- Calculating fission barrier and ν -bar⁴ data to 150 MeV;
- Using the results of GNASH (nuclear reaction code) to generate model-based cross-sections; and
- Using advanced statistical methods to combine discrepant experimental data in the adjustment of the GNASH-generated results to produce new evaluated cross-sections.

As part of these activities, NJOY data processing of new ENDF evaluations and generation of data files of the new ENDF evaluations using the NJOY code will be performed.

⁴ Average number of neutrons released per fission.

The nuclear data tasks also include improving ^{208}Pb inelastic scattering ENDF cross-section and production of a new version of ENDF ^{208}Pb neutron cross-section that improves the inelastic scattering in the few MeV energy regions.

Initially, an effort was started to upgrade the CINDER90 activation libraries to 150 MeV. This effort was terminated in November due to budget limitations.

Highlights

- MCNPX version 2.4.j was released to the Beta Test Team.
- MCNPX classes were taught at UNLV on January 14–18 and in Tokyo, Japan, on February 18–22.
- We completed our new data evaluation for the LA150 nuclear data library of inelastic scattering to the first excited state in Pb at 2.61 MeV, which will be made available for use in MCNPX and other codes.

MCNPX Code Development

MCNPX version 2.4.j was made available to the beta test team. This version is fully updated to MCNP4C, and has also been rewritten in Fortran90. It has dynamic memory allocation, and uses the now standard auto-configuration installation procedure. This marks the first time the source code has been released on the MCNPX beta test web site. Since not all users have Fortran-90 compilers, we have also posted pre-compiled executables for seven platforms: PC Windows, IBM AIX, DEC Ultrix, HP HPUX, Linux, SGI IRIX, and Sun Solaris.

The code contains a number of enhancements, including

- repeated structures source path improvement;
- 14 standard dose functions available through a DF card;
- logarithmic interpolation in defining energy bins with E cards;
- cosine bins may be specified in degrees or for F2 flux tallies; and
- source particles may be specified by descriptors.

Work is also underway to extend the multitasking capabilities of the code to higher energies. We are using a newly established 64-node computer cluster at LANL Group NIS-1 to test the improvements.

The MCNPX team taught a class at the University of Las Vegas, Nevada, from January 14–18. The class included 14 UNLV and 2 Idaho Accelerator Center collaborators. This was a beginning-level class, especially suited to students funded under the AAA University Program. A second class was held in Tokyo, Japan, from February 18–22 and attracted students from the JAERI high-energy physics facility.

We are waiting for delivery of the Cugnon INC and Schmidt Evaporation models from CEA, Saclay. A Memorandum of Understanding on implementation of these modules was prepared at LANL and forwarded to CEA, and CEA is now in the process of obtaining signatures from the code authors. Work on implementing these modules cannot proceed until the MOU has been signed and the software delivered to the MCNPX team.

Nuclear Data

²⁰⁸Pb Inelastic Scattering at Fast Neutron Energies – Deficiencies in the existing LA150 Pb inelastic evaluation were first noted by Obninsk researchers (Ignatyuk *et al.*) and ANL researchers (Finck *et al.*), who were concerned about the impact this would have on ATW k_{eff} predictions. We studied this question and concluded that the ENDF LA150 evaluation does need improvement below 5 MeV.

We completed our new evaluation of inelastic scattering to the first excited state in Pb at 2.61 MeV. We will be incorporating this work into our ENDF evaluation (LA150) and will process the evaluation with NJOY for use in AAA MCNPX simulations. Accurate inelastic scattering in Pb is important for predictions of ATW criticality in a Pb-Bi cooled transmuter, and our new evaluation, which reduces the previous ENDF cross-section by ~0.5 barns at 3.5 MeV, should provide a significant improvement.

Experimental data on inelastic scattering (MT51 in ENDF parlance) to the first excited state (2.61 MeV) below 5 MeV neutron energy are limited. Existing measurements are shown in Fig. 78. A more recent measurement (1994) from Los Alamos by Vonach also provides valuable information. The Vonach experiment measured the (n,n'g) gamma-ray decay of the 2.61-MeV state, and included inelastic cross-section to the 2.61-MeV state, but also to higher states that gamma-ray decay to the 2.61-MeV state. By restricting ourselves to energies below 3.75 MeV, we only have to consider the first three excited states. At an energy of 3.2 MeV, the Vonach data are identical to the inelastic MT51 cross-section. Between 3.2 and 3.75 MeV, we can infer the MT51 cross-section by subtracting the inelastic cross-sections to the second and third excited states from the Vonach (n,n'g) data. In this way, we obtained the experimental Vonach points shown in Fig. 78.

We have also undertaken nuclear model calculations to guide our evaluation of this cross-section. These include compound nucleus Hauser-Feshbach calculations using the GNASH code, as well as direct reaction coupled-channel calculations using the ECIS optical model code based on the coupling scheme developed by Young.

Based on the aforementioned experimental data and the nuclear reaction model calculations, we evaluated the MT51 inelastic scattering cross-section as shown by the bold line in Fig. 78. The modification is rather large, with the inelastic cross-section being about 0.5 barns smaller at its peak. For comparison, we also show the recent Japanese JENDL3.2 evaluation, which peaks at a similar value but has a somewhat unphysical behavior at higher energies.

Since the total neutron cross-section is known rather precisely from experiments, and the partial cross-sections must sum to the known total value, we have increased the neutron elastic cross-section accordingly in the 2.6–5-MeV region. The maximum percentage increase in the elastic scattering cross-section is 8%, at 3.5 MeV.

Actinide LA150 Evaluations: ²³⁹Pu, ²³⁸U – We made progress in optimizing our GNASH model calculations for n+²³⁹Pu up to 150 MeV. Use of an optical potential developed by Ignatyuk provided us with a neutron reaction cross-section lower than our previous results, which enabled us to fit the fission cross-section well (measured by Lisowski, Stapes, and Scherbakov). We used nuclear fission barriers for nuclides near stability from our extensive work on n+²³⁹Pu, ²³⁸U, etc., for weapons research; to obtain barriers for the many (more than 50) excited nuclei away from stability that are produced in high-energy reactions, we extrapolated barriers using a mass dependence taken from Sierk's rotating liquid-drop model.

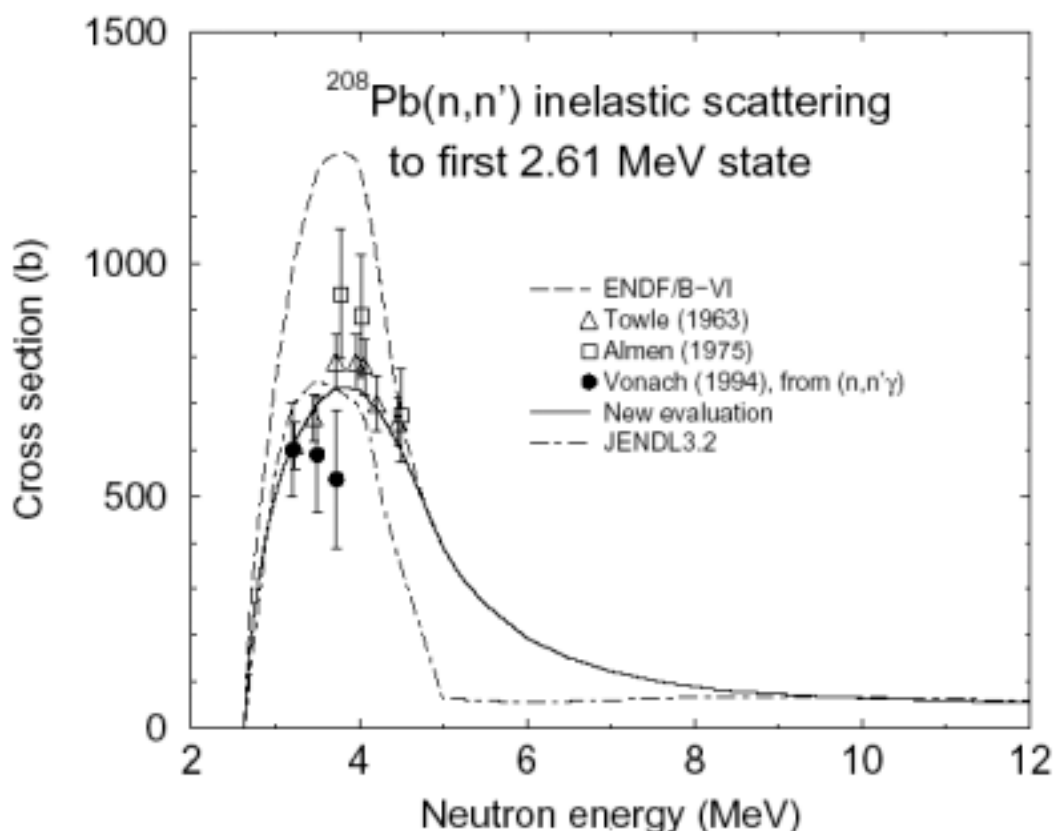


Fig. 78. ^{208}Pb inelastic scattering cross-section evaluations.

Figure 79 shows our GNASH-calculated fission cross-section compared to recent measurements. Agreement is seen to be good, though at the highest energies the fission cross-section over-predicts the data when the default optical-model reaction cross-section is used. However, the high-energy behavior of the neutron-reaction cross-section is not well known. If the reaction cross-section is decreased to a somewhat smaller value in the 90–150 MeV region, as shown by the dashed line in Fig. 80, we obtain agreement with the Lisowski fission data (dashed line in Fig. 80). Further work is needed to determine which reaction cross-section is best to use.

We have had discussions with Lisowski on the systematic uncertainties associated with the recently released high-energy Lisowski fission data (2001). This is needed so we can combine these data with Scherbakov's new St. Petersburg data in a covariance analysis of the $^{239}\text{Pu}(n,f)$ cross-section up to 150 MeV.

Future work that will be required after we finalize the GNASH model calculations includes (1) adding information on fission neutrons from CEM2k; (2) completing elastic scattering calculations; (3) running GSCAN to generate ENDF-type data and using Talou's covariance analysis of the fission cross-section data up to 150 MeV; and (4) creating a new ENDF file merging the 20–150 MeV information with the existing ENDF data below 20 MeV and undertaking a similar analysis for ^{238}U .

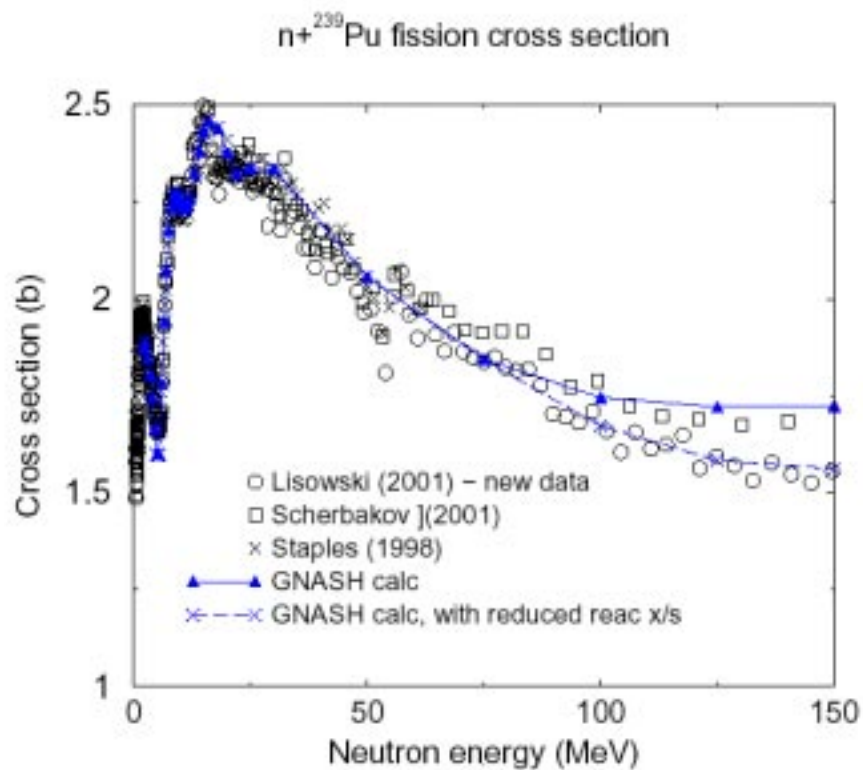


Fig. 79. GNASH-calculated fission cross-section compared to recent measurements.

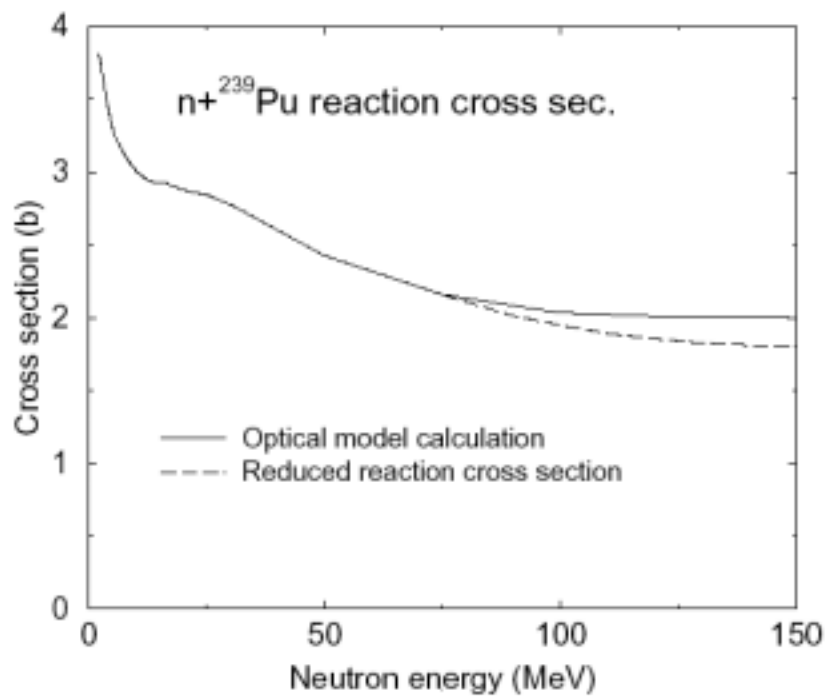


Fig. 80. Comparison to Lisowski's fission data.

Fission Neutrons for the LA150 Actinide Library – During this quarter, we worked on the development of a modified version of the CEM2k code to describe fission fragment production with the subsequent evaporation of neutrons and other particles. To describe fission and light-fragment (heavier than ^4He) production, the CEM2k code has been merged with the GEM2 code of Furihata, which contains evaporation of up to 66 different particles and a fission model based on Furihata's modification of the Rutherford-Appleton fission model by Atchison from LAHET.

With our modified code, CEM2k+GEM2, we can describe fission fragments and particle spectra for proton-induced reactions in the sub-actinide region. However, we met difficulties in correctly describing the total fission cross-section for actinides, and as a consequence, all fission characteristics including fission neutrons. After a special study, we were able to modify Atchison's expression in Furihata's code so that now we can accurately describe the actinide fission cross-sections, and all other characteristics of fission. So far, we have tested this modification of our code on fission cross-sections, mass distributions and yields of fission fragments for several reactions on actinides where we found available data. An example of our results for the mass distribution of the products from $p(100 \text{ MeV}) + ^{238}\text{U}$ with experimental data from Titarenko (ITEP, ISTC Report 839B-99, Moscow, 2001) is shown in Fig. 81.

We compared our results to predictions by the NASA phenomenological model YIELDX of Sliberberg, Tsao, and Barghouty, and to the LANL phenomenological code CYF by Arthur Wahl. We found that our new CEM2k+GEM2 code describes these measurements reasonably well, while both the phenomenological codes fail. Our CEM2k code can now be used to predict fission neutrons for the LA150 actinide libraries.

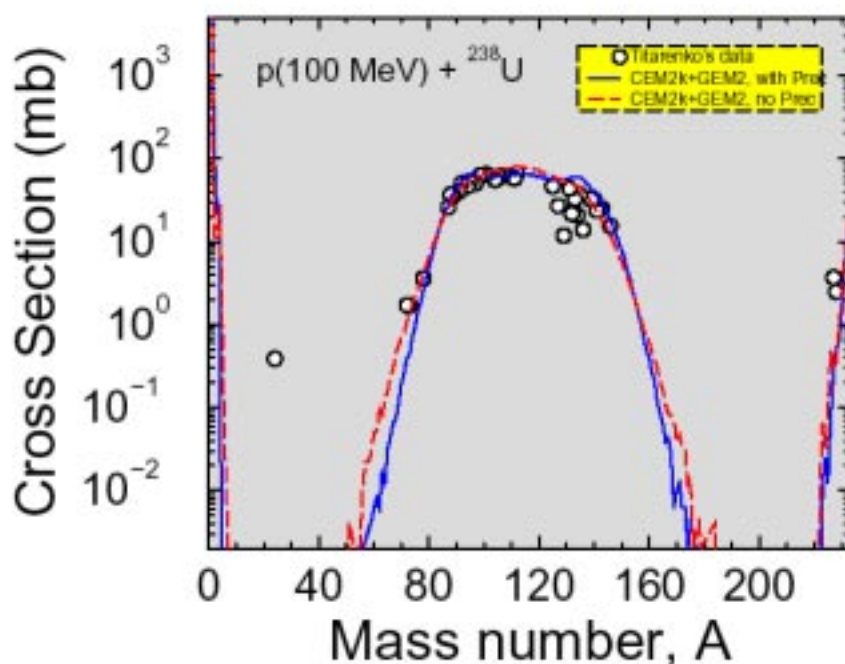


Fig. 81. Example of CEM2k calculations in comparison with the data.

3.6 Reactor Physics

The reactor physics task involves the codes and methods used to assess the transmutation process. The objective also includes defining and designing long-term experiments needed to advance the TRL in this area.

Scope

Experiment and Safety Analysis

This task consists of analyzing physics experiments and developing a safety analysis strategy applicable to accelerator-driven system (ADS) design. Part of the physics experimental work consists of providing high-quality experimental data; and for this purpose, ANL personnel will participate in collaboration with CEA to perform the critical and subcritical experiments of the MUSE4 configuration. To validate data and methods for the neutronic design of an ADS, an analysis of the experimental results obtained in the MUSE4 program will be performed using both deterministic and stochastic codes with different data files (e.g., JEF2 and ENDF/B-VI). Additionally, the irradiation experiments PROFIL-1 and -2 will be analyzed, in which samples of actinide isotopes were irradiated in the French Phenix reactor. The objectives for safety analysis are to develop the conceptual safety design basis and criteria for ADS reactors, to develop and verify the computational safety analysis methods and computer codes necessary for safety assessment of ADS reactors, and to perform initial scoping analyses of design basis and bounding accident sequences for an ADS reactor conceptual design.

Physics Needs and Methods Development

Physics needs will be assessed by performing uncertainty evaluations and developing new capabilities for computational tools used for the neutronic analysis of ADS. Work will be performed to define physics needs and needs related to cross-section data uncertainties. In a first phase, sensitivity and uncertainty analyses will be performed for minor-actinide-dominated fuel compositions. A significant effort will be devoted to extend the present field of applicability of deterministic tools to energies >20 MeV, taking into account phenomena (e.g., gas productions) that can be affected by uncertainties in this energy range. Code and methods upgrades are needed to improve our capability to correctly calculate coupled systems with deterministic tools. The iteration strategies for equilibrium concentrations in the REBUS-3 burnup code will be modified to eliminate instabilities observed for subcritical and deep burnup conditions. Implementation of multivariate cross-section fitting capability will also be performed. Coupling with high-energy (spallation) source calculation has to be extended to the 3-D geometries (Cartesian and hexagonal) and needs to be implemented in a more flexible manner. Considerations will also be given to the possibility of developing an entirely deterministic coupled calculation (i.e., spallation and high-energy charged-particle transport treated deterministically).

Physics Experiment Planning

The purpose of this task is the definition of an experimental plan conceived to support the needs of the neutronic design of an ADS. To simulate the physics and dynamic behavior of accelerator-driven systems and to support their design, an action will be taken to investigate the possibility of using the TREAT and ZPPR facilities located at

ANL-W. The information coming from the potential experiments performed at these facilities will play a critical role in validating data, codes, and methods needed for reducing uncertainties and margins for the actual design of an ADS. These experiments will be planned to be complementary of existing and future experimental programs (e.g., MUSE, TRIGA) carried out by foreign partners. The scope of this work is to provide an experimental plan, to perform sensitivity analysis for justification of the program, and to define the objectives and the feasibility of the experiments.

Highlights

- A preliminary analysis of the MUSE benchmark, corresponding to the critical configuration of the MUSE-4 experiment, has been performed.
- An uncertainty assessment quantifying the impact of nuclear data on integral parameters relevant to the neutronic design of an ADS has been carried out for systems containing fuels with high content of minor actinides.

MUSE Benchmark

Work continued on the MUSE subcritical benchmark. Results for the deterministic calculations were obtained and indicate good agreements between experiments and calculations when either JEF 2.2 or ENDF/B-V nuclear data libraries are used. ENDF/B-VI data seems to produce large discrepancies that still need to be explained. Continuous-energy Monte Carlo analyses will be used to investigate this discrepancy.

MUSE Experimental Activity

An ANL staff member has been running the experimental activities for the MUSE subcritical measurements. The preliminary experimental analysis of the Cf source traverses was completed and a report drafted. These data will be released from MASURCA in the near future. Additionally, the fission reaction rate traverses are underway, but will not be completed until late spring. Thus, the full set of experiments with the GENEPI accelerator coupled to MASURCA will not begin until June. At that point, it is planned to have three configurations: the SC0 configuration (-450 pcm), followed by SC2 (-3000 pcm) and SC3 (-5000 pcm). After SC3, it is likely that an expanded lead buffer will be added to the SC3 configuration. These four phases are expected to last until the end of 2003.

Kinetics data have been obtained in four experiments to date: one with the reference core (noise techniques), and three with SC0 (pulse neutron source, frequency variation, and rod drop). The data are in the process of being analyzed.

PROFIL Experiment

Work regarding the analysis of the PROFIL Minor Actinide Burnup experiments started this quarter. The purpose of this study is to perform a validation of different sets of cross-section data (i.e., JEF and ENDF/B files) for minor actinides to quantify their reliability in ATW-design calculations. During the PROFIL irradiation campaign, one or two standard pins, with separated capsules (46 in PROFIL-1, 2x42 in PROFIL-2) containing separated U, Pu, Np, Am, and Cm isotopes, were placed in a standard subassembly in the first row of the inner core of the Phenix reactor, far away from neutronics perturbations to obtain clean irradiation conditions. Currently, work is

concentrated on reanalyzing the PROFIL-1 experiment by using JEF2 cross-section data and the ECCO/ERANOS system code. Preliminary results indicate good agreement between our results and results published by the French.

Safety Analysis

To provide a capability for scoping analyses of accelerator-driven subcritical operation of TREAT, modeling upgrades are being implemented in SAS4A/SASSYS-1 Version 3.1. Modifications and additions were made to the DIF3D-K/VARIANT-K spatial kinetics options to enable cross-section input via the MACOEf macroscopic file format. In the pin heat-transfer formulation, the structure field was eliminated, the cylindrical fuel and cladding circumferences were replaced with appropriate TREAT fuel element periphery, and the convective heat-transfer correlation was revised. In the incompressible coolant dynamics model, air thermo-physical properties replaced the liquid-sodium properties, and the pressure-drop calculation was eliminated. Testing and verification of the heat-transfer and coolant dynamics modeling changes were completed. In the spatial kinetics model, implementation of the MACOEf cross-section handling code was completed, and testing progressed. Both Eigenvalue and external source problems were executed at the steady state for infinite, semi-infinite 1-D, and finite 3-D models of TREAT. Preliminary estimates of the TREAT reactivity temperature coefficient were obtained; the calculated value compares favorably with available historical data.

Uncertainty Assessment

A report that summarizes the uncertainty analysis on ADS with minor-actinide-dominated fuel has been issued. The uncertainty analysis work is now focusing on the high-energy effects, in particular to study the impact of cross-sections over the 20 MeV threshold, especially on gas-production rates. These types of parameters are the ones that could be more sensitive to uncertainties in that high range of energy. A MC²-2 library was generated using the Los Alamos-evaluated data files LA150. The data files were used to generate cross-sections over the 20-MeV energy, while under this energy the usual ENDF/B-VI files were kept. The LA150 files contain mostly structural materials. Where data were not available (i.e., minor actinides), cross-sections were extrapolated using the data from under 20 MeV. It is believed that most of the uncertainty would come from the structural materials, for parameters like gas productions and damages, while the minor actinide data would have a lesser impact. The initial calculations have shown that the multiplication factor is affected in a negligible way by the 20-MeV data. A larger impact can be observed on the external source importance, where there is an effect of ~4%. In the future, sensitivity calculations will be performed to assess the uncertainty on the main integral parameters.

Method Development

Efforts to upgrade codes and methods have been initiated to improve ANL capability to analyze the coupled systems with deterministic tools. The REBUS-3 fuel-cycle analysis code is being modified to eliminate the instabilities of feed-enrichment search observed for subcritical and deep-burnup conditions, and a utility code that couples the high-energy spallation-source calculation with the deterministic codes is being developed. The improvement and modification needs of the REBUS-3 code

were defined and work priorities determined. As first priority, it was decided to combine the current two-step calculations for the fixed source problem into a single-step calculation and to improve the iteration strategies for the feed-enrichment search. The code requirements for a utility code to couple the high-energy spallation-source calculation with the deterministic codes were defined, and the development strategies were established. This code would read the log file for low-energy neutrons written by the special version of the MCNPX code and write the fixed-source file FIXSRC for DIF3D and VARIANT calculations.

TREAT-Coupling Experiments

The TREAT minimal critical-core configuration was calculated with a detailed 3-D MCNP model of the reactor. A crucial uncertainty in the calculation is represented by the boron impurities in the graphite. Using different information taken from available literature, an average value of 7.6 ppm has been applied. The resulting effective multiplication factor of the system is $k_{\text{eff}}=1.00945\pm0.00201$. This value reflects the critical state of the reactor; therefore, in the future we recommend using the above calculated density of boron in the fuel. For the proposed ADS experiments using the TREAT reactor (TREACS: TREAT Experiment for ACcelerator-driven System), it is important to evaluate the worth of different fuel elements in the core, as well as fuel-slotted elements because of the location of the target and accelerator beamline. The worth of the central-fuel element vs. void was calculated with MCNP code. The agreement between calculated and measured value is satisfactory. The design and optimization efforts of the external neutron source design continued during this period. A target composed of tungsten material (cylindrical geometry of various lengths) and of tungsten cylinder surrounded by a shell of Be has been considered. While the importance of the Be shell is clear when the thickness of the W converter is small (<1cm), it plays almost no role when the tungsten thickness is above 2 cm. Hence, it can be concluded that a thick (2–3 cm in length, 5 cm in diameter) W target would not require being surrounded by a Be shell. Modeling of different target compositions and geometry will continue.

3.7 International Support

International support and collaboration is a strong part of the research conducted under transmutation science. A major collaborator is CEA in France. However, this collaboration is defined at the basic research level, and there are no tasks specifically conducted or funded in support of CEA's efforts. All the tasks discussed in Sections 3.1–3.6 directly or indirectly benefit this collaboration.

Some tasks are specifically funded in support of the MEGAPIE Project at Paul Scherrer Institute (PSI) in Switzerland, as well as the import of the Russian IPPE (Institute of Physics and Power Engineering) LBE target. Those tasks are discussed below.

Scope

MEGAPIE is a 1-MW LBE spallation target experiment being set up at PSI in Switzerland. DOE signed a partnership agreement on the MEGAPIE Project that includes having a US engineer participate in the MEGAPIE design and analyses on change-of-station at PSI. The objective is to provide technical support to the

MEGAPIE Project and to transfer knowledge gained and related research on the Project to US laboratories to advance the TRL for the US LBE target development.

We will provide analysis support to MEGAPIE in US laboratories. The specific scope of this support has not yet been determined, but it will be defined soon in collaboration with PSI scientists and engineers.

The IPPE LBE target was designed and built in Russia with the initial objective of irradiating it at LANSCE (LANL). However, because of the unavailability of the irradiation facility, the target will be used as another LBE loop for basic research. Currently, the objective is to bring the target to the US, to deliver it to UNLV, and to set it up as another research loop.

Highlights

- In partial fulfillment of the MEGAPIE collaboration agreement, a resident engineer from LANL is stationed at PSI for a 5-month duration. He is working on the MEGAPIE target engineering design and development tasks.

Summary

After negotiations between the DOE-AAA Program and the Paul Scherrer Institute, Switzerland, an agreement was reached in December 2001. As part of this agreement, the DOE is committed to providing support at PSI at the level of 1-man-year per year to the MEGAPIE target development and testing program. MEGAPIE is to be a Pb-Bi spallation neutron target to be tested at PSI in the SINQ neutron production facility. Beam conditions are nominally to be 570 MeV and 1.4 mA.

This report cannot comprehensively encompass the quarterly progress of the entire project. A brief summary of the system operation is provided, followed by a similarly brief discussion of the status and current issues on major system components. The work performed on assignment here at PSI is also reported. The amount of information available on MEGAPIE is extensive, and the amount of new information generated quarterly is beyond the scope appropriate for an AAA Quarterly Report. The MEGAPIE server posts all relevant documents and is available for viewing by all MEGAPIE partners.

By the start of DOE involvement, the project had been ongoing for about 2 years. Roughly speaking, the project is in the final stages of design and moving as rapidly as possible to fabrication, with the intent of staging the completed target and ancillary systems for out-of-beam testing during the spring of 2003. Overall the project design is very solid and comprehensive, but the schedule is very tight.

Even while rapidly approaching final design, some design questions remain, some testing is still ongoing or yet to be performed, and some design decisions are being made, to some extent with an insufficient data basis. In the report below, we will attempt to briefly summarize the status of major components and subsystems, highlight any significant issues, and present the plan and schedule of further work.

As would be expected, the project involves an extensive number of meetings at all levels. Minutes and reports are posted on the MEGAPIE server.

MEGAPIE General Description

MEGAPIE is a new element in the AAA Program, but work has been ongoing for 2 years at PSI and at other European organizations, both collaborators and contractors. Extensive documentation, including drawings, is available for review on the MEGAPIE server for those who need a more detailed understanding of the design. Perhaps the easiest path to a complete overview is to access the presentation material for the Third Technical Review, recently held in Bologna, Italy.

MEGAPIE (megawatt pilot experiment) is to be a molten LBE spallation neutron target. It will be operated in the SINQ neutron production facility at PSI. This test is currently scheduled to begin in 2005. SINQ, which was brought into operation about 10 years ago, was originally intended for liquid-metal targets, so it was designed for a vertical, upward proton beam with the intent to maximize the contribution of natural convection to the circulation of the metal target. The beam at SINQ is 540 MeV. MEGAPIE will most likely be operated at 1.4 mA.

MEGAPIE will be placed in the existing SINQ well, a cylindrical space defined by shielding, moderators, detectors, etc. The well diameter and the vertical upward beam constrains the design and the arrangement of components considerably. The decision was made to put all LBE-containing components, except an external fill and drain system, into the well. As a result, the arrangement of the target with the pumps, heat exchanger, power lines and instrumentation is very compact and complex.

The target window and lower target containment are to be made of T91 martensitic-ferritic stainless steel. All other parts are to be of SS-316L. An AlMg3 safety hull cooled with heavy water surrounds the lower part of the target to provide containment in the event of a LBE leak.

The external systems include a fill-and-drain system, an LBE cover-gas system with gas sampling, the oil-coolant system, coupled to a house-water system as the final heat sink, and an isolation-gas system to provide a low-pressure gas gap between the target and the safety hull.

The target is to be filled with LBE just once and drained at the conclusion of the test. Heaters are provided to maintain liquid LBE at all times, and the oil-heat removal system is designed to pump 240°C oil during beam interrupts. Instrumentation includes thermocouples throughout the target, EM flow meters on the main and bypass flows, pressure on all gas and external liquid systems, level sensors, oil flow rate, etc.

Current Status of MEGAPIE

During this quarter and the preceding months, MEGAPIE has been coming to final design on the target and all external systems. The following summary indicates the status of each subsystem and some of the issues.

Target – The target was designed by SUBATECH. The design, which is ready for fabrication, is very professional and the documentation is thorough. A review is scheduled for April. Given the design constraints and requirements, the design is very compact and thus very complex. SUBATECH has successfully integrated components designed in whole or in part by other participants. Plans for quality assurance and acceptance testing are to be discussed at the upcoming review.

Heat Exchanger – The target includes the heat exchanger, about which there has been considerable discussion. A single-pin heat exchanger test was conducted at Brasimoni by ENEA. In this test, measured heat transfer was in acceptable agreement with analytical predictions, but the pressure drops measured on the oil side were significantly higher than had been calculated. The higher value for pressure drop was accepted, and the oil-side pump system was modified accordingly. Additional testing may be needed, perhaps including a simple mock-up with water as the flow media for resistance measurements.

EM Pumps and Flow Meters – The pumps are electromagnetic-inductive type, designed by specialists in Riga, Latvia. A pump prototype is to be fabricated and tested this spring, with final pump design and fabrication to follow. Several issues related to the pumps are unknown. First, if the pump capacity is less than design, the space constraints severely limit the options for design modifications. Delays in fabrication and testing of a prototype have made it difficult to change the target design to accommodate any significant changes in pump size or shape. Second, the issue has been raised that there may be cavitation in the pump due to low pressures, based on observations in similar pumps with Hg. Although it seems highly unlikely that this will be a problem in the MEGAPIE system, the design pressure of the LBE system has been raised. The result is that the LBE cover gas pressure has been increased from subatmospheric to above atmospheric. Positive pressure operation of the cover gas in turn results in a requirement for double enclosure of the entire cover gas system. Third, the neutron field in the vicinity of the pumps results in cumulative radiation damage to some of the pump materials in excess of any previous experience. So the pumps could fail, or the performance may degrade with time, thus effectively ending the experiment. Neutron irradiation tests of questionable pump materials will be conducted. Last, there is a concern about flow meter signal corruption due to the high magnetic field of the nearby pump. Benchtop tests have led to minor design changes in electrical shielding, which apparently will solve this problem.

Target Window – Of all components, the target window is the weakest link because of the severe environment and the lack of experience with metals at these temperatures under these conditions and in the presence of Pb-Bi. Although LISOR and other experiments will help understand and quantify SS-T91 performance, there will be too little information and it will come too late. A further complication for now is that the thermal modeling of the window cooling is not complete, and planned cooling tests have yet to be conducted (planned now for June–July 2002). It is difficult to see how sufficient knowledge and experience can come to bear on the window design and material choice problem in time to impact MEGAPIE. Liquid-metal embrittlement (LME) has come to the forefront of attention. LME is a brittle failure of a ductile material, apparently due to interactions on an atomic level at the tip of a crack or defect. Since the window will be embrittled in any case, LME can only be important if it results in crack propagation and failure at lower stresses than would otherwise be the case. Because of the high difficulty in predicting window life, the MEGAPIE Advisory Committee, in a meeting in March, recommended operating under the assumption that window failure is eminent, and this failure is an acceptable end to the experiment. Such an assumption may be the only justifiable position for the safety case, but this imposes very high acceptance and performance demands on the safety hull.

Safety Hull – At this time, it is not clear that MEGAPIE will adopt the suggestion of planning for the end of the experiment to be determined by window failure, but in any case, the ability of the safety hull to contain the LBE under any failure scenario is critical. A spill of LBE down the beam tunnel could delay any further use of SINQ by up to 2 years. A detailed analysis of the safety hull in what is believed to be a bounding set of accident scenarios has been conducted. The report on this analysis is not yet available, nor is it clear what design acceptance criteria will be used or what QA and testing will be performed. Some testing with small LBE leaks onto the safety-hull window are planned to begin in April. More extensive testing is under discussion, but it is difficult and expensive to replicate the most severe accident scenarios.

External Systems – External systems include the oil heat-transfer loop, the cover-gas system, the isolation-gas system, and the fill-and-drain systems. Final reviews of these systems will be held soon, and fabrication could begin thereafter. An extensive amount of work has been completed and documented. While there are still some outstanding issues as well as work to be done on these designs, these systems, which were designed by ANSALDO (oil cooling system and cover gas system) and ENEA (fill-and-drain system), are in a very good state.

US MEGAPIE Activities

The work done by the US in the MEGAPIE collaboration for this quarter has been performed mainly by our resident engineer from LANL, who is on assignment at PSI. Several other AAA staff have made visits to PSI and the facilities of other European collaborators, and some attended the MEGAPIE Technical Review meeting in March.

Heat Exchanger – The LANL resident engineer at PSI performed spreadsheet analysis of the heat-exchanger design and test as performed by ENEA and had discussions with other scientists on the experiment and results. Although some want to change some of the instrumentation and run again, the general conclusion is that the heat transfer has predictable to acceptable accuracy, but the measured pressure drop is not consistent with the geometry. Some parametric studies on the effect of flow rate were performed. Preliminary reports by ENEA have been released. Their three-dimensional CFD models also cannot predict the measured pressure drop. Our resident engineer, Keith Woloshun, conducted some parametric studies on the heat exchanger test to try to understand the high measured-temperature rise on the inner pass of oil (measured rise is 5°C, while analysis shows 1°C). In addition, we evaluated mechanical stresses in the heat exchanger tubes as a result of differential expansion between the oil manifolds and the LBE side. The design has vertically mounted bellows to give some horizontal compliance. Because of the short lengths, the stresses would be very high without the bellows. A test to demonstrate the ability of the bellows to handle a large number of cycles (up to 9000) of small lateral movement would be appropriate.

The conclusion of these analyses and discussions with PSI and ENEA personnel working on the heat exchanger and tests suggest that the higher pressure-drop measured by ENEA is most likely a geometry effect not representative of the MEGAPIE design.

LBE Expansion – We studied the problem of LBE expansion after freezing. Work done at PSI shows that there is significant volume increase in LBE after freezing. This expansion depends upon geometry of the sample and temperature history. It is possible that in closed or partially enclosed systems, such as the MEGAPIE target,

high wall stresses exceeding yield stress can result from this expansion. This should be considered in the design of all LBE systems. In MEGAPIE, the LBE will never be allowed to freeze inside the target.

Gas Systems – We studied the overall gas system design and functionality. The overall schematic has minor errors in functionality, and there are inconsistencies between this PSI schematic and the cover-gas subsystem design by Ansaldo. There is no overall P&ID, although Ansaldo has a complete P&ID for the cover-gas system that should be integrated into a comprehensive P&ID that numbers and tracks all components and instruments. The resident LANL engineer is working to make progress on this item.

Small LBE Leak Experiment – We began work on the design of a simple experiment to look at the process of a slow leak of LBE onto the safety hull window. The question is whether the LBE will flow down off the spherical surface and into the trough, formed by the intersection of the concave sphere and the cylindrical side wall, or if it will freeze in place or splatter in such a way that the leak is not detected by the wire placed in that trough. Looking at other failure scenarios, more complex experiments may follow. A fabrication drawing of the safety window mock-up has been generated. The LBE leak apparatus has been designed and is being fabricated; experiments should start in April. Some scoping calculations for the drop, falling and hitting the surface were performed.

LBE Flow Analysis – The flow of LBE at the top of the pump, where the flow turns 180° and enters the pump, and the flow connected to the expansion tank by 0.5-cm holes was analyzed. Velocities are slow (0.1 m/s), so small gas bubbles can readily escape and rise to the expansion tank. Only gas bubbles smaller than 0.16 mm will be entrained and carried into the heat exchanger.

Water Leak Analysis – A water leak into insulation gas space was investigated as a possible serious accident case. Preliminary analysis conducted assumed the most extreme leak scenario of 7.5 liters of water suddenly enters the insulation gas space. Analysis shows that if no venting is allowed, equilibrium is reached at about 230°C and 28 bars in 13 seconds. Pressure rises in about 10 seconds to a limit of 10 bars (180°C), controlled by a pressure relief valve. The tube diameter of 1 cm is sufficient to vent the steam generated thereafter, based on fairly conservative assumptions. Possible accumulation of condensate in the tubing may cause unsteady flow conditions, depending upon the configuration and location of components. The spreadsheet generated for this analysis serves as a baseline for further analysis as the system design evolves. It may be prudent to perform an experimental simulation of this accident scenario. The possibility of a water leak, followed immediately by brittle failure of the window (induced by thermal shock), needs to be considered.

Heat Removal System and Cover Gas System Specification Reviews – Ansaldo has delivered to PSI complete system specifications along with procurement specifications for both the oil Heat Removal System (HRS) and the LBE Cover Gas System (CGS). We reviewed these documents and wrote detailed review reports. In summary, although the design appears to be complete and adequate, the documentation is lacking in the level of detail needed for procurements and operation. Perhaps the most serious observation is that there is no redundancy of components or instruments, although the space for these external systems (the TKE) is not easily accessible due to radiological controls.

3.8 LANL-Sponsored University Programs

Scope

University support is an important part of the AAA Program. In addition to the general University programs run by the DOE-HQ, a number of universities are supported directly by the programmatic funds to provide technical assistance to the AAA Program. The directly supported universities include University of Michigan, UC-Berkeley, UT-Austin, and North Carolina State University.

University of California – Berkeley

Provide technical support to the Systems Analyses and Transmutation science teams via specific tasks defined and coordinated through the AAA Program leads, including:

- Benchmark of the simple model for fuel cycle analysis;
- Resolve the discrepancy with ANL on actinide built-up with cycles;
- Apply fuel-cycle analysis methods to compare design alternatives;
- Compare Na vs. LBE-cooled ATW;
- ATW performance assessment using molten salt and alternative (${}^7\text{LiF-BeF}_2$);
- ATW assessment during approach to equilibrium using molten salt; and
- Perform optimization and analyses of pebble-bed ATW.

University of Michigan

Provide technical support to the Systems Analyses and Transmutation science teams via specific tasks defined and coordinated through the AAA Program leads, including:

- Analysis of coupled accelerator core dynamics with emphasis on k_{eff} predictions and control;
- LWR-based reactor transmutation studies for equilibrium cycles;
- Assessment of LBE slowing down spectrum and the associated cross-sections;
- In collaboration with technical staff at LANL, use proton irradiation to simulate spallation neutron radiation damage in accelerator-driven systems. This work is to investigate the effect of higher gas production at significant doses (several dpa) to lay a foundation for a full-scale radiation campaign;
- Develop a detailed description of the irradiation campaign (temperatures, dose rates, doses, and He-implantation levels); and
- Conduct a single irradiation campaign (~240 hours of irradiation) on SS-T-91 at three dpa levels.

University of Texas – Austin

Provide technical support to the Systems Analyses and Transmutation Science teams via specific tasks defined and coordinated through the AAA Program leads, including:

- Participation in the helium and hydrogen production experiments in LANL/Blue Room (Summer 2002);

- Development of a test plan, and post-test analyses for spallation product benchmark experiments for targets (emphasis on LBE);
- Time-dependence incorporation on the proliferation metrics development and analysis; and
- Development of the uncertainty analysis methodology for the proliferation metrics, providing results to the Systems Analysis Team.

North Carolina State University

The purpose of the proposed research is to calculate radiation damage (production of displacements, helium, hydrogen, and heavier transmutation products) and energy deposition in the target materials, containment structures, and entrance windows of the target assemblies for the SINQ spallation neutron sources that are under design and development at the Paul Scherrer Institute (PSI). These targets include the Mark II and Mark III designs. The Monte Carlo code MCNPX will be the primary computational tool, but other codes such as SPECTER and SRIM (or TRIM) and cross-section information sources such as ENDF and LA150 will be used. These calculations are two-fold in nature: (1) a detailed simulation model will be constructed incorporating the materials and geometry of the spallation-neutron-source targets by means of which the spatial variance of proton and neutron fluxes will be determined, and (2) cross-section sets for the production of the damaging entities (displacements, helium, etc.) will be created to cover the full applicable energy range of protons and neutrons in each of the affected materials. The damage production rates will then be determined by folding the radiation fluxes into the cross-sections.

In addition to the direct production of displacements due to incident and secondary protons and due to spallation neutrons, the PI must be cognizant of less obvious (and less well studied) mechanisms for the transfer of energy to the irradiated materials and hence the production of displacements. These mechanisms include recoil-atom damage (i.e., the damage due to primary knock-on atoms (PKAs) and other interaction products produced in the heavy-metal target material, which become implanted near the surface in the surrounding structural materials) and n-gamma capture damage (due to absorption of thermal neutrons followed by emission of a capture gamma-ray and motion of the capturing atom in order to conserve momentum). These mechanisms could be important in special cases. Furthermore, the PI will consider the spectrum of transmutation products upon spallation and their possible effects on corrosion properties.

Finally, the effects of the calculated radiation damage on mechanical and other property changes will be analyzed and reasonable and safe lifetimes for the radiation-damaged components will be assessed.

University of California – Berkeley

Optimization of an Accelerator-Driven Molten-Salt Transmuting Reactor

Research was continued on the performance of a graphite-moderated molten-salt subcritical transmuter. The molten-salt reactor uses NaF:ZrF₄ as the coolant fuel, with an inlet/outlet temperature of 600°C/700°C. The molten salt with actinides, where U and fission products are completely removed, is continuously fed and removed from the reactor at a rate of 0.8 liters/day and an actinide concentration of 12.87 mol%; the molten-salt effluent contains a different composition and smaller actinide

concentration than the feed. It is also assumed that fission products are removed from the core as soon as formed. The central question addressed is whether or not it is possible to design such a reactor to have an acceptable k_{eff} (>0.92) when at equilibrium composition, while the actinide concentration is constrained by the solubility limit of 1.56 mol% and what is the corresponding transmutation efficiency.

Iterative numerical calculations using MCNP and steady-state rate equations were performed to obtain equilibrium states of the reactor, with the graphite-to-fuel ratio (C/MS) ranging from zero (the case of a homogeneous reactor composed only of molten salt and actinide) up to a value of C/MS of 12 or greater, for three different fuel-channel diameters of 1, 3.5, and 7 cm. For the 7-cm-diameter fuel channel, the peak k_{eff} of 1.03 is reached at C/MS~1 (Fig. 82). The peak in k_{eff} is lower (1.025) as the fuel-channel diameter decreases to 3.5 and 1 cm, corresponding to a larger C/MS of 3. All k_{eff} values are in the vicinity of unity; radial leakage will reduce them by a few%. At the peak k_{eff} , the actinide equilibrium concentration (Fig. 83) reaches a minimum of ~0.9 mol% for $d=1$ cm, ~1 mol% for $d=3.5$ cm, and ~1.3 mol% for $d=7$ cm, all of them below the solubility limit of 1.56 mol%. A peak actinide transmutation efficiency is reached at C/MS=1.03 for all of the fuel-channel diameters (Fig. 84), and its maximum value of 94% is achieved for the case of 1-cm-diameter fuel channels.

In conclusion, based on the analysis done so far, the molten-salt transmuter is highly attractive. An important question is to what extent imperfect removal of fission products will impair its performance. This question will be addressed in the future.

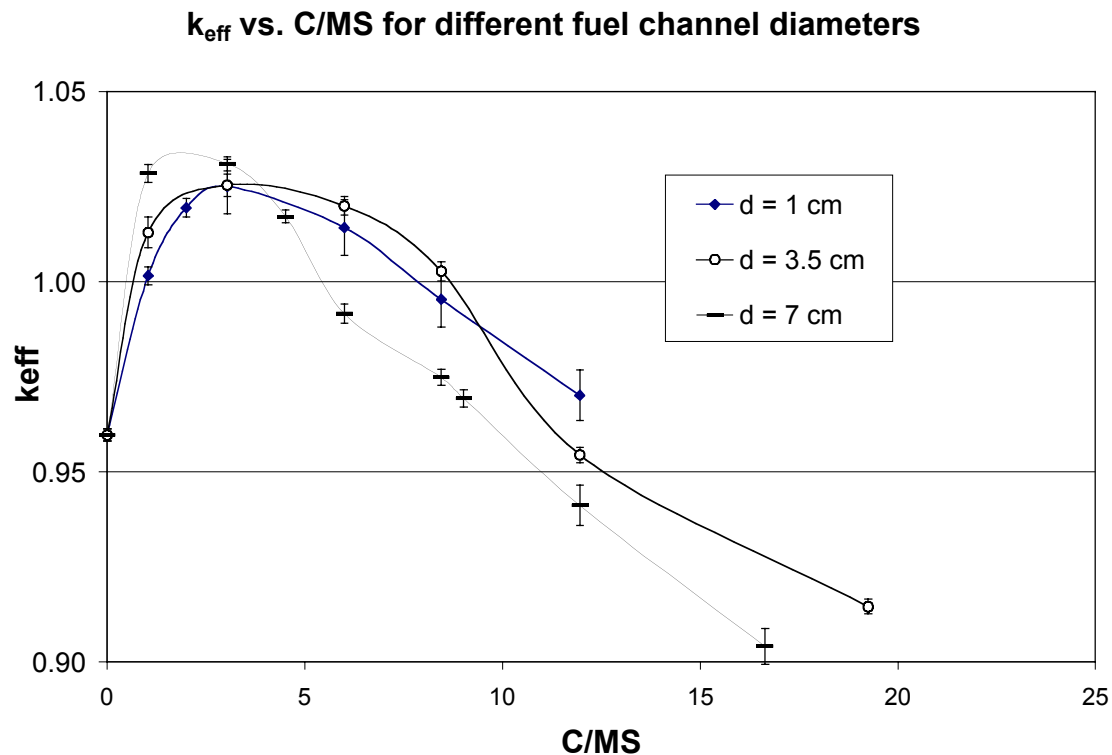


Fig. 82. Dependence of k_{eff} on graphite-to-fuel ratio (C/MS) for different fuel-channel diameters.

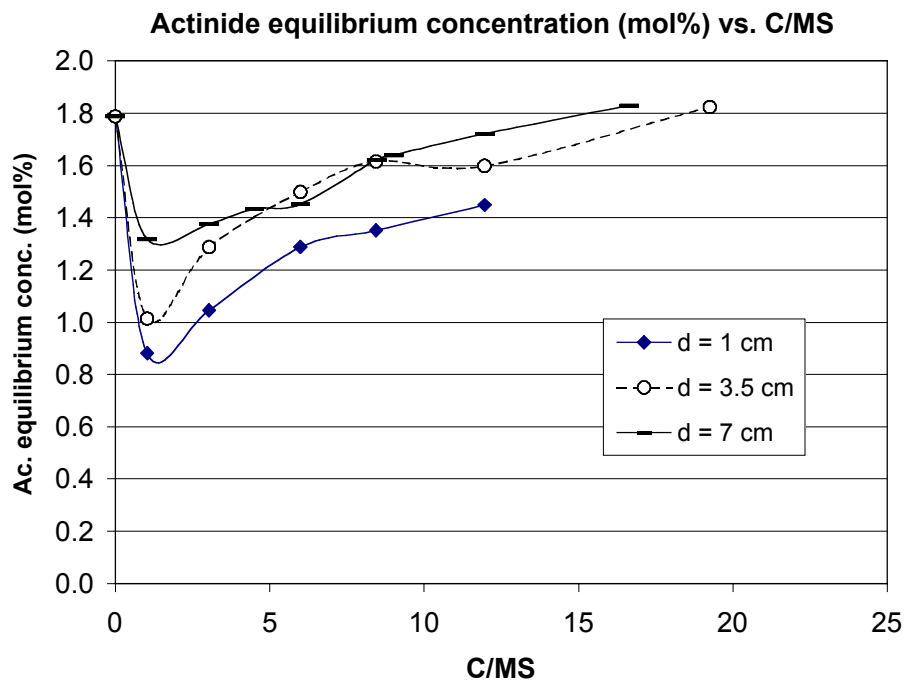


Fig. 83. Dependence of actinide equilibrium concentration (mol%) on graphite-to-fuel ratio (C/MS) for different fuel-channel diameters.

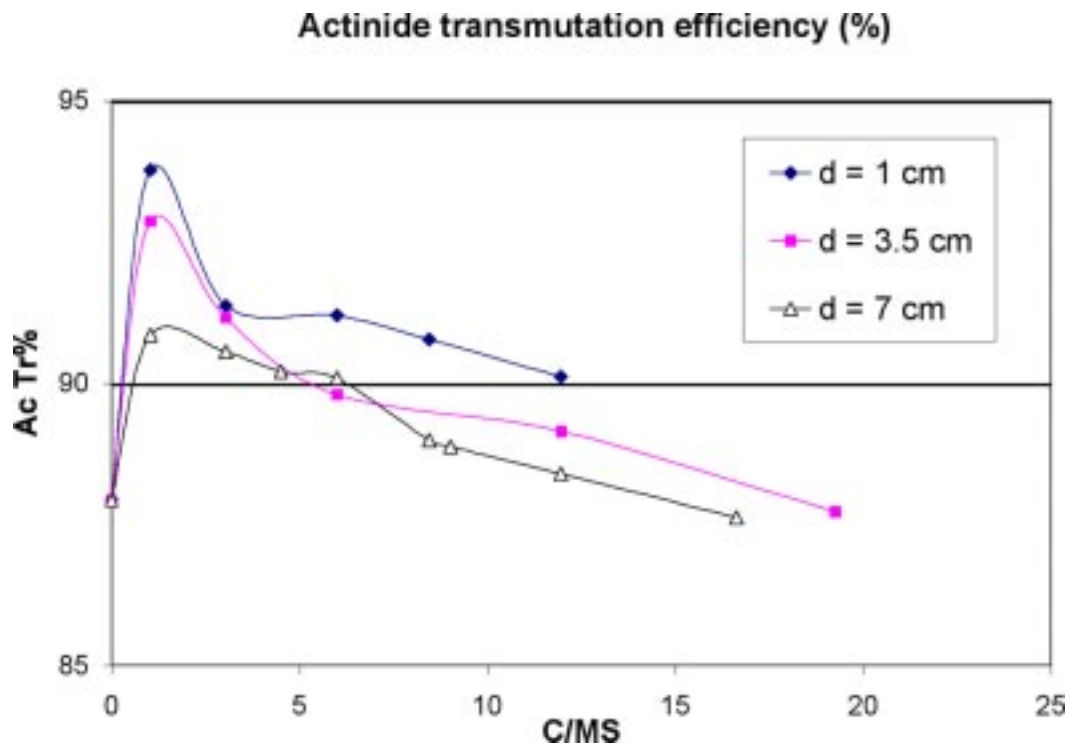


Fig. 84. Actinide transmutation efficiency for different fuel-channel diameters and graphite-to-fuel ratios.

Transmutation Capability of Accelerator-Driven Pebble-Bed Reactor

A parametric study was carried out of the transmutation capability of accelerator-driven pebble-bed reactors. Design variables of this study include the heavy-metal loading per fuel kernel and the graphite-to-fuel volume ratio. So far, the transmutation efficiency we managed to get from the pebble-bed transmuter is significantly lower than from the molten-salt transmuter, even though both use a graphite moderator and both have continuous (or semi-continuous) fueling. One difference is that the pebble-bed transmuter retains all of the fission products it generates. Whether or not this difference is responsible for the entire difference in the transmutation efficiency will be the subject of follow-on research.

A Simplified Model for Fuel Isotope Evolution in ATW Systems

We continued development of a simplified model for simulating the evolution of the fuel-isotope inventory in an ATW and its fuel cycle, as well as to characterize the actinide waste that gets into the repository. We focused on benchmarking the model. Numerical results from our model on fuel isotopes that change due to neutron irradiation in the reactor was compared with that from an MOCUP calculation for 17 isotopes, including Am and Cm. The comparison showed a significant difference in the concentration of Am and higher actinides. Much of this discrepancy was found due to the neglect of the ground state of ^{242}Am in our model. The benchmarking against MOCUP continues.

Comparison Between Na and Pb-Bi as Coolants for Liquid-Metal ATW

A research plan was laid out to elaborate on and expand a previous study comparing liquid-metal coolants for ATW reactors. The old study compared LBE and Na on an optimized-core basis, which featured differing core designs that take advantage of the properties of each coolant rather than using the same core design for both coolants. The new study will follow the same procedure, but will consider accelerator-driven cores for a double-tier strategy and will use more accurate modeling.

Cost/Risk Analysis of Candidate Approaches for P&T

One of the latest AAA reports (LA-UR-01-5572, 2001) cites nine candidate approaches for partitioning and transmutation (P&T) of nuclear waste. A cost/risk methodology was applied to study four of those alternatives: two double-tier and two single-tier systems, and to compare them with the open fuel cycle. The main questions addressed are (a) would it be cost-effective to undergo the increased short-term risks and costs associated with P&T in order to derive the benefit of decreased long-term risks? (b) what is the effect of considering the sale of electricity produced by the transmuting reactors? (c) what alternatives—single-tier or double-tier approaches—are most cost-effective? Applying the US NRC-recommended limit of \$1000 expended per person-rem averted, it is concluded that all the P&T options are cost-effective if the electricity from the transmuters is sold, and that two-tier systems are preferred over single-tier systems. It should be noted that cost uncertainties are large.

Neutronics Computational Laboratory

The neutronics computational laboratory, which provides reference materials and computational support for our students, is in the process of being updated. This

quarter, we put into operation the MONTEBURNS code. We are benchmarking it against MOCUP, with which we have extensive experience.

University of Michigan

Transmutation of Transuranics in Pressurized Water Reactors

In our continuing effort to study the feasibility of recycling and transmuting transuranics (TRUs) in light-water reactors, we initiated an evaluation of the French CORAIL concept for Pu multi-recycling in pressurized water reactors. Our investigation involved assembly-level lattice physics calculations with the CASMO-3 collision probability code, and effort was made to compare our results with the WIMS8 lattice physics calculations performed at ANL and global diffusion theory results reported in the CORAIL papers. WIMS8 utilizes a 172-group library, which originated from the JEF2.2 data, while CASMO-3 uses a 70-group library, which contains mostly the ENDF/B-IV data. Thus, one important objective of this initial benchmarking work is to establish whether the 70-group structure of the CASMO-3 library is sufficient to treat the low-energy Pu or TRU resonances. We have also begun to compare the isotopic transmutation and decay chains of CASMO-3 and WIMS8. In addition to benchmarking the CASMO-3 library and depletion chains, we plan to evaluate if and how much the heterogeneous distribution of Pu in the fuel assembly, i.e., the CORAIL concept, increases the ability to perform multiple Pu recycles in PWRs, when compared against a partial loading of MOX assemblies comprising homogenous Pu loading within each assembly.

Analysis in Support of the LANSCE Experiments

We have begun the task of analyzing the December 2001 LANSCE data received from ANL in February. The data consist mainly of gamma-ray spectra from metal foils irradiated on a Pb-Bi spallation target subject to an 800-MeV proton beam. The spectra are being analyzed to identify relevant peaks and determine which foils would be best for the next irradiation at LANSCE planned for July. Co, Bi, Tb, and Ag have been identified to date as good candidate foils, and effort is continuing to perform analysis of the other foils. We are also evaluating time-of-flight measurements taken in December. Although an initial analysis of the TOF data did not yield much useful information, we plan further counting and analysis of the data at the University of Michigan. Along with the spectrum analysis, numerical simulation of the LANSCE experiment is underway using the MCNPX high-energy physics code. The simulation results will be compared to the December irradiation data and will be used to aid in planning the July irradiation.

Space-Time Analysis of Coupled Accelerator-Core Dynamics

We continued efforts to investigate the influence of spatial effects on subcriticality measurements in the accelerator-driven systems. A review of recent literature on methods for subcriticality analysis suggests that the reactivity determination in the ADS depends heavily on the relationship between the neutron source location and detector position. This spatial dependence due to higher harmonic contaminations increases with subcriticality, indicating a limited validity of conventional point kinetics model. To account for the spatial effects in ADS reactivity determination, we are studying noise analysis techniques and efficient methods to utilize the data available during accelerator startup and trip events. For this purpose, we studied modal

expansion techniques to represent space-time dynamics subject to a localized source, and efforts are underway to evaluate the performance of these methods with the FX2-TH time-dependent diffusion theory code.

Cross-Section Processing with the NJOY Code

In our effort to acquire in-house ability to update the cross-section libraries for various neutronics codes, we have used the NJOY99 code to generate new cross-section data for ^{235}U in the ACE format for the MCNP code. The current ACE library contains limited cross-section data for fission products that would be needed for waste transmutation analysis with a Monte Carlo depletion code such as MONTEBURNS. The absence of the ^{90}Sr data is most noticeable in this regard. Our effort to date has concentrated on verifying various options for the MCNP library generation. Once our own NJOY99-generated cross-section data are verified against existing datasets for a few select nuclides, effort will be made to generate an augmented MCNP library that can accommodate a number of fission products. We also plan to update the cross-section library for the MC² code, which is currently based on the ENDF/B-V dataset. The goal is to create an ENDF/B-VI library, so that MC² results may be compared more directly with MCNP-4C results. This endeavor will allow us to more closely examine the MATXS11 library and help us understand the discrepancies between the TRANSX and MC² cross-section libraries presented at the 2001 ANS meeting in Reno.

Radiation Effects in Candidate Materials for Spallation Neutron Environments

Candidate materials for the spallation neutron environment will require radiation tolerance to doses of 30 dpa at temperatures between 350°C and 550°C and injection of H or He in the range several hundred to a few thousand appm. These are extremely severe and demanding conditions and basic data as well as understanding of material response to these conditions is lacking. Given the sparse database and understanding of radiation response under these conditions, proton irradiation of candidate spallation materials is planned. Proton irradiation has proven to be an extremely effective tool in emulating the effects of neutron irradiation in austenitic stainless steel used in LWR cores.

It was jointly decided by LANL and UM to focus on two ferritic-martensitic alloys for the first set of experiments, HT-9 and T-91. HT-9 is a 12Cr-1Mo steel and T-91 is a 9Cr-1Mo steel containing Nb with optimized V and C. HT-9 is a swelling-resistant alloy that has been proposed for applications in conditions where swelling will be a problem for austenitic alloys (400°C–600°C and high dose). T-91 is also expected to be swelling resistant in the same range and has greater high temperature creep strength due to the alloying additions. Small sections of sheet stock (0.5–1.0 mm thick) of both alloys were received from LANL. Samples in the form of 2-mm-wide (\times 30 mm long) bars and 2-mm-wide tensile bars will be made from the sheet stock. The straight bars will be used for microhardness indentation experiments following irradiation and also for microstructure analysis via transmission electron microscopy. Samples will be made by electric discharge machining, followed by heat treatment.

University of Texas (UT) Austin

Proliferation Resistance Assessments

Questionnaires for determination of weighting factors for the proliferation resistance assessments were collected from 24 individuals. Questionnaires were originally distributed to 32 different experts in the fields of nuclear security, nonproliferation, international security, nuclear safeguards, nuclear smuggling, and law enforcement. Twenty-four of these questionnaires have been completed and their results have been compiled to generate an unbiased set of weighting factors for use in the MAUA-based proliferation assessment methodology. This is sufficient data to allow for good reliance on the weightings factors; however, if more questionnaires are returned in the future, their results will also be added to the weights.

Input data was collected to allow for the application of the proliferation resistance assessment methodology to four basic static facilities: storage facilities (including wet storage of spent fuel and the storage facility at PANTEX), separations facilities (including a sample UREX process), fuel fabrication facilities, and transmuters (both reactor-based and accelerator-based).

Four basic long-term systems were constructed which would include a time-dependence and consider a material flow from initial input into the system to a long-time into permanent disposal. The four systems constructed were (a) a once-through PWR cycle, (b) a closed PWR cycle based on PUREX separations, (c) a closed PWR cycle based on UREX separations, and (d) a closed accelerator-based transmuter cycle based on UREX separations.

The theoretical background for adding time dependencies to the proliferation resistance assessment methodology was established. This included development of the equations and analysis of proper normalization strategies to allow for relative assessments of radically different fuel cycles. This methodology consists of the assessment of the proliferation resistance (termed the Total Nuclear Security Measure) inherent to 1 metric ton of material initially input into the cycle and following its history until the simulation is terminated (presumably at some time long after permanent geological disposal). Given a system which involved $i=1, 2, 3, \dots, I$ processes, we can determine the aggregated total nuclear security measure (NS) for the system using the following:

$$NS = \sum_{i=1}^I m_i \cdot \Delta t_i \cdot PR_i$$

where m_i is the amount of material in process i , Δt_i is the time the material is in process i , and PR_i is the static proliferation resistance value for process i .

Spallation Product Studies

A study assessing the radiological impact of various spallation target designs was completed. This study involved the simulation of various target designs and operational histories using a linked MCNPX and ORIGEN2 code at UT. The results of this study could be important for decay heat analyses, accident scenarios, maintenance of the target and target area, and target decommissioning and disposal. It was found that the geometrical design of the target, the choice of materials used, and the initial beam-energy were all important factors in the short-, medium-, and

long-term external radiological dose from the target following irradiation. It was also found that for many materials the spallation product yields currently available might be lacking in the accuracy needed for the AAA Program. Future studies are planned to perform a set of experiments in collaboration with the Los Alamos Neutron Science Center (LANSCE) to measure spallation products in various materials. This will produce more data and allow for more accurate assessments of target designs.

4. SYSTEMS TECHNOLOGIES

Scope

The scope of Systems Technologies is to coordinate all technical elements to define requirements, perform system-level evaluations, develop preconceptual designs, and establishing technology development activities in a comprehensive R&D proof-of-principle (POP) effort. Overall system objectives, system performance requirements, and POP requirements are used to correlate R&D needs, data quality objectives, experimental facilities, resources, and materials. Preconceptual designs serve as fundamental bases in defining critical R&D and focusing POP testing. Systems Technologies provide a solid foundation for focused and coordinated AAA R&D efforts.

Accelerator-Driven Test Facility (ADTF)

The preconceptual and conceptual design phases of the Accelerator-Driven Test Facility (ADTF) includes the Target and Materials Test (TMT) Station, the Subcritical Multiplier (SCM), the accelerator, and the balance of facility segments. The work performed in connection with the ADTF design must be documented, including the reference preconceptual designs of the TMT and the Na-cooled SCM-100, with a Pb-Bi reference target, and the studies of alternative engineering design solutions considered. The scope also includes collaboration with CEA. The following specifics are included:

- Completion of the ADTF preconceptual design documentation;
- Development of an ADS reference design—US will work on liquid-metal-cooled designs (Na and LBE) and CEA will work on a gas-cooled design;
- Proof-of-performance coupling tests—a work plan for experimental POP of the coupling between an accelerator and a multiplier will be developed; and
- POP for accelerator reliability and accelerator development.

Integration activities include:

- Development of functional and performance requirements for the ADTF project;
- Definition and control of design interfaces between major facility segments;
- Coordination of internal and external design reviews;
- Technical risk assessment; and
- Cost estimating.

ADS Reference Design

The purpose of this task at ANL is to develop a preconceptual design for a Na-cooled, accelerator-driven system. LANL will lead the reference design for a Pb-Bi-cooled system. This work involves development of a preconceptual design for a large-scale (~800 MWth) ADS with liquid-Na cooling and a Pb-Bi eutectic target. The focus is on defining a set of top-level requirements for the ADS engineering design concept for the facility as a whole, including:

- Identifying the containment structure with ingress and egress routes for personnel, services, and radioactive and nonradioactive equipment;
- Routing and shielding of the accelerator beam;
- Configuring the subcritical multiplier, the vessel in which it is housed and its cover, and all other in- and ex-vessel ancillary components and systems; and
- Handling schemes for all of the above.

The ADS design will be used to update, as necessary, requirements developed for the ADTF.

Micro Accelerator-Driven System Proof-of-Principle

Coupling Experiments – This task will investigate the use of an experimental facility such as the Transient Reactor Test (TREAT) facility, located at ANL-W, for the study of accelerator-driven-system control issues related to the coupling of a multiplier to an external source. The feasibility of using the TREAT reactor coupled with an accelerator-driven external source to be part of a POP for ADS will be assessed. The dynamic behavior of the experimental coupled system will provide useful information for simulation of operation of an actual ADS power system.

Fuels and Materials Experiments – The main deliverable for this year is to develop a preconceptual design, cost estimate and schedule for the implementation of an irradiation experiment in the high power beam at LANSCE.

Advanced Cavity Development – The main effort is the procurement and testing of two $\beta=0.175$, 2-gap, 350-MHz superconducting spoke resonator cavities and the completion of the design of the power coupler for these cavities.

Highlights

Accelerator-Driven Test Facility (ADTF)

- We issued the ADTF Preconceptual Cost Study, which provided parametric estimates for the Total Project Cost of four alternate design concepts for the ADTF. The results of this study were also presented at the AAA Quarterly Review Meeting held at UNLV in January.
- We revised the ADTF Missions, Functions, and Requirements document to reflect the removal of the tritium production mission from the AAA Program. This document was submitted as part of the close-out documentation for the ADTF, which also included system descriptions and design drawings for both the Subcritical Multiplier (SCM) and Target Multiplier (TMT) plant concepts.
- We initiated the preparation of the Transmutation Technology Development Plan, which involved a guidance package consisting of the document outline

and detailed schedule of activities, and a videoconference meeting with all project participants to kickoff the effort.

ADS Reference Design

- The Na-cooled ADS reference design for the reactor core shroud was established using the core shroud design for an existing 300-MWe (~800 MWth) ANL point design and the core design previously developed, with no scaling necessary.
- A Pb-Bi target assembly for the 800-MW reference Na-cooled ADS was dimensioned on the basis of scaling the ADTF target design.
- LANL, BNL, DOE, and ANL agreed on the set of neutron physics calculations to be performed this year in support of the two liquid-metal-cooled ADS reference designs. The calculations will be based on the existing core point designs.

Coupling Experiments

- Meetings were held at ANL-W and at the Idaho Accelerator Center (IAC) to discuss the engineering feasibility of coupling the IAC accelerator to the TREAT reactor at ANL-W. The coupling appears to be feasible and no engineering show-stoppers were identified.
- Concepts for cooling the target in a TREAT-accelerator coupling experiment were developed.

Accelerator-Driven Test Facility (ADTF)

Preconceptual Cost Estimate

In March 2001, a draft preconceptual cost estimate was prepared for the Accelerator Driven Test Facility (ADTF) as part of the submittal for Approval of Mission Need, CD-0. Due to uncertainties in the outyear budgets, the project did not receive the approval to start conceptual design. In the interim, the preconceptual design was advanced to allow an improved draft cost estimate to be prepared for alternate ADTF configuration options. These options are:

- Option A: ADTF with SCM and TMT; tritium upgrade capability
- Option B: ADTF with TMT; SCM and tritium upgrade capability
- Option C: ADTF with TMT; no tritium upgrade capability
- Option D: LEDA add-on with TMT; no SCM or tritium upgrade capability

The draft cost estimates (in \$K) for the four options are summarized below:

Project Option	TEC	OPC	TPC	TPC Range	
				Low	High
Option A - ADTF with SCM and TMT; tritium upgrade capability	1,983	614	2,597	2,141	3,284
Option B - ADTF with TMT; SCM and tritium upgrade capability	1,308	439	1,747	1,471	2,255
Option C - ADTF with TMT (green-field); no tritium upgrade capability	843	556	1,399	1,087	1,723
Option D - LEDA Add-On with TMT; no SCM or tritium upgrade capability	586	527	1,113	878	1,358

Preconceptual Design

To ensure that the status of the ADTF design is adequately documented, there has been a significant effort to capture all of the relevant design information that was developed in FY01 to support the pre-project planning effort and submittal of the CD-0 package. This design information includes the following:

- ADTF Missions, Functions, and Requirements (updated to take into account the deletion of the tritium production missions)
- Design trade studies
- System Descriptions
- Drawings and sketches (equipment arrangements, building layouts, etc.)

Documentation summarizing the engineering activities on the ADTF was issued in March. The following documents were issued:

- Report ANL-AAA-001, "Assessment of Beam Entry and Primary Circuit Configuration Alternatives for Application to the Sodium-Cooled Subcritical Multiplier System for the Accelerator-Driven Test Facility," describes the process by which the final reference design, incorporating a vertical accelerator entry into an isothermal-pool-type subcritical multiplier system, was chosen from among other alternatives.
- Report ANL-AAA-002, "Final Report on the Preconceptual Design of the Sodium-Cooled Subcritical Multiplier System for the Accelerator-Driven Test Facility," is the SCM-100 system design description (SDD) that provides a detailed summary of the preconceptual reference design features, including analyses relating to reactor physics, thermo-hydraulics, spallation target, and shielding aspects of the design.
- Report ANL-AAA-004, "ADTF Preconceptual Design: SCM-100 Selection of Pool Design," documents the choice of a pool configuration for the Na-cooled SCM.
- Report ANL-AAA-007, "Neutron Physics Analyses of the Sodium-Cooled Subcritical Multiplier System for the Accelerator-Driven Test Facility", documents neutron physics analyses performed for alternative configurations of the beam tube entry, target and multiplier.
- Memorandum ANL-AAA-005, "Thermal Fatigue Effects in the SCM-100 Blanket of the ADTF," on thermal fatigue analysis
- Memorandum ANL-AAA-006, "Preliminary Neutron Physics Analysis for two SCM-100 Models," comparing metal and oxide cores.

Additional reports documenting the complete target design activities for the SCM are being finalized and will be distributed next quarter.

Transmutation Technology Development Plan

The DOE guidance letter for WBS 1.03 requested the preparation of a Transmutation Technology Development Plan by September 1, 2002. This document will address the facilities and associated research needed to demonstrate POP for transmutation technologies. These activities will support decisions on the preferred technologies and path forward, and on the decision to proceed with the POP phase.

The following schedule was established to complete this document.

Milestone	Date
Draft Missions, Functions, and Requirements	April 30, 2002
Cost estimate of R&D to support each technology area	May 1, 2002
Interim status review meeting with DOE	May 16, 2002
Narrative sections complete	June 3, 2002
Integration and Prioritization Review Meeting	June 12, 2002
Final cost and schedule input	July 1, 2002
Issue draft Development Plan for review	July 31, 2002
Comment Resolution Meeting	August 15, 2002
Issue final report to DOE	August 30, 2002

A videoconference meeting was held to kickoff the work to develop the Transmutation Technology Development Plan. Program representatives from ANL, LANL, BNL, SRS, and DOE participated in the meeting. A general consensus was reached on the objectives and content of the document. It was also agreed that the AAA Program must develop a top-level strategy that will help guide the overall R&D program. This strategy may be published in a separate document or incorporated into the technology plan itself.

ADS Reference Design

Sodium-Cooled ADS Engineering Design

The ANL team that was involved in ADTF preconceptual mechanical design activities has been assigned to work on a preconceptual design for an SCM to be used in a full-scale (~800 MW_{th}) ADS for transmutation of LWR-spent fuel and generation of electricity. This assignment was discussed at the AAA Quarterly Review to establish assumptions upon which to base the preconceptual design. It was agreed that the multiplier physics designs presented in the AAA Program Report, "Compendium of Initial System Point Designs for Accelerator Transmutation of Radioactive Waste,"⁵ would be used as the basis for the multiplier core concept in lieu of additional physics analyses. The question of accelerator definition for the ADS reference was not completely resolved; whereas the physics point design uses a 1-GeV accelerator, LANL felt that the same energy accelerator used in the ADTF preconceptual design (600 MeV) should be used to minimize the requirements for new MCNPX shielding analyses. This question has yet to be settled, although it was agreed that a simple scale-up of the ADTF lead-bismuth eutectic (LBE) target would suffice for the current activity.

Information on a reactor design under development at ANL could be used in the ADS reference design. Both designs are about 800 MW_{th}. The similarity in sizes and anticipated commonality of components, analogous to the ADTF and EBR-II correspondence, allows for cross-fertilization between engineers on the two teams and minimization of design effort for both. Consequently, pending resolution of the completion of the accelerator design issue, work has been initiated on the design of part of the in-vessel fuel-handling system, namely the transfer arm that will be used in

⁵ AAA-RPO-SYS-01-0008, February 2001

both concepts. A conceptual design was completed on this sub-system, which moves fuel from the core gripper to the storage basket and from the basket to the fuel unloading machine gripper. The design was presented to the team working on the design of an advanced fast reactor of about the same size and power. Several suggestions for improvements were made, and also for further development of an alternative scheme that had not been brought to the same level of detail.

Superposition of the 840-MW SCM point design onto the reactor structure mentioned above (whose physics aspects were developed previously and chosen as the basis for the current work) was initiated. An elevation view of the core region of the concept is shown in Fig. 85, and a plan view is shown in Fig. 86.

In the development of this concept, a target was assumed that is simply a scaled-up version of the one used in the ADTF. The vertical dimension was scaled to be consistent with the deeper primary tank of the larger SCM, which was necessitated by the longer fuel assemblies. The lateral dimension was increased to accommodate the 27-mA beam of 600-MeV protons required for the 840-MW SCM⁶ at a current density of 40 $\mu\text{A}/\text{cm}^2$ and the increased LBE flow area required for removing the heat generated in the larger target without exceeding a lineal flow velocity of 2 m/sec. It is to be noted that this is quite a large target module, or in-pile beam tube (IPBT); its LBE content is ~24 tons, and the LBE supply and return tubes are ~30 cm in diameter. As yet, no consideration has been given to the high-energy beam transport (HEBT) that interfaces the IPBT to the accelerator proper, nor to the thermal or structural design of the window through which the protons must pass to reach the LBE target. It is obvious, however, that the HEBT will differ considerably from that developed for the ADTF, since the IPBT is so much longer, forcing the final HEBT beam handling magnet to be located at a greater distance from the target. The greater static head of LBE acting on the larger-diameter beam window will complicate its design as well. Moreover, the length of the IPBT will necessitate a very large shielded cask for removal from the SCM for replacement. It is clear that target design and handling will be challenging for this large system.

No control rods are tentatively anticipated for the reference design ADS. Unless their inclusion is absolutely necessary, it is preferable not to include them to simplify the placement of equipment on the small rotating plug of the primary tank cover and access to the IPBT for support and movement. This was a problem with the ADTF SCM and is exacerbated with the larger ADS because of the larger components located on the rotating plug and the intermediate heat exchangers and primary Na pumps (there are three of each) which extend some distance above the tank cover. The exclusion of control rods is based on a very preliminary evaluation, and could change if a compelling reason for their inclusion is found.

The direct scale-up of the ADTF systems for the ADS reference design is becoming increasingly problematic. The magnitude of the target assembly and the control approach that were deemed adequate for the test facility may not be adequate for the larger production facility. Therefore, some of the basic assumptions of the ADTF approach will be reconsidered and evaluated for applicability to the ADS facility. In particular, a target assembly that would be more practical for ADS will be studied, and evaluation of the ADS control approach—utilization of control rods, desirable k_{eff} for

⁶ "Effects of Buffer Thickness on ATW Blanket Performance," W.S. Yang *et al.*, presented at the 2001 Winter Meeting of the ANS, Reno, NV, November, 2001

ADS mission and safety considerations—will be initiated. As a result, it may become necessary to redefine the reference core.

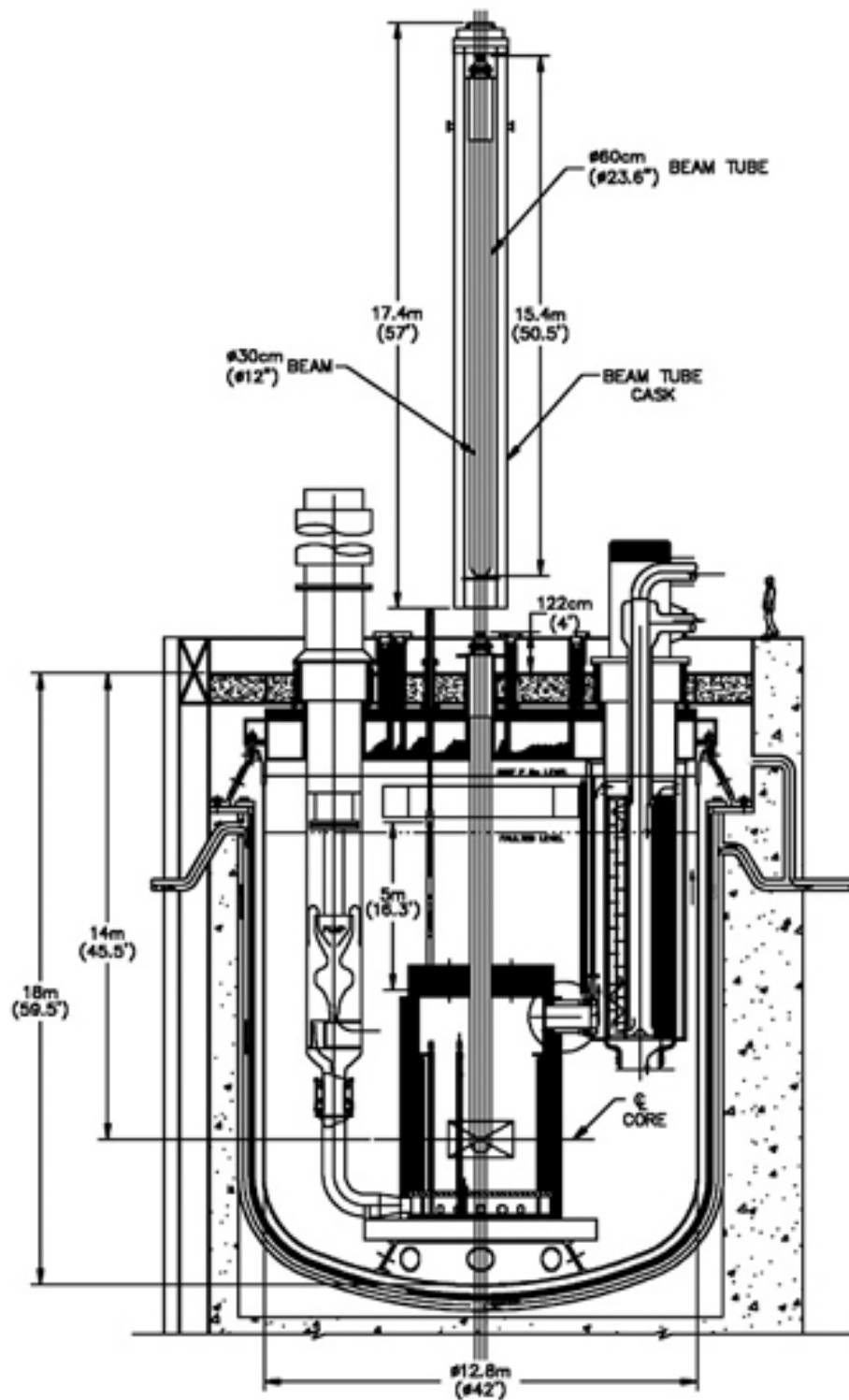


Fig. 85. Elevation view of the 840-MW Na-cooled SCM.

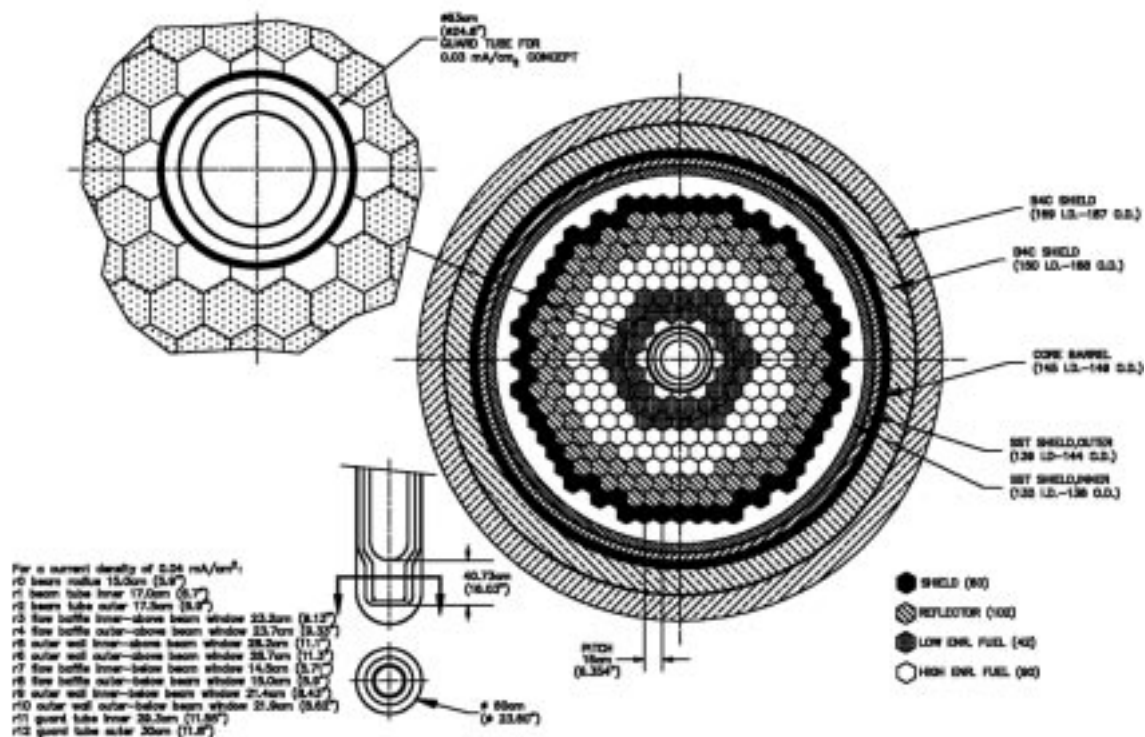


Fig. 86. Plan view of core region of 840-MW Na-cooled SCM.

Micro Accelerator-Driven System (ADS) Proof-of-Principle (POP)

Coupling Experiments

Accelerator-TREAT Coupling Experiments

A meeting was held to coordinate and plan activities among ANL and IAC participants in the TREAT coupling experiments. The required activities and costs involved in the TREAT facility restart were summarized and discussed. It appears that the dominant costs are associated with training four reactor operators, procedure writing, maintenance, and I&C system work. An environmental assessment will also be needed prior to restart. DOE has rejected a categorical exclusion for restart, in part at least because the environmental impact statements approved for a couple of INEEL facilities assumed that TREAT would not be operational and took advantage of using the environmental emissions that would normally have been due to TREAT operations (thus necessitating further analysis to evaluate the incremental effect of TREAT). In addition, the ANL-W participants indicated that the TREAT restart would involve the first NEPA action from ANL/INEEL since the intervention by local environmental organizations against the proposed BNFL mixed-waste treatment facility.

The use of TREAT as a POP test bed for an ADS subcritical facility along with associated specific objectives were reviewed. Ideas for the location of the accelerator and electron beam tube, for the target, and for target cooling were presented and discussed. It appears that the best configuration for the accelerator and beam consists of the accelerator located inside the TREAT equipment room just east of the reactor. The beam would be coming through a hole in the wall of the room and directly into the reactor core through the existing thermal column. For a depleted-U target, the acquisition of the U in a suitable geometry is an issue; potentially an array of EBR-II blanket pin segments could be used, if available. Containment of the U and its fission products will require a wall of minimal thickness to avoid excessive attenuation of the electron beam. Cooling approaches for the target, including the use of water, silicone oil, and air was also discussed.

Physics Modeling for TREAT Experiments

An assessment on the use of TREAT in the coupling experiments was initiated. The issues that can be studied in coupling experiments of TREAT and an external source are being investigated. The most relevant items are as follows:

- To perform a study of start-up and shutdown procedures for an ADS and to validate the instrumentation needed for monitoring such a procedure;
- To study the domain of reliable operation of an ADS system at different levels of subcriticality;
- To simulate different status of fuel irradiation (burn-up swings) by control rod movements;
- To validate different techniques of subcriticality measurements in a power system; and
- To study the correlation between power and current.

The choice of external source in coupling experiments using TREAT has been investigated. Three different possibilities have been considered: (1) proton-induced spallation source (base choice for ADS), (2) $\text{Be}^9(d,n)\text{B}^{10}$ reactions, and (3) use of an electron accelerator to ignite photo-neutron reactions. This last option has been considered in more detail, as an electron accelerator is available at the IAC. The availability and relatively low operating cost of this system, when compared to the other neutron source options considered, make it an attractive choice for an external neutron source for the coupling experiments. The highest total neutron flux that is expected from the 30-MeV LINAC at IAC, using a composite $^{238}\text{U}/\text{Be}$ target would be 3.7×10^{13} n/s; additional increase in the neutron flux, up to 10%, can be achieved by optimizing the target thickness and geometry.

Photo-neutron cross-section libraries have been linked to the MCNPX code. MCNPX models for the external neutron source have been initiated. TREAT core models are also being developed. More details are provided under Subtask 1.25.01.03.

Engineering Design

The ADTF engineering team is also responsible for the mechanical design portion of the AD-POP activity. Engineering team members participated in initial brainstorming sessions with physicists and thermal-hydraulics analysts at ANL, and accelerator experts from IAC.

Several sketches were prepared of a concept for integration of the small electron accelerator with the TREAT reactor. These sketches were presented and discussed at the ANL-W meeting with the director of IAC, and the ANL group representing TREAT operations and ANL-W management. Many interesting refinements of the basic ideas in the sketches were discussed. It was concluded that there are no basic scientific or engineering show-stoppers to the coupling of the IAC accelerator to TREAT, but it appears that the cost of TREAT restart may become the critical hurdle.

A conceptual design was initiated of a layout that uses fresh Fermi-1 reactor-blanket elements as a target for the electron beam from the accelerator. These elements sit in a capsule containing water so that heat from the target material is carried off as steam (from nucleate or film boiling at the surface of the elements) and either condensed in the cooler upper regions of the capsule or in an external condenser. A thin metal window in the wall of the tube admits electrons with minimal losses. A similar arrangement using EBR-II blanket elements is being prepared (there is a larger inventory of EBR-II blanket elements).

TREAT In-core target

The “vehicle” for positioning the target at the center of the TREAT core must permit target cooling and must ensure thermal isolation from the TREAT fuel and containment of any target debris. Present target vehicle concepts envision a long (~4 m) cylindrical tube with the target at one end and a heat exchanger on the other. For purposes of preliminary studies, a cylindrical target is assumed (diameter and height each ~10 cm) generating ~10 kW of heat. The target end of the vehicle is located at the center of the TREAT core through an assumed ~20-cm-diameter vertical test hole. Two cooling concepts, illustrated in Fig. 87, are presently under study: (1) forced flow of single phase coolant past the target and (2) a free-convection water boiler with a closed evaporation/condensation cycle.

Scoping analyses of these cooling methods, using the above parameters and dimensions, indicate that temperature rise in the boundary layer at the target surface (surface ΔT) is a more limiting concern than either pressure drop or bulk coolant temperature rise. Forced flow with liquid coolant requires volumetric flows ~100 gpm to keep surface ΔT s within ~100°C. The alternative of sub-sonic forced air flow leads to unacceptably high surface ΔT s ~1000°C. On the other hand, surface ΔT s with the water boiler concept are small provided target cooling takes place in the regime of nucleate boiling. Roughly, this boiling regime requires that the target have at least ~1cm² of cooling surface for every 100 W of heat generated within its volume.

The principal design goal is to maximize neutron production. This suggests using (1) high atomic weight materials for the target, and (2) low-density and/or low atomic number materials for insulation, vessel wall, and heat transfer fluid. Both neutron production and heat generation depend on the effective target thickness facing the incident electron beam. Calculations of these dependencies are currently underway. Cooling the target requires good internal conduction paths and sufficient target surface shaped to optimize contact with the heat transfer fluid. Detailed thermal analyses to guide preliminary designs of target size and shape will follow.

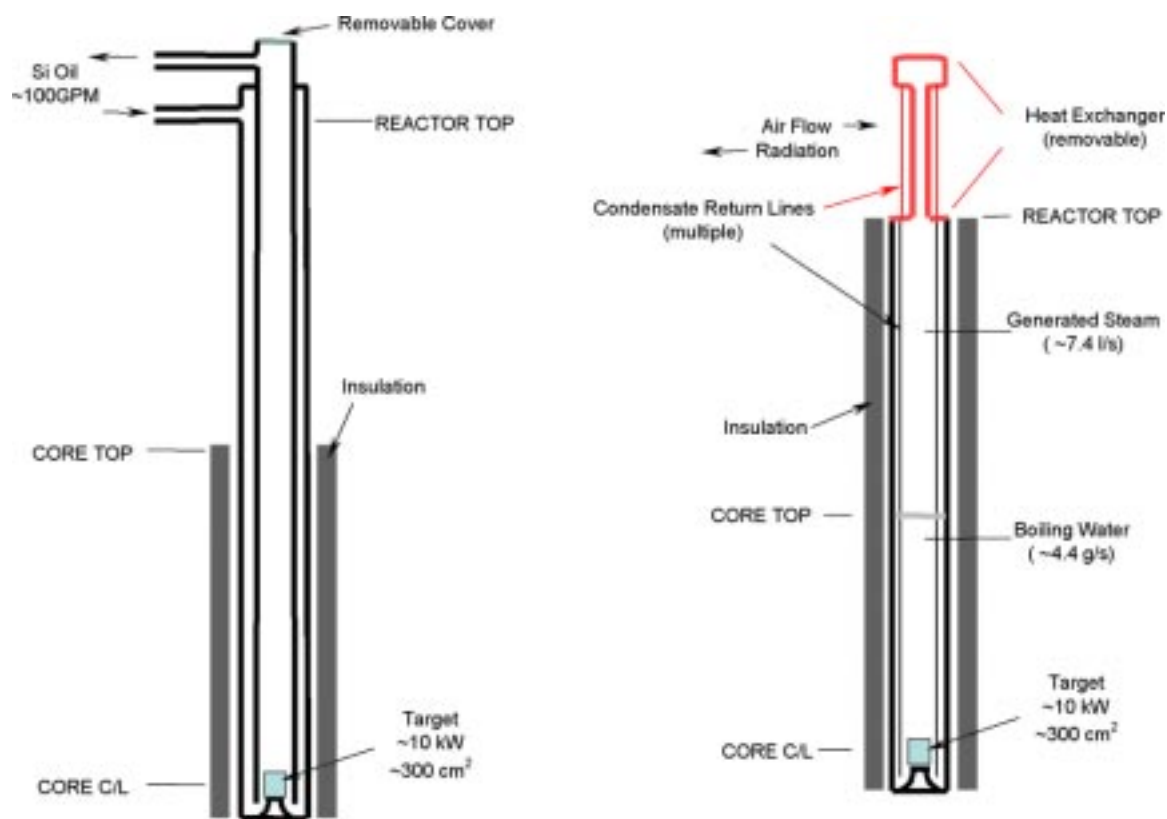


Fig. 87. Two concepts for mounting, containing, and cooling the target in a TREAT/ADS experiment.

Fuels and Materials Experiments

LANSCe will deliver 800 kW of beam power (800 MeV, 1 mA) to a neutron producing spallation target. To date, the overall vessel, shielding, and target insert configuration have been developed. In addition, preliminary physics analyses have been performed. The target will be a flowing lead-bismuth eutectic (LBE) contained in stainless steel structures, similar in configuration and size to the ISTC target. Allowances will be made for the insertion of material and fuel samples directly into the LBE, making it possible to perform tests in a prototypic irradiation and coolant environment. Surrounding the target will be additional irradiation positions for direct proton irradiation, mixtures of protons and neutrons, and pure neutron environments with both fast and thermal spectra. The design features allow for easy insertion and retrieval of samples without target removal. Calculations show that the proton fluxes of 4×10^{14} p/cm²/s are achievable for direct proton irradiation of materials. A fast neutron flux of up to 1×10^{15} n/cm²/s are also achievable providing an excellent environment for fuel tests. The calculations were performed assuming a fuel sample height of 11 cm, which is sufficient for meaningful testing. Helium generation to dpa ratios can be varied from 2:1 to 20:1 depending on the needs of the experimenter.

Both the testing of structural materials and fuels will be performed. Materials experimenters will be able to investigate the irradiation effects of both protons and high-energy neutrons on the structural properties of window and target materials.

Materials testing in the LBE coolant will provide the synergistic effects of material corrosion and irradiation.

Over a 9-month irradiation campaign, fuels experimenters will be able to achieve burn-ups of up to 5 atom%. Testing will be performed to understand fuel material behavior in a fast spectrum environment, and allow experimenters to test the effects of fuel composition, swelling interaction due to fission product growth and gas retention, fuel phase stability, and constituent separation behavior. In addition, the experimenters will test fission product targets of Tc and I in prototypic environments. With the addition of closed coolant loops, a variety of test temperatures can be achieved, and transient and overpower conditions can be imposed safely.

The cost and schedule for the experiment will be estimated. The current goal is to implement the experiment in a time period of three years at a cost of less than \$20M. To minimize cost, an existing target location has been chosen for modification (Fig. 88). The old target and experimental hardware will be removed, and a new vacuum vessel inserted (Fig. 89). The existing shielding (iron plates and concrete blocks) will be used to the extent possible.



Fig. 88. Experiment location at LANSCE. Existing shielding (steel plates) to remain in place.

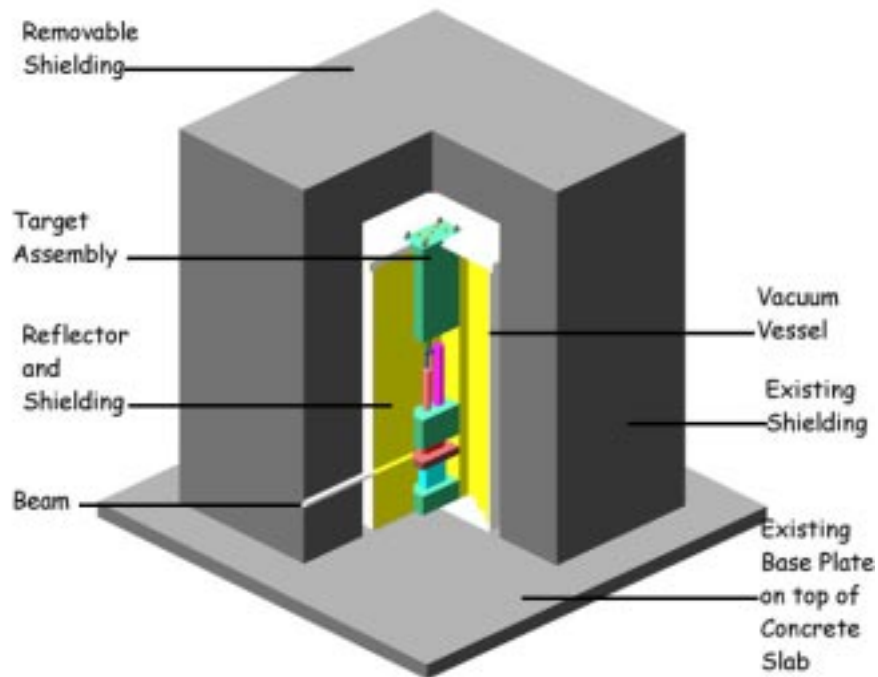


Fig. 89. Isometric of vessel and shielding for the LANSCE LBE spallation target.

POP Facilities Requirements Document

An outline of the documentation of the requirements for the AD-POP for an ADS facility was developed in collaboration with SRS and LANL. The initial emphasis of the document was to identify what proof-of-principle was required before a test facility (e.g., ADTF) to demonstrate the ADS transmutation concept could be built. Of special importance was the identification of the facilities (existing and/or modified) and tests that would be needed for the proof-of-principle. After the NERAC subcommittee meeting in February, there has been discussion within the project regarding the scope of the document. In particular, the discussion has centered on using the document in support of the recommended approach for the program, including the down-selection to preferred systems in the future. This document, called the Transmutation Technology Development Plan (as discussed earlier), will provide a top-level strategy to help guide the overall R&D program.

Advanced Cavity Development

Progress on the fabrication of the $\beta=0.175$, 2-gap, 350-MHz superconducting spoke resonator cavities continued at the vendor, Zanon. The work continued to progress on schedule, and the first cavity is scheduled for delivery in June of 2002. The photographs in Fig. 90 show the status of components at the end of March 2002.

We continued our collaboration with ANL, and began testing the ANL $\beta=0.4$, 2-gap 340-MHz spoke resonator cavity. This work will be completed early next quarter.

Optimization of the design of the power coupler for the spoke cavity continued. The current concept of the power coupler is shown in Fig. 91.



Fig. 90a. Copper facsimile of spoke cavity.



Fig. 90b. Spoke cavity endwall stiffeners.



Fig. 90c. Spoke cavity ports and flanges.



Fig. 90d. Spoke cavity endwalls.

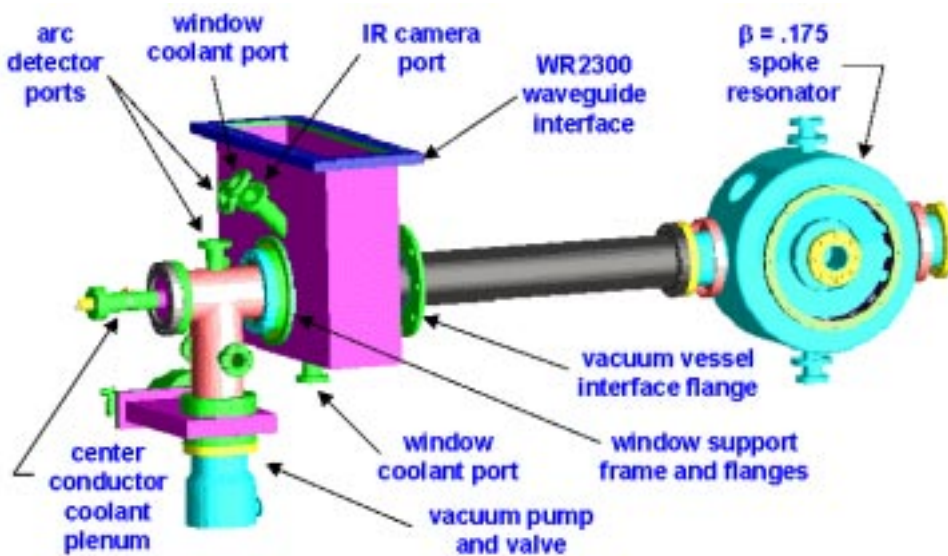


Fig. 91. Preliminary concept of spoke cavity power coupler.

5. PROJECT INTEGRATION

5.1 Systems Studies

Scope

Transmutation System Selection Studies

The FY02 AAA Systems Studies is focused on analyses to support selection between the multi-tier transmutation system approaches. Based on the results of the recently completed multiple strata task force report and feedback from the NERAC ATW Subcommittee Meeting, two primary systems studies needed for this assessment are (1) the evaluation of options to achieve deeper burnup in the Tier 1 thermal system, and (2) the refinement of systems evaluation techniques (e.g., include cost comparisons and more robust fuel cycle consequence analysis). To this end, proliferation resistant and conventional ALWR fuel cycles are being evaluated to clarify and assess the practical limits for Tier 1 partial destruction of the transuranics (TRU). As demonstrated in the FY01 study, partial burning of the TRU in a first tier thermal spectrum system will impact the performance of the second tier transmuter; thus, the Tier 2 fast-system performance impact must be considered. If the TRU content can be reduced sufficiently, the repository licensing dose rates of the long-lived fission products (LLFPs) may dominate. Thus, the potential for LLFP transmutation is also being evaluated. In brief, Systems Studies scope includes:

- assess practical limits for Tier 1 partial destruction of TRU;
- consider the impact on Tier 2 fast system performance;
- evaluate the potential for LLFP transmutation.

Report To Congress

The Department of Energy was directed to prepare a report for Congress by May 1, 2002 identifying the benefit of alternative nuclear fuel cycles employing transmutation and addressing a specific list of questions. These questions included (1) comparison of processing techniques, (2) comparison of transmutation approaches, (3) resulting waste streams, (4) life-cycle costs, (5) proliferation resistance, and (6) strategy for facility siting.

Highlights

- The AAA report on the CORAIL-Pu deep burn analyses was completed, and three papers on the CORAIL fuel cycle analyses were submitted to upcoming nuclear conferences.
- The transmutation performance of a second tier fast spectrum accelerator driven system (ADS) to follow the CORAIL-Pu design was evaluated.

Transmutation System Selection Studies

Recently, the French CEA proposed the use of the so-called CORAIL assembly design for stabilizing the production of Pu in a PWR. One of the attractive features of the CORAIL concept is that it makes use of a retrofit-able PWR fuel assembly design.

The CORAIL assembly employs a standard 17x17 PWR fuel assembly with a heterogeneous loading of UO_2 and MOX fuel pins as shown in Fig. 92.

The multi-recycling of Pu in the CORAIL assembly was assessed with the WIMS8a LWR lattice code. After each irradiation cycle, the discharge UO_2 and MOX pins are recycled with 99.9% recovery of the Pu, and the minor actinides are discharged to the second tier. As shown in Figure 93, the Pu content in the MOX and the U enrichment increase each recycle because of the degradation of the Pu fissile content. However, the Pu content stabilizes around 8% and the ^{235}U enrichment at 4.57%. While a typical UO_2 fueled assembly produces about 6 kg of Pu/assembly, the CORAIL assembly can achieve an almost zero Pu mass balance (only 0.5 kg per assembly). Furthermore, the reactivity coefficients with CORAIL assemblies are quite similar to a reference UO_2 assembly. However, the pin power peaking in the heterogeneously loaded CORAIL assembly is more severe (1.2 as compared to 1.06 for a homogeneous assembly); thus, increased utilization of burnable absorbers may be needed to flatten the power distribution.

By multi-recycling the Pu in the CORAIL assembly, this approach effectively achieves a deep burnup in the thermal reactor system. All of the Pu and roughly 75% of the total TRU mass is consumed. It was observed that complete Pu consumption reduces the long-term radiotoxicity relative to the reference UO_2 assembly by a factor of 2-5; however, the minor actinide inventory has roughly doubled—a key consideration for repository performance. Thus, a subsequent fast-spectrum system would be required to consume the remaining minor actinides.

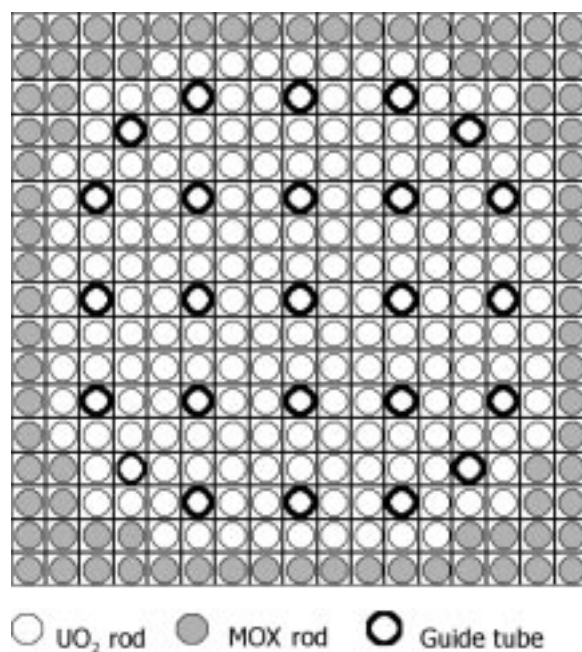


Fig. 92. Heterogeneous pin loading pattern in the CORAIL-Pu assembly.

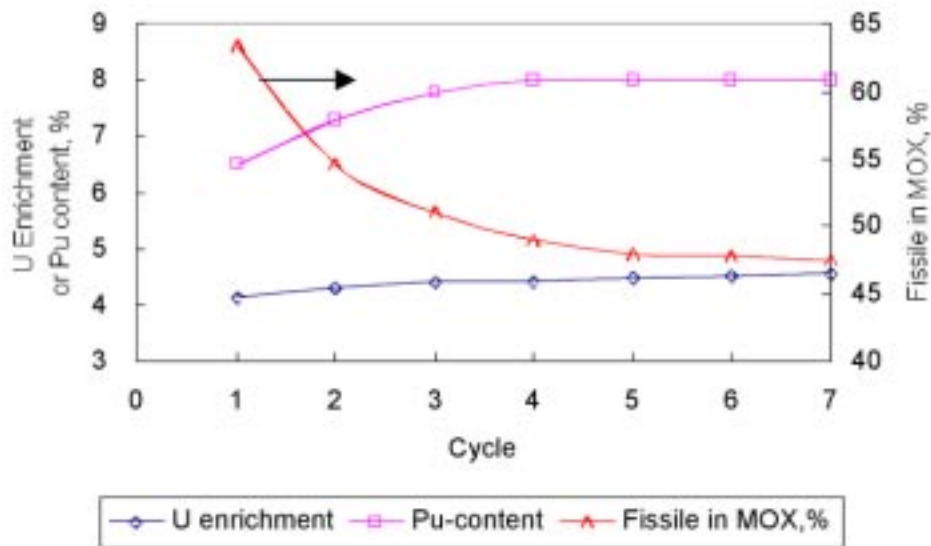


Fig. 93. Multi-Recycling of the CORAIL-Pu Assembly

Fuel cycle analyses were also started for the CORAIL heterogeneous assembly with recycle of all transuranics, denoted CORAIL-TRU. With recycle of the TRU, the minor actinides would not build up in the LWR waste stream. However, much larger increases in the TRU enrichment were observed for the CORAIL-TRU case, over 20% TRU enrichment at equilibrium. In addition, the power peaking is much worse in this case. Thus, alternative assembly configurations are being evaluated to both reduce the TRU enrichment and improve the peaking behavior. It is important to note that recycle of the TRU in LWRs will introduce significant fuel handling and processing complications. Thus, work was also initiated to identify and evaluate practical limits for utilization of repeated recycle fuels in conventional LWR systems.

The AAA report on the CORAIL-Pu deep burn analyses was completed this quarter. In addition, three papers on the CORAIL fuel cycle analyses were submitted to upcoming nuclear conferences, both the CORAIL-Pu and CORAIL-TRU results are discussed.

Also this quarter, the transmutation performance of a second tier fast spectrum accelerator driven system (ADS) to follow the CORAIL-Pu design was evaluated. As described above, the make-up feed for this system is composed solely of minor actinides recovered from both the UO_2 and MOX pins of the CORAIL-Pu design. The low fissile content results in some performance degradation (e.g., burnup decrease from 28 to 22%); however, the equilibrium system performance is similar to double tier cases evaluated in the FY01 multiple-tier study. Because of the deep burn in the LWR, the Tier 2 support ratio increases to 14 for the CORAIL-Pu case. This cuts the number of required ADS systems roughly in half compared to the 50% burnup cases in the FY01 study, and a significant fuel cycle cost benefit is observed.

Evaluation of the potential to transmute the long-lived fission products (LLFPs) in the various transmutation systems was also initiated. Effective transmutation of LLFPs requires both significant transmutation rates and the avoidance of radiotoxic product isotopes (e.g., activation products of the target materials). The radiotoxicity was evaluated for the entire spectrum of fission products, and ^{99}Tc , ^{129}I , and ^{135}Cs were identified as the most problematic isotopes because of their high radiotoxicity and

geochemical mobility. However, isotopic separation would likely be required for effective transmutation of ^{135}Cs , thus it was excluded. Preliminary analyses have considered ^{99}Tc and ^{129}I target transmutation rates in a typical ADS; variations in both target composition and location (changing neutron spectrum) are being investigated.

Report To Congress

Sections of the Congressional Report were composed to explain the potential and urgency of waste disposal benefits achieved by transmutation. Descriptions of the options for partitioning and transmuter technology were provided. Several international studies focused on transmutation were summarized, including the AAA Program FY01 multi-tier fuel-cycle study. Refinements to the systems studies were completed to provide key information to answer the questions posed by Congress; in particular, fuel cycle economics were assessed and deep burnup LWR options were considered.

(1) Regarding processing techniques, the key attributes of aqueous processes are the capability to process large quantities of LWR spent fuel and high technology readiness based on European experience. Nevertheless, these technologies all result in producing highly separated plutonium streams. Pyroprocessing is desirable for treating highly radioactive spent fuel having large concentrations of transuranics (TRU) or short cooling time; further development is needed to allow pyroprocessing to treat large quantities of LWR spent fuel; another favorable feature is that the TRU are not separated, avoiding the creation of a pure plutonium stream.

(2) Electricity generation costs of accelerator-driven systems (ADS) will be higher than fast reactor approaches. Thus, fast reactors are ideal for either single-tier or dual tier systems with deep burnup in the first tier, while ADS are best suited to a double-tier system with deep burnup in the first tier. Future nuclear energy will be a key consideration, with reactors favored in growth scenarios. Fast reactor technology is closer to deployment, but fuel cycle research and development will be required in any case.

(3) Life cycle costs were separately considered for the development and implementation phases. The total research and development cost was estimated in detail. This included separate evaluations of the separations and transmuter demonstration facilities. The relative cost of electricity for a single-tier fast reactor transmutation system is estimated 10% higher than the once-through LWR cycle; and the cost of an ADS single-tier system is significantly higher. The marginal cost of either system can be reduced by performing multiple recycle in Tier 1 LWRs. For the deep-burn LWR case, the marginal costs of the double-tier ADS is comparable to the single-tier fast reactor scenario.

(4) For all transmutation scenarios, the high-level waste volume is reduced significantly, by roughly a factor of 4 compared to the once-through LWR fuel cycle. However, the low-level waste volume becomes much larger due to the removal of uranium into this waste stream. This change is beneficial because high level waste disposal is much more expensive.

(5) All transmutation approaches nearly eliminate the long-term proliferation risk (plutonium disposal in the repository) at the cost of a short-term increase of proliferation risk (during the transmutation campaign). However, these short-term

risks should be readily manageable using conventional safeguards. Co-location and the avoidance of separated plutonium are perceived advantages in some scenarios.

(6) The AAA Program will make use of existing facilities to the greatest extent possible. An extensive infrastructure for spent fuel storage, processing, and transmutation will be required. The large-scale deployment of transmutation requires a comprehensive siting strategy.

A detailed presentation was provided to the NERAC Subcommittee; previous studies and recent analytical results were shown and answers to the Congressional questions were discussed.

5.2 University Programs

Scope

University Programs consists of four major aspects: the University of Nevada-Las Vegas (UNLV) University Participation Program (UPP), AAA Program at the Idaho Accelerator Center (IAC) of Idaho State University (ISU), University Fellowships Program (UFP), and AAA Directed University Research within the Transmutation Sciences technical area.

UNLV AAA University Participation Program — The University of Nevada supports the AAA Program through “research and development of technologies for economic and environmentally sound refinement of spent nuclear fuel...”⁷ The UNLV Program has four components: student-based research, infrastructure, international collaborations, and support.

Idaho Accelerator Center — The IAC at Idaho State University received \$1.5 M in FY02 for unspecified research. They will develop a long-term plan and a research program to conduct a variety of investigations that depend on high-energy electron accelerators.

University Fellowships Program — The University Research Alliance (URA, formerly ANRC—the Amarillo National Research Center) acts as the executive agency for the AAA Program to select, award, and administer fellowships for ten graduate students who were selected last year and ten more to be selected in FY02.

AAA-Directed University Research — Three universities currently support R&D and technology development: the University of Michigan, the University of California-Berkeley, and the University of Texas-Austin. North Carolina State University is being added.

In addition, the scope of this effort involves coordination between other AAA activities and academia.

⁷ ref. H.R. 5483, P.L. 106-377

Highlights

LANL University Programs

- An annual report that describes all FY01 AAA University Programs was completed and distributed.
- UNLV hosted a University Workshop to bring together researchers from a number of AAA university programs. PIs and others from Michigan, Berkeley, and UT-Austin traveled to Las Vegas and presented their research. In addition, UNLV PIs and students gave presentations. Other attendees came from LANL, DOE/NE, and URA.
- The University Projects Leader, D. Beller, invited philanthropist and actor Paul Newman, and the Chairman of the HWGC Board, Raymond Lamontagne, to UNLV to discuss nuclear waste and transmutation, to view the DOE-sponsored UNLV hydrogen-fueled bus project, and to visit Yucca Mountain.
- Additionally, Beller gave several presentations on AAA to audiences at the Univ. of Tennessee, ORNL, and ORAU.

University Participation Program

- The UNLV AAA Director submitted a fourth-quarter summary report that described progress, technical status of the first research projects, budget status, and other topics.
- UNLV coordinated and hosted a technical working meeting for the Dose Conversion Coefficients Project.
- UNLV hosted a week-long training course for the MCNPX radiation transport code. Attendance included 13 from UNLV and about the same from a number of other organizations including ISU and LANL.
- UNLV coordinated and hosted the second AAA Quarterly Technical Review.
- UNLV received a third round of research proposals, four for continuation of ongoing research, and seven for new funding. Two proposals were selected for funding beginning this summer.
- US Senator Pete Domenici's senior science advisor, Dr. Peter Lyons, visited UNLV to discuss the AAA Program.
- AAA seminars were conducted weekly.

Idaho Accelerator Center

- The IAC received authorization to begin work the end of March.

University Research Alliance

- The University Research Alliance (URA), formerly the Amarillo National Research Center, conducted the selection of ten AAA Fellows.

Directed University Research

University of Michigan extended their work in five areas: they modeled transmutation of transuranics in pressurized water reactors, conducted analysis in support of the LANSCE experiments, developed a method to evaluate space-time analysis of

coupled accelerator-core dynamics, and investigated cross-section processing with the NJOY code. In addition, a new project was initiated to examine radiation effects in candidate materials for spallation neutron environments by irradiating LANL-supplied samples with protons. The contract has been extended through Dec 2002.

UC Berkeley began a comparison of the MONTEBURNS code and the MOCUP depletion code. They also completed a study of equilibrium characteristics of molten-salt reactors, studied the transmutation capability of accelerator-driven pebble-bed reactor, developed a simplified model for fuel isotope evolution in ATW systems, conducted a comparison between Na and Pb-Bi as coolants for liquid-metal ATW, and began a cost/risk analysis of candidate approaches for partitioning and transmutation

UT-Austin established a methodology and collected data (questionnaires from individuals) for adding time dependencies to proliferation assessment for four systems. They included (a) a once-through PWR cycle, (b) a closed PWR cycle based on PUREX separations, (c) a closed PWR cycle based on UREX separations, and (d) a closed accelerator-based transmuter cycle based on UREX separations. In addition, students who are not supported by LANL funding have contributed in two areas: UREX process modeling and spallation product studies. The contract has been extended through May 2002.

North Carolina State University received an RFP to initiate a project in support of the SINQ spallation neutron source at the Paul Scherrer Institute (PSI) in Switzerland. The purpose of the research is to calculate radiation damage (production of displacements, helium, hydrogen, and heavier transmutation products) and energy deposition in target materials, containment structures, and entrance windows of the target assemblies for the SINQ spallation neutron sources.

Technical Progress

Technical progress of ongoing investigations by direct university research projects is reported under appropriate technical areas (e.g., Transmutation Science). Some technical progress made under the UNLV program has been reported separately (viz., quarterly progress reports by primary investigators).

References

1. Y.S. Touloukian, *et al.*, *Thermophysical Properties of Matter*, vol. 1, IFI/Plenum, New York (1970).
2. Y. Takahashi, M. Yamawaki and K. Yamamoto, *J. Nucl. Mater.* 154 (188) 141.
3. J.K. Fink and L. Leibowitz, *J. Nucl. Mater.* 226 (1995) 44.
4. T.A. Sandenaw, in *The Metal Plutonium*, eds., A.S. Coffinberry and W.N. Miner, University of Chicago Press, pp.152 – 156, 1961.
5. R. Schenkel, *Solid State Communications*, 23 (1977) 389.
6. W. Muller, R. Schenkel, H.E. Schmidt, *et al.*, *J. Low Temp. Phys.* 30 (1978) 561.
7. J.A. Lee, in *Progress in Nucl. Energy*, Series v: Metallurgy and Fuels, III, pp.453-467, 1961.
8. S. Tamura, *J. Mater. Sci. Lett.* 15 (1996) 1752.
9. A. Matthiessen and C. Vogt, *Annal. Physik.* (Leipzig), 122 (1864) 19.
10. K. Schroder, *CRC Handbook of Electrical Resistivities of Binary Metallic Alloys*, CRC, Boca Raton, FL, 1983.
11. D.A.G. Bruggeman, *Annal. Physik.* 24 (1935) 636.
12. R. Landauer, *J. Appl. Phys.* 23 (1952) 779.
13. Z. Hashin and S. Shtrikman, *J. Appl. Phys.* 33 (1962) 3125.
14. J.P. Stora, *Nucl. Technol.* 17 (1973) 225.
15. T.J. Shankland and A.G. Duba, *Geophys. J. Int.* 103 (1990) 25.
16. F.D. Stacey and O.L. Anderson, *Phys. Earth and Planetary Interiors*, 124 (2001) 153.
17. G.N. Dul'nev and Yu.P. Zarichnyak, *Thermal Conductivity Of Mixtures And Composition Materials* [in Russian; *Teploprovodnost' Smesei I Kompozitsionnykh materialov*], Energiya, Leningrad, 1974.
18. Yu.P. Zarichnyak and T.A. Lisnenko, *Izv. Vyssh. Uchebn. Zaved. Priborost.* 19, No.5 (1976).
19. Yu.P. Zarichnyak and T.A. Lisnenko, *Inzhenerno-Fizicheskii Zhurnal* (Byelorussian SSR), 33 (1977) 642; Journal title of translation: *Journal of Engineering Physics* (USA), 1978.
20. G.L. Hofman, *et al.*, *Metallic Fuels Handbook*, Argonne National Laboratory, Report ANL-IFR-29, 1985.
21. H.A. Saller, R.F. Dickerson, A.A. Bauer and N.E. Daniel, Battelle Memorial Institute, Report BMI-1123 (1956).
22. E.L. Francis, UKAEA Report IGR-R/R-287 (1958).
23. K.A. Long, *Plutonium and other actinides*, eds., H. Blank and R. Lindner, North-Holland Pub. Co., Amsterdam, pp.449-457, 1976.

24. T. Matsui, T. Natsume and K. Naito, *J. Nucl. Mater.* 167 (1989) 152.
25. P.M.G. Damen, A. van Veen, H.J. Matzke, H. Schut, J.A. Valdez, K.E. Sickafus, "Helium Behavior in Amorphous Spinel," in preparation for *J. Nuc. Materials*.
26. T.M. Besmann and T.B. Lindemer, *J. Nucl. Mat.* v. 130, pp. 489-504, 1985.
27. T.M. Besmann and T.B. Lindemer, *Trans. Amer. Nucl. Soc.* v. 45, pp. 280-281, 1983.